Advancing the understanding of hydro-climatic controls on water balance and lake-level variability in the Tibetan Plateau

-

Hydrological modeling in data-scarce lake basins integrating multi-source data

Dissertation

zur Erlangung des akademischen Grades *doctor rerum naturalium*

(Dr. rer. nat.)

vorgelegt dem Rat der Chemisch-Geowissenschaftlichen Fakultät

der Friedrich-Schiller-Universität Jena

von Dipl.-Geogr. Sophie Biskop

geboren am 03. Mai 1984 in Weimar

Gutachter:

1. Prof. Dr. Alexander Brenning (Friedrich-Schiller-Universität Jena)

2. Prof. Dr. Wolfgang-Albert Flügel (ret.) (Friedrich-Schiller-Universität Jena)

Tag der Verteidigung: 3. Februar 2016

ABSTRACT

The Tibetan Plateau with its surrounding mountain ranges (TP) reacts sensitive to climate variability and change. Specifically, the numerous high-elevation lakes are considered as important indicators for climate variability and climate-related changes within the hydrological cycle. Contrasting patterns of lake-level changes indicate differences in the water balance over the TP. The water balance of the several closed lakes across the TP included in this study is controlled by the net difference between input (on-lake precipitation, runoff from glaciers and non-glacierized areas) and output (lake evaporation). Hydrological models are an important tool to quantify several water-balance components and to analyze climate effects on hydrological processes. However, hydrological modeling in the remote TP region is challenging, due to data scarcity.

The overall goal of this thesis is to contribute to an improved understanding of the hydro-climatic controls on the water balance and lake-level variability in the TP region. Therefore, the present thesis deals with the development of a modeling framework linking spatially distributed hydrological modeling with model-derived atmospheric and remote-sensing data. The distributed conceptual model J2000g was adapted and extended according to the specific characteristics of closed-lake basins on the TP. The High Asia Refined analysis (HAR) data at 10 km resolution were used as driving force for the modeling period 2001-2010. In addition, satellite-derived lake-water surface temperature served as input for the estimation of lake evaporation. Due to a lack of lake-level in-situ data, satellite-derived lake-volume changes were used as a model-performance criterion. The model was applied to four selected closed lakes in the south-central part of the TP: Nam Co and Tangra Yumco (increasing water levels), and Mapam Yumco and Paiku Co (stable or slightly decreasing water levels). The Nam Co basin had the best available hydrological data and thus was selected as case-study site for model development and evaluation.

The presented results provide novel knowledge on spatiotemporal patterns of the water-balance components and their relative importance for the lake-level regime in the four selected basins. Differences in the mean annual water balance among the four basins are primarily related to higher precipitation totals and attributed runoff generation in the basins with a higher monsoon influence (Nam Co and Tangra Yumco). Precipitation and associated runoff are the main driving forces for inter-annual lake variations. The glacier-meltwater contribution to the total basin runoff volume (14-30 %) plays a less important role compared to runoff generation from rainfall and snowmelt on non-glacierized land areas. However, considering the small part of glacier areas in the study basins (1-6 %), glaciers make an important contribution to the water balance. Using a hypothetical ice-free scenario, it is indicated that ice melt is an important water supply for the Mapam Yumco and Paiku Co basins to maintain a state close to equilibrium; whereas, the water balance in the Nam Co and Tangra Yumco basins remains positive under ice-free conditions.

This thesis highlights the benefits of combining hydrological modeling with multi-source data such as atmospheric-model output and satellite-based data. This is in order to advance our understanding of hydrological dynamics and their influencing variables in the data-sparse TP, which is critically important for water-resources management in Tibet. It provides a robust modeling tool that can be readily transferred to other remote and difficult accessible mountainous regions, and forms a valuable basis for further model improvement, opening new directions and priorities for research.

ZUSAMMENFASSUNG

Das Tibetische Plateau mit seinen angrenzenden Hochgebirgszügen (TP) reagiert sensibel auf Klimavariabilität und -änderungen. Insbesondere die zahlreichen abflusslosen Seen stellen einen wichtigen Indikator für Klimavariabilität und klimabedingte Veränderungen im hydrologischen Kreislauf dar. Rezente Seespiegeländerungen auf dem TP weisen gegensätzliche Muster auf und deuten somit auf regionale Unterschiede in der Wasserbilanz hin. Das Verhältnis zwischen Netto-verdunstungsüberschuss (Differenz zwischen Verdunstung und Niederschlag über dem See) und der Wasserzufuhr durch Gletscherschmelze und Abflüsse von gletscherfreien Landflächen bestimmt die Gebietswasserbilanz bzw. die Änderung des Seespiegels. Hydrologische Modelle sind wichtige Werkzeuge zur Quantifizierung der Wasserhaushaltsgrößen sowie zur Erfassung des Klimaeinflusses auf hydrologische Prozesse. Hydrologische Modellanwendungen in Tibet stellen jedoch aufgrund der mangelhaften Datengrundlage eine große Herausforderung dar.

Vor diesem Hintergrund ist die übergeordnete Zielstellung der vorliegenden Arbeit, einen Forschungsbeitrag zum besseren Verständnis der hydroklimatischen Einflussfaktoren auf die Wasserbilanz und die Variabilität von Seespiegeländerungen auf dem TP zu leisten. Die Arbeit beschäftigt sich mit der Entwicklung eines Modellverfahrens, das raum-zeitlich differenzierte Modellierung mit atmosphärischen Modelldaten und Fernerkundungsdaten verknüpft. Hierfür wurde das distributive prozessorientierte Einzugsgebietsmodell J2000g hinsichtlich der spezifischen Gegebenheiten abflussloser Seeeinzugsgebiete auf dem TP angepasst und erweitert. Als meteorologische Eingangsdaten für den Modellierungszeitraum 2001-2010 dienten die 10-km aufgelösten atmosphärischen Modelldaten des High Asia Refined analysis (HAR) Datensatzes. Zusätzlich sind aus Fernerkundung gewonnene Wasseroberflächentemperaturen als Modellinput für die Berechnung der Verdunstung freier Wasserflächen (Seeverdunstung) verwendet worden. Zur Kompensation fehlender Seespiegelmessungen wurden fernerkundungsbasierte Seevolumen-änderungen als Maß für eine plausible Wiedergabe der Wasserbilanz herangezogen. Die Modellanwendung erfolgte in vier ausgewählten Seen in Zentral- und Südtibet: Nam Co und Tangra Yumco mit ansteigenden Seespiegeln sowie Mapam Yumco und Paiku Co mit relativ stabilen bzw. leicht fallenden Seespiegeln. Das Nam Co Einzugsgebiet diente aufgrund der besseren Datenverfügbarkeit als Fallstudie für die Modellentwicklung und -evaluierung.

Die vorliegende Studie liefert neues Wissen über raum-zeitliche Muster der einzelnen Wasserhaushaltsgrößen und deren relativer Bedeutung für die Wasserbilanz in den vier selektierten Einzugsgebieten. Die Unterschiede in der mittleren Gebietswasserbilanz (2001-2010) sind vor allem durch höhere Jahresniederschläge und damit verbundene Abflussmengen in den stärker vom Monsun beeinflussten Einzugsgebieten (Nam Co und Tangra Yumco) bedingt. Der simulierte Anteil der Gletscherschmelze am Gesamtabfluss (zwischen 14 und 30 % in den vier Einzugsgebieten) spielt eine geringere Rolle im Vergleich zu dem durch Niederschlag und Schneeschmelze generierten Abfluss auf den gletscherfreien Landflächen. Unter der Berücksichtigung des geringen Gletscherflächenanteils in den einzelnen Einzugsgebieten (1-6 %) leisten die Gletscher jedoch einen wichtigen Beitrag zur Wasserbilanz. Unter Zuhilfenahme eines hypothetischen Szenarios konnte aufgezeigt werden, dass ohne den Beitrag der Gletschereisschmelze eine negative Wasserbilanz im Paiku Co und Mapam Yumco vorherrschen würde. Die Einzugsgebiete Nam Co und Tangra Yumco würden hingegen auch ohne Gletschervorkommen eine positive Wasserbilanz aufweisen.

Weiterhin zeigten die Modellsimulationen, dass interannuelle und saisonale Seespiegel-schwankungen in den Untersuchungsgebieten generell durch Variationen des vom Niederschlag gespeisten Abflusses bestimmt werden. Der 10-jährige Modellierungszeitraum lässt keine endgültigen Aussagen über hydrologische Trends zu. Die Ergebnisse bestätigen jedoch die Vermutungen weiterer Autoren, dass räumliche Unterschiede in Niederschlagstrends die Hauptursache für räumliche Variationen in Seespiegeländerungen sind. Zugleich widerlegen sie die Vermutungen anderer Autoren, dass die abschmelzenden Gletscher der Haupteinflussfaktor für die ansteigenden Seespiegel in Zentraltibet sind.

Durch die Verknüpfung von distributiver hydrologischer Modellierung mit freizugänglichen atmosphärischen Modelldaten und Fernerkundungsdaten ermöglicht die vorliegende Arbeit die Quantifizierung einzelner Wasserhaushaltsgrößen in der datenarmen Region von Tibet. Sie trägt somit zu einem verbesserten Verständnis der hydrologischen Systemdynamiken und deren Einflussgrößen auf dem TP bei, was von wichtiger Bedeutung für ein nachhaltiges Wasserressourcenmanagement in Tibet ist. Das entwickelte Modellverfahren kann ohne das Vorliegen von In-situ-Messdaten eingesetzt werden und ist dadurch besonders für hydrologische Modellanwendungen in schwer zugänglichen Hochgebirgsregionen geeignet. Es schafft damit eine wichtige Grundlage für weiterführende Untersuchungen von Klimaauswirkungen auf den Wasserhaushalt im tibetischen Hochland sowie für andere Gebiete mit ähnlichen Gegebenheiten.

TABLE OF CONTENTS

LIST OF FIGURES

LIST OF TABLES

LIST OF ACRONYMS

AET	Actual Evapotranspiration
a.s.l.	Above Sea Level
AWS	Automatic Weather Station
BMBF	Bundesministerium für Bildung und Forschung
CAS	Chinese Academy of Sciences
CAME	Central Asia – Monsoon Dynamics and Geo-Ecosystems (BMBF Program)
DEM	Digital Elevation Model
FAO	Food and Agriculture Organization of the United Nations
GIS	Geographical Information System
GLUE	Generalized Likelihood Uncertainty Estimation
GRACE	Gravity Recovery and Climate Experiment
HAR	High Asia Reanalysis
HRU	Hydrological Response Unit
IDW	Inverse Distance Weighting
ITP	Institute of Tibetan Plateau Research
JAMS	Jena Adaptable Modeling System
LAI	Leaf Area Index
Landsat TM/ETM+	Landsat Thematic Mapper/Enhanced Thematic Mapper Plus
LSWT	Lake-Surface Water Temperature
LST	Land-Surface Temperature
MAAT	Mean Annual Air Temperature
MAP	Mean Annual Precipitation
MODIS	Moderate Resolution Imaging Spectroradiometer
NASA	National Aeronautics and Space Administration
NCDC	National Climatic Data Center
PUB	Predictions in Ungauged Basins
RSA	Regional Sensitivity Analysis
SCAF	Snow-Covered Area Fraction
SEB/MB	Surface Energy Balance / Mass Balance
SOTER	Soil and Terrain
SRTM	Shuttle Radar Topography Mission
SWE	Snow-Water Equivalent
TLR	Temperature-Lapse Rate
TP	Tibetan Plateau (with surrounding mountain ranges)
TRMM	Tropical Rainfall Measuring Mission
WET	Variability and Trends in Water Balance Components of Benchmark Drainage Basins on the Tibetan Plateau (BMBF project)
WRF	Weather Research and Forecasting (model)

1 INTRODUCTION

1.1 Background and Research Questions

The Tibetan Plateau with its surrounding mountain ranges (TP) plays a key role for climate and hydrology in Central and High Asia (IMMERZEEL *et al.*, 2010). Due to its large areal extent and high altitude, it acts as a major driver in both the regional and global climate systems. With an average elevation of more than 4500 m above sea level (a.s.l.) the TP contains the largest ice masses outside the Polar Regions; thus, it is therefore referred to as '*The Third Pole*' (QIU, 2008; YAO *et al.*, 2012a). The TP also holds the largest high-elevation inland lake area on Earth and is the origin of major Asian rivers such as the Indus, Ganges and Brahmaputra (LEI *et al.*, 2013).

Widespread climate trends and climate-induced cryosperhic and hydrological changes (e.g., glacier retreat, lake expansion, etc.) have been widely reported in the TP region in recent years (e.g., KANG *et al.*, 2010; YAO *et al.*, 2012b). Although in the recent past a large number of environmental studies have been performed, the knowledge on atmosphere, cryosphere and hydrosphere linkages in this unique environment is still limited. As a consequence, the '*Third Pole Environment (TPE)*' program bringing together international scientists from interdisciplinary research field was initiated by scientists from China, India, Germany, Italy, Japan, Nepal, the Netherlands, Norway, Pakistan, US, Canada, Tajikistan, and Switzerland in 2009. The research effort of the TPE program has been directed towards the synergy of joint theoretical, field and laboratory studies indicating that interdisciplinary and integrated approaches are needed to understand and to assess the changing ecosystem dynamics (YAO *et al.*, 2012a).

In this context a Sino-German priority program '*Tibetan Plateau: Formation - Climate - Ecosystem (TiP)*' was initiated as the German contribution to the large international TPE program. This then was complemented by the Federal Ministry of Education and Research (BMBF) program '*Central Asia and Tibet: Monsoon Dynamics and Geo-Ecosystems (CAME)*'. The present study was embedded in the WET-Project ('*Variability and Trends in Water Balance Components of Benchmark Drainage Basins on the Tibetan Plateau*'), which was initiated in 2011 as a part of the CAME-program.

The drainage system of the interior TP is characterized by numerous closed-lake (endorheic) basins. While most of the lakes located in the central part of the TP are characterized by a water-level increase over recent decades, there are also several lakes with nearly stable or slightly decreasing water levels in the south part of the TP (e.g., PHAN *et al.*, 2012a; ZHANG, G. *et al.*, 2011). These high-elevation lakes, which are less affected by direct anthropogenic factors, are considered to be one of the most sensitive indicators for regional differences in the water balance over the TP (e.g., LEI *et al.*, 2014; SONG *et al.*, 2014c; 2015; ZHANG, G. *et al.*, 2013b). However, little is known about the region's key hydrological processes controlling this variability. Detailed knowledge about the actual state of the hydrological system at catchment scale in the TP region

is essential to gain a better understanding of the hydrological response of high-elevation lakes to climate-related changes. Therefore, it is important to analyze the spatiotemporal variability of the several hydrological components and to quantify their contribution to the basin water balance under current climate conditions.

Previous studies addressing the controlling mechanism of water-level fluctuations of endorheic lake basins are mostly qualitative or rely on simple water-balance analyses (e.g., LI, L. *et al.*, 2014; MORRILL, 2004; ZHANG, B. *et al.*, 2011; ZHOU *et al.*, 2013; ZHU *et al.*, 2010). Recent studies emphasize the urgency of hydrological modeling to enable quantitative estimates of the factors controlling the water balance and lake-level variability (e.g., CUO *et al.*, 2014; LEI *et al.*, 2014; SONG *et al.*, 2014c; YE *et al.*, 2008). However, detailed hydrological modeling studies of Tibetan lakes are lacking. Especially, the sparse distribution of hydro-meteorological stations and associated data for the inner TP constitutes the major limitation of comprehensive hydrological modeling studies of endorheic lake basins in the TP region. This raises the questions:

- How is it possible to overcome the lack of ground-based data for hydrological modeling studies of endorheic lake basins over the TP?

- What are the relevant hydrological processes in Tibetan lake basins? How do they vary spatially and temporally? What are the controlling factors of spatiotemporal hydrological patterns?

- What are the contributions of single components to the water budget of Tibetan lakes?

- What are the key factors governing water balance and lake-level variability on the TP?

1.2 Research Objectives and Methodological Approach

Addressing the aforementioned research questions, the objectives of this study are:

i) Development of a distributed, process-oriented hydrological model that is applicable in data-scarce lake basins in the TP region and capable to account for spatial heterogeneity of hydrological processes within the catchments.

ii) Distributed hydrological modeling of selected endorheic lake basins in the TP in order to:

  - analyze spatiotemporal patterns of water-balance components and to contribute to a better understanding of their controlling factors,

  - quantify single water-balance components and their contribution to the water balance, and obtain a quantitative knowledge of the key factors governing the water balance and lake-level variability.

A methodological approach combining hydrological modeling with multi-source data, such as satellite-derived data and atmospheric-model output for the period 2001-2010, is proposed to fulfill the above-stated study objectives. Four endorheic lakes along a west-east lake transect across the southern-central part of the TP (between 28°N~32°N and 81°E~92°E) are selected for this study: Nam Co and Tangra Yumco with increasing water levels (i.e. positive water balance), and Mapam Yumco and Paiku Co with stable or slightly decreasing water levels (i.e. stable or slightly negative water balance, respectively). The Nam Co basin is chosen as a case

study site for model development and evaluation, because it is the basin with the best hydrological data availability. The hydrological model developed and evaluated in the Nam Co basin is then transferred to the other three basins. Comparing the model results of the several basins, the most relevant factors influencing the hydrologic conditions for endorheic lake basins on the TP are identified, and thereby the impact of the spatial-temporal variability of climate conditions on catchment hydrology.

1.3 Structure of the Thesis

The thesis is organized as follows:

- *Chapter 2* outlines a state-of-the-art review of key scientific topics providing the background and research context of this thesis.

- *Chapter 3* describes the climatic and physio-geographic characteristics of the study area.

- *Chapter 4* gives an overview of data sets used in this study.

- *Chapter 5* gives details of analytical methods used for data analysis, processing, observation and hydrological modeling.

- *Chapter 6* presents the study results with a strong focus on hydrological modeling results.

- In *Chapter 7* the results, limitations, and implications of this research are discussed.

- The concluding *Chapter 8* highlights the principal outcomes of this study and concludes with remarks on future research needs.

1.4 Published Research Papers

The author was responsible for/contributed to following publications which are of relevance for this thesis:

Peer-reviewed articles

I.   **Biskop, S.**, Maussion, F., Krause, P. and Fink, M. (2015): What are the key drivers of regional differences in the water balance on the Tibetan Plateau. *Hydrol. Earth Syst. Sci. Discuss.*, *12*, 4271–4314 (*in review*). (*S.B. designed the study, extended the J2000g model, performed modeling studies, analyzed data and wrote the main paper and the supplementary information*)

II. **Biskop, S.**, Krause, P., Helmschrot, J., Fink, M., and Flügel, W.-A. (2012). Assessment of data uncertainty and plausibility over the Nam Co Region, Tibet. *Adv. Geosci.*, *31*, 57–65. (*S.B. designed the study, analyzed the data and wrote the main paper*)

III. Hochschild, V., Kropacek, J., **Biskop, S.**, Braun, A., Chen, F., Fink, M., Helmschrot, J., Kang, S., Krause, P., Leiterer, R., Ye, Q. and Flügel, W.-A. (2011). Multisensoral remote sensing based modelling of the water balance of endorheic lakes on the Tibetan Plateau, IAHS Publ. 352, 253-256. (*S.B. responsible for hydrological modeling part*)

IV. Krause, P., **Biskop, S.**, Helmschrot, J., Flügel, W.-A., Kang, S. and Gao, T. (2010). Hydrological system analysis and modelling of the Nam Co basin in Tibet, *Adv. Geosci.*, *27*, 29–36. (*S.B. contributed to study design, input data preparation and analyzing, writing*)

Conference contributions

I. **Biskop, S.** and Fink, M. (2014): Lake levels as indicator for the water balance of endorheic lake basins under present-day and paleo conditions. 5th Third Pole Environment Workshop, December 8-9, Berlin, Germany.

II. **Biskop, S.**, Maussion, F., Krause, P. and Fink, M. (2014). The role of snow and glacier dynamics in endorheic lake basins on the Tibetan Plateau. 18th Alpine Glaciology Meeting, February 27-28, 2014, Innsbruck, Austria.

III. **Biskop, S.**, Maussion, F., Krause, P. and Fink, M. (2013). Analyzing atmosphere, cryosphere and hydrosphere interactions to understand water balance changes of data-scarce lake basins, Tibet. AGU Fall Meeting, December 9-13, 2013, San Francisco, USA.

IV. Schneider, C., Yao, T., Scherer, D., Kang, S., Buchroithner, M., Fink, M., Hochschild, V., Bendix, J., Kropacek, J., Maussion, F., Yang, W., Huintjes, E., **Biskop, S.**, Curio, J., Zhang, G., Rüthrich, F., Thies, B., Spiess, M., Neckel, N., Holzer, N. and Schröter, B. (2013). Advances in the process-related understanding of atmosphere-cryosphere-hydrosphere couplings on the Tibetan Plateau. 28th Himalayan Karakorum Tibet Workshop & 6th International Symposium on Tibetan Plateau, August 22-24, 2013, Tübingen, Germany.

V. **Biskop, S.**, Krause, P. and Fink, M. (2013). A multiple response validation approach to estimate the modelling uncertainty in data-scarce lake basins, Tibet. "Kos 2013- Facets of Uncertainty", 17-19 October, 2013, Kos, Greece.

VI. **Biskop, S.**, Maussion, F., Kropacek, J., Fink, M. and Flügel, W.-A. (2013). A comprehensive data assimilation approach for reliable hydrological predictions in data-scarce endorheic basins, Tibetan Plateau. EGU General Assembly, April 7-12, 2013, Vienna, Austria.

VII. **Biskop, S.**, Maussion, F., Fink, M. and Flügel, W.-A. (2012). Integrated multi-scale hydrological system analysis approach in data-scarce high elevation basins, Central Asia, EGU General Assembly, April 22-27, 2012, Vienna, Austria.

VIII. **Biskop, S.**, Krause, P., Leiterer, R. and Helmschrot, J. (2010). Linking large-scale, long-term modeling and micro-scale, short-term process studies to assess climate-driven changes in hydrological dynamics in the Nam Co Basin, Tibet, China. AGU Fall Meeting, December 13-17, 2010, San Francisco, USA.

2 RESEARCH CONTEXT

Many studies suggest that high-elevation environments (including glaciers, snow, permafrost, lakes, etc.) are strongly impacted by climate change (e.g., BENISTON, 2003; DIAZ *et al.*, 2003; RANGWALA *et al.*, 2013). In particular, high-elevation lakes are considered as sensitive indicator for climate-related changes, because lake-level dynamics represent integrated effects of climate and associated cryospheric and hydrological dynamics within their drainage basin (e.g., LI, Y. *et al.*, 2014; LIU *et al.*, 2009). Because this study aims to contribute to the understanding of the hydrological response of high-elevation endorheic lakes in the TP region to climate variability and change using hydrological modeling, the research review is structured as follows:

- Section 2.1 provides a general overview of climate variability and change over the TP.

- Section 2.2 summarizes climate-induced cryospheric and hydrological changes in the TP region.

- Section 2.3 gives basic background on the water balance of endorheic lake basins, summarizes the current scientific knowledge of lake-level changes across the TP and outlines their potential driving factors.

- Section 2.4 introduces challenges and limitations of hydrological modeling studies, and recent efforts and progress in hydrologic science to overcome such research constraints.

2.1 Climate Variability and Change over the Tibetan Plateau

2.1.1 Climatic Drivers

Climate variability in the TP is principally related to the large-scale atmospheric circulation systems in the Northern Hemisphere, namely the mid-latitude westerlies and the East Asian and South Asian Monsoon (e.g., MAUSSION *et al.*, 2014). In turn, the TP with its unique topographic features exerts profound influences on the atmospheric circulation systems, acting as an elevated heat source and a mechanical barrier. Although the influence of the TP on atmospheric circulation has been the subject of research for a long time (e.g., HAHN & MANABE, 1975; RAGHAVAN, 1973), the mechanical and thermal controlling factors of the global circulation patterns are not yet clear and still involve considerable research (e.g., BOOS & KUANG, 2010; RAJAGOPALAN & MOLNAR, 2013; WU *et al.*, 2012).

The interplay of the large-scale atmospheric drivers over the TP varies from subregion to subregion and over monthly to millennial timescales (e.g., BENN & OWEN, 1998; MAUSSION *et al.*, 2014; MÖLG *et al.*, 2014). The combined and competing influences of the mid-latitude and monsoonal dynamics on the climatological and hydrological patterns across spatial and temporal

scales are not yet fully understood and promote active debate within the research community (BOTHE *et al.*, 2011; 2012; MÖLG *et al.*, 2014).

The spatial distribution and the seasonal cycle of precipitation are strongly related to the location and intensity of the westerly jet (MÖLG *et al.*, 2014; SCHIEMANN *et al.*, 2009). In many studies the westerly jet has been identified as key element connecting the mid-latitude and monsoonal dynamics (e.g., BOTHE *et al.*, 2011; DING & WANG, 2005; MÖLG *et al.*, 2014). During the winter and summer seasons, the position of the westerly jet, respectively, is south and north of the TP. Indeed, the jet transition from south of the Plateau to the north as consequence of the summer hemisphere heating indicates large meridional variability from year to year (SCHIEMANN *et al.*, 2009) and thus strongly influences the interplay or 'competition' of mid-latitude and monsoon circulation (MÖLG *et al.*, 2014). A northerly jet location in late spring intensifies the north-south pressure gradient and therefore promotes moisture advection from the mid-latitudes toward the TP cyclonic system; whereas, jet occurrences far south over the western Plateau and also over the Plateau reduce the north-south pressure gradient and limit the moisture import from mid-latitude circulation as well as the northward penetration of the monsoonal flow (MÖLG *et al.*, 2014).

During the Indian summer monsoon onset period (late spring/early summer), the mid-latitude wave train (BOTHE *et al.*, 2011) which is part of a circumglobal pattern (BRANSTATOR, 2002; DING & WANG, 2005) and, being closely linked with the North Atlantic climate (BOTHE *et al.*, 2011; BRANSTATOR, 2002), determines the strength of the regional atmospheric flow over the whole Plateau and associated local precipitation conditions (MÖLG *et al.*, 2014). Weak flow or low wind speed, respectively, over the TP enhances deep convective precipitation (FUHRER & SCHÄR, 2005; KIRSHBAUM & DURRAN, 2004; MÖLG *et al.*, 2014). Hence, the mid-latitude westerlies are a major driving force for the spatial-temporal climate variability not only during the winter, as has been previously assumed, but even during the monsoon season (MÖLG *et al.*, 2014).

Beside mid-latitude intrusions during the monsoon period, local to meso-scale processes forced by the complex topography may modify the large-scale monsoonal flow. Moreover, lakes interact with the atmosphere by exchanging moisture and thermal energy. As shown by MAUSSION (2014) large lakes across the TP have a major influence on local climate by weakening convection during the summer and enhancing snowfall in the autumn. Unfortunately, lake-atmosphere interactions over the TP have been studied only to a limited degree (BIERMANN *et al.*, 2013; HAGINOYA *et al.*, 2009; MAUSSION, 2014).

Increasingly undergoing research but still a matter of debate is the relevance of the monsoon and westerlies for the amount, origin, and transport of atmospheric moisture over the TP and of their respective influences on precipitation and associated regional water resources (CHEN *et al.*, 2012; CURIO *et al.*, 2014; FENG & ZHOU, 2012). CURIO *et al.* (2014) concluded that local water recycling plays a major role in the TP's hydrological cycle. Thus, the TP itself is a major source for atmospheric moisture and provides more moisture than external sources (on average 60 % versus 40 %) (CURIO *et al.*, 2014).

2.1.2 Climate Trends

Based upon long-term observational data, significant warming trends have been detected on the Plateau during the last half century, with an accelerated temperature increase since the late 1980s and a higher-than-normal warming during winter and spring seasons (e.g., CHEN *et al.*, 2003; FRAUENFELD *et al.*, 2005; KANG et al., 2010; LIU & CHEN, 2000; QIN *et al.*, 2009; WANG *et al.*, 2008; XIE *et al.*, 2009b; YOU *et al.*, 2008; 2010a; 2010b; 2013; ZHAO *et al.*, 2004). Using almost all available ground-based weather-station data located principally in the eastern TP, the annual mean surface air-temperature averaged using 90 stations increased by 0.36°C/decade between 1961 and 2007 (WANG *et al.*, 2008), which is double the rising trend based on weather-station records between 1955 and 1996 (LIU & CHEN, 2000). Increase of minimum air-temperature is more pronounced than the maximum air-temperatures (LIU *et al.*, 2006; YOU *et al.*, 2008).

Using 71 stations, annual precipitation increased on average by 5 mm/decade during the period 1961-2007 (YOU *et al.*, 2012). However, spatial variations of precipitation changes occurring throughout the TP are more complex compared to the continuous temperature rise. The central and northeastern TP indicated a slightly increasing trend in precipitation during the last decades, whereas stable or slightly decreasing precipitation were observed in the southern, western and northwestern TP (LI, Y. *et al.*, 2014; XU *et al.*, 2008; YANG *et al.*, 2011; 2014; YIN *et al.*, 2013; YOU *et al.*, 2012). However, available meteorological stations are mostly located near population centers in lower elevations in the eastern part of the Plateau. Thus, the limited number and uneven distribution of observational data may not represent all spatial patterns of precipitation changes occurring throughout the TP (QIN *et al.*, 2009).

Based upon 75 stations, average wind speeds decreased by ~0.02 m s^{-1} yr^{-1} between 1970 and 2009 (~27 % over the 39 years) (XIE & ZHU, 2013), although winds seemed to be steady and even recovering during the last decade (LIN *et al.*, 2012; YIN *et al.*, 2013). Changes in surface wind speed are similar to changes in the upper-air zonal wind speed and are strongly related to changes in geopotential height gradient at 500 hPa. These, in turn, are correlated with the changes of latitudinal surface temperature gradient, suggesting that the spatial gradient of surface global warming or cooling might change surface wind speed through atmospheric thermal adaptation (LIN *et al.*, 2012).

The solar radiation over the TP decreased by ~0.008 MJ m² day^{-1} yr^{-1} between 1970 and 2009 (XIE & ZHU, 2013). YANG *et al.* (2012) reported that radiation extinction due to aerosol loading over the TP has a minimal effect. Instead, this study suggests that solar dimming is primarily determined by an increase in water vapor amount and deep cloud cover, which in turn might be related to surface warming and an increase in convective available potential energy.

2.2 Cryospheric and Hydrological Changes

2.2.1 Snow Cover

Monitoring of the snow pack on the TP is limited to snow-depth measurements at conventional ground-based meteorological stations principally located in the inhabited lower-altitude regions. Because snow measurements in the remote and difficult accessible region of the TP are sparse

and not representative for larger scales, snow dynamics have been examined based on MODIS snow-cover products and passive microwave remote-sensing data (e.g., CHE *et al.*, 2008; PU & XU, 2008; QIU *et al.*, 2012; QUIN *et al.*, 2006; TANG *et al.*, 2013; XU, 2010). Snow-cover and snow-depth data of the TP indicate a large inter-annual variability, with no discernible time-trend during the last decades (CHE *et al.*, 2008).

2.2.2   Glacier Area and Mass Balance

Based upon remote-sensing analysis, the glacier area in the TP region gives an overall decreasing tendency during the last decades (e.g., BOLCH *et al.*, 2010; 2012; HE *et al.*, 2003; KANG *et al.*, 2010; KÄÄB *et al.*, 2012; NECKEL *et al.*, 2014; YAO, 2010; YAO *et al.*, 2007; 2012b). Although glacier-area changes provide only an indirect indicator of global climate change and depend on the glacier response time, glacier mass budgets reflect almost a direct relationship to climate (e.g., BOLCH, 2011).

Because in-situ measurements of glacier mass budgets are currently limited, laser-altimetry data acquired by the *Geoscience Laser Altimeter System* (*GLAS*), transported onboard the *Ice Cloud and Elevation Satellite* (*ICESat*), were used in recent studies to derive estimations of glacier elevation and mass-balance changes on the TP (e.g., KÄÄB *et al.*, 2012; NECKEL *et al.*, 2014). The mass-balance changes indicate contrasting patterns with highest specific mass loss rates in the north- and south-eastern parts of the TP and balanced mass budgets or even slight mass gain in the north-western part (Figure 2.1, NECKEL *et al.*, 2014). However, accurate quantifications of glacier mass-balances remain difficult due to the limited number of field observations.

The summer-accumulation-type glaciers in the central and eastern parts of the TP which undergo simultaneous accumulation and ablation are more sensitive to climate change than winter-accumulation-type glaciers in the western TP (FUJITA & AGETA, 2000). A reduced percentage of snowfall in summer (wet season) caused by rising temperatures not only leads to a decrease in accumulation, but also to an increase in ablation associated with surface albedo lowering (e.g., FUJITA & AGETA, 2000; KANG *et al.*, 2009; MÖLG *et al.*, 2014). In order to better understand the interactions between atmospheric conditions and glacier dynamics at a local scale, detailed *surface energy balances/mass balance* (*SEB/MB*) studies are required (MÖLG *et al.*, 2012). However, due to the scarcity of direct field measurements, the number of such studies is limited for the TP (e.g., FUJITA & AGETA, 2000; MÖLG *et al.*, 2012; ZHANG, G. *et al.*, 2013a).

MÖLG *et al.* (2014) evaluated the influence of large-scale circulation systems on local mass balance and emphasized the high sensitivity of the annual glacier mass-balance in the TP region to the amount of snowfall during the late spring and early summer (May-June). As previously mentioned, precipitation in spring is not only strongly related to the intensity of Indian summer monsoon onset but also influenced by the mid-latitude dynamics. Although it is evident that interacting large-scale atmospheric flows largely determine the annual mass-balance, local features (e.g., topography, debris coverage) also affect the heterogeneous glacier changes on the TP over short distances (e.g., SCHERLER *et al.*, 2011; VENKATESH *et al.*, 2012). However, further investigations are needed to quantify the influence of several factors on present glacier changes across time and spatial scales.
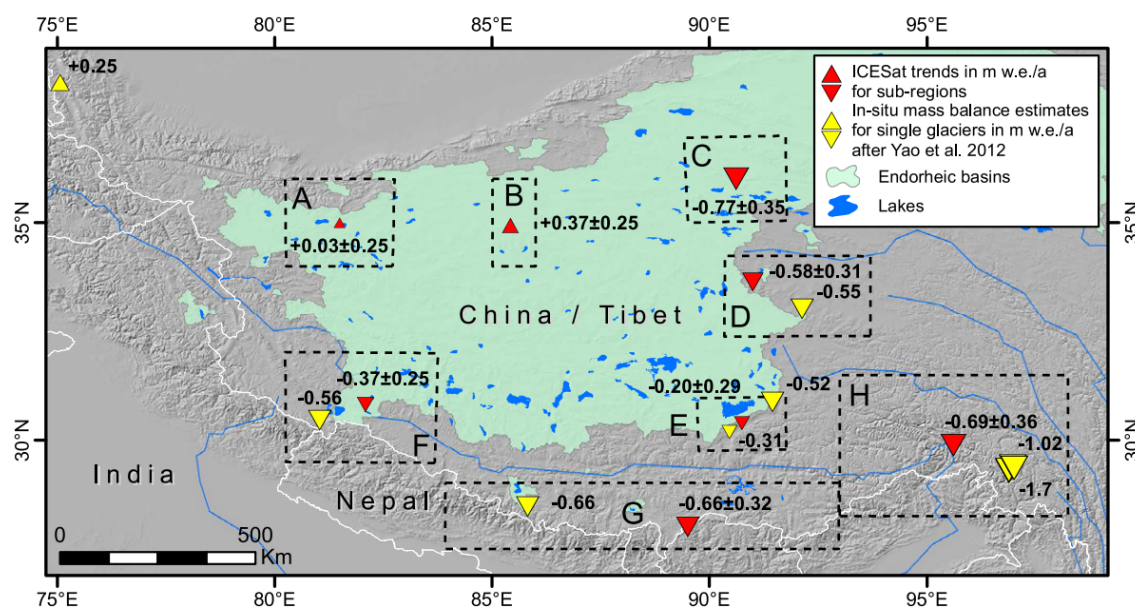
Figure 2.1: Mass balance estimates in m w.e.a⁻¹ derived from ICESat measurements for eight subregions (comprising 80 % of the glacier area on the TP) in comparison to in-situ mass balance measurements of single glaciers (2006-2010, YAO et al., 2012) (Neckel et al., 2014).

2.2.3 Permafrost

Permafrost in the TP region degraded during the last decades associated with a rise in permafrost temperature and an increase of the permafrost's active layer thickness (GUO, D. *et al.*, 2012; LI, R. *et al.*, 2012; WU & ZHANG, 2008; 2010; YANG *et al.*, 2010). Permafrost long-term monitoring (10 boreholes up to 10.7 m depth) from 1966 through 2006 along the Qinghai-Tibetan Highway indicated that mean annual permafrost temperatures at 6.0 m depth increased by 0.12°C to 0.67°C. Increasing rainfall in summer and decreasing snowfall in winter may have a cooling effect and explain the less degree of permafrost warming compared with the magnitude of air-temperature increase (WU & ZHANG, 2008). The active layer thickness increased by 3.1 cm yr⁻¹ from 1998 to 2010 in permafrost regions above 4700 m a.s.l. along the Qinghai-Tibetan Highway (LI, R. *et al.*, 2012). The depth of seasonal frozen ground decreased up to 20 cm over the last 30 years). The duration of seasonal ground freezing has been shortened up to 20 days over the last 30 years, principally caused by an increase in winter air-temperature (LI, X. *et al.*, 2012; ZHAO *et al.*, 2004).

A research review on permafrost degradation and the environmental effects in the TP region is given by YANG *et al.* (2010). The implications of changes in permafrost and seasonal freeze-thaw processes on spatiotemporal patterns in hydrogeology (e.g., ground-water table), soil-moisture, and land-surface evapotranspiration have been studied in only a limited way, because observational studies and adequate field measurements are rare.

2.2.4 Evapotranspiration

Because of the warming trend, an increase in the potential evaporation is expected (ZHANG, 2007). Indeed, potential evaporation indicated an overall decrease during the last four decades, (LIU *et al.*, 2011; XIE & ZHU, 2013; YIN *et al.*, 2013; ZHANG, 2007; ZHANG *et al.*, 2009). Reference

evapotranspiration (ET_{ref}) estimates derived from 75 meteorological stations using Penman-Monteith method, recommended by the FAO (ALLEN *et al.*, 1998), indicated that ET_{ref} decreased on average by 0.7 mm yr^{-1} between 1970 and 2009 (XIE & ZHU, 2013).

In order to explore the impact of the increase in air temperature (~0.0057°C yr^{-1}) and actual vapor pressure (~0.0019 KPa yr^{-1}) as well as the decrease in wind speed (~-0.02 m s^{-1} yr^{-1}) and solar radiation (~-0.008 MJ m² day^{-1} yr^{-1}) on ET_{ref} changes during the 1970-2009 period, XIE & ZHU (2013) quantified the contribution of these four variables. Reduced wind speed was the dominant factor with the contribution of -0.7 mm, followed by air temperature (0.51 mm), actual vapor pressure (-0.4 mm) and solar radiation (-0.1 mm). The combined effect of reduced wind speed, increased vapor pressure and decreased solar radiation have tended to negate the effects of rising temperature (XIE & ZHU, 2013). However, the decreasing trend of potential evapotranspiration has reversed in the 2000s (LI, Y. *et al.*, 2014; YIN, *et al.*, 2013), indicating an upward tendency possibly due to increasing wind speeds after 2000 (LIN *et al.*, 2012).

Theoretically, decreased potential evaporation indicates a reduced capacity of water evaporation in the atmosphere and hence a decrease in actual evapotranspiration. However, a complementary relationship exists for potential evaporation and actual evapotranspiration on the TP, known as the 'pan evaporation paradox' (e.g., YIN *et al.*, 2013; ZHANG, 2007; ZHANG *et al.*, 2009). Simulated actual evapotranspiration rates revealed an increase during the last decades for most parts of the TP, which coincided with the increased precipitation, especially in the central TP (YANG *et al.*, 2011; YIN *et al.*, 2013). Indeed, regions with decreasing precipitation (e.g., along the south-west periphery of the TP) indicated a decline in actual evapotranspiration.

2.2.5 Runoff

The exhoreic drainage area of the TP comprises the upstream areas of the major Asian rivers (e.g., Indus, Ganges, Brahmaputra, etc.), covering about 50 % of the entire Plateau (CAO *et al.*, 2006). Time-trend analysis for observed discharge in the upstream area of the large river systems revealed both increasing trends (mostly towards the central TP) as well as decreasing trends (particularly in the south and east Plateau) (e.g., CAO *et al.*, 2006; CUO *et al.*, 2014; LIN *et al.*, 2008; YANG *et al.*, 2012; 2014; ZHANG *et al.*, 2006; ZHANG, Y. *et al.* 2012). However, previous studies revealed that stream flow trends may vary from headwater region to downstream reaches and for different time periods within the same river system.

To investigate the impact of climate change on runoff, many hydrological modeling studies have been conducted in the entire upstream areas of the large river systems originating from the margin areas of the TP (e.g., IMMERZEEL *et al.*, 2009; 2010; ZHANG, L. *et al.*, 2013) or in individual upstream sub-catchments (e.g., IMMERZEEL *et al.*, 2013; NEPAL *et al.*, 2014; PELLICCIOTTI *et al.*, 2012; PRASCH *et al.*, 2013; RAGETTLI *et al.*, 2013; TAHIR *et al.*, 2011; ZHANG *et al.*, 2007). Moreover, LI, F. *et al.* (2013; 2014) analyzed and compared conditions in multiple catchments in the Yarlung Tsangpo river basin in the south-eastern part of the TP.

In contrast to the exhoreic drainage area in the marginal region of the TP, the interior drainage system is characterized by a large system of endorheic lake basins along with a sparse stream network. Due to the harsh conditions and limited logistics of access, very limited runoff measurements are available in the central TP (e.g., GAO *et al.*, 2011; ZHOU *et al.*, 2013) and thus there are no information about temporal trends in runoff. Only a few catchment-modeling

studies using limited river discharge measurements have been completed for this remote region (e.g., GAO *et al.*, 2011; LI, F. *et al.*, 2014). Using a simplified procedure, YIN *et al.* (2013) developed spatial patterns of the surface-water budget over the entire TP for the 1981 through 2010 period by estimating the difference between precipitation (P) and actual evapotranspiration (AET). P-AET showed increasing time-trends particularly in the interior regions of the TP (semi-arid zone) and decreasing trends in most of the semi-humid and humid regions (YIN *et al.*, 2013). In regions where precipitation decreased while evapotranspiration increased, the decreasing trend of P-AET is much stronger (e.g., in the humid zone in southeast). This spatial pattern of surface-water budget change is reflected by lake-level changes which will be discussed in the next section.

2.3 Lakes as Indicator for a Land-Surface Water Budget

2.3.1 Water Balance of Endorheic Lake Basins

Because an endorheic lake basin integrates all aspects of the hydrological cycle in a defined landscape unit, lake-level or volume changes provide an integrative (or cumulative) measure of the water balance. The annual water balance or lake-volume change, respectively, is simply the net difference between the water inputs and outputs (MASON, 1994). Neglecting the influence of long-term storage changes such as deep groundwater and lake-groundwater exchange, the net water balance of an endorheic lake basin with water supply from glaciers can be expressed as:

$$\Delta V_{lake} = P_{lake} - E_{lake} + R_{land} + R_{glacier} \qquad \text{[Eq. 2.1]}$$

where ΔV_{lake} is the lake-volume change (net annual lake water storage), P_{lake} the on-lake precipitation, E_{lake} the evaporation rate from the lake, and R_{land} and $R_{glacier}$ are the runoff from land surface and from glaciers (in units of volume per unit time).

Under constant climatic conditions, endorheic lakes will eventually tend towards a stable equilibrium ($\Delta V_{lake} = 0$), where the several water-balance terms such the net surface evaporation (E_{lake} - P_{lake}) and the total runoff are balanced (MASON, 1994). Lake-volume changes thus result from a shift in the water input or output. If the water gain is higher than the water loss, the lake area will increase over time. For an endorheic lake, where the lake evaporation is higher than the precipitation over the lake, the net surface evaporation rate will increase, which in turn will reduce the lake-volume change over time (MASON, 1994).

The time lag in the response of the area of an endorheic lake to climate fluctuations or, in other words, the time required to reach an steady state depends upon the climate over each lake and associated catchment area and the geomorphological characteristics of the lake. The more arid the climate conditions and the higher the rate of change of a given lake's area with volume, the faster is the lake response time to compensate for a given increment in net inflow (MASON, 1994).

2.3.2 Lake Variation over the Tibetan Plateau

According to ZHANG, G. *et al.* (2013b), the TP contains a total of 4.345 lakes, three are larger than 1000 km². The majority of Tibetan lakes are located in sparsely populated areas in the central part of the TP at elevations exceeding 4500 m a.s.l.. Because of the remote location of these lakes and the harsh environmental conditions, it is not feasible to perform continuous in-situ measurements for most Tibetan lakes (SONG *et al.*, 2013). GLAS/ICESat laser altimeter data provide reasonable estimates of water-surface elevation changes for the period 2003 to 2009, with centimeter-level accuracy (KROPACEK *et al.*, 2012; PHAN *et al.*, 2012a; 2012b; SONG *et al.*, 2013; 2014a; 2014c; WANG *et al.*, 2013; ZHANG, G. *et al.*, 2011; ZHANG, B. *et al.* 2013; ZHANG, G. *et al.*, 2013b). The number of Tibetan lakes with available ICESat data for 4-7 years is limited to 200, from which 118 are located in the interior TP (see Figure 2.2) (ZHANG, G. *et al.*, 2013b).
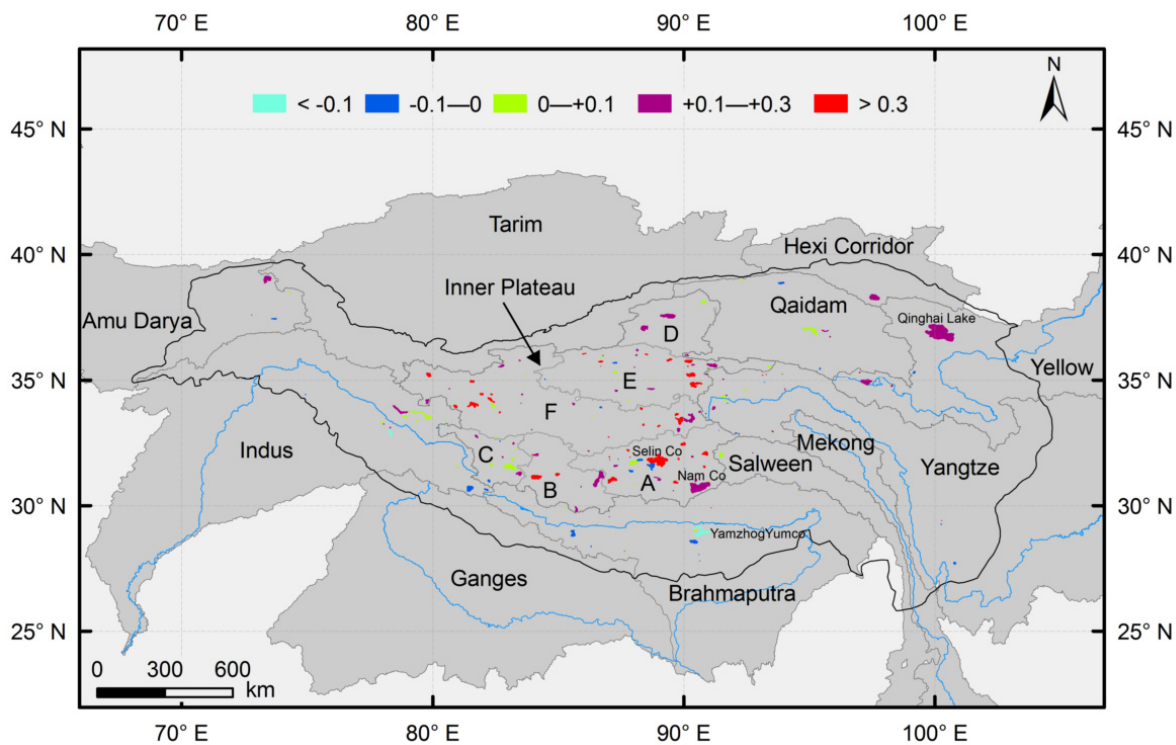
Figure 2.2: Rate of lake-level changes (m yr⁻¹) from 2000 to 2009 and the nine great lake sub-basins over the TP, with the Inner Plateau basin consisting of sub-basins A, B, C, D, E, F (ZHANG, G. et al., 2013b).

Based upon differences between ICESat elevations and *Shuttle Radar Topographical Mission* (*SRTM*) *Digital Elevation Model* (*DEM*), ZHANG, G. *et al.* (2013b) estimated mean annual lake-level changes from 2000 to 2009 for these 200 lakes (Figure 2.2). The interior TP with the highest density of lakes indicated a mean water-level increase of +0.20 m yr⁻¹. In contrast, most of the lakes along the southern periphery of the TP exhibited slight inter-annual water fluctuations or even a lake-level decline. A decrease in lake levels on the southern TP and along the Himalaya mountain ranges and the reverse (increasing lake levels) for most of the observed lakes of the rest of the TP were also reported in other studies analyzing ICESat data (e.g., PHAN *et al.*, 2012a; 2012b; SONG *et al.*, 2013).

Due to the short time span of water-level data derived from satellite altimetry, Li, Y. *et al.* (2014) analyzed lake-extent changes between 1972 and 2010 using Landsat MSS and TM/ETM+ images. During this period, lakes in the central TP experienced a continuous expansion (<10 % in lake-extent change) before 2000, but they expanded rapidly after 2000 (20-40 %). Lakes in the southern and western TP indicated a continuous shrinkage or were relatively stable since 1970s.

Based upon the statistical relationship between a given lake's surface area and water level from 2003 to 2009, SONG *et al.* (2013) estimated lake volumes from the 1970s through 2011 for a number of Tibetan lakes. During the last four decades, the total lake-water volume increased by 92.43 km³ (SONG *et al.*, 2013). The comparison of the empirically modeled lake-volume changes between 2003 and 2010 with mass changes in water storage over the TP derived from *Gravity Recovery and Climate Experiment* (*GRACE*) data (TAPLEY *et al.*, 2004) indicated a good agreement in the mean annual rising rate of lake-water storage and provided a similar spatial pattern of water-mass changes, with significantly positive water-mass balance in the north and the interior Plateau and mass loss in south-eastern Tibet (SONG *et al.*, 2013).

As shown by ICESat data, there are contrasting patterns of seasonal lake-level variations throughout the TP (PHAN *et al.,* 2012b; SONG, *et al.*, 2014b). Lakes in the south of Tibet with nearly stable or decreasing lake levels indicate larger water-level declines in the cold-dry seasons compared to the water-level rises in the warm-wet seasons. In contrast, lakes in the interior regions of the TP with primarily increasing lake levels exhibit a relatively large lake-level increase during the rainy season and nearly changeless or slightly decreasing lake levels in the dry season. In the west and north of the TP, the inner-annual lake dynamics are different compared to the other parts of the TP. Most of the lakes decrease little during the summer season and increase slightly or indicate no lake-level change during the winter season; however, small lake level increases occur on an annual basis (PHAN *et al.*, 2012b).

2.3.3   Potential Driving Factors of Lake Changes across the Tibetan Plateau

Although lake changes in the TP region have been widely investigated based on remote sensing data, there is an ongoing scientific debate concerning the hydro-climatic controls on lake-level fluctuations. Due to the accelerated glacier mass loss, it has been hypothesized that the lake growth, particularly in the central part of the TP, is mainly induced by an increased inflow of glacier-melt runoff (WANG *et al.*, 2013; WU & ZHU, 2008; YAO *et al.,* 2007; ZHANG, G. *et al.*, 2011; ZHU *et al.*, 2010). Nevertheless, as pointed out by ZHANG, G. *et al.* (2013b), glacier melting into lakes itself should not increase the overall mass on the TP, as indicated by GRACE satellite gravimetry data. Furthermore, numerous lakes of the TP are not linked to glaciers (Li, Y. *et al.*, 2014; PHAN *et al.*, 2013) and the rates of change of lakes without glacier-meltwater supply in the 2000s were as high as those of glacier-fed lakes (SONG *et al.*, 2014c).

In other studies, increased precipitation and decreased evaporation were generally considered to be the principal factors causing the rapid lake-level increases (LEI *et al.*, 2013; LIU *et al.*, 2009; MENG *et al.*, 2012; MORRILL, 2004; SONG *et al.*, 2014c; WU & ZHU, 2008; ZHANG, Y. *et al.*, 2011). SONG *et al.* (2014c) examined the spatial and temporal patterns of water-level changes of 105 Tibetan lakes in relation to climate variations over the last decade. Based on the analysis of a few available meteorological station records and gridded precipitation data from the *Global Precipitation Climatology Project* (*GPCP*), this study found a broad consistency between lake variations in the

2000s and precipitation changes across the TP. Because potential evapotranspiration has tended to increase during the last decade, it is very unlikely that the rapid lake expansion on the central TP after 2000 is caused by changes in potential evapotranspiration (LI, Y. *et al.*, 2014).

In some studies permafrost degradation has also been proposed as a potential factor for lake changes in the TP region (LI, Y. *et al.*, 2014; LIU *et al.*, 2009; 2010). In particular, the study of LI, Y. *et al.* (2014) emphasizes the potentially important contribution of permafrost melt to lake-level changes. They suggest that spatial variations in lake-level changes might be related to different distributions and types of permafrost.

2.4   Current State of Hydrological Modeling

2.4.1   Challenges and Limitations in Hydrological Modeling

In order to improve the understanding of hydrological system dynamics and changes, hydrologists benefit from the application of hydrological models. A hydrological model is by definition a simplified conceptual representation of the real system it attempts to describe (WAGENER & KOLLAT, 2007). The representation of a specific hydrological system is always simplified, as a model never incorporates every aspect of the represented system. The degree of simplification depends on a series of decisions. Due to insufficient scientific understanding of hydrological system dynamics associated with gaps in the knowledge of the system properties and boundary conditions, important modeling decisions may be far more ambiguous (CLARK *et al.*, 2011). CLARK *et al.* (2011) pointed out *"[...] there is currently little agreement regarding what a 'correct' model structure is, especially at relatively larger spatial scales such as catchments and beyond".*

Hydrological models can be grouped into stochastic and deterministic models. Stochastic models are based on probabilistic laws and stochastic elements, with known or estimated distributions. Most hydrological models, however, are based on mathematical relations (deterministic models). In the last decades, a plethora of deterministic model approaches varying in complexity of the model structure (empirical – 'black-box', conceptual – 'grey box' or more physically-based – 'white box') and the degree of spatial discretization (lumped, semi-distributed or distributed) has occurred (see e.g., DANIEL *et al.*, 2011; KAMPF & BURGES, 2007; REFSGAARD, 1997).

Distributed approaches such as the *Hydrological Response Unit (HRU)* approach (FLÜGEL, 1995; LEAVESLEY *et al.*, 1983) account for spatial heterogeneity in the catchment. This is an advantage over lumped approaches which treat a catchment as one homogenous unit. According to FLÜGEL (1995) HRUs are understood as *"[...] distributed, heterogeneously structured entities having a common climate, land use, and underlying pedo-topo-geological associations controlling their hydrological dynamics".* The variation of processes controlling the hydrological dynamics within a HRU class is assumed to be relatively small in comparison with the dominant processes in a different HRU class (FLÜGEL, 1995). Distributed models are mainly used for process-based approaches. A high spatial discretization of model entities allows a more physically-based process description. In contrast, the coarser the spatial scale, the simpler the model structure should be (BEVEN, 2001). MIKE-SHE (JAYATILAKA *et al.*, 1998), WaSIM-ETH (SCHULLA, 2013), J2000 (KRAUSE, 2002), and PRMS/MMS (LEAVESLEY *et al.*, 1983) are some examples of complex (distributed, physically-based) hydrological models.

The choice of an appropriate spatial discretization depends on fundamental inter-related, sometimes opposing considerations (DEHOTIN & BRAUD, 2008):

i)   What is the modeling objective?

ii)   Which data are available and at which spatial and temporal resolution?

iii)   Which output variables are required and at which spatial and temporal resolution?

iv)   What are the dominant hydrological processes within the catchment scale and what are their functional scales?

v)   Which representation of hydrological processes is relevant and at which temporal and spatial scale?

vi)   Which degree of heterogeneity is acceptable within modeling units?

The challenge for a hydrological modeler in ungauged or poorly gauged regions such as the TP is to balance the desire to adequately represent hydrological processes with the need to simplify models for regions with limited data availability (WAGENER & KOLLAT, 2007; WAGENER *et al.*, 2001). As demonstrated in Figure 2.3, a degree-of-complexity trade-off is needed, in order to achieve a balance between model performance supported by the available data and uncertainty assumed acceptable to achieve the modeling purpose or the accuracy desired (WAGENER & KOLLAT, 2007; WAGENER *et al.*, 2001).
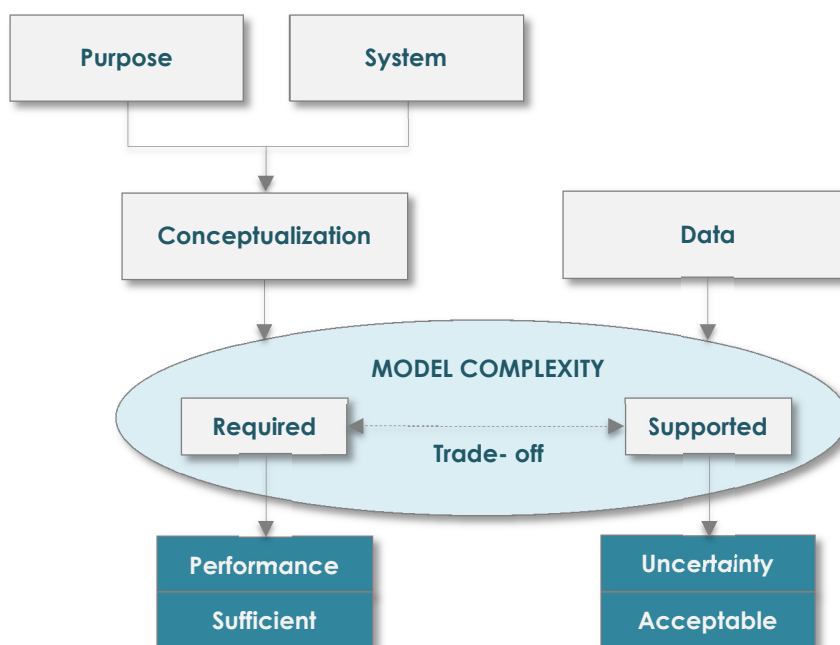
Figure 2.3: Model complexity evaluation (WAGENER & KOLLAT, 2007).

To account for the lack of understanding of hydrological processes, it should be engaged in more complex model building; the practical applicability of these models however is limited (BLÖSCHL, 2006). Complex (distributed, physically-based) models focusing on better representation of underlying physical processes may become a paradox, because excessive model complexity increases the problems of model-parameter identifiability (VACHÉ & MCDONNELL, 2006). The more complex the model, the more data needed and experience in model-parameter estimation. This leads to an 'interesting' question from *Keith Beven*, one of most highly cited hydrologists: *"How far can we go in distributed hydrological modelling?"* (BEVEN, 2001). Analyzing this question BEVEN (2001) has revealed a number of limitations on the realism of process representation and discussed in relation to resulting issues of nonlinearity, scale, uniqueness, equifinality and uncertainty. A brief description of these limitations modelers have to deal with is given below.

Although the nonlinear character of hydrologic systems has been known for a long time, much of early hydrologic research (1960s-1980s) was restricted on 'linear' assumptions, i.e. the relation between cause (e.g., input) and effect (e.g., output) is linear or proportional (SIVAKUMAR & SINGH, 2012). Despite the fact that linear transfer functions have been prevalent in hydrology, recently, computational advances have been developed during the last decades to account for nonlinearity in the formulation and application of distributed models. Indeed, the effects of nonlinearity can lead to high sensitivity to initial and boundary conditions, which are not well known in hydrology (ZEHE & BLÖSCHL, 2004), and potentially to chaotic behavior (SIVAKUMAR, 2000; SIVAKUMAR & SINGH, 2012).

A further problem related to nonlinearity is the inherent linkage to scale issues such as upscaling/downscaling of nonlinear process descriptions. The scale dependence of process descriptions is a well-known and often discussed problem in the literature (e.g., BLÖSCHL, 2001; BLÖSCHL & SIVAPALAN, 1995; SIVAPALAN & KALMA, 1995). There have been difficulties to apply nonlinear descriptions based on small-scale physics or theories to larger scales (e.g., catchment scale). Because each field study is unique in both space and time, it reflects only local conditions at the particular time of measurement and cannot represent the spatial heterogeneity in landscape properties and nonlinearity of hydrological processes or process interactions at all scales (BEVEN, 2001). The difficulty of uniqueness of place also becomes apparent by applying hydrological models in particular catchments which are unique in terms of land-surface conditions, topography, soils, hydrogeology, vegetation, land cover, and space-time variability of climatic inputs. Because of the inability to observe processes over a broad range of scales and at the same time, there is limited information on the multi-scale heterogeneity encountered in hydrology (SIVAPALAN, 2003).

Due to the uniqueness of catchments and the space-time limitations of measurements in representing the multi-scale landscape and process heterogeneity, model parameters have to be estimated by calibration which is typically conducted by minimizing the residuals between the simulated and the observed system response (usually the streamflow hydrograph) (GUPTA *et al.*, 2006). This optimization can be carried out manually or automatically with numerical methods. Also semi-automatic approaches were proposed which combine manual with automatic methods (GUPTA *et al.*, 2006).

Because most distributed modeling studies are based on the comparison of observed discharge at the watershed outlet and predicted runoff alone, the effects of local heterogeneity on the system behavior and the interaction of different hydrological processes might not be well reflected in the model. Mathematically optimal parameterizations may be considerably different from hydrologically plausible solutions, which are a more realistic representation of the processes within the catchment (e.g., ANDRÉASSIAN *et al.*, 2012; HRACHOWITZ *et al.*, 2013; SEIBERT & MCDONNELL, 2002).

Due to the fact that parameters are commonly adjusted or optimized against data observed at a particular location (and even at a certain time-period) under specific (unique) system conditions, there is no guarantee that they are valid under any other circumstances and they may well be unreliable to be used when the system is driven beyond the range of previously observed variability (BEVEN, 2001; KIRCHNER, 2006; WAGENER, 2007). As a consequence, extrapolation of local knowledge and understanding of underlying process controls gained from gauged catchments to other time scales or other places has caused tremendous difficulties, because models are often tailor-made to analyze the system behavior at particular places at a defined time scale (SCHAEFLI *et al.*, 2011).

Hydrological models focusing on locally acceptable solutions, rather than transferable hydrological understanding are usually over-parameterized (BLÖSCHL *et al.*, 2013). Over-parameterization means that many different model structures and parameter-set combinations may yield equally acceptable or behavioral representation of the (often limited) calibration data, which is referred to as the equifinality problem (e.g., BEVEN, 2001; BEVEN & FREER, 2001). Thus, it is likely that a large number of parameters will increase the degree of model uncertainty, resulting from a lack of parameter identifiability (BEVEN, 2001). Beside model-parameter uncertainty, errors in climate inputs and model-structure inadequacies, which reflects the inability of a model to describe precisely the systems behavior, are major sources of uncertainty arising from the modeling process (Figure 2.4).
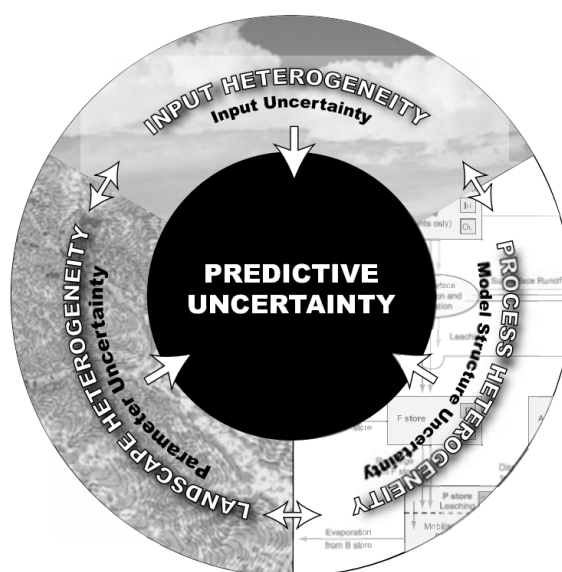
Figure 2.4: Predictive uncertainty and links with climatic and landscape heterogeneity (SIVAPALAN et al., 2003).

2.4.2 Paradigm Shift in Hydrology

Driven by the increasing speed of environmental change and the complexity in the manner that basins respond to these changes, it has been widely recognized that traditional model-calibration exercises targeted at finding the parameter set which matches best the runoff observations are often inadequate (or deceptive) for predictions, even more so in ungauged basins or poorly gauged basins. Due to the limitations of the classical approach of rainfall-runoff 'curve-fitting' in regions where measurements are too short, of too poor quality or even inexistent, there have been numerous calls by the scientific community in recent times for a new unified theory of hydrology, in order to bring about profound changes in conducting hydrological science. One also speaks of a paradigm shift in hydrology from one that has a strong reliance on calibration to a new exciting one that seeks to yield deeper insights and new transferable generalizations of hydrological functioning at multiple space-time scales (BLÖSCHL & MONTANARI, 2010; BLÖSCHL *et al.*, 2013; EHRET *et al.*, 2014; MCDONNELL *et al.*, 2007; SCHULZ *et al.*, 2006; SIVAPALAN, 2003; TROCH *et al.*, 2009; WAGENER *et al.*, 2004; 2010).

WAGENER *et al.* (2010) suggest that *"[...] hydrologists must become both synthesists, observing and analyzing the system as a holistic entity, and analysts, understanding the functioning of individual system components [...]"*. Research efforts to go beyond model calibration and to move toward a more comprehensive hydrologic understanding have been reported under the umbrella of the decadal research initiative '*Predictions in Ungauged Basins (PUB)*' (SIVAPALAN *et al.*, 2003), which was launched in 2003 by the *International Association of Hydrological Sciences (IAHS)*. According to SIVAPALAN *et al.* (2003) *"An ungauged basin is one with inadequate records (in terms of both data quantity and quality) of hydrological observations to enable computation of hydrological variables of interest (both water quantity and quality) at the appropriate spatial and temporal scales, and to the accuracy acceptable for practical applications"*. The PUB initiative engaged the scientific community to advance current methods of prediction (Target 1), to develop new innovative approaches (Target 2), and to link these two strategies (Figure 2.5).
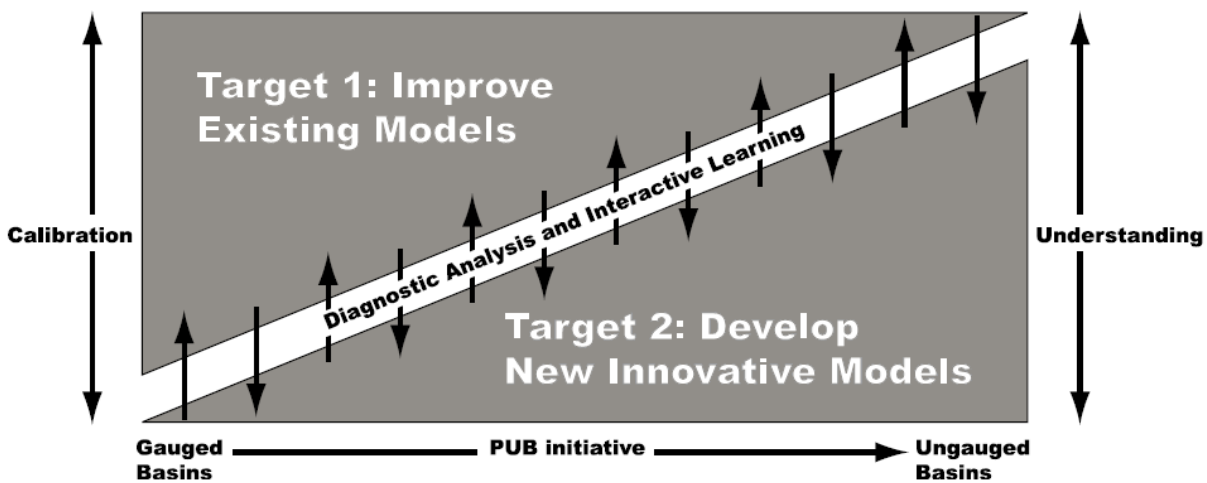
Figure 2.5: Targeted research -towards paradigm change- from model calibration to models based on increased understanding (SIVAPALAN et al., 2003).

Beside the fact that small-scale process studies and laboratory studies are crucial to improve the understanding as well as to conceive new hypotheses from controlled experiments (KLEINHANS *et al.*, 2010), larger scale studies are needed to achieve a greater coherence in the understanding of hydrological response patterns in different places and across a range of time scales (GUPTA *et al.*, 2014). Particular attention must be paid to seeking descriptions and explanations for spatio-temporal hydrological patterns and their controlling factors, in order to gain knowledge of how the system behavior is varying or changing across time and space scales (e.g., BLÖSCHL, 2006; BLÖSCHL *et al.*, 2013; SCHULZ *et al.*, 2006; SIVAPALAN, 2006).

In recent years there was a growing preference for model simplification by using a minimal number of free parameters (e.g., KIRCHNER, 2006). However, even a simplified model structure cannot prevent the risk of model over-parameterization (UHLENBROOK *et al.*, 1999). In view of this, much research has been directed toward a more robust model parameterization (see review of ANDRÉASSIAN *et al.*, 2012; GUPTA *et al.*, 2006). Many authors advocated to maximize the profit from any available hydrological information within the basin during the calibration instead to use only conventional calibration data from the catchment outlet (i.e. stream flow measurements) (e.g., ATKINSON *et al.*, 2002; CLARK *et al.*, 2011; MONTANARI & TOTH, 2007; SCHAEFLI & ZEHE, 2009; SEIBERT, 2000; SEIBERT & BEVEN, 2009; SEIBERT & MCDONNELL, 2002; WAGENER *et al.*, 2003; WINSEMIUS *et al.*, 2008; 2009). Several researchers (e.g., DEUS *et al.*, 2013; SUN *et al.*, 2015) have used satellite-derived information for hydrological model calibration.

Improved parameter-estimation procedures such as multi-objective strategies have been suggested in a variety of studies (e.g., EFSTRATIADIS & KOUTSOYIANNIS, 2010; GUPTA *et al.*, 1998; KUCZERA & MROCZKOWSKI, 1998; KUCZERA *et al.*, 2006; POKHREL *et al.*, 2012; SEIBERT, 2000; VRUGT *et al.*, 2003). Multi-objective approaches comprise parameter fitting on multiple responses or on various aspects of a single response. A comprehensive review of multi-objective approaches is given in EFSTRATIADIS & KOUTSOYIANNIS (2010). Rejecting the idea of finding an optimal model, ensemble approaches have been proposed to identify equally acceptable (behavioral) models in terms of predefined objective functions (e.g., BEVEN & FREER, 2001; MCINTYRE *et al.*, 2005). In spite of much research efforts to avoid over-parameterization (e.g., multi-objective trade-offs, ensemble modeling) research is still needed to identify hydrologically optimal parameter sets (ANDRÉASSIAN *et al.*, 2012).

In the last decades, it became increasingly apparent that model applications have inherent uncertainty that also is for the most part unavoidable (e.g., MCINTYRE *et al.*, 2005; MONTANARI & KOUTSOYIANNIS, 2012). Hydrological modeling studies in data-scarce regions are generally fraught with uncertainty most related to the fact that reliable input data are not available and process dynamics are often unknown and/or unobservable. BLÖSCHL *et al.* (2013) stated *"If one calibrates parameters to compensate for the real uncertainty this is likely a 'quick fix' which may jeopardize the realism of the model"*. As a much better strategy BLÖSCHL *et al.* (2013) suggest *"[...] to allow for the uncertainty in an explicit way rather than to seek a best fit of the model to the one realization of hydrologic response available"*. To reveal the critical uncertainties on which the future research work should focus, judicious assessment of the reliability of prediction is required by incorporating uncertainty estimation in process-based modeling (MONTANARI & KOUTSOYIANNIS, 2012). In this context, uncertainty analysis has become a research topic gaining increasing attention in the hydrologic scientific community.

MONTANARI (2007) provides an overview of the issues and challenges related to uncertainty assessment. Despite numerous contributions in the recent scientific literature, there is still an active debate on which approach, either probabilistic or non-probabilistic, is most appropriate, given the needs of the purpose of the model application (e.g., CLARK *et al.*, 2011; MONTANARI *et al.*, 2009). In the presence of sufficient information, MONTANARI *et al.* (2009) suggest a probabilistic statistical approach to summarize efficiently the information content of data. Conversely, in the occurrence of limited data, a formal statistical approach would not be reliable and a non-probabilistic approach is required. Given that the latter method often integrates 'soft' information, these approaches are unavoidably subjective (MONTANARI *et al.*, 2009). Soft data are *"[...] qualitative knowledge from the experimentalist that cannot be used directly as exact numbers but that can be made useful through fuzzy measures of model simulation and parameter value acceptability"* (SEIBERT & MCDONNELL, 2002).

3 STUDY AREA

This chapter provides an overview of the various Tibetan Plateau (TP) lake basins investigated in this study (Section 3.1), and describes the climatic conditions (Section 3.2) and physio-geographic characteristics (Section 3.3) of the study region.

3.1 Geographic Location and Basic Basin Information

This study comprises four endorheic lake basins in the south-central part of the TP (between 28°N~32°N and 81°E~92°E) (Figure 3.1). Based on GLAS/ICESat data, the lake levels for Nam Co and Tangra Yumco rose by approximately 0.25 m yr^{-1} between 2003 and 2009; whereas, the lake levels for the Paiku Co and Mapam Yumco slightly decreased by around -0.05 m yr^{-1} (PHAN et al., 2012a; ZHANG, G. et al., 2011). The lakes Mapam Yumco, Tangra Yumco and Nam Co are located along a west-east lake transect, whereas the lake Paiku Co is situated south of this transect (Figure 3.1). Basic characteristics (lake area, basin area, etc.) of the selected lake basins are summarized in Table 3.1.

The *Nam Co* (30°42'N, 90°33'E, 4725 m a.s.l.), the easternmost lake of the transect, is the second largest lake on the TP and it is located in a graben structure at the northern foot of the Nyainqêntanglha mountain range with elevations of over 7000 m a.s.l. (highest peak Nyainqêntanglha Feng with 7162 m a.s.l.).

The *Tangra Yumco* (31°00'N, 86°34'E, 4540 m a.s.l.) in the center of the lake transect is associated with a north-south trending graben system along the northern slope of the Transhimalaya (MIEHE et al., 2014). The Transhimalaya mountain range (~1600 km in length), extending in a west-east direction parallel to the main Himalayan range, is comprised of the Gangdise range to the west and the Nyainqêntanglha range to the east.

The *Mapam Yumco* (30°42'N, 81°28'E, 4585 m a.s.l.) in the west of the transect is located between the Gangdisê mountain range in the north with Mt. Kailash as the highest peak (6638 m a.s.l) and the western Himalayan Mountains in the south (highest peak Mt. Naimona′nyi with 7694 m a.s.l) (YE et al., 2008).

The *Paiku Co* (28°55'N, 85°35'E, 4580 m a.s.l.), which is also located in a tectonic depression, is controlled by both an east-west structure and a north-south structure. The Paiku Co is located along the northern flank of the central high Himalayas near the Mt. Qomolangma (Everest) (NIE et al., 2012).
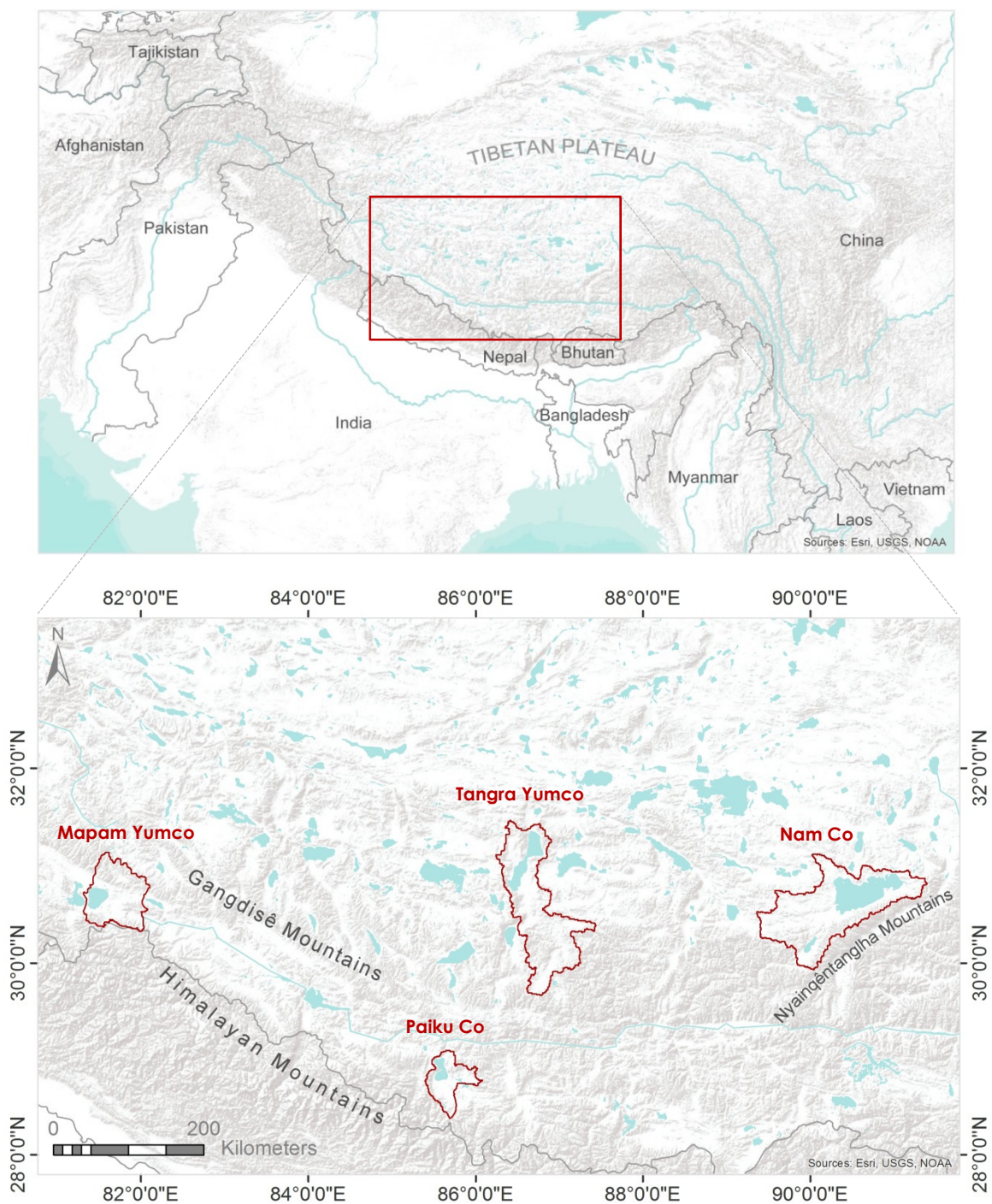
Figure 3.1: Location of the study region. Basins and mountain ranges noted in the text are indicated.

Table 3.1: Basic information of selected lake basins in the study region.

Lake name	Elevation (m a.s.l.)	Lake center		Lake area (km²)	Basin area (km²)	Water supply coefficient (ratio basin area/lake area)
		Lat	Long			
Nam Co	4725	30°42	90°33	1950	10760	5.5
Tangra Yumco	4540	31°00	86°34	830	9010	11
Paiku Co	4580	28°55	85°35	270	2380	8.8
Mapam Yumco	4585	30°42	81°28	420	4440	10.6

3.2 Climatic Conditions

The study region encompasses a semi-arid zone and is characterized by two distinct seasons: a temperate-wet summer season from June through September dominated by the Indian Monsoon and a cold-dry winter season determined by the Westerlies (LEBER *et al.*, 1995). The mean annual air temperature (MAAT) is between 0°C and -5°C (Figure 3.2), as indicated by the *High Asia Refined analysis* (*HAR*) data (MAUSSION, 2014; MAUSSION *et al.*, 2014; see Section 4.2 for data description). The study region features a climate gradient, with increasingly cooler and drier conditions in a westward direction.
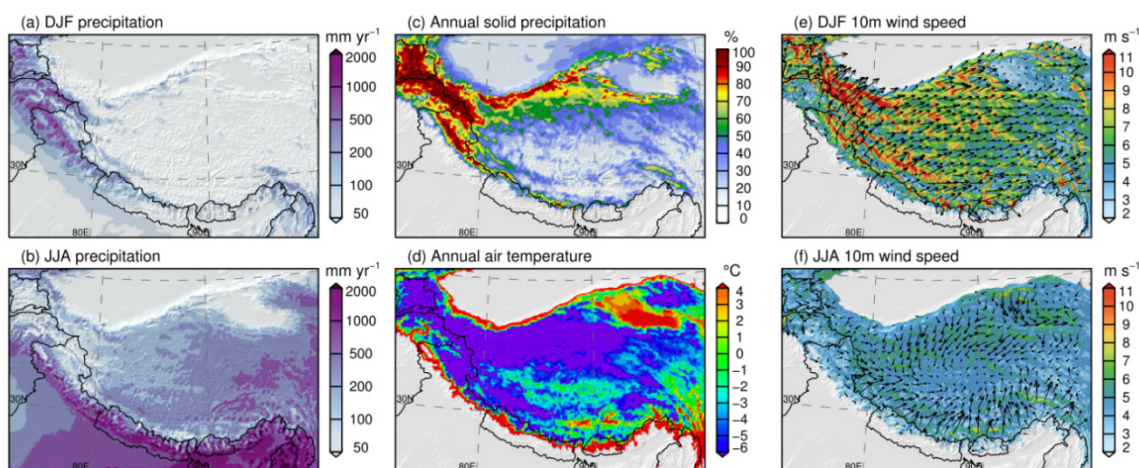
DJF…December-February; JJA…June-August

Figure 3.2: Average climate variables from HAR10. For (d), (e), (f) the altitudes below 2000 m a.s.l. are masked for clarity (Maussion, 2014).
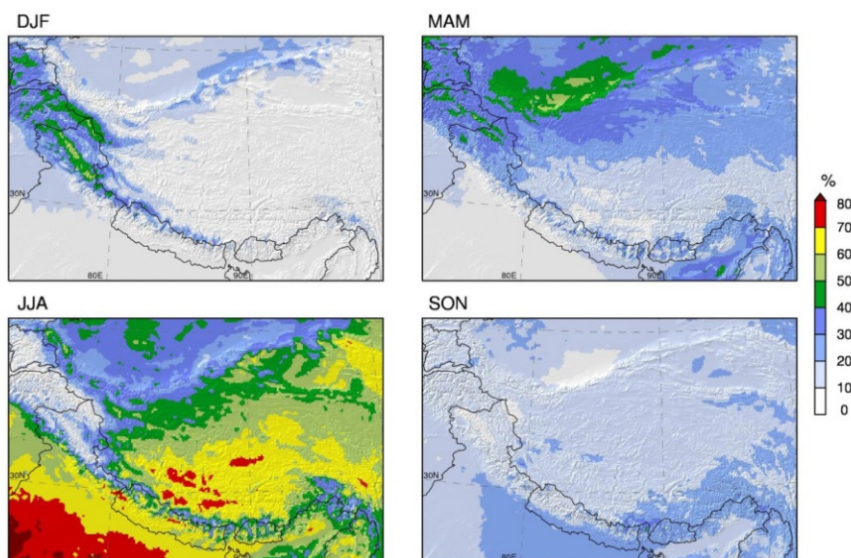
Figure 3.3: Contribution (%) of December-January (DJF, winter), March-May (MAM, spring), June-August (JJA, summer) and September-November (SON, fall) to the HAR10 mean annual precipitation (MAUSSION et al., 2014).

According to MAUSSION *et al.* (2014), the *mean annual precipitation* (*MAP*) ranges between 200 and 500 mm, with more than 60-80 % of this total occurring between June through August (Figure 3.3). Summer precipitation in the central TP is characterized by rather constant intensity due to frequent local convective activity (MAUSSION *et al.*, 2014). The snow season is from early October to late April (PU & XU, 2008). The dominant west-east wind direction, the constant zonal flow pattern, and the high velocities in winter all indicate the strong influence of the westerlies (Figure 3.2). During the summer season, however, the situation changes, as indicated by lower wind velocities and a cyclonic circulation (MAUSSION *et al.*, 2014).

3.3 Physio-Geographic Characteristics

The TP is composed of a series of continental fragments (terranes) which were accreted successively to the Eurasian plate during Paleozoic and Mesozoic eras (YIN & HARRISON, 2000). The lake basins in the study area are mainly located on the southernmost terrane, the Lhasa terrane, which is separated from the Qiangtang terrane in the north by the Bangong-Nujiang suture and from the Indian terrane in the southern part by the Yarlung Tsangpo suture zone. The Lhasa terrane is characterized by intrusive, metamorphic and sedimentary rocks partly covered by Quaternary deposits of glacial, fluvial, eolian and lacustrine origin (YIN & HARRISON, 2000).

Owing to the uplift of the TP, the lakes in the study region are situated in quite high elevations (above 4500 m a.s.l.). Valley floors and flood-plains with shallow slopes (< 5°) occur along the rivers courses in the lower elevation range (< 5000 m a.s.l.). Hilly relief structures with moderate slopes (5°-15°) are widespread between 5000 and 5500 m a.s.l.. The headwater areas are characterized by steep inclinations (> 15°) and high elevations (> 5500 m a.s.l.). The spatial distributions of topographic features in the four study basins are illustrated in Figure A.1. - Figure A.4. Table A.1 summarizes the proportion of the area in various elevation, slope and aspect classes for all four basins.

Due to the semi-arid and cold climate conditions as well as the complex topography, soils in the study area in general are poorly developed. According to the *Soil and Terrain* (*SOTER*) data base (VAN ENGELEN & DIJKSHOORN, 2013) *Leptosol* is the dominant soil type in the study region (Figure A.1 - Figure A.4). Leptosol is either limited in depth by continuous hard bedrock within 25 cm of the soil's land surface or is extremely gravelly and/or stony, with less than 20 % (by volume) fine earth averaged over a depth of 75 cm (VAN ENGELEN & DIJKSHOORN, 2013). In flat areas and on shallow slopes, *Cambisol* is the typical soil developed in medium and fine deposits.

A characteristic feature of soils in the study area is the high enrichment of organic matter added from the thick, deep-root system of grasses. A high content of remains of living and dead roots increases the soil porosity, aeration and water movement. However, the decomposition of the biomass occurs slowly due to the cold and semi-arid climate conditions in the study region. Burrowing small mammals belonging to the Plateau Pika species (*Ochotona curzoniae*) are widespread in the TP region. Besides the plant-root system, they can loosen soil particles and promote penetration of air and water (bioturbation). Depending on the burrow density, Plateau Pika may positively affect the soil structure by increasing soil permeability, by accelerating infiltration of top soil water into deep soil and by increasing the silt fraction (GUO, Z. *et al.*, 2012).

Because of the low temperatures during the winter, the soil is seasonally frozen from November into May. The study region is characterized by sporadic permafrost (10 to 50 % of area underlain by permafrost) and isolated patch permafrost (< 10 % of area underlain by permafrost) (CHENG & JIN, 2013). According to TIAN *et al.* (2008), the lower altitude limit of permafrost in the Nam Co basin is 5300 m a.s.l.. This corresponds to an area of ~16 % of the total basin which might be underlain by permafrost. Figure A.1 - Figure A.4 indicate the permafrost distribution for the study basins, based on the model-derived *Global Permafrost Zonation Index Map* (GRUBER, 2012). The permafrost index with a value range of 0.01-1 indicates to what degree permafrost exist (GRUBER, 2012). Only 1.7 % (Nam Co) / 4 % (Tangra Yumco) / 15 % (Paiku Co) / 15 % (Mapam Yumco) of the total basin area indicate a permafrost index > 0.9. Thus, it is very likely that the relatively low elevation areas of the basins with less slope inclinations, denser vegetation cover and deeper soils compared to the steep inclined and high elevated regions are not affected by permafrost.

Influenced by cold climate and poorly developed soils, vegetation throughout the study area is generally sparse and composed of species adapted to the high-cold, alpine conditions. The growing period lasts approximately five months, from late April/early May to late September or mid-October, depending on the climate conditions for any given year (ZHANG, B. *et al.*, 2013). *Leaf Area Index* (*LAI*) measurements of an alpine grassland site indicate that the LAI increases rapidly from ~1 m² m⁻² in early June to 3 m² m⁻² by mid-June, reaches the maximum of ~4 m² m⁻² in mid-July and then decreases rapidly from ~3 m² m⁻² to 1 m² m⁻² in September (ZHU *et al.*, 2014). Vast areas of the basins (32-64 % of the total basin area, Table 3.2) are covered by alpine meadows and steppe grasses. According to the climate gradient, the vegetation cover decreases westward, and the dominant vegetation types gradually change from close alpine mats of different species of the genus *Kobresia* (*Cyperaceae*) (Figure 3.5a) in the more wet regions in the east to open short-grass steppes (*Alpine Steppe*) (Figure 3.5b) in the drier region in the west (Figure 3.4).
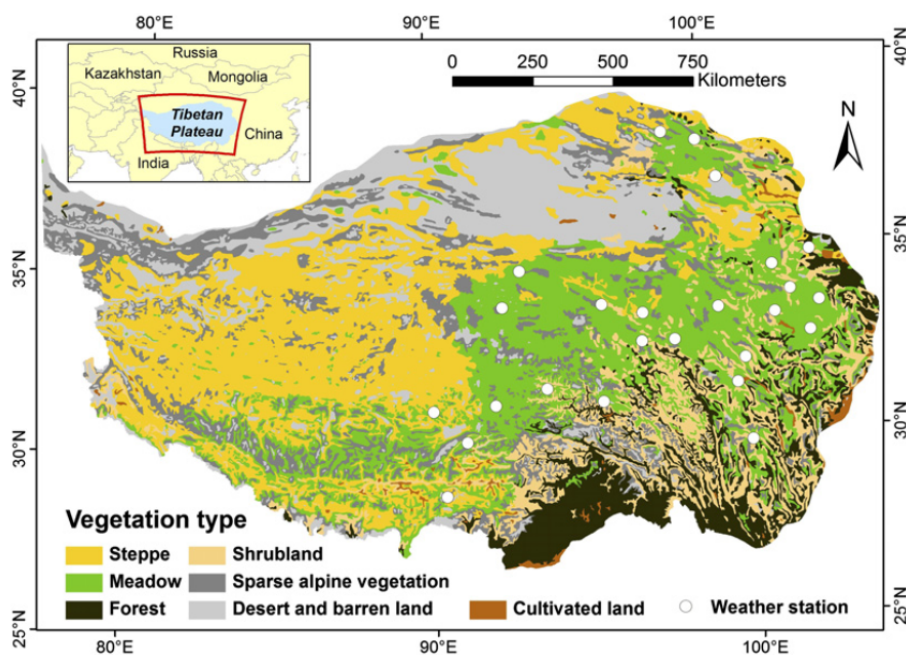
Figure 3.4: Vegetation types of the Tibetan Plateau according to the Atlas of the Tibetan Plateau (YU et al., 2010).

Kobresia pygmaea is the most widely distributed vegetation species type of alpine meadows. These tiny sedge species with only few centimeters in height occur in nearly all relief positions and cover different substrates and soil types. *Alpine Steppe* with average plant heights of around 15 cm dominates at dry sites, with prevailing substrates of sand and loess. Based upon field observations, the average rooting depth of the sedge mats and the steppe grasses is approximately 30 cm, with a very dense root system in the top 15 cm of soil. Vegetation communities in the study region have been studied in detail by several authors (e.g., CHANG, 1981; MIEHE *et al.* 2008; 2011; 2014).

The spatial extent of wetland areas within the basins (1-8 % of the total basin area, Table 3.2) is strongly controlled by topography, soil saturation, and water table. Wetlands occurring in the basins can be divided into two principal types: *i)* wetlands next to the lake shore and river estuaries (characterized by permanent water saturation), and *ii)* wetlands along foothills of surrounding mountains affected by fluctuating groundwater. The latter wetland type shows a well-developed hummock-and-hollow micro-topography, i.e. the topography is characterized by elevated mounds (hummocks) alternating with flatter hollows (Figure 3.5c). The size of the hummocks ranges in height from several centimeters to about one meter, and in diameter from several decimeters to meters. Some hollows are permanently filled with water, whereas others dry up during the summer season. Wetland sites located in groundwater-affected depression and foothills areas are dominated by *Kobresia schoenoides* swamps. The *Kobresia schoenoides* species may form tussocks 80 cm high (MIEHE *et al.*, 2011). In comparison to *Kobresia pygmaea*, the roots of *Kobresia schoenoides* plants that were observed in the field reach greater depths (~50 cm).

The barren land class represents 33 % of the total basin area (Table 3.2) and comprises *i)* flat areas surrounding the lake and along river beds which are covered by well-rounded pebbles, *ii)* bare soil areas (partial very sparsely vegetated), and *iii)* high-lying barren areas characterized by bare rock and rock debris (Figure 3.5d). The high mountains are covered by glaciers and permanent snow (Figure 3.5e). The equilibrium line altitude is about 5800 m a.s.l. (YAO *et al.*, 2012b). Among all basins, the Paiku Co catchment exhibits the largest glacier coverage (6.5 % of the total basin area). The area covered by glaciers in the other three basins accounts for 1-2 % of the total basin area.

Due to the harsh climate, the study region is characterized by a sparse human population. There are no bigger settlements; rather, several small villages are in the region. Nomadic herding is wide-spread in the Tibetan highland pastures (Figure 3.5f*)*. Eroded topsoil and desertification can be found in large areas in the TP region, indicating that much of the *Kobresia* pastures are severely overgrazed by livestock (yaks, goats and sheep) (MIEHE *et al.*, 2008; 2011).

Table 3.2: Area percentages of land-cover classes in the four study basins.

	Land cover (area proportion in %)				
	water	glacier	grassland	wetland	barren land
Nam Co	18	2	39	8	33
Tangra Yumco	9	1	32	1	57
Paiku Co	11	6.5	42	0.5	40
Mapam Yumco	10	1.5	64	2.5	22

a) Kobresia pygmaea mats

b) Alpine Steppe

c) Typical wetland site with hummocks alternating with water-filled and dried out hollows

d) Low mountains with barren lands
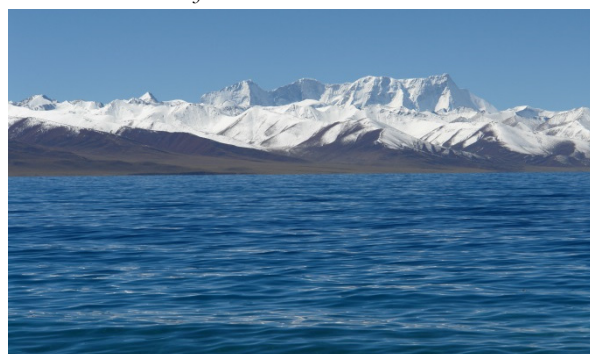
e) Lake Nam Co surrounded by snow covered high mountains (Nyainqêntanglha range)

f) Extensive grazing

Figure 3.5: Typical landscape features in the study region (Photographs: S. Biskop, 2009-2012).

4 DATA

Various environmental data, including hydro-meteorological and geospatial data varying in spatial and temporal resolution, were acquired from several institutions, provided by other databases (e.g., public sources), generated by data processing or collected in the field.

Available data sets were comprised of:

i) **In-situ observations** (Section 4.1)

ii) **Model-derived atmospheric data** (Section 4.2)

iii) **Remote-sensing and satellite-derived data** (Section 4.3)

4.1 In-Situ Observations

4.1.1 Hydro-Meteorological Measurements

The *Nam Co Monitoring and Research Station for Multisphere Interaction* (*Nam Co station*) (*http://www.namco.itpcas.ac.cn/*) was established in the summer of 2005 at the south-eastern shore of the Nam Co (90°59.31 E, 30°46.44 N, 4730 m a.s.l.) by the *Institute of Tibetan Plateau Research* (*ITP*), *Chinese Academy of Sciences* (*CAS*). Due to the strict rules of the CAS, only records from an automatic weather station from November of 2005 to July of 2008 and lake-level observations from 2006 to 2010 were provided for this study. Specifically, lake-level values during the freezing (wintertime) periods are missing, because the lake-level gauge was destroyed by lake ice, and therefore rendered inoperable each winter. Due to an unknown shift between the consecutive years, it was not possible to compare modeled year-to-year lake-level changes with in-situ measurements (only seasonal lake-level fluctuations).

Fully *automated weather stations* (*AWS*) with long-term measurements (over several decades) were only available outside the Nam Co basin (Figure 4.1, Table 4.1). Nevertheless, meteorological stations surrounding the Nam Co basin are sparsely distributed and are located at lower altitudes (< 4800 m a.s.l.), primarily south of the Nyainqêntanglha mountain range. Thus, they were only considered for regional estimates, but not as being representative for the Nam Co basin.
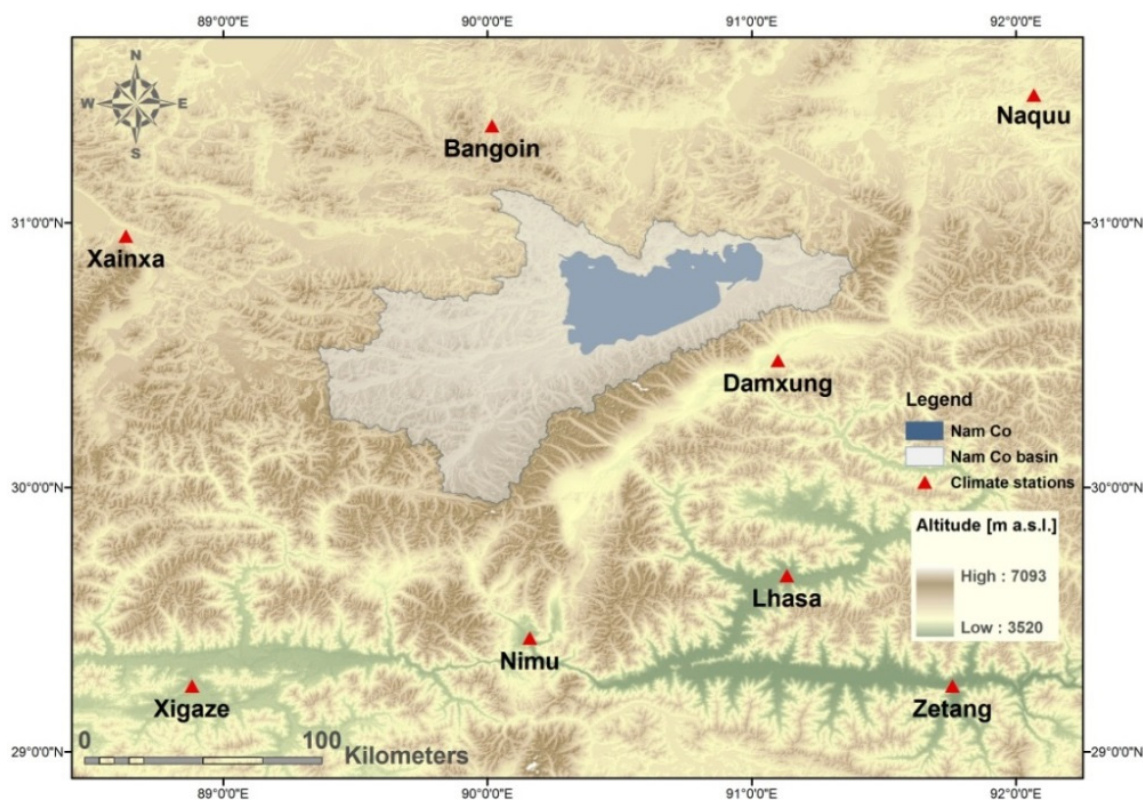
Figure 4.1: Location of meteorological stations with long-term measurements.

Table 4.1: Meteorological station list.

Meteorological Station	Longitude (E)	Latitude (N)	Altitude (m)	Institution*
Xainxa	88.63	30.95	4670	NOAA/NCDC
Bangoin	90.02	31.37	4701	NOAA/NCDC
Naquu	92.07	31.48	4508	NOAA/NCDC
Damxung	91.10	30.48	4200	ICIMOD
Zetang	91.76	29.25	3552	ICIMOD
Lhasa	91.13	29.67	3650	NOAA/NCDC
Nimu	90.16	29.43	3809	ICIMOD
Xigaze	88.88	29.25	3837	NOAA/NCDC

*NOAA/NCDC = National Oceanic and Atmospheric Administration/National Climatic Data Center
ICIMOD = International Centre for Integrated Mountain Development

4.1.2 Field Observations

During several sampling surveys between 2009 and 2012, which were conducted in close cooperation with German project partners as well as Chinese project partners at the ITP/CAS, empirical observation and information of Nam Co catchment characteristics have been compiled. For model development and application, various field data were available comprising soil-profile descriptions, soil temperature and moisture measurements, and vegetation and wetland characteristics.

4.2 Model-Derived Atmospheric Data

Because of limited data availability in the TP region (Figure 4.2), a new model-derived atmospheric dataset for the TP, the *High Asia Refined analysis* (*HAR*) (MAUSSION *et al.*, 2014), was used as hydrological-model input. The HAR data were generated by dynamical downscaling of large-scale meteorological data, using the *Weather Research and Forecasting* (*WRF*) model (SKAMAROCK & KLEMP, 2008). The advantage of dynamic downscaling, as opposed to statistical downscaling, is that this procedure relies upon physical relationships instead on statistical relationships. The latter may not be valid under changing boundary conditions or time scales (MAUSSION *et al.*, 2014).

The *Final Operational Model Global Tropospheric Analyses* at regular time intervals (6 hours), with a spatial resolution of 1.0° (generated by the *Global Forecast System* provided by the *National Centers for Environmental Prediction*), were used as inputs to the WRF model (SKAMAROCK & KLEMP, 2008). The HAR data were developed by consecutive model runs, reinitialized every day, using a procedure called the *Global Forecast System's final analysis*. Thus, the atmospheric model is constrained by the observed large-scale state of the atmosphere. Because the atmospheric modeling procedure represents a regional atmospheric reanalysis it differs from regional climate simulations (MAUSSION, 2014). The modeling strategy used to create the HAR is described more in detail in MAUSSION (2014).

The HAR data sets provide time series of various meteorological variables at a high spatiotemporal resolution for the time frame 2001 to 2011. The HAR data sets are freely available (*http://www.klima.tu-berlin.de/*) in different spatial (30 km x 30 km and 10 km x 10 km) and temporal resolutions (hourly, daily, monthly and annual). The HAR10 data were used in daily time step as meteorological input for the hydrological modeling.
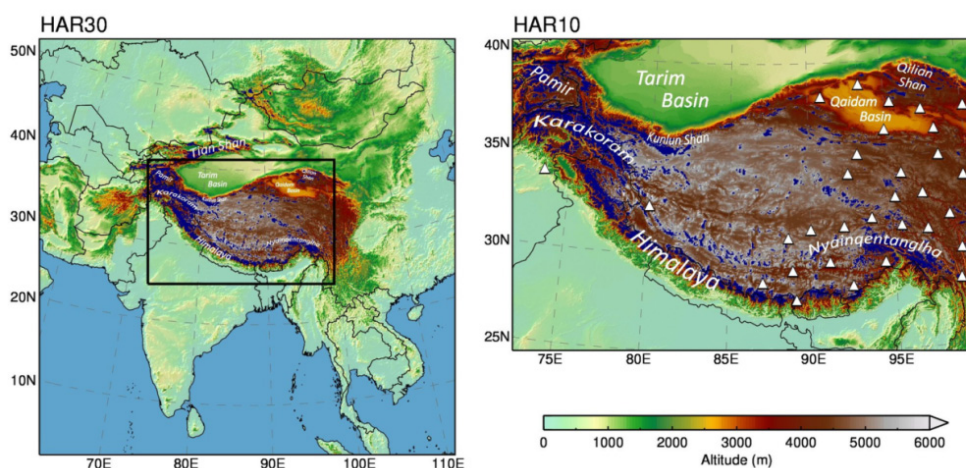
Figure 4.2: *Maps of the model domains HAR30 (South-Central Asia domain, 30 km x 30 km resolution, 200 x 200 grid points) and HAR10 (High Asia domain, 10 km x 10 km resolution, 270 x 180 grid points). Glacier outlines from the Randolph Glacier Inventory are drawn in blue, and the positions of the NCDC stations used for the validation are indicated by white triangles (MAUSSION, 2014).*

Table 4.2 summarizes meteorological variables of the HAR10 data which were used in this study.

Table 4.2: Meteorological variables of the HAR10 data used in this study.

Meteorological variable	Unit
Mean air-temperature	Kelvin
Maximum air-temperature	Kelvin
Minimum air-temperature	Kelvin
Precipitation	mm
Relative humidity	%
Wind u component (10 m)	m/s
Wind v component (10 m)	m/s
Solar radiation	W m^{-2}
Cloud cover	dimensionless (0-1)

Air temperature was converted from Kelvin into degree Celsius and solar radiation from W m^{-2} into MJ m^{-2}. Based on a right-angled triangle, the wind speed was estimated from longitudinal and latitudinal wind components (10-m altitude) by using a trigonometric function (HAZEWINKEL, 2001). The wind speed at 10-m altitude (v_{10}) was converted to wind velocity at 2-m altitude (v_2) using the following equation (DVWK, 1996):

$$v_2 = v_{10} \frac{4.2}{\ln(10) + 3.5} \quad [ms^{-1}] \qquad \text{[Eq. 4.1]}$$

In the WRF version 3.3.1, which was used for the generation of the HAR10 data, the lake-surface temperature is initialized by averaging the surrounding land-surface temperatures. MAUSSION (2014) analyzed the influence of the assimilation of satellite-derived lake-surface temperatures (ST) and found that the standard WRF method leads to a much cooler lake-surface temperature than observed (Figure 4.3). This, however, has a strong influence on local climate. Therefore, the HAR10 data points over water surfaces were not included for hydrologic modeling purposes. Instead, surrounding HAR10 data points were used as input data for any given lake.
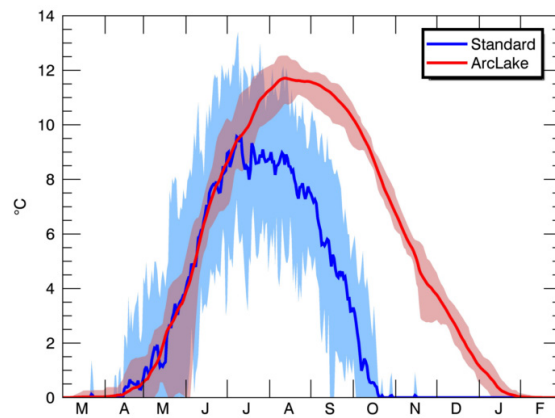
Figure 4.3: Decadal mean of the daily lake-surface temperature of the lake Nam Co, according to the WRF standard parametrization (blue) and to the ARC-Lake dataset (red). Shaded areas indicate the decadal minimum and maximum range (MAUSSION, 2014).

The HAR10 precipitation output was compared to rain-gauge data and to *Tropical Rainfall Measuring Mission (TRMM)* satellite precipitation estimates by MAUSSION *et al.* (2014). HAR10 accuracy in comparison to rain gauges was slightly less than TRMM. However, orographic precipitation patterns and snowfall were more realistically simulated by the WRF model. The comparison of HAR10 precipitation with observations from stations primarily located near population centers in lower elevations in the eastern part of the Plateau revealed a non-systematic error pattern (MAUSSION *et al.*, 2014). In particular, precipitation totals in the summer of years 2007-2010 indicate a positive bias (MAUSSION *et al.*, 2014). The reasons for these discrepancies for some years are unclear. The differences after 2007 may be associated with changes in the global data assimilation system (MAUSSION *et al.*, 2014). However, the uncertainty of HAR10 precipitation in complex terrain, where no measurements are available, is unknown.

The overall seasonality of air temperature observations is well reproduced by HAR10 temperature data (MAUSSION, 2014). Daily HAR10 temperature fits well to in-situ measurements on the Zhadang glacier in the Nam Co basin (r = 0.98, bias = -1.98) (MAUSSION, 2014). In general, HAR10 temperatures in the summer months are closer to ground observations than in winter (MAUSSION, 2014). The effect of the winter cold bias on the accuracy of the hydrological modeling results is assumed to be low, because hydrological processes governing lake-level changes (e.g., precipitation, snow and glacier melt, evapotranspiration) are more critical during the other three seasons of the year.

4.3 Remote-Sensing and Satellite-Derived Data

A variety of data sets comprising *i)* satellite-derived lake-level and water-volume data (Section 4.3.1), *ii)* lake-surface water temperature (Section 4.3.2), *iii)* MODIS surface temperature and snow product (Section 4.3.3), *iv)* topographic data (Section 4.3.4), and *iv)* land-cover information (Section 4.3.5) have been acquired. GIS layers required for HRU delineation as well as MODIS data extracted for several basins were projected into the UTM coordinate system (Zone 44N for Mapam Yumco, Zone 45N for Tangra Yumco and Paiku Co, Zone 46N for Nam Co) using the WGS-84 geodetic datum.

4.3.1 Satellite-Derived Lake Level and Water Volume

Due to the absence of continuous lake-level measurements, satellite-based lake-level and water-volume data were obtained for the four studied basins from the *HydroWeb* data base (*http://www.legos.obs-mip.fr/en/soa/hydrologie/hydroweb/*) provided by *LEGOS* (*Laboratoire d'Etudes en Geodesie et Oceanographie Spatiales from the Oceanographie, et Hydrologie Spatiales*) (CRÉTAUX *et al.*, 2011). LEGOS lake-level and water-volume data for the lakes included in this study were available for different time spans (see Table 4.3). The start and end date of each time series were taken from the same season (as far as available), in order to make lake levels or volumes comparable.

Water-volume data calculated through a combination of satellite images (e.g., MODIS, Landsat) and various altimetric height level data (e.g., Topex/Poseidon, Jason-1) (CRETAUX *et al.*, 2011) were used for model calibration. The mean annual lake-level changes derived from LEGOS data for the four basins are close to the change rates estimated by PHAN *et al.* (2012a) and ZHANG, G. *et al.* (2011) using GLAS/ICESat data (2003-2009) (see Table 6.16).

Table 4.3: Lake-level and water-volume changes derived from LEGOS data for the four studied lakes.

Lake name	Start date	Start volume (km³)	Start level (m)	End date	End volume (km³)	End level (m)	Δ Lake volume (km³ yr⁻¹)	Δ Lake level (m yr⁻¹)
Nam Co	27/09/2001	1.3	4722.683	01/10/2010	5.3	4724.697	0.44	0.22
Tangra Yumco	07/10/2001	0	4533.997	25/10/2009	1.7	4535.987	0.21	0.25
Paiku Co	02/06/2004	0	4578.067	04/03/2008	-0.08	4577.768	-0.02	-0.07
Mapam Yumco	30/10/2003	0.02	4585.551	21/11/2009	-0.1	4585.231	-0.01	-0.05

4.3.2 Lake-Surface Water Temperature

Lake-surface water temperature (*LSWT*) estimates from the ARC-Lake v2.0 data products (*http://www.geos.ed.ac.uk/arclake/*) (MACCALLUM & MERCHANT, 2012) were used as additional input for the hydrological modeling in the Nam Co and Tangra Yumco basins. ARC-Lake v2.0 data products contain daytime and nighttime LSWT observations from the series of (advanced) along-track scanning radiometers for the period 1991-2011. Comparison of satellite-derived LSWT with in-situ observations from several lakes reveals differences of 0.3 ± 0.9 K for daytime and -0.3 ± 0.8 K for nighttime observations (mean ± standard deviation) (MACCALLUM & MERCHANT, 2012) .

4.3.3 MODIS Data Products

The *Moderate Resolution Imaging Spectroradiometer* (*MODIS*) instrument aboard both the *National Aeronautics and Space Administration's* (*NASA's*) Terra (launched 1999) and Aqua (launched 2002) satellites provides data of the Earth surface and clouds in 36 spectral bands, ranging in wavelength from 0.4 to 14.4 μm (BARNES *et al.*, 1998). The Terra satellite passes from north to south over the equator at 10:30 AM, with a sun-synchronous, near-polar, circular orbit; whereas, the local equatorial crossing time of the Aqua satellite is approximately 1:30 PM in an ascending node. MODIS Terra and Aqua data have been available since 24 February 2000 and July 2002, respectively.

The globally-gridded MODIS data products are produced at four spatial resolutions (250 m, 500 m, 1 km, and 0.05°). Most of the higher-resolution MODIS data sets are gridded in adjacent non-overlapping tiles (10° x 10° (lat/lon)) in a sinusoidal map projection. For this study, the most recent version of following MODIS data products (so-called collection 5) were downloaded from the NASA's Reverb Earth Observing System Data and Information System platform (*http://reverb.echo.nasa.gov/*).

- MODIS/Terra Snow Cover 8-Day L3 Global 500m SIN Grid V005 (MOD10A2)
- MODIS/Aqua Snow Cover 8-Day L3 Global 500m SIN Grid V005 (MYD10A2)
- MODIS/Terra Land Surface Temperature 8-Day L3 Global 1km SIN Grid V005 (MOD11A2)

The MODIS snow-cover 8-day data of Terra (MOD10A2) and Aqua (MYD10A2) satellites at a spatial resolution of 500 m were used for model validation. The MODIS snow-detection algorithm is primarily based on the *Normalized Difference Snow Index* which is a normalized ratio of the difference in the reflectance of snow in band 4 (0.545 - 0.565 μm, visible green) and band 6 (1.628 - 1.652 μm, short wavelength near infrared). The snow-mapping procedure incorporates many threshold-based criteria tests and decision rules (HALL *et al.*, 2002). Details of the MODIS snow algorithm are described in the *Snow Product User Guide* (RIGGS *et al.*, 2006).

The 8-day MODIS snow-cover products at 500-m resolution are based on the daily snow-cover data (MOD10A1/MYD10A1). The 8-day MODIS snow-cover products were chosen for this study, because cloud cover problems are reduced (KROPACEK *et al.*, 2010). The snow-mapping algorithm classifies pixels as snow if snow cover is found for any day during a given 8-day period. In the case that no snow cover is detected, the pixel is labelled with the observed value. For the study area, the following classes with associated coded integer values of the *Maximum Snow Extent* attribute field were used: non-snow (25), inland water (37), cloud (50), lake ice (100), and snow (200).

The MODIS Land-Surface Temperature (LST) 8-day data at 1 km spatial resolution (MOD11A2) were used to derive time series of lake-surface temperature for the Paiku Co and Mapam Yumco where no ARC-Lake v2.0 data were available. This 8-day composite daytime and nighttime LST product is composed from the daily 1 km LST product (MOD11A1) and is the average value of clear-sky LSTs during an 8-day period. The LST was retrieved from MODIS thermal channels for all land-cover types including inland water bodies. A detailed description of the day/night LST algorithm is given by WAN (2009).

4.3.4 Topographic Data

Spatial information representing spatially varying topographic basin characteristics are important input data for distributed hydrological modeling due to their major impact on hydrological processes (MOORE *et al.*, 1991). *Digital Elevation Model's* (*DEM's*) are primarily used to analyze catchment topography. Homogeneous digital elevation data in a 3-arc second resolution (around 90 m) originally produced by NASA are freely available for over 80 % of the globe from the 11-day *Shuttle Radar Topographical Mission* (*SRTM*) in February 2000 (FARR *et al.*, 2007). The absolute height error of the DEM's is stated to be less than 16 m (90 % confidence level) (RODRÍGUEZ *et al.*, 2006).

The SRTM Version 4 data were retrieved from the *Consortium for Spatial Information* (*CGAIR-CSI*) *Geoportal* (*http://srtm.csi.cgiar.org*) and were used to derive catchment-related information like catchment boundary, river network, flow accumulation and flow direction, as well as terrain attributes such as slope angle and slope aspect. Moreover, a digital bathymetric model for the lake Nam Co with a grid resolution of 90 m x 90 m was generated in ArcGIS using the isobathic map which has been developed by WANG *et al.* (2009), based on lake-bathymetric survey data measured from 2005 through 2008.

4.3.5 Land-Cover Information

A land-cover map of the Nam Co basin for the year 2010 was provided by project partners (*University of Tübingen*) within the WET-project. This map was generated by land-cover classification using Landsat TM/ETM+ satellite imagery and several mapping campaigns. A hybrid classification approach was applied that combines a maximum likelihood classifier with a decision-tree approach. The decision rules were based on thresholds of multi-spectral bands and on terrain properties derived from the available digital elevation model (SRTM DEM). The land-cover classification consists of five classes used for this analysis: water, wetland, grassland, barren land and glacier.

The land-cover data for the Paiku Co and Mapam Yumco were obtained from the *Himalaya Regional Land Cover* data base, which is available at *http://www.fao.org/geonetwork/srv/en/main.home*. The Himalaya land-cover map at a 1:350.000 scale was produced as part of the *Global Land Cover Network Regional Harmonization Program* (*http://www.glcn.org/activities/himalaya_en.jsp*), an initiative to compile land-cover information for the Hindu Kush-Karakorum-Himalaya mountain range using a combination of visual and automatic interpretation of recent Landsat ETM+ data (acquired primarily during the period 2000-2005). A mapping accuracy assessment has not been performed. The land-cover legend of categories, comprising 35 classes, is based on the FAO's *Land Cover Classification System* (*LCCS*). The land-cover classes were reclassified into five classes according to the classification of the Nam Co basin. Classes with similar characteristics (e.g., vegetation type, degree of vegetation cover) were consolidated into a single class.

Because the Tangra Yumco basin is not completely covered by the Himalaya land-cover map, a land-cover classification (overall accuracy: 93 %) was produced for the entire basin using Landsat ETM+ data (VETTERMANN, 2014). The land-cover classification was conducted using the object-oriented image analysis software *ILMSImage* developed at the Department of Geography, Chair of Geoinformatics, Friedrich-Schiller University Jena. *ILMSImage* is based on a two-step concept combining unsupervised classification of cells (clustering) with supervised classification according to reference data. A detailed description of the two-stage classification procedure is given in VETTERMANN (2014).

5 METHODS

This chapter outlines the application of the following analytical methods for this study:

        i)   **Hydro-meteorological time-series analysis** (Section 5.1)

        ii)   **Geo-data processing** (Section 5.2)

        iii)   **Field surveys** (Section 5.3)

        iv)   **Hydrological modeling** (Section 5.4)

5.1 Hydro-Meteorological Time-Series Analysis

Analysis of long-term meteorological data from sites surrounding the Nam Co basin

Due to lacking long-term climate observations within the study basins, time series from eight stations located outside the Nam Co basin (see Figure 4.1) were analyzed statistically to assess spatial and temporal variations of climate conditions in the Nam Co region. Regarding quality control of the climatological data from the *Global Summary of the Day* provided by the *National Climatic Data Center* (*NCDC*) (Section 4.1.1), the raw data undergo extensive automated quality control before they are provided to the public.

To check the measured time series with respect to consistency and plausibility, daily time series were plotted as graph and visually examined. Because daily time series of air temperature (mean, maximum, minimum), precipitation, wind and relative humidity from the eight stations surrounding the Nam Co basin indicate data gaps of only few days between 1981 through 2010, this period was selected for the analysis of long-term meteorological data. For three stations (Damxung, Zetang, Nimu) there are data only available for mean temperature, precipitation and wind and only from 1981 through 2003.

Due to large distances from one station to the next (Figure 4.1), the calculated values of the coefficient of determination (r²) for nearby stations were lower than 0.7 for all climatic variables (daily data). Thus, linear interpolation within each time series was used to fill data gaps. Annual and monthly averages as well as seasonal means for the pre-monsoon (March-May), monsoon (June-September), post-monsoon (October-November) and winter season (December-February) were computed, in order to provide information on temporal dynamics.

The non-parametric rank-based *Mann-Kendall test* (*M-K test*) (MANN, 1945) was applied for climatic long-term trend detection. The M-K test has been widely used to detect trends in hydro-meteorological time series (e.g., BURN & HAG ELNUR, 2002; MAIDMENT, 1993; YIN *et al.*, 2013). The null hypothesis H_0 of no trend, i.e. the assumptions that observations x_i are

randomly ordered in time, is tested against the alternative hypothesis, H_1, that there is an increasing or decreasing monotonic trend. By applying the M-K test, each data value of a time series is compared with all subsequent data values. The M-K test statistic S is estimated as the summation of signs (*sgn*) using the formula:

$$S = \sum_{j=1}^{n-1} \sum_{k=j+1}^{n} \text{sgn}\left(x_j - x_k\right)$$

[Eq. 6.1]

where x_j and x_k are the annual or seasonal values in years *j* and *k*, *j>k* respectively.

In this study, three different significance levels ($\alpha = 0.05$ (*); $\alpha = 0.01$ (**) and $\alpha = 0.001$ (***)) were used to test trends in temperature, precipitation and wind.

The non-parametric *Sen's Slope Estimates* (SEN, 1968) was used to estimate the slope Q (change per unit time). The slopes of all data pairs are calculated as follows:

$$Q_i = \frac{x_j - x_k}{j - k} \, i = 1,2, ... \, N, j > k$$

[Eq. 6.2]

Sen's estimator of slope is the median of the N values of Q_i. A positive value of the *Sen's Slope* means that an upward trend exists and a negative value indicates a downward trend (LIN *et al.*, 2008).

Analysis of lake-level measurements of the lake Nam Co

As mentioned in Section 4.1, lake-level measurements of the Nam Co contain an unknown shift between the consecutive years and are only available for the ice-free period (May/June – November/December). Because the lake-level measurements provided a consistent time series between the months of June through November for the years 2006-2010, this period was chosen to analyze seasonal lake-level fluctuations. To be able to compare seasonal lake-level changes of all years, the lake-level value of the 1st of June was set to zero in each year and all subsequent values were adjusted accordingly. Then, monthly-average lake levels for the months of June through November were calculated for the individual years, and years with relatively higher or lower lake-level changes during the June-November period were identified.

5.2 Geo-Data Processing

This section describes the processing of various remote-sensing and GIS data, which will be used for the modeling.

5.2.1 Digital Elevation Data Processing

Hydrological terrain analysis was performed comprising following work steps:

i) DEM pre-processing

ii) Basin delineation

iii) Derivation of hydrologically relevant terrain attributes

iv) Generation of a DEM of the bathymetry of Nam Co

An *AML* (*Arc Macro Language*) based script tool consisting of *ArcInfo* commands, namely the *AMeLie-HRU Tool* (PFENNIG, in prep.), was used for the DEM pre-processing and the basin delineation. The derivation of terrain attributes and the digital bathymetry model generation were conducted using *ArcGIS*.

DEM Pre-Processing

A usually essential step for watershed delineation is the filling of sinks in the DEM to avoid internal drainage. However, for delineation of closed drainage basins where water drains into a water body, but where nothing flows out, the following procedure was used:

i) Extraction of endorheic water bodies

ii) Filling of sinks

iii) Merging of filled DEM and extracted water bodies

Initially, endorheic lakes were extracted from the SRTM-DEM, in order to exclude them from the filling procedure. Within the framework of the *AMeLie-HRU Tool*, additional information such digitalized shore lines or land-cover classifications including a class for water bodies can be used to select corresponding raster cells. Otherwise, a mask of flat areas (regions with an aspect of -1) with a user-defined minimum size is derived automatically from the DEM. Because lake areas within the SRTM-DEM have been corrected and obtained a uniform elevation, the latter method was used to identify endorheic lakes within the DEM. The *Standard Fill Algorithm* (JENSON & DOMINGUE, 1988) was applied to eliminate any remaining small sinks. Finally, the filled elevation grid was merged with the original raster cells of the lake areas extracted in the previous step, in order to obtain a filled DEM with endorheic water bodies as the only natural sinks.

Basin Delineation

Based on the developed DEM, closed drainage basins were delineated for selected lakes using the *AMeLie-HRU Tool*. First, drainage parameters, such as flow direction and flow accumulation, were obtained according to a method described in detail by JENSON & DOMINGUE (1988).

The direction of flow from each raster cell to its steepest downslope cell was determined. Next, the flow into each cell was calculated by accumulating flows from the cells that flow into each downslope cell. For the watershed delineation, selected lakes were specified as outlet points within the drainage network, assuming that all cells upstream drain into this natural sink. Based upon the calculated flow direction and flow accumulation, the catchment boundary could be derived.

Derivation of Terrain Attributes

Primary terrain attributes, such as slope angle (slope) and slope aspect (aspect), were derived from the SRTM-DEM based upon a moving 3 x 3-grid cell window using the *Surface* toolset in *ArcGIS*. Slope is the rate of maximum change in z-value from each cell to its eight neighbors; whereas, aspect identifies the steepest downslope direction of each cell. The computed slope and aspect grid were classified and used as input data for the delineation of spatial model entities.

Digital Bathymetry Model Generation

Based on the isobatic map of the Nam Co (WANG *et al.*, 2009) presented in Figure 5.1, a digital bathymetric model for the lake Nam Co (Figure 5.2) was generated. Following steps were conducted using *ArcGIS*:

i)   Georeferencing of the isobatic map

ii)   Digitizing of the bathymetric contour lines

iii)   Interpolation of the digitized contour lines (grid resolution 90 m x 90 m) using the *Topo to Raster* tool in *ArcGIS*

The interpolation method *Topo to Raster* has been designed for the generation of DEMs and is based on the *ANUDEM* program developed by (HUTCHINSON, 1989). *Topo to Raster* uses a discretized thin plate spline technique (WAHBA, 1990).

After merging the digital bathymetry model with the SRTM DEM, water-storage volume data for various lake levels were obtained by using the *Surface and Volume* module in *ArcGIS*. Then, the relationship between water volume (y) and water level (x) of the lake Nam Co was derived (Figure 5.3). The water level-volume curve was used to convert simulated lake-volume values in respective lake-level values.
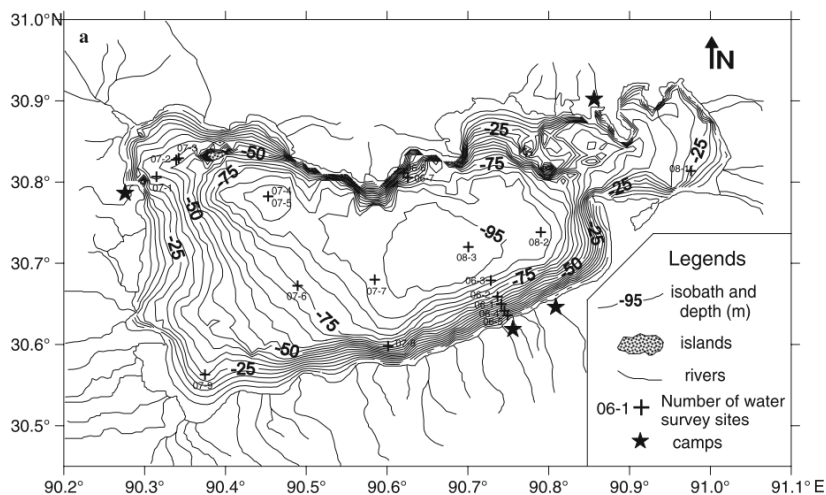
Figure 5.1:Isobathic map of lake Nam Co, generated based on lake-bathymetric survey data measured from 2005 through 2008 (WANG et al., 2009).
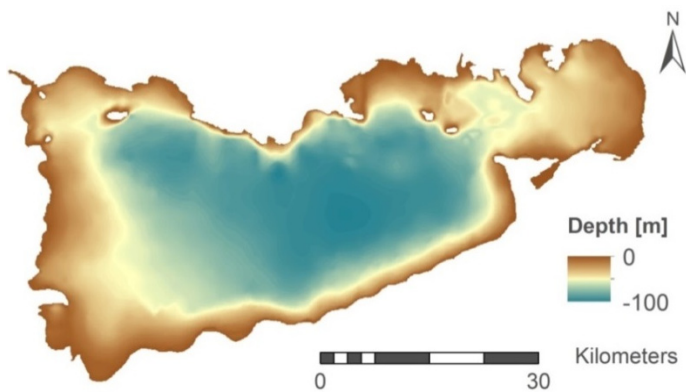
Figure 5.2: Digital bathymetry model (90 m x 90 m resolution) of the lake Nam Co.
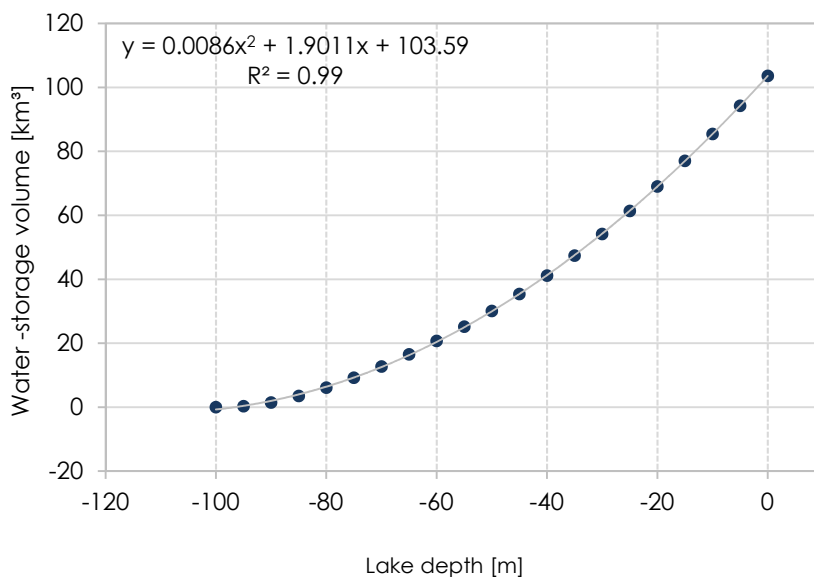
Figure 5.3: Water level-volume curve for the lake Nam Co.

5.2.2 MODIS Snow-Cover Data Processing

With respect to the crucial role of snow in catchment hydrology of mountainous environments and a lack of snow in-situ measurements for this study area, the MODIS snow-cover data from Terra (MOD10A2) and Aqua (MYD10A2) satellites (Section 4.3.3) were used for validation purposes of the snow modeling approach applied in this study. First, various pre-processing steps were conducted using *ArcGIS* and the *statistical software R* (IHAKA & GENTLEMAN, 1996). As proposed in the literature (e.g., GAO *et al.*, 2010; PARAJKA & BLÖSCHL, 2008; XIE *et al.*, 2009a; ZHANG, G. *et al.*, 2012), MOD10A2 and MYD10A2 products were combined on a pixel basis to reduce cloud-contaminated pixels. Due to the 3-hour difference between the Terra (10:30 AM) and Aqua (1:30 PM) sources, cloud pixels in the Terra images were replaced by the corresponding Aqua pixel. In order to combine the Terra and Aqua products for each time step, a *R* script developed by STURM (2013) was applied. After the combination procedure the cloud cover percentage was on average less than 1 %, with higher values during the wet summer season (~1 %) than in the drier winter season (~0.6 %). Then, the *snow covered area fraction* (*SCAF*) were obtained from the combined 8-day MODIS snow-cover data for the period 2001-2010 using *R*. For the period before the Aqua satellite was launched (May, 2002), the combination procedure was not possible, and the original MODIS/Terra snow-cover data were used for the calculation of SCAF.

5.2.3 MODIS Land-Surface Temperature Processing

In order to derive daily time series of lake-surface water temperature as a model input from the MOD11A2 product (Section 4.3.3), different processing steps had to be performed. MODIS pixels covering selected lakes were extracted and all pixel values for each 8-day time step were stored in a single *comma-separated value* file. Then, a mean lake-surface temperature value for the entire lake was generated for daytime as well as nighttime by averaging all pixel values of daytime or nighttime LST, respectively. Although MOD11A2 is an 8-day composite, it may contain outliers, particularly during the summer season. These often are caused by long-term cloud cover (XU *et al.*, 2013). Outliers were excluded through manual inspection from the daytime and nighttime time series, in order to eliminate cloud-affected values. Later, removed invalid values were filled by linearly interpolating between the remaining values. Finally, a continuous daily time series was computed by averaging the fitted daytime and nighttime 8-day LST and performing linear interpolation between the 8-day data points.

5.2.4 Delineation of Spatial Model Entities

In order to provide spatially distributed information of landscape characteristics for the hydrological modeling (see Section 5.4 below), the HRU approach (FLÜGEL, 1995) was used. In the absence of highly spatially distributed input information regarding landscape parameters (e.g., geology, soil, relief, vegetation), as is the case for the TP, the spatial scale of model entities becomes coarser, whereby the spatial homogeneity of an HRU decreases. The catchment size should also be taken into account, because fine representations of the landscape heterogeneity are not feasible for large catchments (such as the Nam Co basin, investigated in this study, with ~11.000 km² catchment size) and simplified assumptions are needed (DEHOTIN & BRAUD, 2008).

HRUs are typically delineated by overlaying spatially distributed information, assumed to be relevant for hydrological system dynamics in a step-by-step procedure. A toolbox for the delineation of spatial entities that considers specific needs for the modeling was created within the framework of the *ModelBuilder* of *ArcGIS*. The created *HRU-toolbox* consists of multiple *ArcGIS ModelBuilder* models. The overall workflow of the *HRU-toolbox* is summarized schematically in Figure 5.4 below.
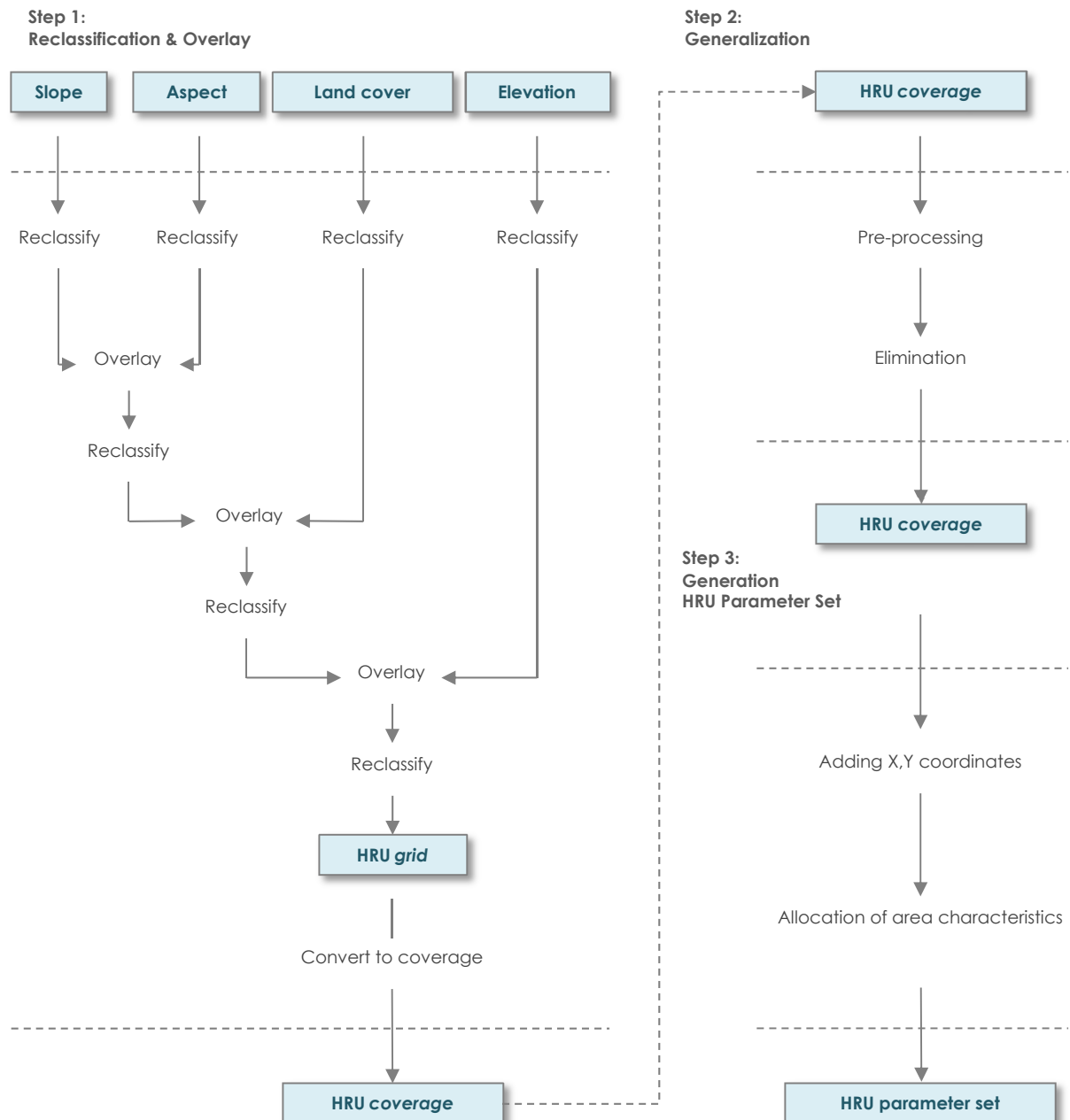
Figure 5.4: Scheme of the HRU-delineation ArcGIS ModelBuilder toolbox.

The principal steps of the HRU derivation can be summarized as follows:

i) *Reclassification and overlay*

Based upon available data, GIS layers of topographic-related information (slope, aspect and elevation) and land cover were selected for the overlay analysis. Soil and hydrogeological information were not included in the overlay analysis, primarily due to a lack of data. The several GIS layers (given in raster format) were reclassified into following classes (Figure 5.5):

- Slope (°): < 5; 5-15; > 15
- Aspect: flat; northerly: NW-NE / 292.5-112.5; southerly: SE-SW / 112.5-292.5
- Land cover: water, wetlands, grassland, barren land, glaciers
- Elevation (m a.s.l.): < 5300, 5300-5550, 5550-5800, > 5800
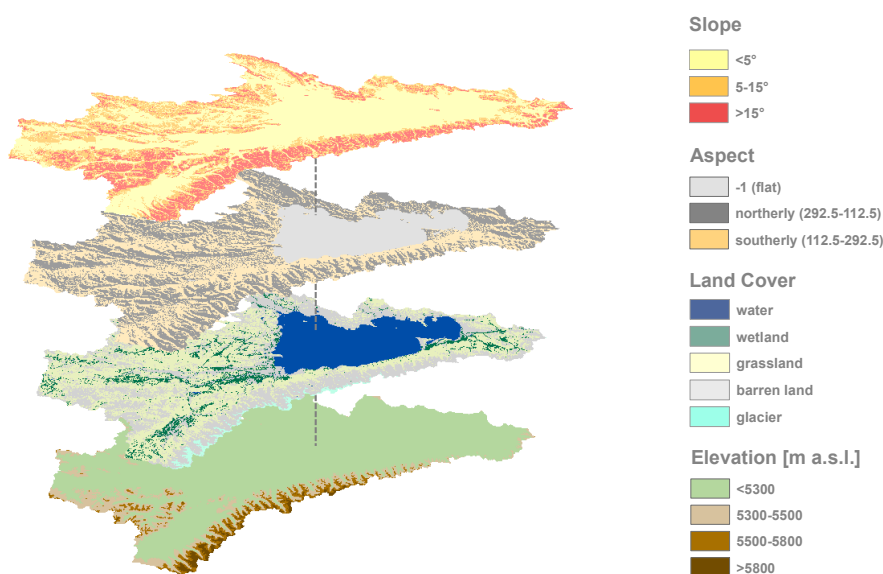
Figure 5.5: Hydrologically relevant classes of several GIS layers defined for the HRU delineation.

After reclassification, the data layers were overlain successively. To reduce the total number of model entities, HRU classes were grouped manually, depending on their size and hydrological relevance for the modeling:

- Wetland HRUs were not divided into different slope or aspect classes, because of the small occurrence of wetlands.
- Grassland or barren land HRUs with a slope < 5° were merged to one class and were not grouped into different aspect classes. This results from the assumption that in relatively flat terrain variations in aspect are negligible for the calculation of net solar radiation.
- Grassland and wetland HRU classes were not divided in different elevation classes, because of the low occurrence in higher elevation classes.
- Only two slope classes (< 5°; > 5°) were differentiated for barren land HRUs.
- Only two slope classes (< 15°; > 15°) and two elevation classes (< 5800 m a.sl.; > 5800 m a.sl.) were differentiated for glacier HRUs. The altitude value of 5800 m a.s.l. corresponds roughly to the median elevation of the glaciers within the study basins.

As result of the overlay analysis and reclassifications, a HRU map with 24 HRU classes (Figure 5.6, Table 5.1) was generated for the selected basins.
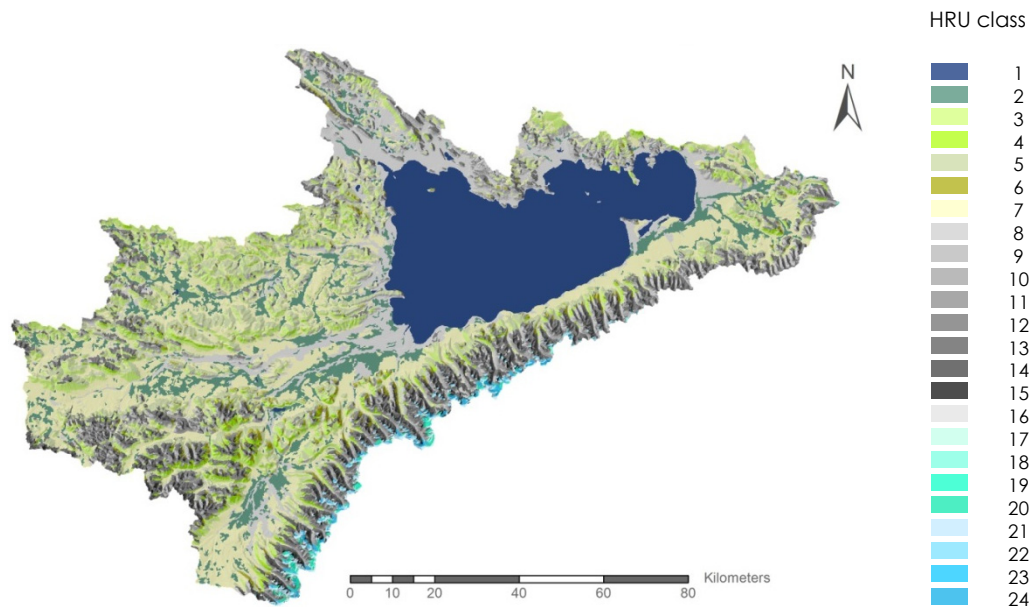
Figure 5.6: HRU map for the Nam Co basin. The numbers in the legend correspond to the HRU class IDs given in Table 5.1.

Table 5.1: Summary of HRU classes. HRU class IDs correspond to those indicated in Figure 5.6.

No.	Land cover	Aspect	Slope [°]	Elevation [m a.s.l.]
1	water	-	-	-
2	wetland	-	-	-
3	grassland	southerly	5-15	-
4	grassland	southerly	> 15	-
5	grassland	northerly	5-15	-
6	grassland	northerly	> 15	-
7	grassland	flat	< 5	-
8	barren land	southerly	> 5	4000-5300
9	barren land	southerly	> 5	5300-5500
10	barren land	southerly	> 5	5500-5800
11	barren land	southerly	> 5	> 5800
12	barren land	northerly	> 5	4000-5300
13	barren land	northerly	> 5	5300-5500
14	barren land	northerly	> 5	5500-5800
15	barren land	northerly	> 5	> 5800
16	barren land	flat	< 5	-
17	glacier	southerly	< 15	< 5800
18	glacier	southerly	< 15	> 5800
19	glacier	southerly	> 15	< 5800
20	glacier	southerly	> 15	> 5800
21	glacier	northerly	< 15	< 5800
22	glacier	northerly	< 15	> 5800
23	glacier	northerly	> 15	< 5800
24	glacier	northerly	> 15	> 5800

ii)   *Generalization*

Because overlaying several types of data can result in HRU entities with very small areas, these sliver polygons were removed by merging them with neighboring polygons that have the longest shared border. Indeed, the model entity of the lake and glacier HRUs were excluded from the generalization procedure, in order to minimize the loss of process-relevant information. Remaining polygons with a size of one pixel (~0.8 ha), two pixels (~1.6 ha) and so on were successively eliminated until a suitable total number of HRUs and an appropriate representation of the landscape heterogeneity with respect to the modeling purpose was attained (in this case, a target level of 20 pixels, or ~16 ha).

After the generalization step, the total number of HRUs for the several basins was: 1928 (Paiku Co), 3421 (Mapam Yumco), 8058 (Nam Co), 8462 (Tangra Yumco). As can be seen in Figure 5.6, the applied distribution concept represents the landscape heterogeneity with a higher spatial resolution in the complex high mountain areas (a large number of small polygons) than in the relatively flat terrains in the lower elevations (smaller number of large polygons).

iii)   *Allocation of area characteristics*

Coordinates for each HRU were added to the attribute table, and the specific values of the GIS layers included in the overlay analysis were assigned to the single HRUs. Accordingly, each HRU is characterized with a specific combination of spatially distributed, but temporally static parameters describing the land-surface heterogeneity. The land-cover and aspect class with largest area fraction within the HRU was allocated; whereas, for slope and elevation the average was generated. Because reliable spatially distributed data of soil and hydrogeology were not available, these characteristics were assigned to the HRUs based on topographic and land-cover information (a more detailed description is given in Section 5.4.3.1).

5.3   Field Surveys

Several field trips between 2009 and 2012 were jointly prepared, organized and carried out with German as well as Chinese project partners at the ITP/CAS who provided strong support in terms of logistics, equipment and staff for field instrumentation. The field work was focused on the installation of equipment measuring soil temperature and moisture (Section 5.3.1) as well as surveys to receive information on soils, vegetation and wetland characteristics (Section 5.3.2).

5.3.1   Soil Measurement Network

In order to continuously monitor soil moisture and temperature dynamics, a measurement network which automatically records (15-minute time interval) soil-hydrological parameters was established in a test wetland site (30.43°, 91.00°) nearby the southeast shore of the lake Nam Co in October 2009 (Figure 5.7). Intensive field work was conducted for the installation of soil measurement stations consisting of *Stevens Hydra Probe* soil sensors.
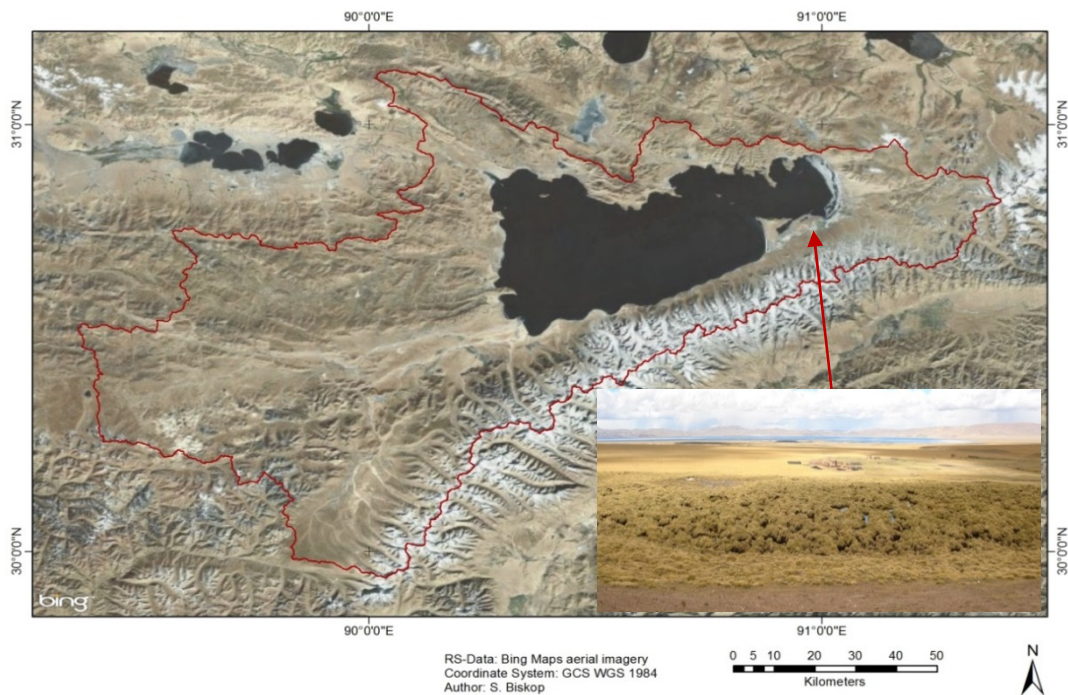
Figure 5.7: Location of the wetland test site within the Nam Co basin.

The concept of the measurement network is shown in Figure 5.8. One station was installed within the wetland area, and the other three stations north, south and east of the wetland. An open pit (approximately 1 m in depth) was dug at each location. As illustrated in Figure 5.9, a *Hydra Probe* was installed in four depths to measure water movement in the soil as well as the differences in soil-moisture fluctuations of distinct horizons. Soil temperature and moisture data were recorded at 15-minute time interval using *Hydra Probe* sensors, with an accuracy of $\pm 0.6°C$ and ± 0.03 volumetric water content, respectively. Recorded data were transmitted analogously to the data-logger *ADCON addIT Unit* (Figure 5.8, Figure 5.9). Near to the wetland (150 m apart), an *ADCON addRelay Station* was installed on the roof of a farm, in order to facilitate the radio-transmission of data to the *ADCON A440 Radio Station* that was installed at the Nam Co research station (7 km apart from the wetland site). The latter site was connected with the *ADCON Telemetry Gateway Server Unit*, which scanned data fully automatically of all incoming *Radio Telemetry Unities*.
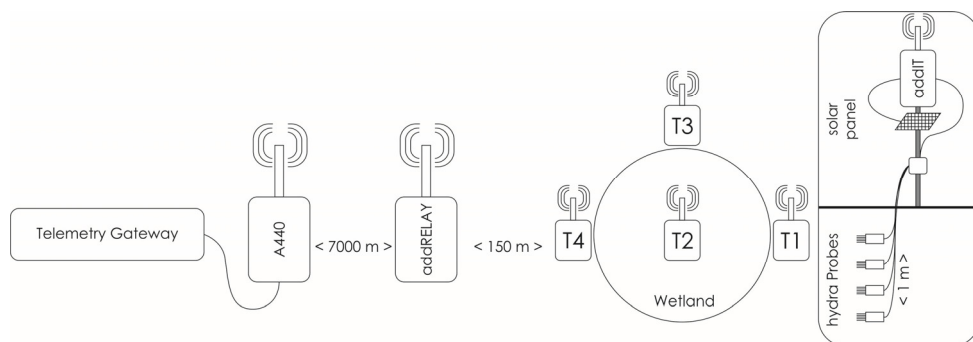
Figure 5.8: Schematic instrumentation structure of station and concept of measurement network.
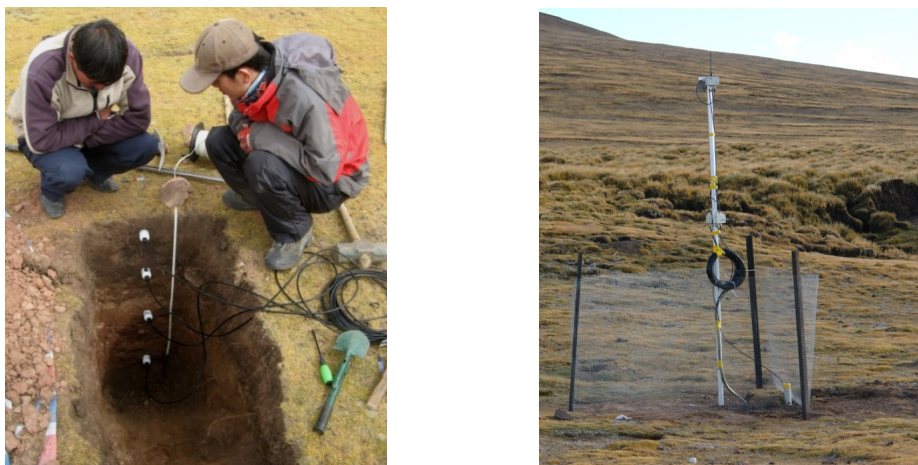
Figure 5.9: *Hydra Probe sensor installation (left). Radio-transmitter station (right).*

From October 2009 data were transmitted continuously via radio from the test site to a radio station established at the Nam Co research station. Unfortunately, the data-transmission process was disturbed several times since June 2010, due to unpredictable problems resulting from the site's remoteness and high altitude (e.g., damaged radio station by lightning strike). Due to the continuous problems with the equipment, only data covering the period October 2009 through the beginning of June 2010 are available. Thus, unfortunately, the analysis of soil-moisture dynamics during the summer season (which in turn influence hydrological processes in the soil profile and on the land surface, such as surface runoff, infiltration, percolation, subsurface and groundwater flow, water storage and evaporation) could not be performed. However, the freeze-thaw cycle was analyzed satisfactorily, based upon soil temperature and moisture measurements for the period October 2009 through the beginning of June 2010. For the analysis of the time-space variations of soil freezing and thawing, the records of 15-minute time interval were averaged to daily time series. The dates for initial freezing and thawing were assumed to correspond to the first day when mean daily soil temperature was below and above 0°C, respectively.

5.3.2 Soil and Vegetation Survey

Because soil information is required to delineate empirical parameters for hydrological modeling, soil profiles were analyzed at the four location of the soil measurement network described previously (Section 5.3.1). The excavated soil pits had a depth of about 1 m. Soil profiles were described according to different horizons, color, texture, rooting depth and abundance of roots. Soil texture was roughly estimated by finger probe, and the soil type was ascertained according to the soil mapping manual '*Bodenkundliche Kartieranleitung (KA5)*' (AD-HOC-ARBEITSGRUPPE BODEN, 2005). In addition, four soil drillings south of lake Nam Co have been described by FINK (2009, pers. comm.). Besides soil-related parameters, information on vegetation characteristics is important for land-surface parameterization. Thus, parameters describing vegetation characteristics (e.g., vegetation height, root length, cover density) have been determined by in-situ measurements at several grassland and wetland sites located south of the Nam Co.

5.4 Hydrological Modeling

Addressing the objectives of this study, the hydrological modeling is an essential component of the scientific method. The *Jena Adaptable Modeling System (JAMS)* (KRALISCH & FISCHER, 2012; KRALISCH & KRAUSE, 2006; KRALISCH *et al.*, 2007) was used as modeling framework. An overview of JAMS, especially the JAMS software architecture and common structure of JAMS models, is given in Section 5.4.1. Then the theoretical and methodological background of the different stages of model development and application are described (Section 5.4.2).

5.4.1 Jena Adaptable Modeling System

JAMS is an open-source software platform for environmental model development, application and evaluation with a thematic emphasis on the simulation of hydrological processes at discrete points in time and/or space (KRALISCH & KRAUSE, 2006). It provides basic functionalities for data input and output, application and communication of single model components as well as an application-programming interface for the implementation of the scientific methods in the form of encapsulated program modules. Primarily, JAMS was developed as a JAVA-based framework for the implementation of model components of the spatially distributed process-oriented hydrological model system J2000 (KRAUSE & KRALISCH, 2005). This system has been successfully applied to meso- or macro-scale catchments (e.g., KRAUSE, 2002; KRAUSE *et al.*, 2006; NEPAL *et al.*, 2014).

During recent years, a comprehensive 'library' of easily manageable components has been developed by implementing a wide range of existent hydrological process descriptions as encapsulated process modules and developing new model modules, as needed. Depending upon the model purpose and available input data, component-based environmental simulation models with process description ranging from simple empirical/conceptual to complex physically-based algorithms and different temporal and spatial resolutions can be easily created for a specific application, scale, and problem focus (KRALISCH & KRAUSE, 2006). In addition to functions supporting the model design and implementation, JAMS provide components for model calibration, parameter optimization, sensitivity and uncertainty analysis, output visualization and parallel computing (KRALISCH & FISCHER, 2012).

JAMS Architecture

The JAMS software structure can be divided into the following: *i)* core library, *ii)* runtime system, and *iii)* component repository. The core library contains JAMS data types and interfaces for the creation of modeling components and the runtime system. The latter manages the model setup, model execution and the communication between JAMS components by accessing the component repository and the model definition. The core library together with the runtime system represents the JAMS core; whereas, the component repository together with the model definition can be regarded as the JAMS knowledge part (KRALISCH & KRAUSE, 2006).

Graphical user interfaces support JAMS users to perform the different stages of the modeling process within this framework. JUICE is a graphical assistant for the creation of problem-tailored models from well-defined model components. For the analysis of JAMS models the data explorer (JADE) offers functionalities for plot and map visualizations of input and output

data. Model calibration in JAMS is supported by a special tool (OPTAS) (FISCHER, 2013; FISCHER *et al.*, 2009) that provides a variety of methods for sensitivity analysis, parameter optimization algorithm, and uncertainty analysis.

JAMS Models

The structure of a JAMS model contains two specific types of building blocks, called component and context component (KRALISCH & KRAUSE, 2006). JAMS components are used especially for the implementation of process algorithm (e.g., the calculation of evapotranspiration), but also for such purposes as reading data-input files, aggregating model results over space and time, etc. The source code of the components includes a set of meta-information such input and output data to support data exchange between the components. JAMS contexts control the execution of components (e.g., iterating of processing routines over time steps), and a set of spatial model entities is managed by the temporal and spatial context, respectively. These special model-building blocks can nest other contexts and components. The spatial context is typically arranged inside of a temporal context.

Figure 5.10 provides the model structure, along with a designated component hierarchy by embedding components within context components. The outermost context is the model context which manages the sequential execution of the ordered list of components.
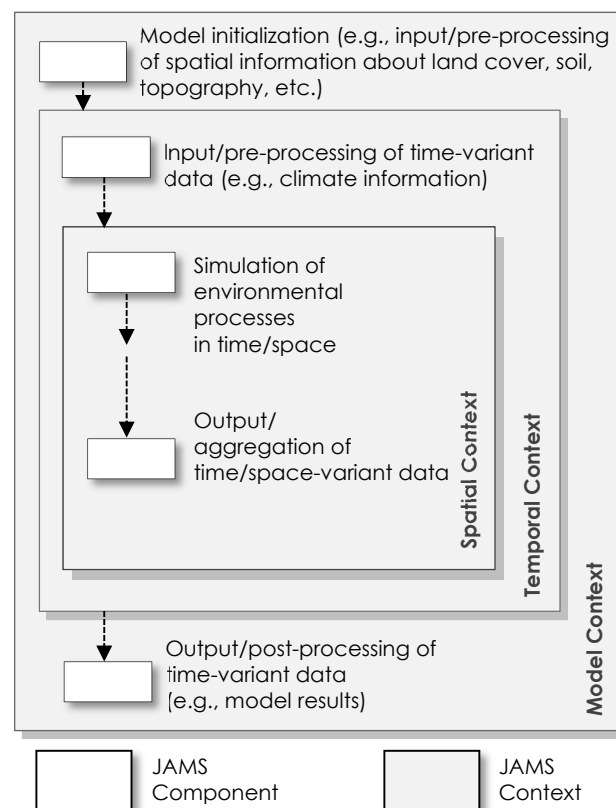
Figure 5.10: Common structure of environmental simulation models in JAMS (after KRALISCH et al., 2007).

5.4.2   General Modeling Approach

A wide variety of suggested modeling procedures can be found in the literature (e.g., JAKEMAN *et al.*, 2006; REFSGAARD & HENRIKSEN, 2004; WAGENER & KOLLAT, 2007). The modeling framework for this study is given in Figure 5.11 below.
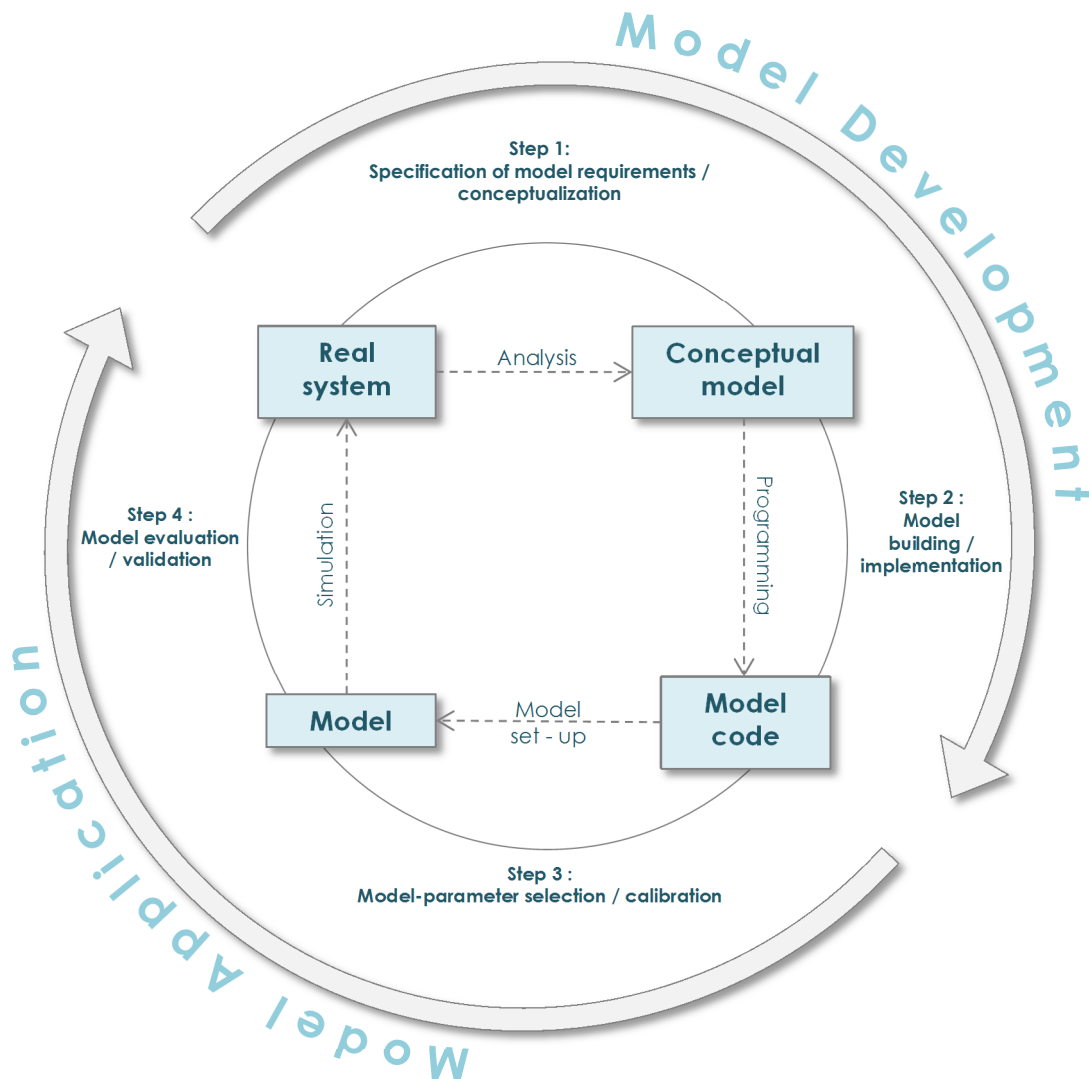
Figure 5.11: Modeling framework (modified after REFSGAARD & HENRIKSEN, 2004).

As illustrated in Figure 5.11 above, **two major modeling stages** can be delineated:

i)   **Model development**
ii)   **Model application**

The model-development stage may be further divided into the steps '***specification of model requirements / conceptualization***' and '***model building / implementation***' and the model application stage into '***model-parameter selection / calibration***' and '***model evaluation / validation***'.

In brief, these several steps include the following tasks:

- ***Specification of model requirements / conceptualization***

An a-priori analysis of the real system under study, based on available data, is a perquisite to define the modeling requirements (e.g., forcing and output variables, the temporal and spatial scope, etc.) and to develop a conceptual system representation that describes how model drivers are linked to internal (state) variables and outputs.

- ***Model building / implementation***

The conceptual model then has to be implemented through the appropriate model code that aggregates the complex and heterogeneous real-world characteristics in a simpler mathematical form.

- ***Model-parameter selection / calibration***

Model-parameter estimation comprises land-surface parameterization as well as the estimation of calibration parameters that reproduce the hydrological response within the range of accuracies assumed sufficient regarding the modeling objective.

- ***Model evaluation / validation***

This step includes the evaluation of model uncertainty and parameter sensitivity. In order to evaluate the model capability, i.e. how well a model describes the system under study, model results are validated against independent data.

5.4.2.1   Model Development

Specification of Model Requirements and Conceptualization

In order to meet the model requirements mentioned in Section 2.4.1, a semi-distributed conceptual model structure was selected. The conceptual structure of the J2000g model (KRAUSE & HANISCH, 2009) has been considered as generally appropriate for this study, regarding the study objective, data availability and the concluding degree of model complexity.

The J2000g model is a simplified version of the fully-distributed J2000 model (KRAUSE, 2002; KRAUSE *et al.*, 2006). The main differences with J2000 are that *i)* complex process descriptions (e.g., soil-water dynamics) are simplified leading to a reduced number of land-surface and calibration parameters in the J2000g model, and *ii)* lateral flow processes between spatial model units and streamflow routing are not accounted for by the J2000g model.

 J2000g was successfully applied for hydrological predictions in data-scarce basins (e.g., DEUS *et al.*, 2013; KNOCHE *et al.*, 2014; POHL *et al.*, 2015; RÖDIGER *et al.*, 2014) including a previous modeling study in the Nam Co basin (KRAUSE *et al.*, 2010). Some modifications of the original J2000g model have been carried out (as described in Section 5.4.2.2), in order to adapt it to the local specifics of endorheic lake basins in the TP region.

The basic concept of the model is schematically summarized in Figure 5.12, including input data requirements, basic hydrological processes considered in the model, and required model outputs variables. Hydro-meteorological data requirements for this application are daily times series of precipitation, minimum, average, maximum air temperature, solar radiation, wind speed, relative humidity and cloud fraction. The daily HAR10 data (Section 4.2) were used as climate input for the period 2001-2010. Daily lake-surface temperatures either provided by the ARC-Lake data (Section 4.3.2) or derived from MODIS data (Section 4.3.3) were used as additional data inputs for the estimation of the long-wave radiation term over the lake surface.

Due to the high altitudinal and spatial variability of climate and landscape properties in the study basins, a spatially distributed representation of the catchment was required. The HRU concept (Section 5.2.4) was applied in this study for the spatial discretization of the catchment. As shown in Figure 5.12, process simulations can be grouped into the following categories: *i)* lake, *ii)* land (non-glacierized), and *iii)* glacier.

The sum of the net evaporation (lake evaporation minus over-lake precipitation), the total runoff (base flow and direct runoff) from the non-glacierized land surface and glacier runoff results in the overall catchment response (in terms of lake-volume change). For simplicity, the terms net evaporation, land runoff, and glacier runoff are used to refer to several water-balance components. A detailed description of several processes considered in the model is given in the next section.
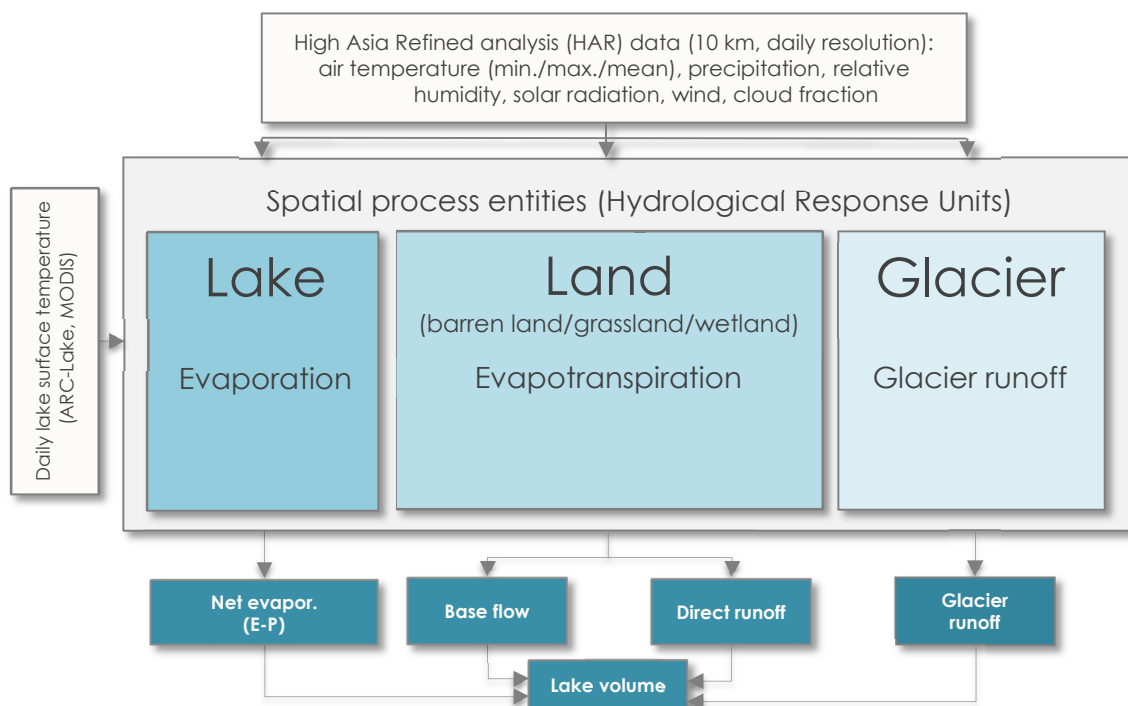
Figure 5.12: Conceptual model representing input data, elementary process simulations and basic model outputs.

Model Building and Implementation

The conceptual model presented herein has been implemented within the JAMS framework (described in Section 5.4.1) using the graphical assistant JUICE. A schematic illustration of the model structure including several model components and contexts is presented in Figure 5.13. The general structure of JAMS models has been described in Section 5.4.1, and is therefore not repeated here. A specific context ('switch context') embedded within the spatial context is used to execute different sequences of process components for specific spatial process entity categories (lake, non-glacierized land and glacier).

A large number of model components could be directly taken from the existing JAMS component repository for the building of a catchment model applicable to data-scarce endorheic lake basins in the TP region. Due to the modular structure, single model components could be easily adapted and enhanced by exchanging single process components and implementing new ones in an iterative manner (involving trial-and-error). Modified components or new implemented components are highlighted in Figure 5.13.

In the following subsections, descriptions of the theoretical and methodological background of the model components used in this study are given as follows:

i) **Regionalization of meteorological data**

ii) **Net radiation**

iii) **Potential evapotranspiration**

iv) **Snow processes**

v) **Glacier melt**

vi) **Soil-water budget and runoff processes**

vii) **Lake-water storage change**

Model adaptions and process implementations that have been performed to enhance the representation of processes, with particular importance for the study area, are integrated in the following model descriptions

.
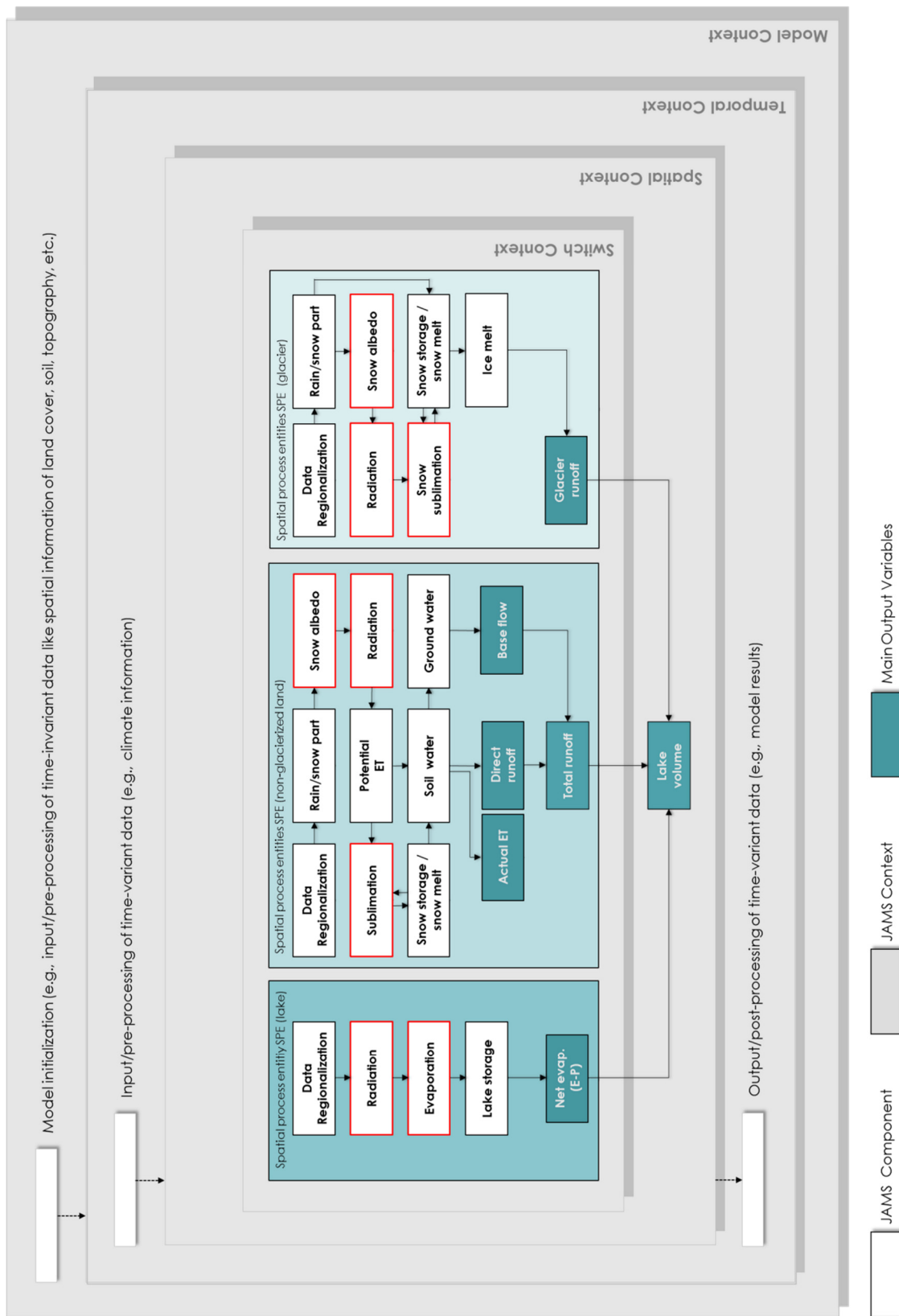
Figure 5.13: *Simplified illustration of the model layout including model components and context components. Modified or new components are indicated in red.*

- **Regionalization of Meteorological Data**

Spatial information of meteorological data is required for distributed hydrological modeling. In order to regionalize point information in this respect, a number of interpolation techniques exist in the literature, which can be grouped into deterministic (e.g., Thiessen Polygon, Inverse Distance Weighting (IDW)) and geostatistical methods (e.g., kriging) (LY *et al.*, 2013).

The regionalization module implemented in JAMS, which was used for the extrapolation of the punctual available HAR10 data to each HRU unit, is based on the IDW method. The principle behind the IDW method is to give more weight to nearby points than to distant points (LY *et al.*, 2013). Thus, the weights decrease as the distance increases. The power of the inverse distance function has to be chosen before the interpolation is performed. A low power means a greater weight towards data from distant points.

To account for horizontal and vertical climate variability, the regionalization procedure within JAMS provides the opportunity to combine distance weighting with an optional elevation correction. The regionalization process can be summarized by following steps. A detailed description of this procedure can be found in the literature (e.g., NEPAL, 2012).

i) Calculation of the linear regression between station values and the station heights for each daily time step (calculation of the coefficient of determination (r^2) and the slope of the regression line)

ii) Estimation of the distance between nearest station and a given HRU (number of stations next to HRUs defined dependently on the density and the spatial position of the stations)

iii) Calculation of the weighted distance via the IDW method (user-defined weighting factor)

iv) Calculation of the data value for each HRU using the weighted values from step iii and an optional elevation correction, based upon the elevation-dependent lapse rate calculated from the regression in step *i*.

In this study the four nearest stations were taken into account for the regionalization of the meteorological input data. All data sets were regionalized using IDW. In the case of air temperature, the elevation correction was done when r^2 was equal or greater 0.75 (default value).

Due to the fact that temperature inversions weaken the temperature-elevation relationship, no elevation correction will be done for time steps when the coefficient of determination of the regression relation between temperature of stations and station elevation is smaller than the threshold ($r^2 = 0.75$). This leads to the problem that higher temperatures can be calculated in glacier areas where data are lacking. This in turn might influence processes such snow evaporation and melting on given days. Therefore, the temperature lapse rate of 0.65 K / 100 m (e.g., MÖLG *et al.*, 2014) has been applied to transfer the temperature values of the closest station to the particular glacier-HRU. The simple temperature lapse-rate method is described by NEPAL (2012) and includes following steps:

i) Calculation of the difference between the mean elevation of a HRU and the closest station

ii) Calculation of the elevation corrected temperature using the elevation difference from step *i* and the defined lapse rate

A recent review of applications and performance of different methods for spatial interpolation of rainfall data is given in LY *et al.* (2013). It was indicated that the results of the comparison of interpolation methods differ from one study to another and that there is no single interpolation method recommended as being universally the best. At a daily time scale, the deterministic interpolation technique of IDW and geostatistical methods are comparable for hydrological modeling approaches (LY *et al.*, 2013).

For the transfer of precipitation values to the HRUs, no lapse rate has been considered due to the high spatial heterogeneity of precipitation distribution and the lack of reliable precipitation lapse rate information. Because precipitation input errors may have a large impact on the accuracy of the model predictions, a precipitation-scaling factor according to the studies of HUINTJES (2014) and MÖLG *et al.* (2014) was implemented to account for *i)* HAR10 precipitation overestimation related to atmospheric-model errors and *ii)* sublimation of blowing or drifting snow which was neglected in the model.

- **Net Radiation**

Net radiation is the principal energy source for evapotranspiration processes. Thus, it is a key variable for the estimation of potential evapotranspiration. Within JAMS, net radiation is calculated following the *Food and Agriculture Organization of the United Nations (FAO)* proposed use of the Penman-Monteith model (ALLEN *et al.*, 1998). For a detailed description of the net radiation calculation it is referred to the FAO Irrigation and Drainage Paper No. 56 (hereafter referred to as FAO56) (ALLEN *et al.*, 1998).

Net radiation (R_n) is the difference between the incoming net shortwave (R_{ns}) and the net outgoing long-wave (R_{nl}) radiation. **Net shortwave radiation** (R_{ns}), the fraction of the solar radiation (R_s) that is not reflected by the surface, depends on the albedo (α) of the land surface. Incoming solar radiation data were provided by the HAR10 data and were extrapolated to each modeling unit as described above. HRU-specific topographical effects (slope-aspect combinations) on the solar radiation were considered by adjusting the extrapolated solar radiation for each HRU, based on the angle between the direction to the sun and the normal to a given modeling unit (the incidence angle).

Land-cover specific albedo values are defined in the land-use parameter file. According to HAGINOYA *et al.* (2009), the lake-surface albedo was set to a value of 0.55 whenever the water surface is covered by lake ice. In the model, it is assumed that the lake is covered by ice if the lake-surface temperature is equal to or less than 0°C. Because in the standard radiation module of JAMS an albedo change during periods of snow cover is not considered, a new component was implemented for the estimation of **snow albedo** for time steps if the snow-water equivalent is greater than zero.

The ageing curve of the albedo of freshly fallen snow was calculated according to ROHRER (1992):

$$\alpha = \alpha_{\min}(t) + (\alpha(t-1) - \alpha_{\min}) \cdot e^{-k}$$
[Eq. 5.1]

where $\quad a_{min}$ minimum albedo [dimensionless]

$\qquad\quad k$ recession coefficient [dimensionless]

The exponential reduction during the time interval since the last considerable snowfall (see below for threshold) depends on the air temperatures. According to PLÜSS (1996) a threshold of > 3 mm d^{-1} was used for the last significant snowfall. If air temperature above or below the freezing the recession coefficients k is set to 0.05 d^{-1} or 0.12 d^{-1}, respectively. The snow albedo decreases until a minimum value a_{min} of 0.55 or is reset to the maximum value of 0.9 when the next considerable snowfall occurs.

For the calculation of the **net long-wave radiation** (R_{nl}), which is the difference between outgoing and incoming long-wave radiation, YIN *et al.* (2008) tested three formulas, including FAO56 (ALLEN *et al.*, 1998), FAO24 (DOORENBOOS & PRUITT, 1977) and Penman (PENMAN, 1948). The comparison with observed R_{nl} at sites throughout the TP has indicated that the Penman's empirical model had the highest accuracy. The R_{nl} simulations using the FAO24 and FAO56 models consistently underestimated the observations. As a consequence, the potential evapotranspiration would be overestimated if the FAO56 model is used without modification in the TP region (YIN *et al.*, 2008). Thus, the Penman simulation method, combined with the minimum and maximum temperature, was recommended by YIN *et al.* (2008) to calculate R_{nl} for conditions applicable to the TP. With regard to this, the long-wave radiation part of the FAO56 calculation was modified according to the recommendations of YIN *et al.* (2008).

$$R_{nl} = \sigma \cdot \left[\frac{T_{\max}^4 + T_{\min}^4}{2} \right] \cdot \left(0.56 - 0.25\sqrt{e_a} \right) \cdot \left(0.1 + 0.9 \cdot \left(\frac{R_s}{R_{so}} \right) \right)$$
[Eq. 5.2]

where $\quad R_{nl}$ net long-wave radiation [MJ m^{-2} day^{-1}]

$\qquad\quad \sigma$ Stefan-Boltzmann constant [4.903 10^{-9} MJ K^{-4} m^{-2} day^{-1}]

$\qquad\quad T_{max}$ maximum absolute temperature during the 24-hour period [K]

$\qquad\quad T_{min}$ minimum absolute temperature during the 24-hour period [K]

$\qquad\quad e_a$ actual vapor pressure [kPa]

$\qquad\quad R_s$ solar radiation [MJ m^{-2} day^{-1}]

$\qquad\quad R_{so}$ clear sky radiation [MJ m^{-2} day^{-1}]

The calculations of the actual vapor pressure (e_a) and clear-sky radiation (R_{so}) are given in ALLEN *et al.* (1998).

In the standard radiation module of JAMS, there is no distinction between the calculations for the net long-wave radiation for land versus water surfaces. Indeed, there is a major difference of the radiation conditions over land surface or large deep water bodies such as occurring in the study area. Although essentially all of the net solar radiation is adsorbed at the land surface and is available for immediate conversion to sensible or latent heat or conduction into the surface (ground energy flux), a part of the net solar radiation, which is not adsorbed at the water surface, penetrates to greater lake depths, where it is stored as energy (JENSEN, 2010). As a result, net radiation captured by the water body is not immediately available at the surface for evaporation and sensible heat.

During the decreasing solar radiation cycle (second half of the year), the stored energy is released gradually and becomes available for evaporation and sensible heat loss, leading to a time lag of water temperature and evaporation rates relative to the net radiation. The larger the amount of energy stored, the greater the time lag is, whereby the energy storage increases with lake depth and greater depth of solar-radiation penetration into the water body.

Due to the fact that the exchange of radiant energy between the lake surface and the atmosphere in the form of long-wave (thermal) radiation is significant for large lakes, a new component for the calculation of the **net long-wave radiation over lakes** (R_{nl}) that takes into account water-surface temperature was implemented in JAMS.

The long-wave radiation fluxes were calculated according to the Stefan-Boltzmann law (BOLTZMANN, 1884; STEFAN, 1879). The incident long-wave atmospheric radiation (R_{il}) at the water surface that is available to the water body after reflection was determined by the air temperature (T) and the effective emissivity of the atmosphere (ε_a). The thermal radiation emitted by the water surface depends on water-surface temperature (T_w) and on the emissivity of water (ε_w). The commonly used nomenclature for calculating the amount of the net long-wave radiation over water surface can be expressed as (JENSEN, 2010):

$$R_{nl} = \overbrace{(1-\alpha_l)\cdot\varepsilon_a\cdot\sigma\cdot T^4}^{R_{il}} - \overbrace{\varepsilon_w\cdot\sigma\cdot T_w^{\,4}}^{R_{ol}}$$ [Eq. 5.3]

where

R_{nl}	net long-wave radiation [MJ m^{-2} day^{-1}]
R_{il}	incoming long-wave radiation [MJ m^{-2} day^{-1}]
R_{ol}	outgoing long-wave radiation [MJ m^{-2} day^{-1}]
α_l	long-wave albedo [dimensionless]
ε_a	effective emissivity of the atmosphere [dimensionless]
ε_w	emissivity of water [dimensionless]
σ	Stefan-Boltzmann constant [4.903x10^{-9} MJ K^{-4} m^{-2} day^{-1}]
T	air temperature [K]
T_w	water-surface temperature [K]

The total reflectivity of the water surface for long-wave radiation (a_l) is assumed to be a constant and is equivalent to (1 - ε_w) or 0.03 (HENDERSON-SELLERS, 1986; JENSEN, 2010). For the calculation of effective emissivity of the atmosphere (ε_a), there are various equations usually depending on vapor pressure, air temperature, and cloud cover. An overview of several formulations is given in CRAWFORD & DUCHON (1999). Most of the previous methods are valid under cloudless conditions and are empirically based. However, the total effective emissivity of the sky increases significantly in the presence of clouds (e.g., CRAWFORD & DUCHON, 1999). CRAWFORD & DUCHON (1999) tested six commonly-accepted, effective clear-sky atmospheric emissivity formulations modified by a cloudiness correction term (DEARDORFF, 1978) for comparison with measured incoming long-wave data. They recommended the physically-based BRUTSAERT (1975) formulation as compared to the others empirical methods. Accordingly, the formulation incorporating the BRUTSAERT (1975) clear-sky parameterization and the DEARDORFF (1978) cloudiness correction was used in this study to estimate effective emissivity of the atmosphere (ε_a):

$$\varepsilon_a = \left(clf + (1 - clf) \cdot \left(1.24 \cdot (e_a \cdot 10 / T)^{1/7} \right) \right) \qquad \text{[Eq. 5.4]}$$

where
ε_a effective emissivity of the atmosphere [dimensionless]
clf cloud fraction [dimensionless]
e_a actual vapor pressure [kPa]
T air temperature [K]

- *Evapotranspiration*

A number of methods exist for the estimation of evapotranspiration. These can be categorized into: *i)* empirical, *ii)* water budget, *iii)* energy budget, *iv)* mass transfer, and *v)* a combination of the previous methods (SINGH & XU, 1997).

The physically-based Penman-Monteith approach (MONTEITH, 1965) recommended by FAO56 is commonly used to compute potential evapotranspiration and has been widely accepted in the scientific community as the most accurate method (ALLEN *et al.*, 1998). The Penman-Monteith method combines the mass-transfer and energy-budget principles in a single equation and has proved to be reasonable in both humid and arid climate conditions (ALLEN *et al.*, 1998).

Within the framework of JAMS, the Penman-Monteith model is implemented, in accordance with the FAO56 report (ALLEN *et al.* 1998). Climate variables of air temperature, wind speed, relative humidity and global radiation are required as input data. Hydro-climatic variables (e.g., vapor-pressure deficit, slope of saturation-pressure curve, psychrometric constant) have to be calculated for the estimation of the potential evapotranspiration. A detailed description of the entire calculation procedure can be found in the FAO56 guideline of ALLEN *et al.* (1998) or in NEPAL (2012).

For the estimation of **open-water evaporation** rates from large lakes, the Penman equation modified by the addition of the lake heat storage was used, which has been applied in various studies (e.g., JENSEN, 2010; YAO, 2009). It has the following general form:

$$E = \frac{\Delta \cdot (R_n - Q_t) + \gamma \cdot E_a}{\lambda \cdot (\Delta + \gamma)}$$ [Eq. 5.5]

where
E evaporation rate of open water [mm day^{-1}]
Δ slope of the saturation vapor pressure curve at temperature [kPa]
λ latent heat of vaporization or sublimation from ice [MJ kg^{-1}]
γ psychrometric constant [kPa °C^{-1}]
R_n net radiation [MJ m^{-2} day^{-1}]
Q_t energy storage change in the water body [MJ m^{-2} day^{-1}]
E_a bulk aerodynamic expression [MJ m^{-2} day^{-1}]

The slope of the saturation vapor-pressure curve at temperature (Δ), the psychrometric constant (γ) and latent heat of vaporization (λ) all are calculated as given in ALLEN *et al.* (1998).

At a water-surface temperature of equal to or less than 0°C a completely frozen lake surface was assumed. The latent heat for sublimation from ice was calculated with the following empirical quadratic function (ROGERS & YAU, 1989):

$$\lambda_{ice} = 2.834 - 0.29 \cdot T - 0.004 \cdot T^2$$ [Eq. 5.6]

where
λ_{ice} latent heat of sublimation from ice [MJ/kg]
T air temperature [°C]

Due to the lack of lake-temperature depth profiles, the energy storage change Q_t in the lake was estimated, based upon the net short-wave and long-wave radiation and using the empirical formulation of JENSEN *et al.* (2005):

$$Q_t = 0.5 \cdot R_{ns} - 0.8 \cdot R_{nl} \quad \text{, for Julian day of year} < 180$$ [Eq. 5.7]

$$Q_t = 0.5 \cdot R_{ns} - 1.3 \cdot R_{nl} \quad \text{, for Julian day of year} > 180$$ [Eq. 5.8]

where
Q_t average daily energy storage in the water body [MJ m^{-2} day^{-1}]
R_{ns} net short-wave radiation [MJ m^{-2} day^{-1}]
R_{nl} net long-wave radiation [MJ m^{-2} day^{-1}]

The bulk aerodynamic expression E_a that contains the empirical wind function and the vapor-pressure deficit then is given by:

$$E_a = 6.43 \cdot (a + b \cdot u) \cdot (e_s - e_a) \qquad \text{[Eq. 5.9]}$$

where   *a, b*   empirical wind function coefficients

                 u   wind speed at 2 m height [m s^{-1}]

                 e_s saturation vapor pressure at the temperature of the water surface [kPa]

                 e_a actual vapor pressure of the air [kPa]

PENMAN (1948) originally suggested setting the parameter values as *a* = 1.0 and *b* = 0.54, respectively. Because the effective value of the aerodynamic resistance (which is inversely proportional to wind speed function) is larger for great lakes, the original Penman formula might systematically overestimate (bias) the 'actual' evaporation for very large lakes by approximately 10-15 % (SHUTTLEWORTH, 1993). Therefore, VALIANTZAS (2006) suggested to use the reduced wind function as proposed by LINACRE (1993), where *a* = 0 and *b* = 0.54, for estimating evaporation from large open waterbody surfaces. The saturation vapor pressure at the water-surface temperature (e_s) and the actual vapor pressure (e_a) were calculated as given by ALLEN *et al.* (1998).

- *Snow Processes*

A large variety of snow models with different degrees of complexity, ranging from physically-based energy balance models to empirical methods, have been developed during recent decades. Although melt rates are controlled by the surface-energy balance, the physically-based approaches are often not applicable in data-scarce regions, because the required data are not readily available.

In order to calculate the daily snow-accumulation rate, the fraction of the total precipitation that falls as snow was estimated previously in a sub module of JAMS. The separation between solid and liquid precipitation phase, thereby, depends on the following: *i)* a defined threshold temperature *snow_trs* (in °C) which conforms to the temperature where 50 % of precipitation is falling as snow and 50 % as rain and *ii)* a transition parameter *snow_trans* (in K) that is taken as the half width of the transition range within which both precipitation forms occur. Snow sublimation was estimated according to the Penman-Monteith equation.

Due to the high importance of the refreezing process in the snow pack in the study region, the simple degree-day snow modeling approach of the standard J2000g model version was replaced by the J2000 snow module that combines empirical or conceptual approaches with more physically-based routines, principally following the approach developed by KNAUF (1980). This snow module takes into account the phases of snow accumulation and the compaction of the snow pack caused by snowmelt or rain on the snow pack (KRAUSE, 2002). It includes the calculation of different state variables, such as snow-water equivalent, snow density, snow depth, snow age, etc. Below, the important calculation steps of the snow module are briefly described. For a more detailed description see NEPAL (2012) and Nepal et al. (2014).

Depending on the air temperature, two phases are distinguished: *i)* the snow-accumulation phase and *ii)* the snow-compaction and snowmelt phase. If the accumulation temperature (T_{acc}) is below a specific temperature threshold (*baseTemp*) and the total precipitation falls as snow, only the snow-accumulation phase is applied. In the case that the melt temperature (T_{melt}) is higher than the user-defined *baseTemp* and the whole precipitation occurs as rain, only the snow-compaction and snowmelt phase is applied. The T_{acc} is calculated, dependent upon the mean and minimum temperature; whereas, the estimation of the T_{melt} considers the mean and maximum air temperature. If the temperature is between T_{acc} and T_{melt}, snow accumulation and snowmelt is simulated within a single time step.

Within the J2000 snow module, the density of new snow is calculated according to KUCHMENT *et al.* (1983) and VEHVILAEINEN (1992), at times when the air temperature exceeds -15°C. In the case that the air temperature is lower than -15°C, the new snow density is assumed to be 0.02875. Liquid water in the snow pack originating from rainfall or snowmelt results in snow subsidence (KNAUF, 1980). The subsidence of the snow pack in the model is calculated according to the snow-compaction scheme reported by BERTLE (1966). Thermal circumstances in the snow pack are considered in the model in such a manner that, if the temperature is below the freezing point, the snow pack cools down and liquid water refreezes. Only when the value of the 'cold' content of the snow pack that is calculated by the product of the air temperature and a calibration parameter (*snowColdContent*) is not negative, snowmelt occurs.

The potential snowmelt rate is given as the sum of different energy fluxes (sensible heat of air temperature, energy from rainfall and soil heat flow), all of which are generated empirically using three calibration parameters (*t-factor, r-factor* and *g-factor*) (KNAUF, 1980). The maximum storage capacity of the snow pack is determined by a certain critical density (*snowCritDens*) and corresponds to a water content of 40 and 45 % in relation to the total snow-water equivalent that includes the actual frozen and liquid water amounts. As long as this maximum storage capacity is not exceeded, liquid water resulting from rainfall or snowmelt can be stored in the pores of the snow pack. When the critical density is reached, the water stored in the snow pack is released as snowmelt runoff.

- **Glacier Runoff**

Glacier-melt models generally can be grouped within energy-balance and temperature-index models. Energy-balance models quantify melt as a residual in the heat-balance equation; whereas, temperature-index models are based on an empirical linear relationship between positive air temperatures and melt rates. Energy-balance models with a more physically-based process description are often difficult to apply due to extensive data requirements. Temperature-index models have been widely used for modeling of snowmelt, because of the lower level of data requirements and a generally 'good' model performance, despite the simplicity of this approach (HOCK, 2003).

In order to bridge the gap between simple degree-day approaches and energy-balance-type expressions, several studies have integrated various input variables into model formulations. In particular, the addition of a factor for radiation, which is the secondary source of heat for melt, overcomes some of the limitations of the 'classical' (commonly-used) degree-day method (HOCK, 2003). The extended temperature-index approach (HOCK, 1999) that has been successfully used

in other studies (e.g., Huss *et al.*, 2008; Nepal *et al.*, 2014; Zhang *et al.*, 2007) was applied in this study. Indeed, snowmelt processes on the glacier surface are calculated according to the approach described previously. If the accumulated snow of any given glacier HRU has been melted completely (i.e. the snow-water equivalent is equal to zero) and the air temperature (T) is above the threshold temperature for melt (T_0), as defined by the user, the ice-melt rate (M) is calculated according to HOCK (1999):

$$M = \left(MF + \alpha \cdot I\right) \cdot \left(T - T_0\right) \quad T > T_0 \qquad \text{[Eq. 5.10]}$$

where
M	melt [mm day^{-1}]
MF	melt factor [mm °C^{-1} day^{-1}]
a	radiation melt coefficient [mm Wh^{-1} m^2 °C^{-1} day^{-1}]
I	incoming solar radiation [MJ m^{-2} day^{-1}]
T	air temperature [°C]
T_0	threshold temperature for melt [°C]

The melt factor *MF* is smaller (approximately 2 mm °C^{-1} day^{-1}) than the degree day factors for a classical temperature-index method, because the radiation term is added to the *MF* (SCHULLA, 2013). The sum of snowmelt, ice melt and rain over glaciers is defined as glacier runoff in the model.

- ***Soil-Water Budget and Runoff Processes***

Due to a lack of detailed soil information in the study area, the simple soil-water module of J2000g described in KRAUSE & HANISCH (2009) was used to fill this data gap. The soil module consists of a simple water storage (i.e. middle-pore storage (*MPS*)) that regulates the relation between evapotranspiration and direct runoff and groundwater recharge. The maximum soil-water storage capacity (*maxMPS*) is defined from the available water capacity (*AWC*) of the specific soil type within the respective modeling unit. During the process of model calibration, the storage-capacity values of all modeling units can be increased or decreased by using a multiplicative calibration parameter (*AWCA*) with the same value for all modeling units.

The *MPS* is filled by precipitation and snowmelt until the *maxMPS* is reached. The amount of water which exceeds the maximum soil-water storage capacity will be used initially for evapotranspiration. In case that the potential evapotranspiration rate is greater than the inflow, the *MPS* is 'emptied' (e.g., lost to the atmosphere) by evapotranspiration. The water loss from the *MPS* through evapotranspiration is controlled by the actual soil-water saturation (*actMPS*), the potential evapotranspiration and a linear evapotranspiration-reduction factor (*linETRed*). The calibration coefficient *ETR* has a range of values between 0 and 1. It defines a specific threshold of the *actMPS* which triggers a linear reduction of the potential evapotranspiration rate if *actMPS* falls below this threshold (KRAUSE & HANISCH, 2009).

Runoff is generated only when the soil-water storage is saturated. Excess water which is not allocated to evapotranspiration is allocated into either direct runoff or percolation, based upon the slope and the maximum percolation rate of any given HRU and a calibration factor (*latVertDist*). The percolation component is transferred to a groundwater-storage component,

where the outflow (base flow) is computed based on a linear-storage approach and a specific-retention coefficient (*GWK*) (KRAUSE & HANISCH, 2009). The total runoff of the non-glacierized land surface occurs, based upon the summation of the direct runoff and the base-flow components from the respective HRUs.

- **Lake-Water Storage Change**

In the lake module, the net evaporation (lake evaporation minus precipitation over the lake's surface area) is calculated. Then the lake-volume change is estimated by summing up the total runoff from glacier and non-glacierized areas minus lake net evaporation. Because the J2000g model does not account for water routing and thus time delay of the discharge, the model is not fully suited to provide continuous and precise estimates of lake-water storage changes. In order to calculate lake-level changes from lake-water storage changes, simplified lake geometry was assumed, because bathymetric maps for most Tibetan lakes are lacking. Hence, lake volume is divided by lake area to derive lake-level variations. Lake-level fluctuations of the Nam Co were also estimated based on the water level-volume relationship derived from the generated bathymetric DEM (see Section 5.2.1).

5.4.2.2 Model Application

The modeling strategy applied in the Nam Co basin is summarized in the Figure 5.14 below. The several steps are described in the following sections.
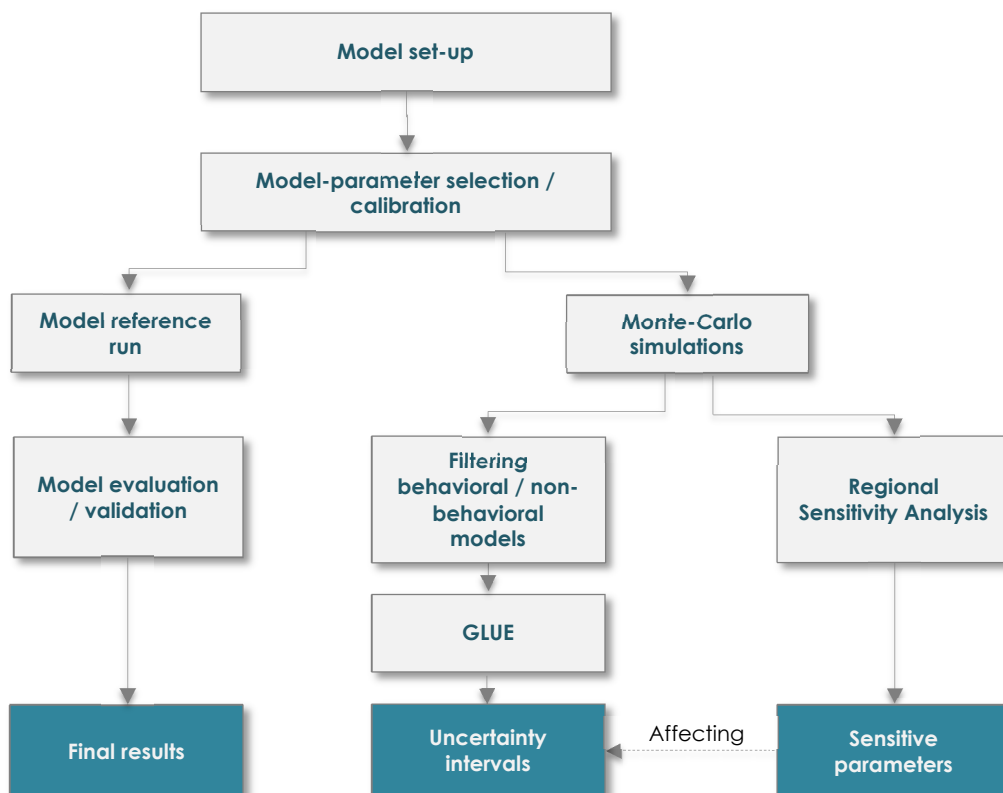
Figure 5.14: Flowchart of the model application in the Nam Co basin.

<u>**Model-Parameter Selection/ Calibration**</u>

- ***Land-Surface Parameterization***

Spatially distributed land-surface parameters describing the heterogenic land surface (e.g., vegetation height, rooting depth, etc.) were derived from field studies or literature values. Reference profiles that have been linked to the SOTER units (several polygons in the soil map in Figure A.1) were judged not to be useful for soil parameterization, because all SOTER profiles are located out of the study basins (up to 2000 km in distance apart). Moreover, the spatial resolution of the SOTER units is very low - in particular, in the high mountain range south of the Nam Co. This leads to unrealistic occurrence of deeper soils in the high elevated and steep areas.

Soil properties characterized through surveys in the Nam Co basin (see Section 6.1.2) correspond very well with the soil characteristics described by KAISER *et al.* (2008) in a neighboring area northeast of the lake Nam Co (near to Nagqu, 31°29'N, 92°04'E). This similarity supports the premise that the soil surveys in the Nam Co basin can be used for soil-related parameter estimates for the hydrological modeling, while taking into account that the punctual soil data cannot represent the complex soil distribution pattern within the Nam Co basin. Based upon the soil mapping manual '*Bodenkundliche Kartieranleitung (KA5)*' (AD-HOC ARBEITSGRUPPE BODEN, 2005), the field capacity was derived as function of the soil types obtained from own field surveys and KAISER *et al.* (2008) (see Table 5.2). Due to the limited availability of spatial soil information, soil parameters were distributed according to different land-cover and slope classes (Table 5.2).

Table 5.2: Soil parameters used as input for hydrological modeling.

Combination land cover – slope	Soil depth [cm]	Field capacity							
		Total [mm]	0-1 dm [mm/dm]	1-2 dm [mm/dm]	2-3 dm [mm/dm]	3-4 dm [mm/dm]	4-5 dm [mm/dm]	5-6 dm [mm/dm]	6-7 dm [mm/dm]
wetland	70	236	60	60	60	14	14	14	14
grassland < 15°	70	120	18	18	18	18	16	16	16
grassland > 15°	40	68	18	18	16	16	-	-	-
barren land < 5°	20	14	7	7	-	-	-	-	-
barren land > 5°	10	7	7	-	-	-	-	-	-

Because of lacking hydrogeological data, maximum possible percolation rates (*maxPerc*) (ground water recharge rates) in mm per time unit were distributed based on the following assumptions (Table 5.3): In valley floors and flood plains the percolation is assumed to be highest (*maxPerc* = 30 mm d^{-1}) due to the relatively high porosity permeability of sedimentary depositions and the flat terrain. Considering the impermeable nature of the crystalline bedrock and the steep slopes in the high mountains, groundwater influence is assumed to be unlikely in these regions (*maxPerc* = 1.5 mm d^{-1}).

Table 5.3: Maximum possible percolation rate used for hydrological modeling.

Combination land cover – slope	maxPerc [mm d^{-1}]
grassland, wetland, barren land < 5°	30
grassland > 5°	15
barren land > 5°	1.5

- *Model Calibration*

Because parameter optimization procedures are difficult to apply in ungauged regions such as the situation on the TP (e.g., REFSGAARD & HENRIKSEN, 2004; WINSEMIUS *et al.,* 2009), calibration parameters were set to default or literature values (see Table 5.4). The parameters *AWCA*, *latVertDist* and *maxPerc* were set to 1, in order to run the model with initial values. Due to the high uncertainty of the precipitation-scaling factor in various regions of the TP (HUINTJES, 2014; HUINTJES *et al.*, 2015; MÖLG *et al.*, 2014; POHL *et al.*, 2015), model runs with precipitation-scaling factors varying between 0.3 and 1.0 (with a 0.05 increment) were performed. Because the precipitation-scaling factor was the parameter that contributes the most to uncertainties in model results, all other climate-forcing variables and model parameters were held constant. Then simulated mean annual lake-volume changes of each model run were compared with water-volume changes derived from remote sensing data. The model run with the minimum difference between modeled and satellite-derived lake-volume change was defined as model reference run and thereby was used for an assessment of model results.

- *Monte-Carlo Simulations*

Because parameter set combinations can lead to equally acceptable models (e.g., BEVEN & BINLEY, 1992; FREER *et al.*, 1996), modeling approaches based on Monte-Carlo simulations incorporating uncertainty assessment have been suggested, in order to identify a set of reasonable parameter sets or behavioral models, respectively, and to give a plausible range of water-balance estimates (e.g., MCINTYRE *et al.*, 2005; WINSEMIUS *et al.*, 2009). Therefore, Monte-Carlo simulations (7500 runs) were carried out to create an ensemble of parameter sets. A quasi-random sampling method, the Sobol sequence (SOBOL, 1967), was used in this study to create a parameter sample with uniformly distributed parameter values. The Sobol sequence belongs to the low-discrepancy sequences where the parameter space is covered evenly (KOCIS & WHITEN, 1997).

The parameter sampling within a range of ±10 % is a common approach when a priori limits of the more critical parameters are lacking (e.g., ANSLOW *et al.*, 2008; HEYNEN *et al.*, 2013; RAGETTLI & PELLICCIOTTI, 2012; RAGETTLI *et al.*, 2013). The calibration parameters (Table 5.4) were sampled within a uniform range of ±10 % of the parameter values of the reference run (except for temperature thresholds), because there is a knowledge gap of reasonable upper and lower parameter limits for the study region. The parameter ranges used for the parameter sampling are provided in Table 5.4. The precipitation-scaling factor was included in the parameter sampling, as it was used to calibrate the model. The precipitation-scaling factor was sampled within a range of ±0.05. The retention coefficient *GWK* was not included in the parameter sampling, because it has no influence on the water balance.

Table 5.4: Calibration parameters and sampling ranges used in this study.

Parameter	Description	Actual value	Range	Reference / note
Precipitation distribution				
snow_trs	Threshold temperature for 50 % rain, 50 % snowfall [°C]	3.75	3 - 4	a
snow_trans	Half width of the transition range within which both precipitation forms occur [°C]	2.75	2 - 3	a
Snow module				
snowCritDens	Critical density of snow pack	0.381	0.343 – 0.419	Nepal et al. (2014)
snowColdContent	Cold content of snow pack	0.0012	0.00108 – 0.00132	Nepal et al. (2014)
t_factor	Melt factor by sensible heat	2.84	2.556 – 3.124	Nepal et al. (2014)
r_factor	Melt factor by liquid precipitation	0.21	0.189 – 0.231	Nepal et al. (2014)
g_factor	Melt factor by soil heat flow	3.73	3.36 – 4.10	Nepal et al. (2014)
baseTemp	Threshold temperature for snowmelt	0	-1 - 1	Default value
Glacier module				
meltFactorIce	Melt factor for ice	2.5	2.25 – 2.75	Nepal et al. (2014)
alphaIce	Radiation melt factor for ice	0.001	0.0009 – 0.0011	Schulla (2012)
baseTemp	Threshold temperature for ice melt [°C]	0		Default value
Soil module				
AWCA	Available water-capacity adaption	1	0.9 – 1.1	Default value
linETRed	Linear evapotranspiration-reduction factor	0.6	0.54 – 0.66	Default value
latVertDist	Lateral/vertical runoff distribution	1	0.9 – 1.1	Default value
Ground water module				
maxPerc	Adaption of maximum percolation rates	1	0.9 – 1.1	Default value
GWK	Retention coefficient	180	-	Default value

a: The upper and lower threshold for precipitation phase corresponds to 6.5°C and 1°C, respectively, according to MÖLG et al. (2014).

- **Identification of Acceptable / Behavioral Models**

In order to identify a group of equally acceptable models, the ensemble was divided in behavioral or non-behavioral models. To select acceptable (behavioral) or to reject unacceptable (non-behavioral) parameter sets, respectively, model performance criteria need to be defined which are assumed to be suitable to achieve the modeling purpose (GUPTA *et al.*, 2006). In the presence of limited and uncertain information, WINSEMIUS *et al.* (2009) suggest the use of hydrologically relevant 'signature measures' as performance criteria. Signature measures can be derived by extracting hydrologically relevant information from any available observations in the basin itself.

For this study, the lake-volume change between 2001 and 2010 derived from remote-sensing data (Table 4.3) was specified as performance criterion for a feasible representation of the water balance. According to the limits of acceptability approach, proposed by BEVEN (2006), only models (i.e. with parameter sets) that reproduce the lake-volume change within defined limits of acceptability were considered as behavioral models. A PBIAS of ≤ 10 % between simulated and satellite-derived lake-volume change for the 2001-2010 period was used to define limits of acceptability. The percent bias (PBIAS) is a common model evaluation criterion that measures under- and over-estimation bias of simulated versus measured values (GUPTA *et al.*, 1999).

<u>*Model Evaluation / Validation*</u>

- ### *Uncertainty and Sensitivity Analysis*

Uncertainty intervals reflecting the range of model outputs encompassed by the behavioral parameter sets were derived, in order to reveal where the highest uncertainty in the model exists. Therefore, the *Generalized Likelihood Uncertainty Estimation (GLUE)* method (BEVEN & BINLEY, 1992) was used. The GLUE approach is an uncertainty method that arose from the equifinality concept (described in Section 2.4.1). Monte-Carlo simulations and the differentiating in behavioral/non-behavioral models are the two major components. As described above, the acceptability of each model run is based upon user-defined model evaluation criteria, what BEVEN & BINLEY (1992) call likelihood measures. Behavioral parameter sets are assigned rescaled-likelihood weights (that sum to 1) which are used to form a cumulative distribution for the output variable of interest (STEDINGER *et al.*, 2008). According to the limits of acceptability defined above, 1479 models were selected from the ensemble. In order to obtain uncertainty ranges for 10-year annual means of relevant model output variables, the 5th and 95th percentile were used. Inner-annual variations of derived uncertainty ranges were analyzed to identify months with higher uncertainty.

Because model sensitivity is closely associated with model uncertainty, sensitivity analysis was conducted, in order to assess which parameters are most strongly affecting prediction uncertainty (e.g., IMAN & HELTON, 1988; SALTELLI *et al.*, 2004). *Regional sensitivity analysis (RSA)*, originally proposed by HORNBERGER & SPEAR (1981), is a common method used in hydrology to evaluate the effect of variations in model parameters on key model outputs of interest (e.g., SIEBER & UHLENBROOK, 2005; TANG *et al.*, 2007; WAGENER & KOLLAT, 2007). Because the precipitation-scaling factor was included in the Monte-Carlo simulations, the influence of variations in precipitation input on model output was also taken into account.

In this study, the RSA was performed using the sensitivity toolbox in OPTAS (FISCHER, 2013). The basic idea of the RSA method is to compare parameter distributions of behavioral/non-behavioral models (HORNBERGER & SPEAR, 1981). Differences between the parameter distributions indicate the sensitivity of the model response to changes in a parameter. According to FREER *et al.* (1996), parameters sets are ranked from best to worst regarding a chosen performance measure and then divided into ten equally sized groups. In this study, parameter sets generated by Monte-Carlo simulations were grouped according to their PBIAS values, considering all model runs with a PBIAS ≤ 50 % (6495 models). The cumulative distribution of each group is then plotted as the likelihood value versus the parameter values to assess the difference between the underlying distributions of the behavioral/non-behavioral models (WAGENER & KOLLAT, 2007) (see Figure 6.36). The larger the vertical distance between cumulative distribution functions, the higher is the impact of any given parameter on the model output, i.e. the model output is highly sensitive to changes in this parameter (WAGENER *et al.*, 2001). Within the sensitivity toolbox in OPTAS, parameters are linearly normalized based upon its sensitivity, in order to create a priority ranking of the parameters (FISCHER, 2013) (see Figure 6.35).

In a second step, a modified RSA approach was applied to identify parameters that affect relevant output variables such as land runoff, glacier runoff, etc. in terms of their mean annual estimates.

Similar to the study of RAGETTLI *et al.* (2013), the parameter sets generated by Monte-Carlo simulations were grouped in parameter sets that lead to more and, respectively, to less than mean annual model outputs. This modified RSA approach is particularly suitable to apply in ungauged catchments, because it avoids the need to rank the parameter sets based on a performance measure that requires observational data of model-output variables (RAGETTLI *et al.*, 2013). From this effort, parameters with a substantial impact on specific output variables were identified.

To examine relationships between climate factors and several hydrological components (lake evaporation, evapotranspiration, runoff from glaciers and non-glacierized areas) as well as lake-level variations, the sensitivity to changes in climate elements was analyzed. Only one climate variable was changed at a time while keeping the others untouched (air temperature, lake-surface water temperature: ±1°C; precipitation, wind speed, relative humidity, solar radiation: ±10%).

- ***Model Validation***

In order to evaluate the model capability in depicting real-world processes, validation tests need to be performed. Similar to the calibration process, data scarcity limited the establishment of rigorous and systematic validation tests. Lake-level observations of the Nam Co were compared with simulated lake levels for the period June through November of the years 2006 through 2010. Given the fact that water routing is not considered in the model, mean monthly, instead of daily, water-level simulations and measurements were used for the comparison.

For an independent assessment of the snow model capabilities, modeled *snow-water equivalent* (*SWE*) simulations of the Nam Co basin were compared with MODIS snow-cover data (see Sections 5.3.3, Section 6.2.2). Because MODIS data provide no information about the amount of water stored as snow (i.e. SWE), this comparison was only possible in an indirect way by comparing the *snow covered area fraction* (*SCAF*) derived from the model simulation and MODIS data. Any given spatial model unit was considered as snow-covered at days when the amount of SWE was larger than 1 mm. Then, SCAF within the Nam Co basin was calculated for each month and hydrological years (September through August).

Model Transfer

The model developed, evaluated and validated in the Nam Co basin was transferred to the Tangra Yumco, Paiku Co and Mapam Yumco catchments (see Figure 3.1). All calibration parameters (with the exception of the precipitation-scaling factor) were set to the same values given in Table 5.4. The precipitation-scaling factor was estimated as described for the Nam Co basin.

6 RESULTS

This Chapter presents the primary results of this study and is structured into three main sections:

- Section 6.1 describes findings achieved through hydro-meteorological time-series analysis and field-based soil analysis.

- Section 6.2 presents the primary results of the model application in the Nam Co basin. As previously mentioned, the Nam Co basin was selected as a case-study basin for the hydrological model development and evaluation.

- By transferring the model developed and evaluated in the Nam Co basin to three other selected ungauged basins (Tangra Yumco, Paiku Co and Mapam Yumco), Section 6.3 contains the comparative analysis of the model results of all four studied basins.

6.1 Analysis of Observational Data

Analyzing climate data from stations surrounding the Nam Co basin, Section 6.1.1 provides information on climate patterns and trends in this region. Observed lake-level fluctuations of the lake Nam Co are evaluated in Section 6.1.2.

6.1.1 Hydro-Meteorological Data Analysis

6.1.1.1 Spatiotemporally Varying Climate Conditions

Temperature

- The stations north of the Nyainqêntanglha mountain range indicate lower mean annual mean air-temperatures (MAAT < 0°C), mean annual maximum (MAAT$_{max}$ ~6°C) and minimum (MAAT$_{min}$ ~-6°C) air-temperatures than the stations in the southern area (MAAT ~5°C, MAAT$_{max}$ ~15°C, MAAT$_{min}$ ~0.5°C) (Figure 6.1, Figure 6.2, Table 6.1, Table 6.2). This is in accordance with the climate classification of LEBER *et al.* (1995), in which the region north of Nyainqêntanglha mountain range is characterized as a subfrigid zone (MAAT < 0°C) and the area south as a temperate zone (MAAT ~0-8°C).

- Mean air-temperature indicates a relatively high seasonal variability with temperature differences of ~15°C between winter and monsoon season (Table 6.1).

- Mean, maximum and minimum air-temperature increased on annual basis with ~0.5°C/decade over the 1981-2010 period (Table 6.3 - Table 6.5).

- Although for mean and maximum air-temperatures, the strongest increasing trends were found in post-monsoon and winter seasons (~0.5-1°C/decade), minimum air-temperature indicates considerably increasing trends in all seasons (Table 6.3 - Table 6.5).

The greater significance of the increasing trend in the colder seasons for mean and maximum air-temperature and in contrast in the warmer periods for minimum air-temperature support the suggestion of other authors (e.g., YOU *et al.*, 2008; YOU *et al.*, 2010a) that increasing mean air-temperature is highly determined by a strong upward trend in winter air-temperature and minimum (nighttime) air-temperature as well.

Figure 6.1: Spatial variation of MAAT and trend per decade (T) (based on Mann-Kendall trend test, see Section 5.1). Significant trend: * if trend at a = 0.05 level of significance, ** if trend at a = 0.01 level of significance, *** if trend at a = 0.001 level of significance).

Figure 6.2: Mean annual air-temperature (MAAT) versus elevation.

Table 6.1: Annual and seasonal means of mean air-temperature for meteorological stations in the Nam Co region.

Station (time period)	Mean air-temperature [°C]				
	Pre-monsoon	Monsoon	Post-monsoon	Winter	Annual
Xainxa (1981-2010)	0.2	8.9	-1.7	-8.1	0.7
Bangoin (1981-2010)	-0.3	8.1	-2.4	-8.7	0
Naquu (1981-2010)	-0.4	8.3	-3.0	-10.3	-0.4
Damxung (1981-2003)	2.0	9.9	-0.4	-7.6	1.8
Zetang (1981-2003)	9.3	15.4	7.2	0.9	8.9
Lhasa (1981-2010)	9.3	15.4	6.6	0.6	8.7
Nimu (1981-2003)	7.6	14.1	4.8	-1.6	7.0
Xigaze (1981-2010)	8.3	14.0	4.6	-1.3	7.2

Table 6.2: Annual and seasonal means of maximum and minimum air-temperature for meteorological stations in the Nam Co region.

Station (time period)	Mean max / min air-temperature [°C]				
	Pre-monsoon	Monsoon	Post-monsoon	Winter	Annual
Xainxa (1981-2010)	5.9 / -6.8	5.8 / 3.3	5.1 / -8.7	5.2 / -15.5	5.8 / -5.9
Bangoin (1981-2010)	5.6 / -6.9	5.5 / 2.5	4.4 / -9.0	4.3 / -14.9	5.3 / -6.1
Naquu (1981-2010)	4.9 / -8.3	4.9 / 2.5	1.9 / -10.1	1.2 / -16.7	5.6 / -7.1
Lhasa (1981-2010)	8.3 / 2.0	7.9 / 9.7	7.1 / -0.6	6.6 / -7.0	6.5 / 1.9
Xigaze (1981-2010)	9.6 / -0.5	9.3 / 7.8	8.8 / -4.9	8.6 / -11.3	8.6 / -1.2

Table 6.3: Annual and seasonal trends of mean air-temperature for meteorological stations in the Nam Co region.

Station (time period)	Mean air-temperature trend [°C/decade]				
	Pre-monsoon	Monsoon	Post-monsoon	Winter	Annual
Xainxa (1981-2010)	0.3	0.2	0.4	**0.5****	**0.4****
Bangoin (1981-2010)	0.4	0.2	**0.7***	**0.7****	**0.5*****
Naquu (1981-2010)	**0.5***	**0.4****	0.5	**0.8****	**0.6*****
Damxung (1981-2003)	0.2	0.1	**0.7****	0.4	0.3
Zetang (1981-2003)	0.2	**0.8***	**0.6***	**0.4***	0.4
Lhasa (1981-2010)	**0.5***	**0.4***	**0.8*****	**0.9*****	**0.7*****
Nimu (1981-2003)	0.4	-0.1	**0.5***	0.5	**0.3***
Xigaze (1981-2010)	**0.5***	0.2	**0.5***	**0.5***	**0.4*****

Table 6.4: Annual and seasonal trends of maximum air-temperature for meteorological stations in the Nam Co region.

Station (time period)	Max air-temperature trend [°C/decade]				
	Pre-monsoon	Monsoon	Post-monsoon	Winter	Annual
Xainxa (1981-2010)	**0.5***	0.3	0.6	**0.8****	**0.6*****
Bangoin (1981-2010)	0.5	0.2	0.5	**0.8***	**0.5*****
Naquu (1981-2010)	0.5	0.2	0.4	**0.9***	**0.5*****
Lhasa (1981-2010)	0.4	0.2	0.5	**1.1****	**0.6*****
Xigaze (1981-2010)	0.5	0.1	**0.5***	**0.8****	**0.5*****

Notes: *Mann-Kendall trend test was used for trend detection (see Section 5.1). Significant trend:* ***** *if trend at a = 0.05 level of significance,* ****** *if trend at a = 0.01 level of significance,* ******* *if trend at a = 0.001 level of significance.*

Table 6.5: Annual and seasonal trends of minimum air-temperature for meteorological stations in the Nam Co region.

Station (time period)	Min air-temperature trend [°C/decade]				
	Pre-monsoon	Monsoon	Post-monsoon	Winter	Annual
Xainxa (1981-2010)	0.2	**0.3****	**0.5***	0.3	**0.3***
Bangoin (1981-2010)	0.4	**0.4****	**0.6***	0.3	**0.5*****
Naquu (1981-2010)	**0.7*****	**0.8*****	**0.6*****	-0.4*	**0.5*****
Lhasa (1981-2010)	**1.1*****	**0.7*****	**1.3*****	**1.4*****	**1.1*****
Xigaze (1981-2010)	**0.5*****	**0.5****	**0.6*****	0.5	**0.5*****

Notes: *Mann-Kendall trend test was used for trend detection (see Section 5.1). Significant trend: ***** if trend at a = 0.05 level of significance, ****** if trend at a = 0.01 level of significance, ******* if trend at a = 0.001 level of significance.*

Precipitation

- The eastern and southern areas are characterized by semi-moist conditions with mean annual precipitation (MAP) of 400-500 mm; whereas, the upper north western part with semi-arid climate (MAP ~300-400 mm) is located in a 'rain shadow' of the southwest-northeast striking Nyainqêntanglha mountain range, which acts as a barrier when the monsoon rains coming from south advance to the north (Figure 6.3, Table 6.6).

- Precipitation varies seasonally with between 80-90 % of the total annual precipitation occurring during the monsoon season (June-September) (Table 6.6).

- Significantly increasing trends (on average 50 mm/decade or 10 % of the annual total) were found. Significant annual trends were detected at three stations (Table 6.7).

- Increasing absolute trend rates are evident in the monsoon period (~40 mm/decade, 10 %), but in relative terms trends are considerably higher in the pre-monsoon season (~10 mm/decade, 20 %) (Table 6.7).
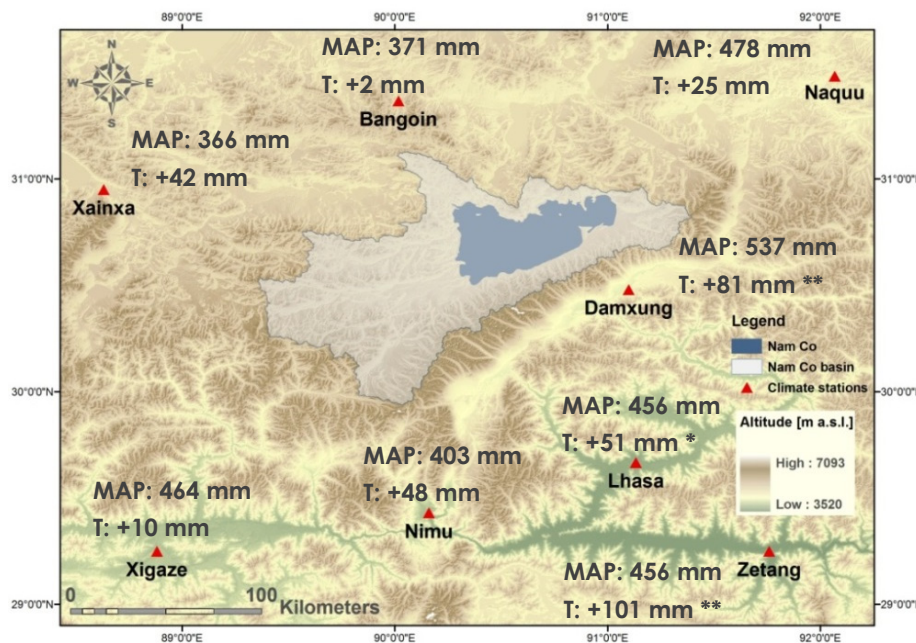
Figure 6.3: Spatial variation of mean annual precipitation (MAP) and trend per decade (T) (based on Mann-Kendall trend test, see Section 5.1). Significant trend: * if trend at a = 0.05 level of significance, ** if trend at a = 0.01 level of significance, *** if trend at a = 0.001 level of significance).

Table 6.6: Annual and seasonal means of precipitation for meteorological stations in the Nam Co region.

Station (time period)	Mean precipitation [mm]				
	Pre-monsoon	Monsoon	Post-monsoon	Winter	Annual
Xainxa (1981-2010)	34	311	15	6	366
Bangoin (1981-2010)	36	310	17	7	371
Naqu (1981-2010)	67	372	28	11	478
Damxung (1981-2003)	62	442	23	11	537
Zetang (1981-2003)	54	391	10	2	456
Lhasa (1981-2010)	44	399	9	4	456
Nimu (1981-2003)	33	360	8	2	403
Xigaze (1981-2010)	42	414	7	1	464

Table 6.7: Annual and seasonal trends of precipitation for meteorological stations in the Nam Co region.

Station (time period)	Precipitation trend per decade abs. trend in mm (rel. trend in %)				
	Pre-monsoon	Monsoon	Post-monsoon	Winter	Annual
Xainxa (1981-2010)	11 (33)	34 (11)	0.1 (1)	0.7 (12)	42 (11)
Bangoin (1981-2010)	**11 (31)***	-3 (-1)	-0.9 (-5)	0.4 (6)	2 (0.5)
Naqu (1981-2010)	9 (13)	13 (3)	4 (13)	0.6 (6)	25 (5)
Damxung (1981-2003)	18 (30)	**61 (14)***	7 (31)	0.7 (7)	**81 (15)****
Zetang (1981-2003)	12 (21)	**82 (21)***	1 (10)	0 (0)	**101 (22)****
Lhasa (1981-2010)	**13 (29)***	40 (10)	2 (17)	0 (0)	**51 (11)***
Nimu (1981-2003)	4 (11)	46 (13)	0.6 (7)	-0.7 (-37)	48 (12)
Xigaze (1981-2010)	5 (13)	30 (7)	0 (0)	0 (0)	10 (2)

Notes: *Mann-Kendall trend test was used for trend detection (see Section 5.1). Significant trend:* ***** *if trend at a = 0.05 level of significance,* ****** *if trend at a = 0.01 level of significance,* ******* *if trend at a = 0.001 level of significance.*

Wind speed

- The stations in the upper north western part of the region surrounding the Nam Co basin are characterized by higher mean annual wind speeds (~4 m/s) as compared to the stations in the lower southern part of this general region (~2 m/s) (Figure 6.4).

- Seasonal variations with generally higher wind speeds were found during winter and pre-monsoon season (Table 6.8).

- Considerably decreasing trends at all stations were detected for the entire year and for all seasons (on average -0.16 m/s per decade or -6 % respective long-term mean) (Table 6.9). The negative trends are significant at a noticeably high significance level (up to 99.9 %) at all stations (except for Damxung) (Table 6.9). The greatest absolute decreases occurred in the pre-monsoon season, but the highest relative values were found for the monsoon period (Table 6.9).
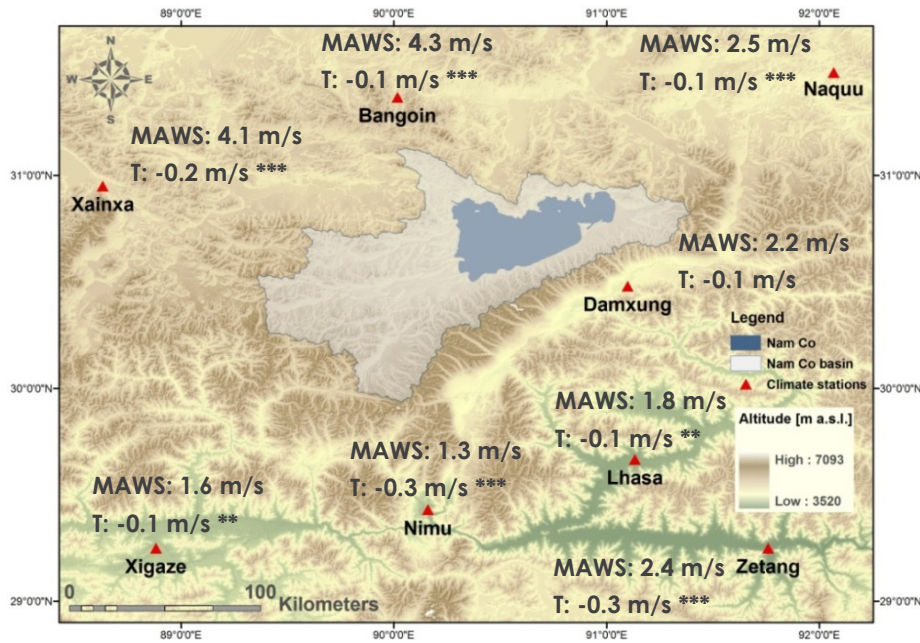
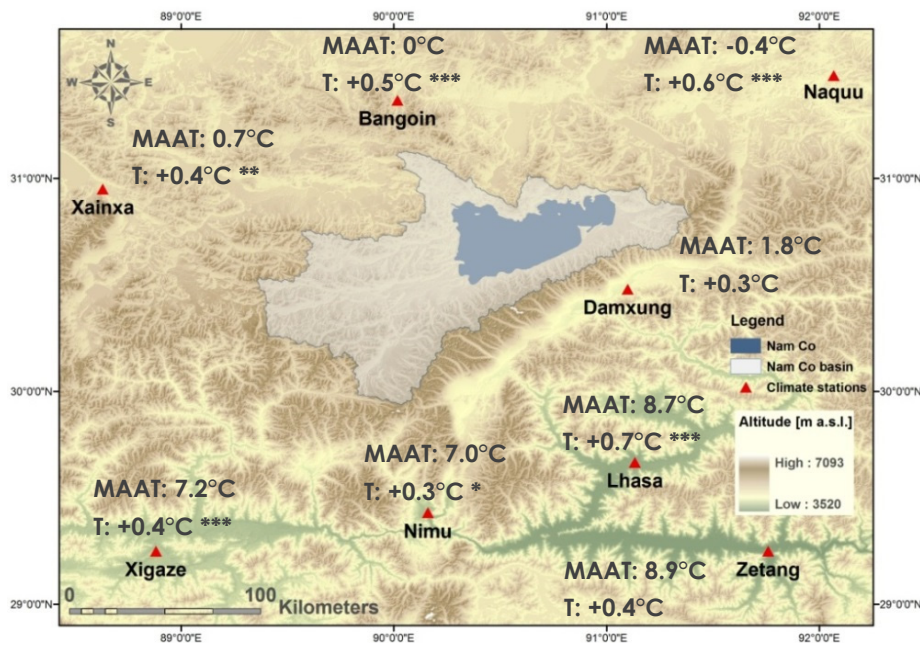*Figure 6.4:* *Spatial variation of mean annual wind speed (MAWS) and trend per decade (T) (based on Mann-Kendall trend test, see Section 5.1). Significant trend: * if trend at a = 0.05 level of significance, ** if trend at a = 0.01 level of significance, *** if trend at a = 0.001 level of significance).*
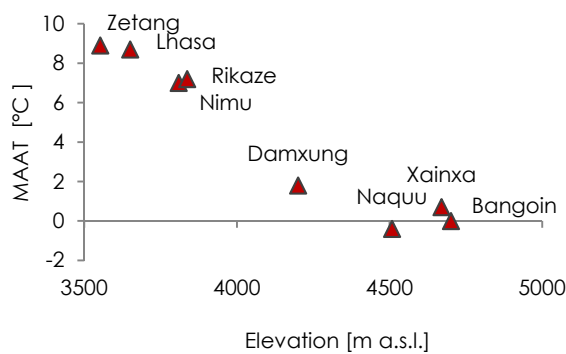
Table 6.8: Annual and seasonal means of wind speed for meteorological stations in the Nam Co region.

Station (time period)	Mean wind speed [m/s]				
	Pre-monsoon	Monsoon	Post-monsoon	Winter	Annual
Xainxa (1981-2010)	4.8	3.1	3.4	5.0	4.1
Bangoin (1981-2010)	4.9	3.4	3.9	5.0	4.3
Naquu (1981-2010)	3.2	2.2	2.0	2.6	2.5
Damxung (1981-2003)	2.7	2.1	1.8	2.1	2.2
Zetang (1981-2003)	3.0	2.3	2.1	2.3	2.4
Lhasa (1981-2010)	1.7	1.5	2.2	1.9	1.8
Nimu (1981-2003)	1.9	1.0	0.9	1.2	1.3
Xigaze (1981-2010)	2.3	1.2	1.1	1.6	1.6

Table 6.9: Annual and seasonal trend of wind speed for meteorological stations in the Nam Co region.

Station (time period)	Wind trend per decade abs. trend in m/s (rel. trend in %)				
	Pre-monsoon	Monsoon	Post-monsoon	Winter	Annual
Xainxa (1981-2010)	**-0.2 (-4)*****	**-0.2 (-5)*****	**-0.1 (-3)***	**-0.2 (-3)****	**-0.2 (-5)*****
Bangoin (1981-2010)	**-0.1 (-2)*****	**-0.1 (-3)*****	**-0.1 (-2)***	**-0.1 (-3)***	**-0.1 (-3)*****
Naquu (1981-2010)	**-0.2 (-6)*****	**-0.1 (-4)*****	**-0.1 (-3)****	**-0.1 (-4)****	**-0.1 (5)*****
Damxung (1981-2003)	-0.1 (-4)	-0.1 (-4)	-0.1 (-5)	-0.1 (-6)	-0.1 (-4)
Zetang (1981-2003)	**-0.4 (-13)*****	**-0.3 (-13)*****	**-0.3 (-14)*****	**-0.3 (-11)*****	**-0.3 (-13)*****
Lhasa (1981-2010)	-0.03 (-2)	**-0.03 (-2)***	**-0.1 (-4)*****	**-0.1 (-5)*****	**-0.1 (-5)****
Nimu (1981-2003)	**-0.3 (-16)*****	**-0.3 (-30)*****	**-0.2 (-24)*****	**-0.2 (-18)*****	**-0.3 (-23)*****
Xigaze (1981-2010)	**-0.1 (-4)*****	-0.03 (-3)	-0.01 (-0.6)	**-0.1 (-4)****	**-0.1 (-6)****

Notes: *Mann-Kendall trend test was used for trend detection (see Section 5.1). Significant trend:* ***** *if trend at a = 0.05 level of significance,* ****** *if trend at a = 0.01 level of significance,* ******* *if trend at a = 0.001 level of significance.*

6.1.1.2 *Lake-Level Fluctuations*

Lake-level observations from 2006 through 2010 (Figure 6.5) indicate a distinct seasonal dynamic with continuously increasing lake-levels during the months of June through September (caused by runoff from glaciers and non-glacierized areas), a lake-level peak during the months of September and October, and decreasing lake-levels in the dry season (primarily caused by lake evaporation). During the months of November and December, the Nam Co begins to freeze and is not completely ice free until April or May. The late freeze-up date is related to the large water volume of the Nam Co.

Between June and November, the monthly-average lake level increased on average by approximately 0.36 m during the period 2006-2010. The monthly-average lake-level increase during the June-November period in the year 2008 (0.70 m) was substantially higher than in the others years (2006: 0.23 m, 2007: 0.29 m, 2009: 0.17 m, 2010: 0.41 m) (Figure 6.5).
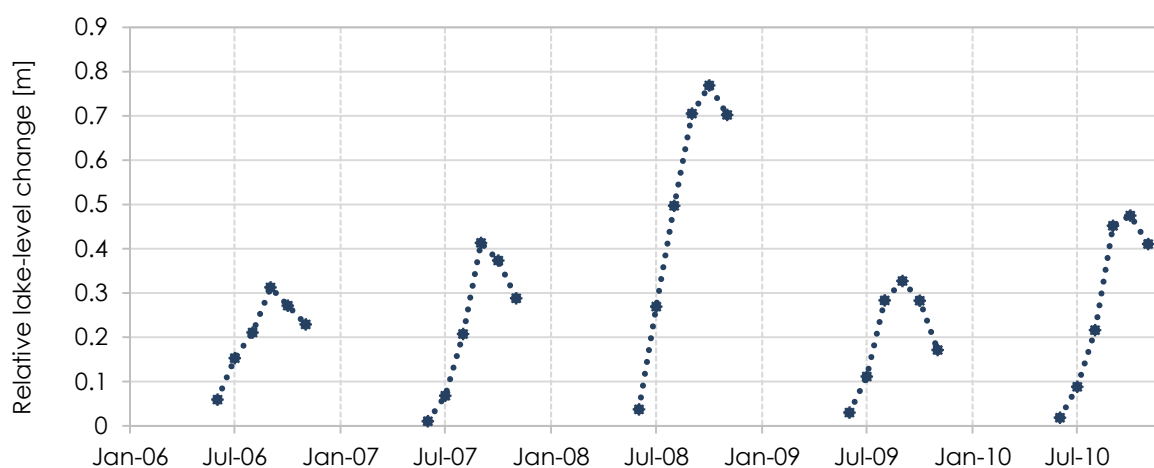
Figure 6.5: Monhtly-average lake levels of Nam Co for the June-November period of the years 2006-2010. Note that for the calculation of monthly-average lake levels, the lake-level value of the 1st of June was set to zero in each year and the subsequent values were adjusted accordingly to make the lake-level changes during the June-November period of the years 2006-2010 comparable.

6.1.2 Soil Analysis

- **Soil Types**

In order to identify dominant soil types in the study catchment Nam Co and to provide information on soil characteristics which are important for soil parameterization for the hydrological modeling, soil analyses were conducted based upon own field surveys. Table 6.10 summarizes information for the investigated soil sites, including location, depth, land form characteristics, land cover and soil type. Due to the limited logistics of access, only soils located south of the Nam Co at elevations between 4730-4950 m a.s.l. were analyzed.

With respect to the soil texture, the soils investigated in the field are primarily composed of medium (0.002-0.05 mm in diameter) and large (0.05-2 mm in diameter) particles (silt and sand, respectively). The low clay content is an indicator for poor weathering processes applicable to soils development in the study area. Depending on landscape positions, land cover and water

saturation, soil classes alternate between *Cambisols* which are predominant on flat-to-moderate slopes, very poorly developed soils belonging to the *Leptosol* soil class in steeper terrain and *Gleysol* at wetland sites. A humic top soil (*Ah*) with deep distribution of soil organic matter (thickness up to a couple of decimeters) is a typical pedological feature, because the decomposition of the biomass is slow due to the low air temperatures over the TP.

Figure 6.6 indicates soil profiles for a wetland site covered by *Kobresia schoenoides* (No. 1 in Table 6.10) and an alpine meadow site covered by *Kobresia pygmaea* (No. 2 in Table 6.10). The profiles were taken southeast of the Nam Co at a relatively slight declined foot-slope. Both the alpine meadow and the wetland site exhibit a humus-rich top soil with black or dark grey color. These so-called turf horizons are characterized by a high enrichment of root biomass and a considerable firmness. According to KAISER (2007), the *Kobresia pygmaea* turfs can be classified as *'Rhizomulls'* or *'rhizic Mulls'*; whereas, the *Kobresia schoenoides* turfs can be classified as *'Rhizo-Hydromors'* or *'rhizic Moor(e)'*. These turf horizons are named *'Afe'* and *'Hfe'* (suffix from *fe* from *felty*; KAISER, 2007), respectively, for *Kobresia pygmaea* and *Kobresia schoenoides* sites. The topsoil horizon at the *Kobresia schoenoides* site (No. 1) indicates a higher amount of rhizogenic organic matter and a higher thickness (*Hfe* ~30 cm) compared with the *Kobresia pygmaea* site (*Afe* ~15 cm). Coarse roots with a diameter > 2 mm are dominant at the *Kobresia schoenoides* site; whereas, fine roots (< 2 mm) prevail at the *Kobresia pygmaea* site. Besides low temperatures, water saturation is an additional factor hindering the decomposition of roots at wet *Kobresia schoenoides* sites.

The soil type at the *Kobresia pygmaea* site (No. 2) can be classified as *Humic Cambisol*, due to the high amount of organic matter within the upper 50 cm soil zone and the brownish B-horizon (*Bw*). The soil profile at the wetland site exhibited a varying degree of wetness and color, indicating that the soil has undergone prolonged periods of intermittent or continuous saturation with water. Changes in the degree of water saturation (i.e. water logging or drainage) lead to alternating reducing and oxidizing conditions, which in turn strongly influences the color of the soil. For instance, the mottled greyish-blue color in the subsoil horizons (Figure 6.6) indicates the presence of ferrous (*Fe++*) iron, which is typical for intermittently wet, so-called hydromorphic soils. Because of the gleyic properties (properties associated with prolonged wetness) in the B-horizon (*Bg*), the soil at the wetland site can be classified as *Gleysol*.

Table 6.10: Location of soils, land form and cover characteristics, and soil type surveyed during field campaigns.

Site No.	Type	Depth [cm]	Long (E)	Lat (N)	Altitude [m a.s.l.]	Aspect	Slope	Land cover	Soil type
1	soil pit	100	91.001	30.719	4817	N	shallow	Wetland (K. schoenoides)	Gleysol
2	soil pit	100	91.002	30.719	4817	N	shallow	Grassland (K. pygmaea)	Cambisol
3	soil pit	100	91.001	30.718	4823	N	moderate	Grassland (K. pygmaea)	Cambisol
5	soil pit	100	91.001	30.720	4813	N	shallow	Grassland (K. pygmaea)	Cambisol
4	soil core	70	90.969	30.777	4739	N	shallow	Grassland (K. pygmaea)	Cambisol
6	soil core	75	90.584	30.543	4933	W	shallow	Grassland (K. pygmaea)	Cambisol
7	soil core	60	90.629	30.563	4462	S	steep	Grassland (K. pygmaea)	Leptosol
8	soil core	40	90.631	30.562	4800	S	steep	Rock substrat	Leptosol
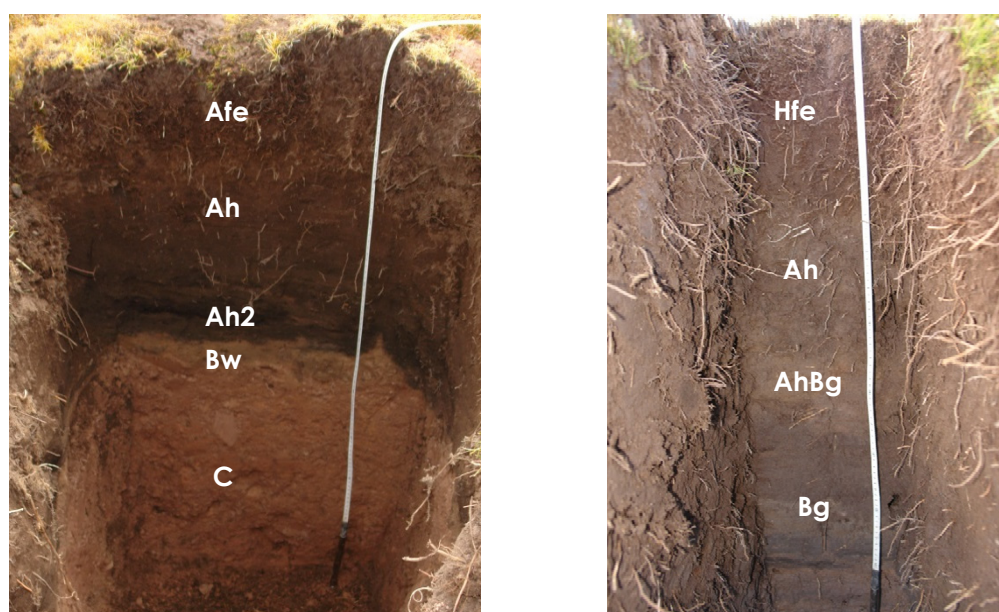
Figure 6.6:   Characteristic soil profiles of a grassland site covered with Kobresia pygmaea (No. 2 in Table 6.10) (left) and a wetland site covered with Kobresia schoenoides (No. 1 in Table 6.10) (right). Length of the ruler = 100 cm.

- **Soil Water**

As described in Section 5.3.1, soil sensors were installed to monitor soil moisture and temperature at depths of 15, 30, 50 and 80 cm on the east side of the lake Nam Co in a selected wetland site. The location of the four soil measurement stations (1 to 4) in Table 6.11 equal to the locations of the soil profiles 1 to 4 given in Table 6.10. As previously mentioned in Section 5.3.1, only data covering the period October 2009 through the beginning of June 2010 could be used for analysis due to unpredictable problems with the data-transmission.

Figure 6.7 - Figure 6.10 indicate daily soil moisture and temperature variations for the distinct soil layers at the four locations. Please note that the water content measured within frozen soils during the winter months is a mixture of the remaining liquid water content in the soil and the drastically reduced signal due to the phase change (liquid to solid) during the freezing process. For spatial-temporal analysis of the freeze-thaw cycle, the first freezing and thawing dates were identified at selected sites and the duration of the freezing period was estimated for four distinct layers at each site (Table 6.11).

Major findings of spatial-temporal variations in the soil freeze-thaw cycle and associated soil moisture content during October 2009 through the beginning of June 2010 are summarized as follows:

- The first freeze and thaw for the surface layers at the four sites were from early-to-mid November through late March/early April, respectively. Indeed, the first freezing and thawing dates became later in time with increase of the soil layer depth.

- The freezing and thawing process of all soil layers took place between a period of 40 to 50 days. However, the two deepest soil layers at the location within the wetland

remained frozen in early June, indicating that wetland areas respond slower to the temperature signal than the surroundings. The duration of the freezing period varied between 130 and 150 days and was more than 150 days at the bottom soil layers within the wetland site.

- The magnitude of soil temperature among distinct soil horizons within the wetland was lower compared to the non-wetland sites, indicating differences in the soil-heat balance across different ecosystems. Further evaluation of the spatial differences of the soil-heat balance was beyond the scope of this study.

- The liquid soil-water content of each layer decreased abruptly when the soil was becoming frozen in November, it remained fairly stable during the winter months, and it increased abruptly when the soil thawing process started. The sharp increase of the soil-moisture content in spring is associated with percolating water from snowmelt and increasing occurrence of precipitation events.

- During the non-frozen stage (October and late May/early June) the near-surface soil-water content was relatively higher (maximum values around 0.2 m³ m⁻³ and 0.4 m³ m⁻³ in the upper layers at the non-wetland sites and the wetland site, respectively) than during the frozen stage (November through April; minimum daily values around 0.07 m³ m⁻³ and 0.14 m³ m⁻³ at the non-wetland sites and the wetland site, respectively).

- With respect to variations within the several soil layers, the soil-moisture content in the non-frozen stage was relatively higher in the upper soil layers than in the bottom soil layers. The small particles (silt and clay) of the finer-textured near-surface soils fit more closely together compared to sandy soils, leading to numerous small pores (hence, high porosity). Moreover, finer particles have a large surface area which facilitates the adsorption of water. As a result of the high porosity and the large surface area more water can be held (high field capacity). In addition to clay, the high organic matter content in the topsoil acts as a further agent that coheres and cements individual soil particles together. Thus, the higher the organic matter, the higher the amount of water content held in the soil (i.e. field capacity) (BONAN, 2008). The low content of organic matter and high fraction of sand particles in the bottom soil layers suggest that the lower part of the profile can be quickly recharged with soil moisture, but their capacity to hold water is relatively low.

Soil moisture data (August 2010 through September 2011) from the *Soil Moisture/Temperature Monitoring Network* (*SMTMN*) (ZHAO *et al.*, 2013), which was established immediately adjacent to the northeast of the Nam Co basin in a grassland site, indicate similar soil-moisture dynamics. As detected in the Nam Co basin, the daily water content was < 0.1 m³ m⁻³ during the 'stable' freezing period (December-March) and increased up to values around 0.2 m³ m⁻³ during the thawing period (April-May). Due to snowmelt and increasing precipitation in spring, the soil moisture increased rapidly up to values around 0.3 m³ m⁻³ in early June. The highest soil-moisture content, with values around 0.4 m³ m⁻³, occurred in late July (ZHAO *et al.*, 2013). A higher water content in the topsoil than in the bottom soil layers was also observed in the study of ZHAO *et al.* (2013) as well as at another alpine meadow site in the central TP (YANG *et al.*, 2009).
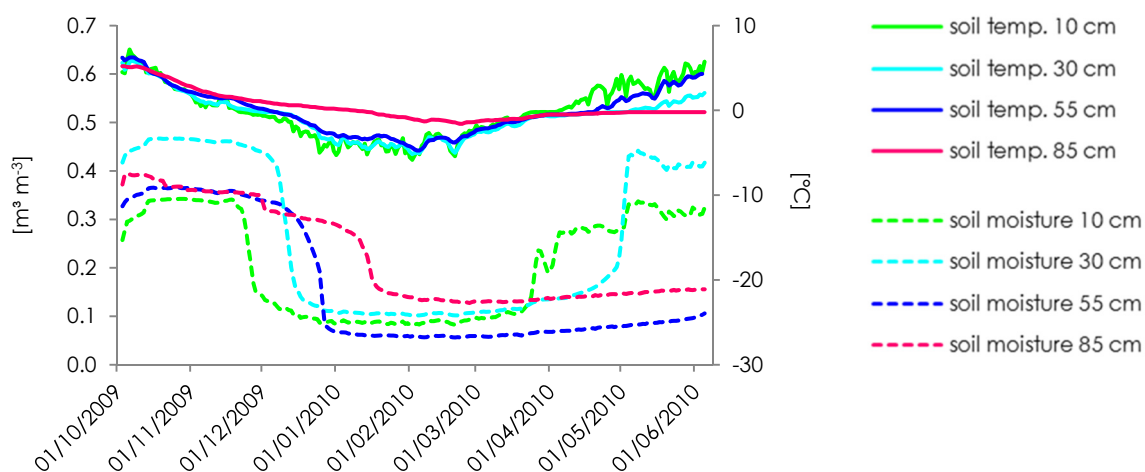
Figure 6.7: Daily soil moisture and temperature variations for distinct soil layers at site No. 1 (wetland).
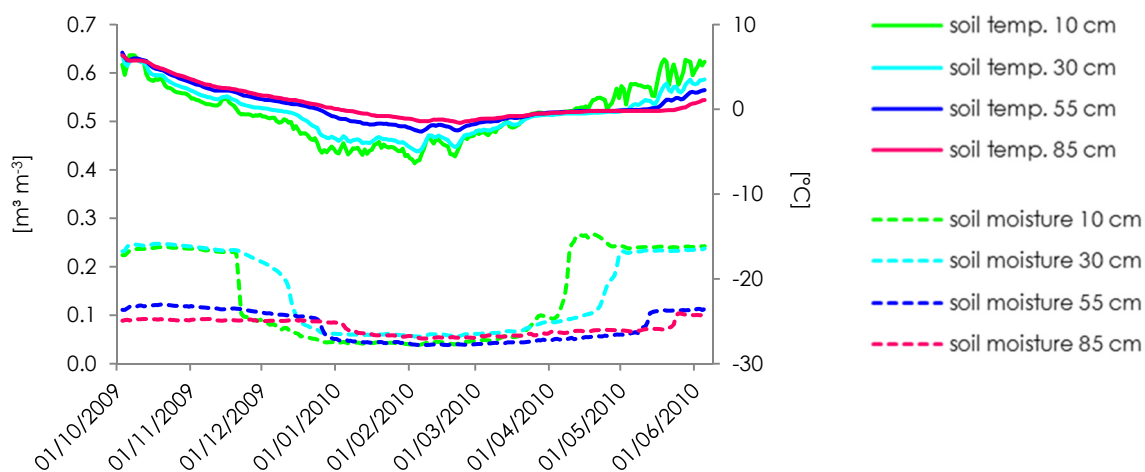
Figure 6.8: Daily soil moisture and temperature variations for distinct soil layers at site No. 2 (grassland).
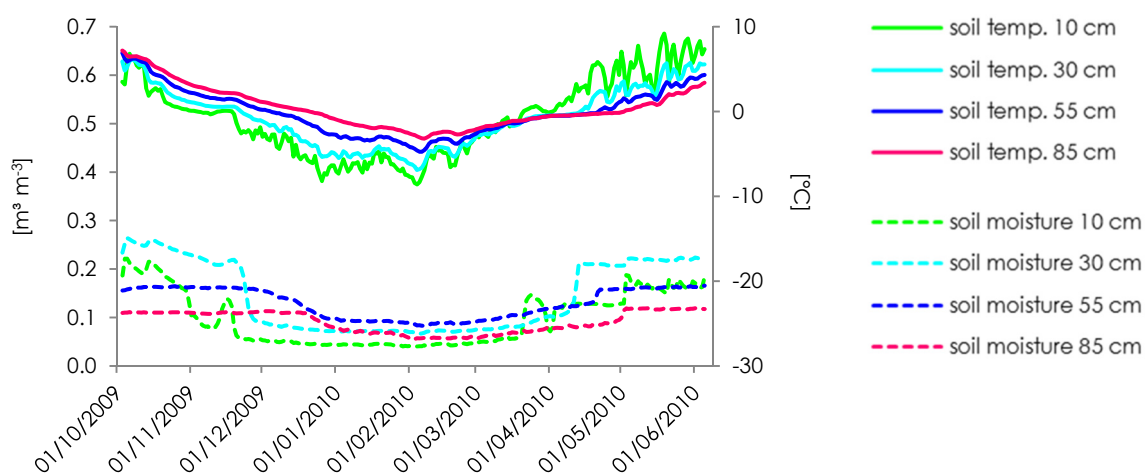
Figure 6.9: Daily soil moisture and temperature variations for distinct soil layers at site No. 3 (grassland).
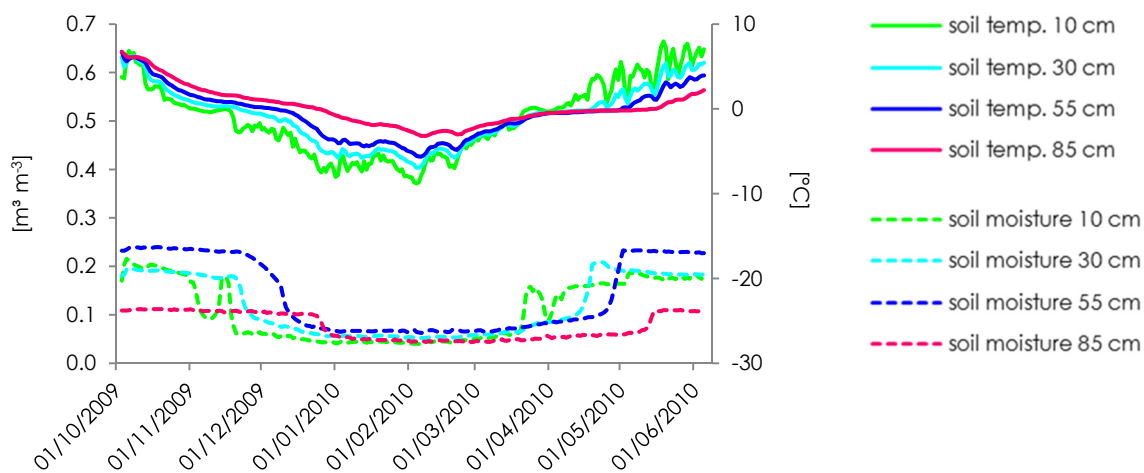
Figure 6.10: Daily soil moisture and temperature variations for distinct soil layers at site No. 4 (grassland).

Table 6.11: *Summary of initial freezing and thawing dates, duration of freezing period and mean daily water content during the frozen and non-frozen stages for soil layers in different depths at four different sites. The locations of the sites 1-4 correspond to the locations of the soil profiles 1-4 given in Table 6.10.*

No.	Depth [cm]	First freezing date [<0°C]	First thawing date [>0°C]	Freezing period [Number of days]	Mean daily water content during the frozen stage [m³ m⁻³]	Mean daily water content during the non-frozen stage [m³ m⁻³]
	10	21-Nov-09	6-Apr-10	135	0.11	0.31
	30	26-Nov-09	6-May-10	160	0.16	0.44
1	55	11-Dec-09	not before 6-Jun-10	>176	0.09	0.35
	85	9-Jan-10	not before 6-Jun-10	>147	0.15	0.34
	10	21-Nov-09	12-Apr-10	141	0.07	0.24
2	30	5-Dec-09	4-May-10	149	0.09	0.23
	55	25-Dec-09	11-May-10	136	0.05	0.17
	85	3-Jan-10	25-May-10	141	0.06	0.16
	10	4-Nov-09	21-Mar-10	136	0.05	0.16
3	30	22-Nov-09	14-Apr-10	142	0.08	0.23
	55	5-Dec-09	22-Apr-10	137	0.10	0.16
	85	21-Dec-09	3-May-10	132	0.07	0.11
	10	3-Nov-09	4-Apr-10	151	0.07	0.18
4	30	22-Nov-09	19-Apr-10	147	0.07	0.19
	55	7-Dec-09	2-May-10	145	0.08	0.21
	85	26-Dec-09	14-May-10	138	0.05	0.15

6.2   Hydrological Modeling – Case Study Basin Nam Co

This section contains the major results of the hydrological-model application in the Nam Co basin. Section 6.2.1 focuses on spatiotemporal patterns of hydro-climatological components and the quantitative assessment of water-balance components. The results of the uncertainty and sensitivity analysis are presented in Section 6.2.2.

6.2.1   Modeling Results

6.2.1.1   *Temperature*

Figure 6.11 illustrates the basin-average mean annual air temperature (MAAT) of the individual years from 2001 through 2010 and the 10-year average annual and seasonal air temperatures. The MAAT in the Nam Co basin was -3.5°C for the 2001-2010 period. The years in the second half of the decade were warmer compared to the first half, which is mostly related to higher winter temperatures during the latter period (Figure 6.11).
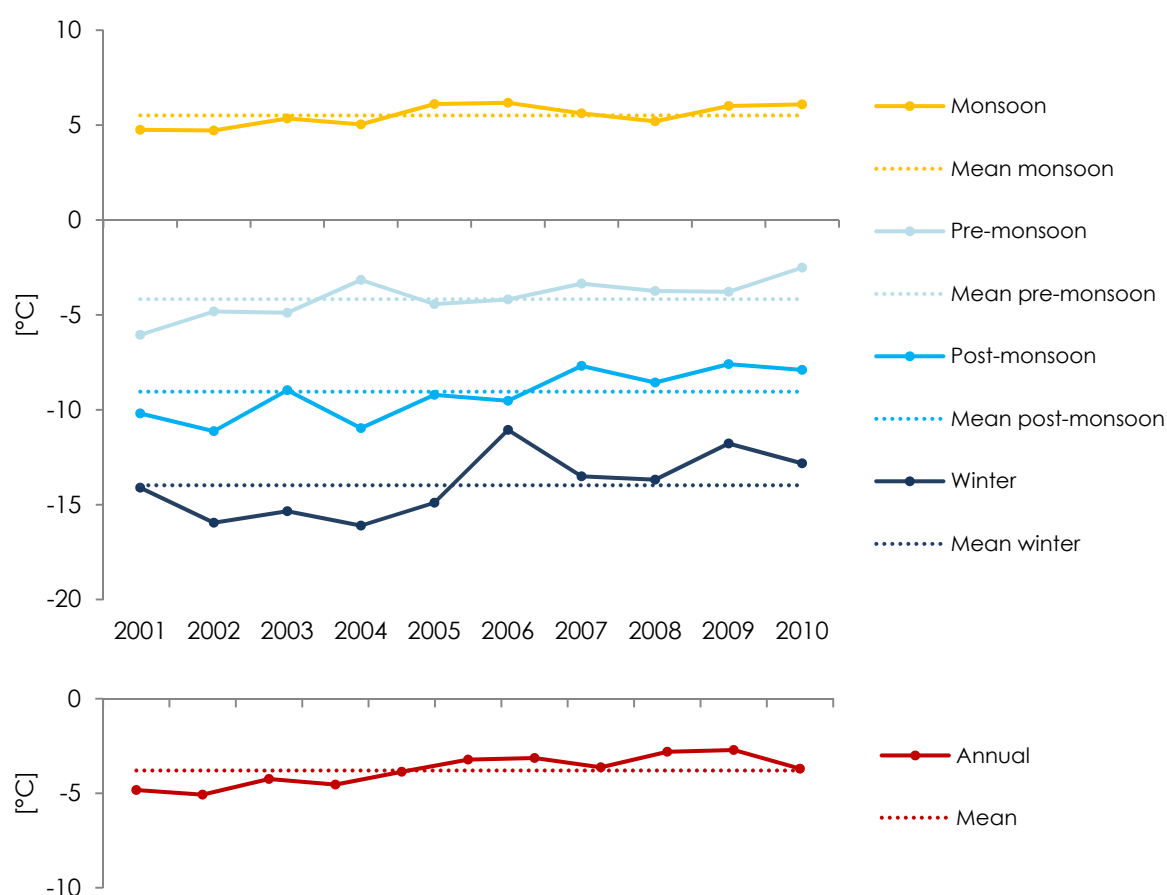
Figure 6.11: Annual and 10-year mean temperature for the entire year and several seasons (winter – December-February, pre-monsoon – March-May, monsoon – June-September, post-monsoon – October-November) averaged over the Nam Co basin.

The warmest month was July, with a spatially averaged MAAT of 7°C, and the coldest month was January, with an average MAAT of -15°C (Figure 6.12). The monthly MAAT was below 0°C for a seven-month period (October through April).
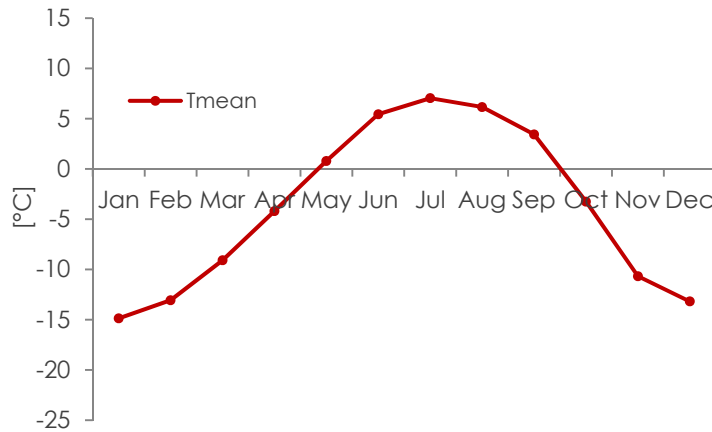
Figure 6.12: Mean monthly mean air temperature averaged over the Nam Co basin.

In order to evaluate the relationship between altitude and air temperature, annual and seasonal *temperature-lapse rates* (*TLRs*) were derived from the regression between mean air-temperature and elevation (Figure 6.13, Figure 6.14). The elevation and corresponding MAAT of the 86 HAR10 data points within the Nam Co ranged between 4736 m a.s.l. and 5630 m a.s.l., and -1.1°C and -7.9°C, respectively (Figure 6.13). Figure 6.13 indicates a linear relationship between MAAT and elevation ($r^2 = 0.94$). The basin-wide annual TLR (-0.64°C/100m) was nearly equivalent to the free-air moist adiabatic lapse rate (-0.65°C/100m) (BARRY & CHORLEY, 2003).
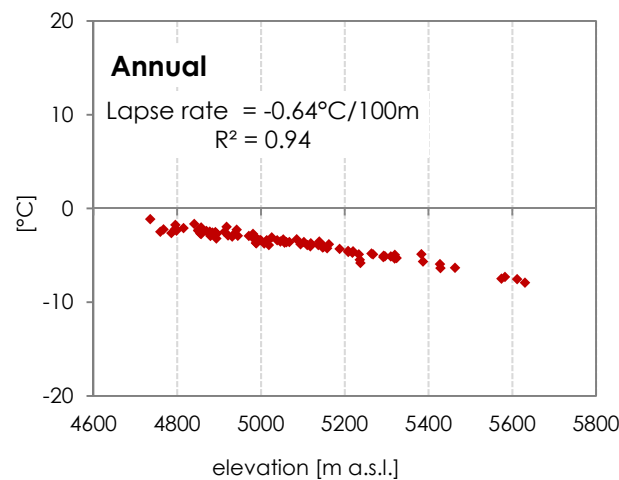
Figure 6.13: Annual TLR for the 2001-2010 period, derived from 86 HAR10 data points within the Nam Co basin.

The pre-monsoon season (March-May) exhibited the highest TLR (-0.75°C/100m). The TLR peak in the pre-monsoon period is consistent with the results of KATTEL *et al.* (2012). The high pre-monsoon TLR is related to strong dry convection. The lowest TLR (-0.52°C/100m) occurred in the winter months (December-February). The low correlation coefficient in the winter season ($r^2 = 0.77$) indicates the occurrence of temperature inversions which may adversely affect the temperature-elevation relationship. Analyzing TLRs at a daily time step, relatively warmer conditions were found at HAR10 data points in higher elevations compared to lower elevations for numerous days during the cold months. Fewer than half of the days of the winter season indicated a TLR with $R^2 > 0.75$; this relationship was used as a threshold for the elevation correction during the regionalization (Figure 6.15). The detected inverted TLRs support the assumption of occurrence of temperature inversions during the winter months in the Nam Co basin. Cold air sinks and displaces warmer air in the valleys and flat terrain areas, resulting in a stable stratification and a temperature inversion. Observations of 11 automatic weather stations, which were set up from 4300 to 5530 m a.s.l. on a south slope of Mount Nyainqêntanglha near Damxung, indicated that temperature inversions during winter months primarily occur under relatively dry conditions when skies are clear and radiative cooling is intense (DU *et al.*, 2007).
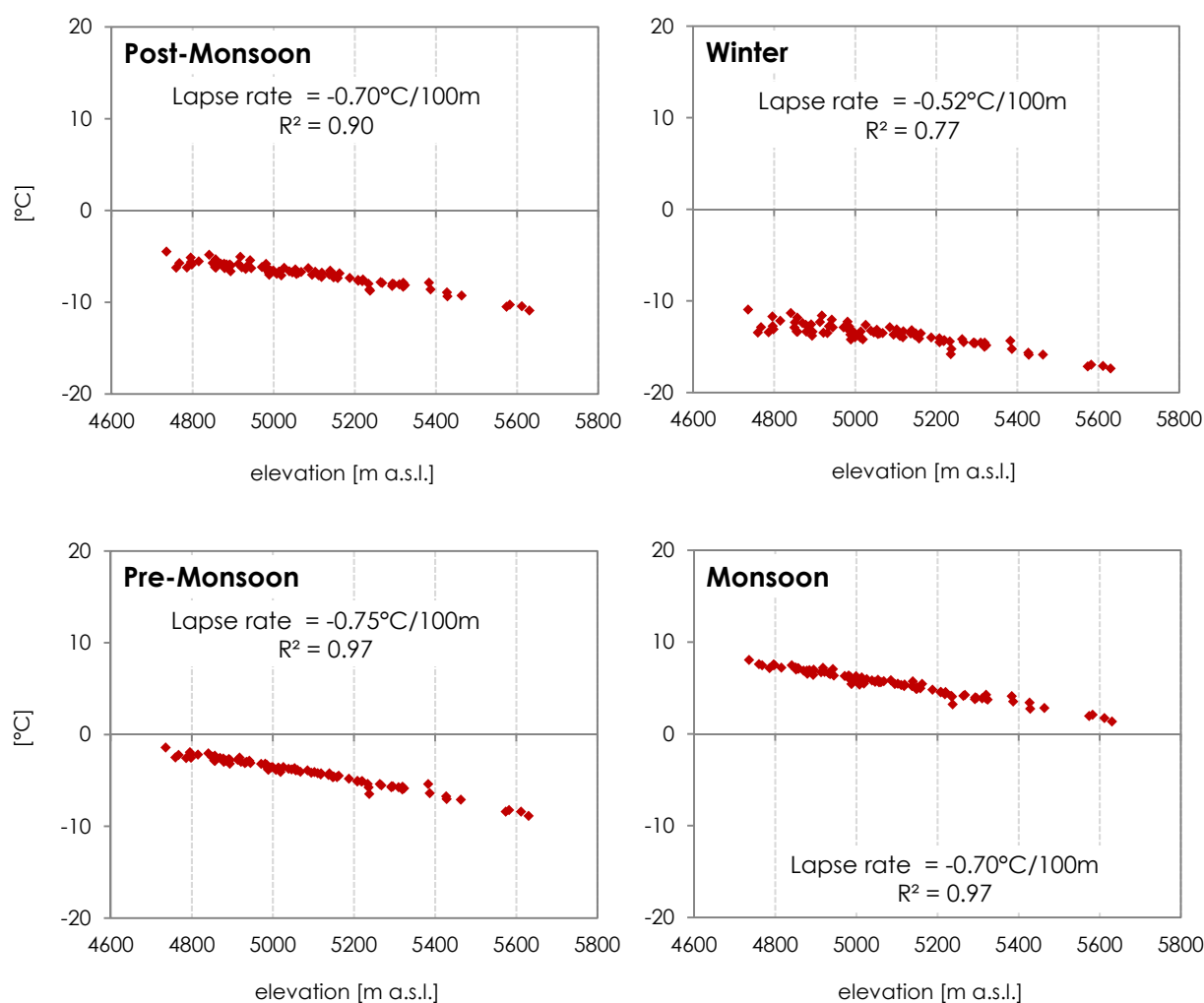
Figure 6.14: Seasonal TLRs for the 2001-2010 period, derived from 86 HAR10 data points within the Nam Co basin.
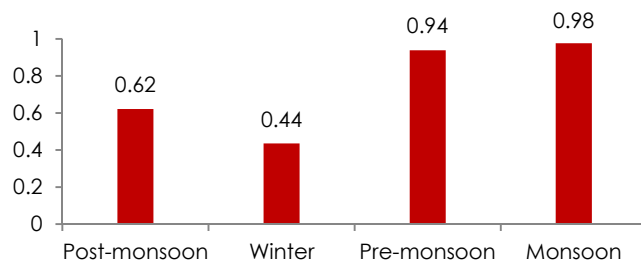
Figure 6.15: Relative frequency of daily TLRs with R² > 0.75 (threshold used for elevation correction) for several seasons.

6.2.1.2   Precipitation

The simulated annual precipitation varied between 270 mm (2005, 2006) and 550 mm (2008), with an average of ~400 mm for the 10-year period (Figure 6.16). In the relatively dry years 2005 and 2006, the precipitation totals decreased by 31 % related to the 10-year average. In the extreme wet year 2008, the Nam Co basin received about 36 % more precipitation than the 10-year average.
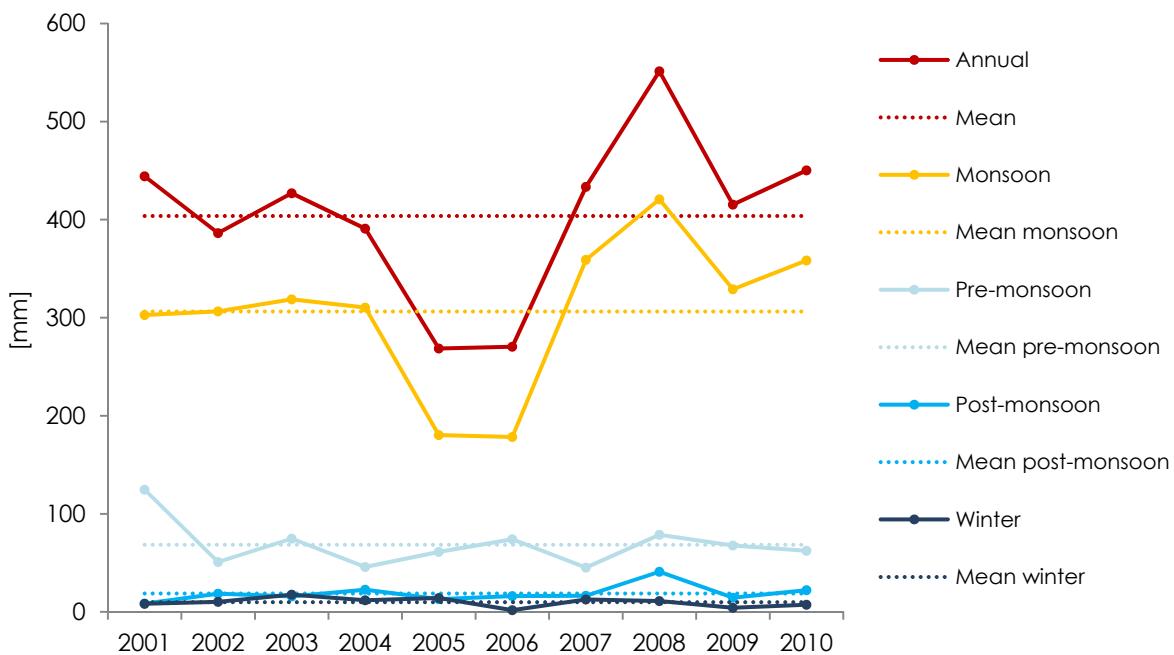
Figure 6.16: Annual and 10-year mean precipitation for the entire year and several seasons (winter – December-February, pre-monsoon – March-May, monsoon – June-September, post-monsoon – October-November) averaged over the Nam Co basin.

As shown in Figure 6.17, HAR10 reproduces the seasonal variability of precipitation, with 80 % of the annual precipitation occurring during June through September. July was the wettest month followed by August. The precipitation was lowest during November through February.
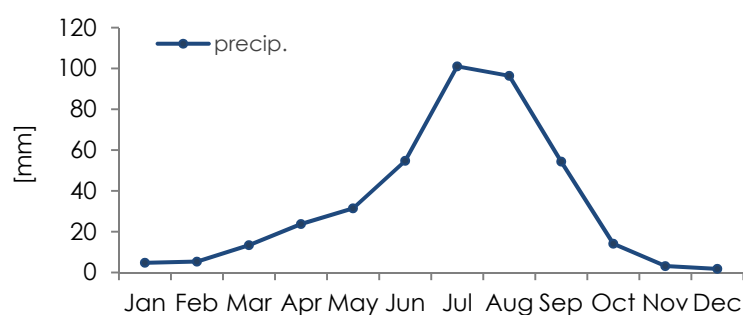
Figure 6.17: Mean monthly precipitation averaged over the Nam Co basin.

The mean annual precipitation (MAP) of individual HRUs varied between 250 and 750 mm within the entire Nam Co basin. Precipitation was highest along the Nyainqêntanglha mountain range in the south and the hilly regions in the headwater areas in the western, northern and eastern parts of the Nam Co basin (Figure 6.18). In general, HAR10 precipitation increases with elevation. However, the HAR10 data points in the southeast, with elevations lower than the high mountain areas of the Nyainqêntanglha mountain range in the southwest, exhibited the highest annual precipitation totals. Based upon the HAR10 precipitation data, only 36 % of the total variation in annual precipitation totals can be explained by variation in altitude (Figure 6.19).

During the monsoon season (June through September) the precipitation-altitude relation was even less ($r^2 = 0.28$) (Figure 6.20). This might be explained by the fact that, during the rainy season, when the monsoon rains comes from the southeast direction and continuing to the northwest, the high-elevation areas are located on the leeward side of the Nyainqêntanglha mountain range. A stronger correlation ($r^2 = 0.73$) between precipitation and elevation was found during the winter months when the dominant wind direction is from the west (Figure 6.20).
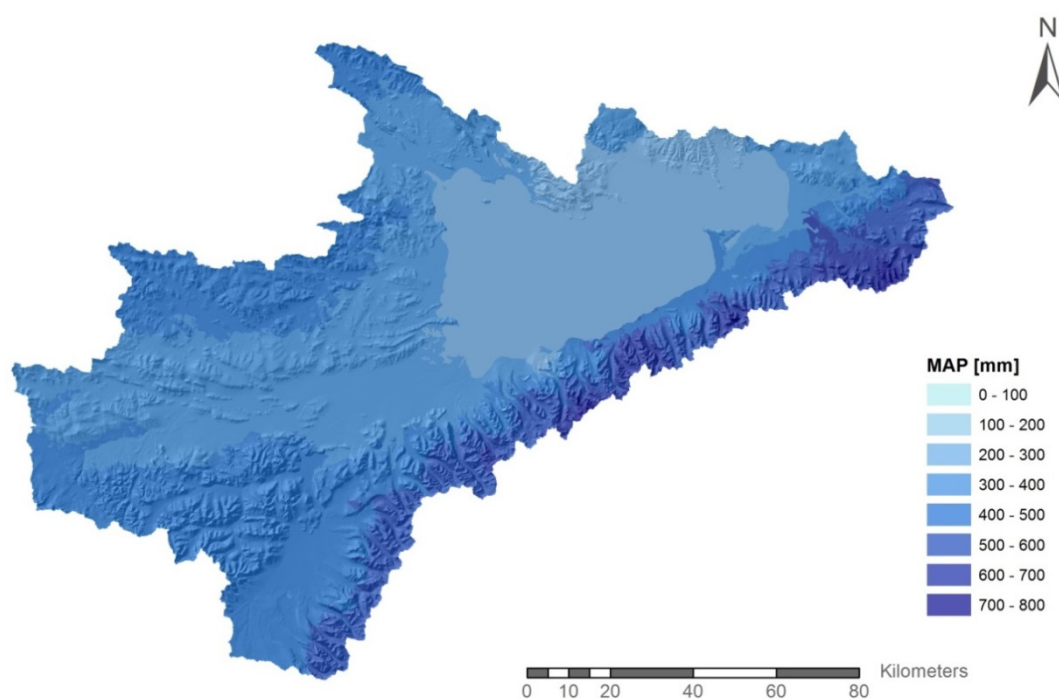
Figure 6.18: Spatial variations of simulated mean annual precipitation (MAP) within the Nam Co basin.
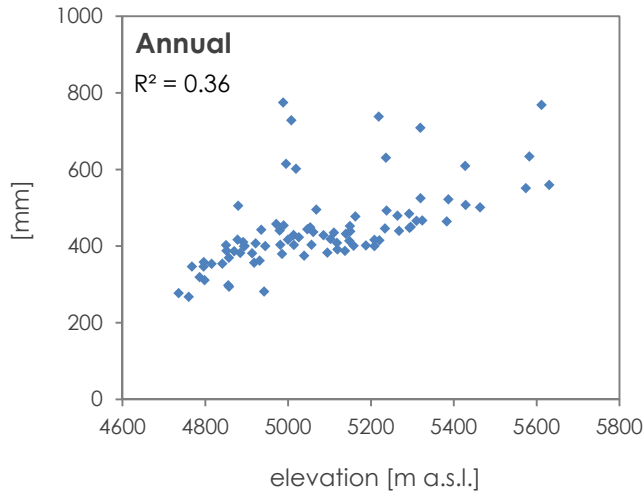
Figure 6.19: Mean annual precipitation versus elevation, based on 86 HAR10 data points within the Nam Co basin.
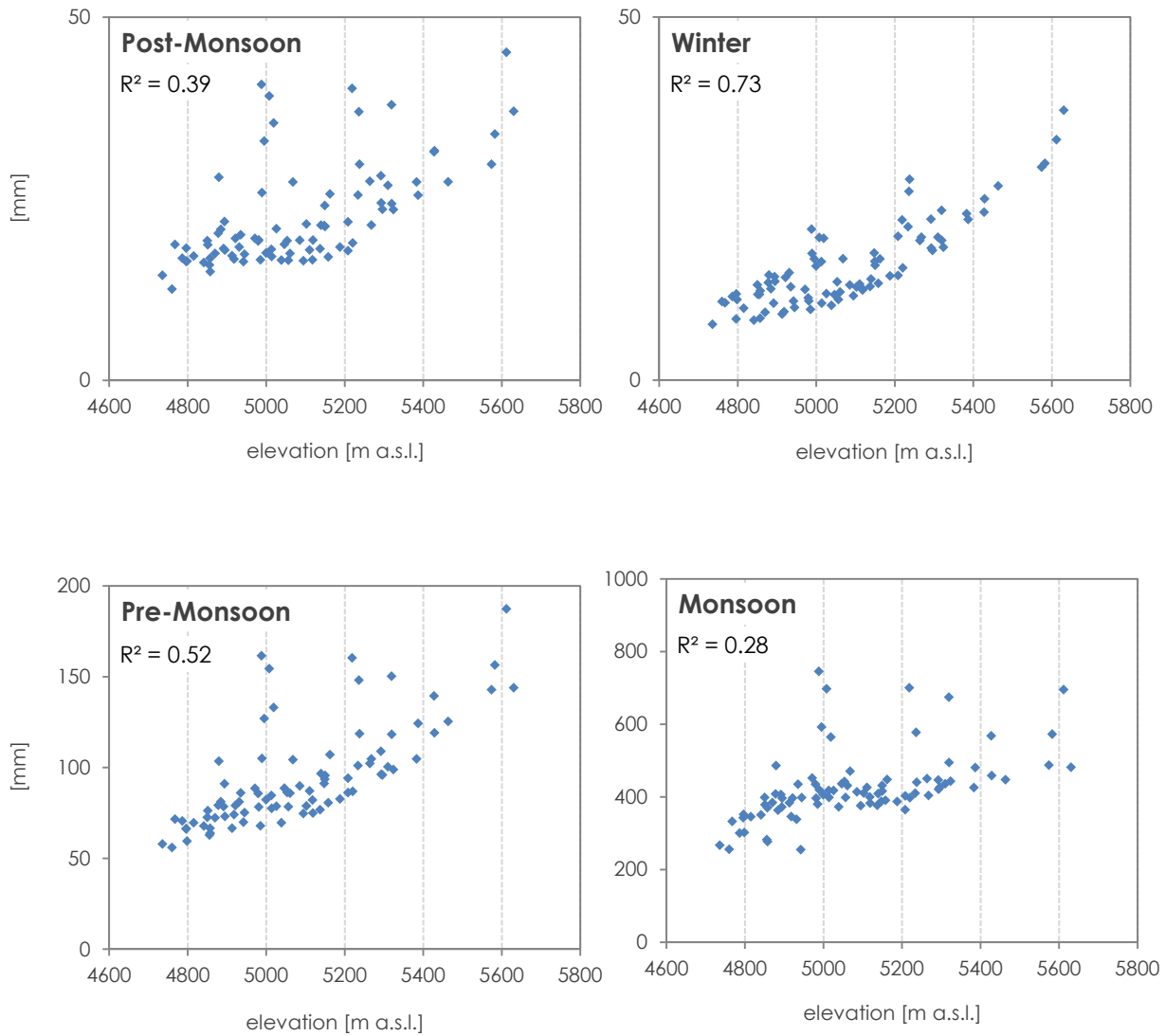
Figure 6.20: Mean seasonal precipitation versus elevation, based on 86 HAR10 data points within the Nam Co basin.

6.2.1.3 *Snow-Process Dynamics*

Simulated snow accumulation in the basin generally occurred beginning in mid-September. The snow-water amount stored in the snow pack reached a first smaller peak in November and the maximum peak between April and May, followed by rapid decrease in snow between May and June and a slower rate of decrease until August (Figure 6.21, left panel). A relatively small amount of simulated snow (between 10-15 %) was lost through sublimation during the winter compared to the snow amount released through snowmelt during the spring and summer months (Figure 6.21, left panel). The modeled annual snowmelt varied between 180 mm (2005) and 410 mm (2008) during the 10-year period (Figure 6.21, right panel), with a mean annual value of 300 mm. The inter-annual variations of precipitation explain most of the year-to-year variability of snowmelt ($r^2 = 0.85$). In spatial terms, mean annual snowmelt amounts ranged from ~100 mm (lower elevation areas) to ~600 mm (higher elevation areas) (Figure 6.22).
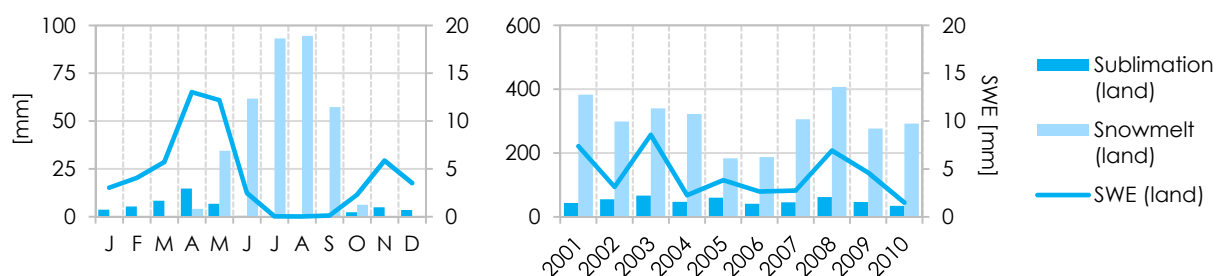
Figure 6.21: Mean monthly and inter-annual variations (2001-2010) of simulated snow-water equivalent (SWE), snow sublimation and snowmelt for the non-glacierized land surface in the Nam Co basin.
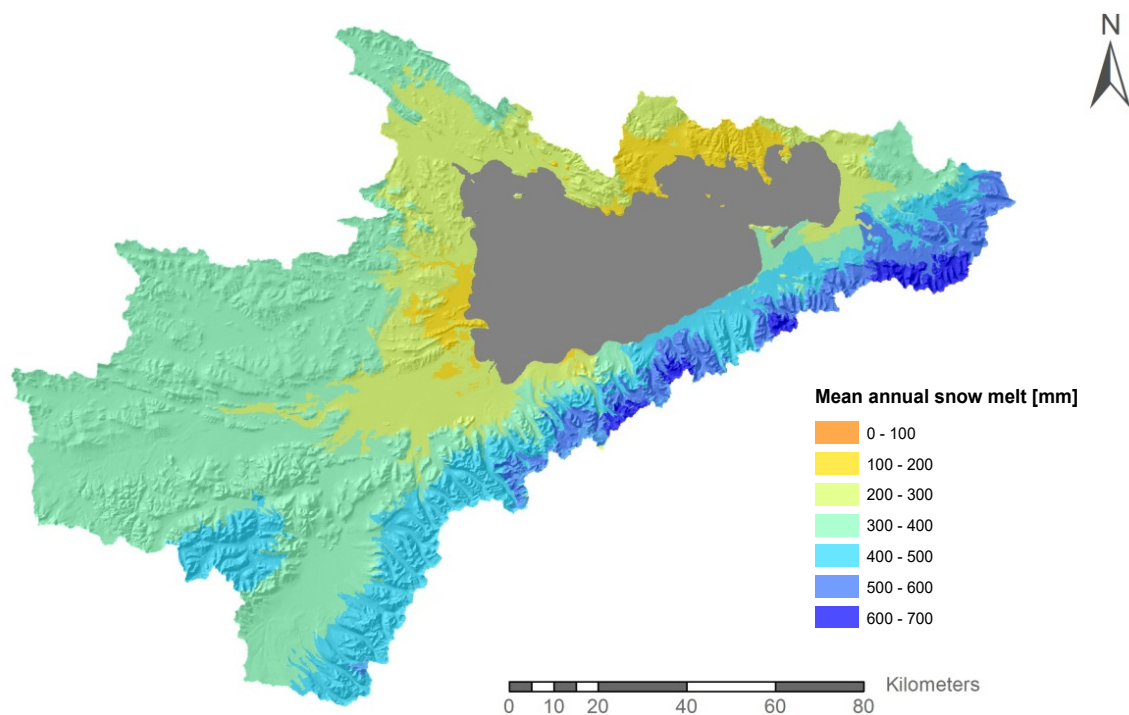
Figure 6.22: Spatial variations of simulated mean annual snowmelt within the Nam Co basin.

As described in Section 5.4.2.2, snow-water equivalent (SWE) simulations of the Nam Co basin were compared with MODIS snow-cover data. The modeled *snow-covered area fraction* (*SCAF*) in the Nam Co basin was on average 33 % greater than MODIS snow cover (SCAF 28 % versus 21 %, Figure 6.23). During the winter months (November through April), the modeled SCAF overestimated the MODIS SCAF by a factor of 2. During the months May through October, however, the modeled snow-cover extent was approximately 40 % lower compared to MODIS. Annual values of modeled SCAF and MODIS SCAF were correlated ($r^2 = 0.74$), indicating that the model incorporates adequately the effects of inter-annual variability.
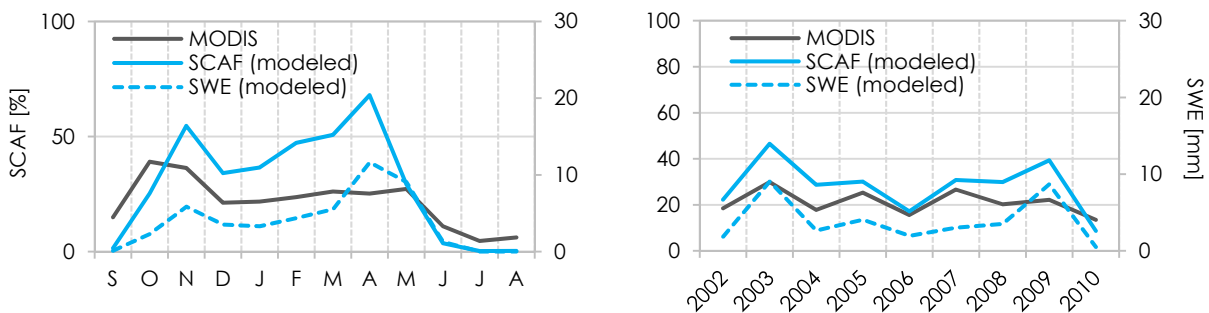
Figure 6.23: Modeled mean monthly and yearly snow-water equivalent (SWE) and snow-cover area fraction (SCAF) versus MODIS SCAF for the Nam Co basin.

6.2.1.4 Glacier Runoff

Model-simulated glacier runoff (snowmelt and ice melt) occurred principally during June through September during the 2001-2010 period (Figure 6.24, left panel). The modeled annual glacier runoff ranged from 900 to 1700 mm yr^{-1} (Figure 6.24, right panel), with a 10-year average of ~1320 mm (38 % snowmelt / 62 % ice melt).
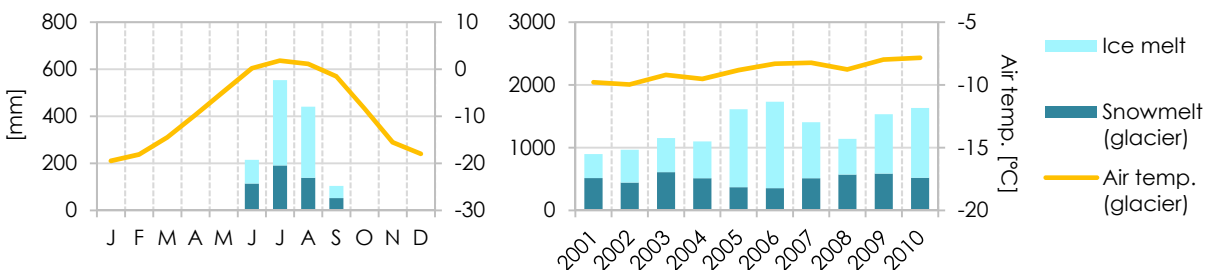
Figure 6.24: Mean monthly and inter-annual variations (2001-2010) of modeled glacier-wide air temperature and glacier melt (snow and ice melt).

The amount and timing of precipitation as well as air temperature were the primary controlling factors of the year-to-year variations. For example, the lower glacier-runoff amounts in the wet years 2001 and 2008 were caused by higher snow accumulation rates between May through June, which led to a shortening of the ice-melt period (Figure 6.25a&c). In contrast, lower snowfall

rates at the beginning and during the ablation season in dry years (e.g., 2006) resulted in the model's estimation of excessive ice melt, because the glacier ice was snow free for a longer time (Figure 6.25b). In the dry years 2005 and 2006, the simulated absolute amount and percentage of ice melt was highest (~80 %). As a consequence of higher temperatures during the last years of the study-period's decade (Figure 6.24, right panel), the modeled percentage of snowfall declined, causing higher ice-melt rates during relatively wet years (e.g., 2010) (Figure 6.25d).
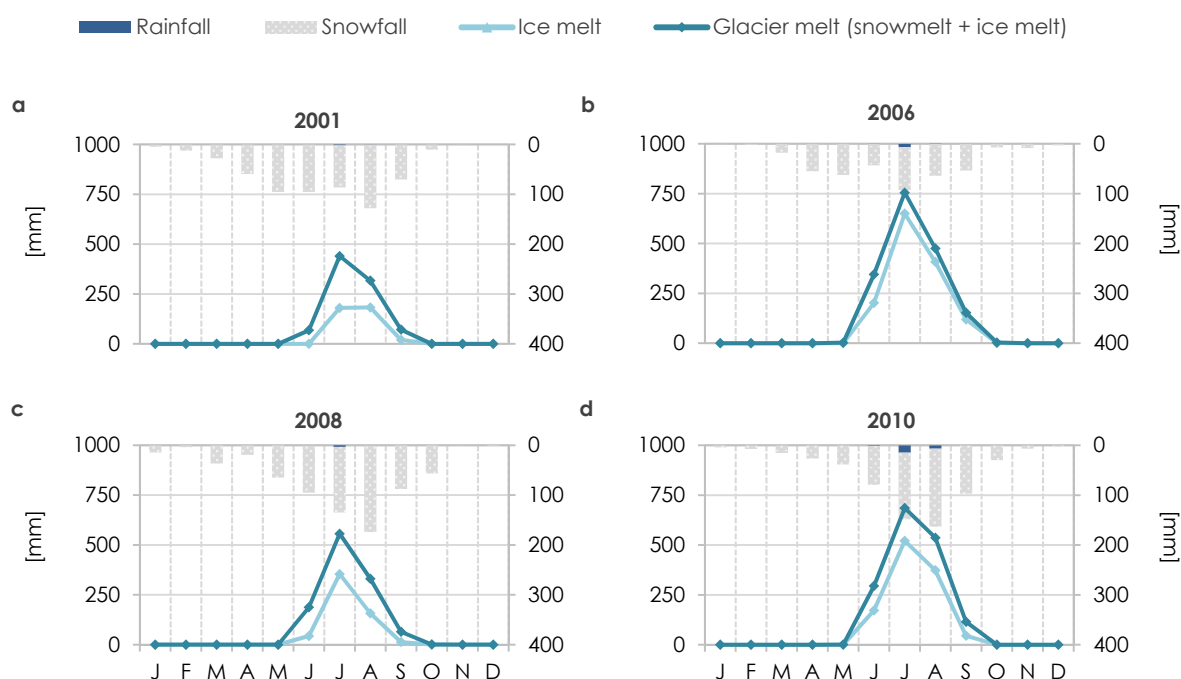
Figure 6.25: Monthly sums of precipitation (rainfall/snowfall), ice melt and total glacier runoff (snowmelt and ice melt) for 2001, 2006, 2008 and 2010 averaged over all glacier areas within the Nam Co basin.

6.2.1.5 Evapotranspiration and Runoff

About 80 % of simulated annual AET occurred during the growing season (May through October) (Figure 6.26, left panel). During the dry spring period before the onset of the monsoon (early June), AET began to increase with the beginning of the growing season and the increases of air temperature, net radiation, and soil-water content. The modeled soil-moisture content increased abruptly during the spring due to water being released from snowmelt. Simulated AET had its maximum in July, when the availability of soil-water and energy is highest. After the peak in July, AET decreased, due to the decrease of available energy and plant senescence.

The simulated mean annual AET was 290 mm, varying between 240 mm (2006) and 320 mm (2008, 2009) (Figure 6.26, right panel). The inter-annual variations of modeled AET were determined principally by precipitation ($r^2 = 0.58$). Indeed, modeled AET in the year 2009 was as high as in the wettest year 2008. By analyzing the temporal variations of further climate factors (air temperature, wind, humidity, radiation), it was noted that conditions during the year 2009 were different from other years, due to relatively high wind speeds during this year, thus intensifying the evapotranspiration process.

Averaged over the study period, about 70 % of annual precipitation was released to the atmosphere through AET and did not contribute to the runoff. The seasonal runoff pattern was similar to that for precipitation and AET, with the highest runoff amounts during the summer. About 80 % of annual runoff occurred between May and October. Runoff started to increase in spring with the beginning of snowmelt and was highest in August. The simulated mean annual runoff from non-glacierized land areas was 130 mm, varying between 50 mm in dry years (e.g., 2006) and 200 mm in wet years (e.g., 2008). The modeled year-to-year variability of runoff from non-glacierized areas was strongly related to inter-annual variations of precipitation ($r^2 = 0.88$).
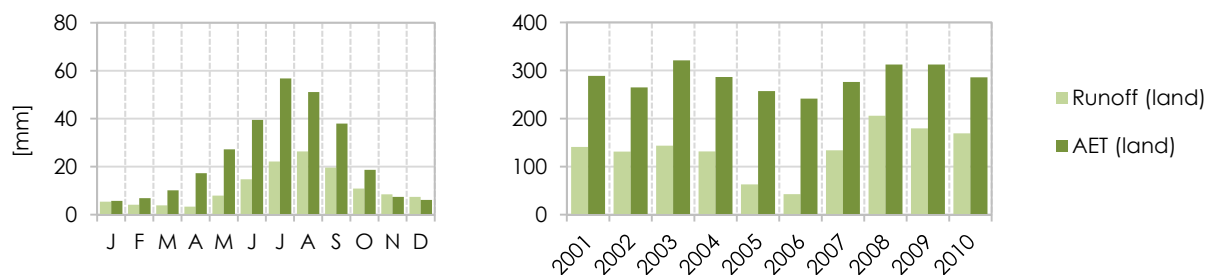
Figure 6.26: Mean monthly and inter-annual variations (2001-2010) of modeled evapotranspiration and runoff for non-glacierized land areas within the Nam Co basin.

The combination of various influencing variables such as local climate, topography, land cover, and soil properties results in a spatially heterogeneous pattern of AET and runoff generation within the catchment. Figure 6.27 presents the spatial variations of mean annual AET and runoff within the Nam Co basin. The wetlands (8 % of the total basin area), which are prevalent in slightly sloping terrain, and grasslands (39 % of the total basin area) indicated the highest AET rates with ~380 mm yr^{-1} (average over all wetland areas) and ~320 mm yr^{-1} (average over all grassland areas), respectively. The dense rooting and high organic-matter content in the topsoil of grassland and wetland sites indicate a high porosity and therefore a high water-holding capacity in the near-surface soil (cf. Section 6.1.2). The lowest AET rates (~210 mm yr^{-1}) were found in non-vegetated areas (33 % of the total basin area), including level gravel areas surrounding the lake and along river beds, and high-lying steep barren areas characterized by bare rock and rock debris.

The decrease of AET with altitude is caused principally by the elevation-dependent decrease of air temperature, the reduction of vegetation coverage and the decline of soil-water storage capacity, which is related to steep topography and poorly developed soils. The basin topography, especially the slope angle, highly affects the relation between evapotranspiration and runoff. The highest runoff rates on non-glacierized land surface (between 400 and 700 mm yr^{-1}) are generated in the high mountains of the Nyainqêntanglha mountain range in the south of the basin and in the hilly headwater areas in the west, north, and east of the Nam Co basin (Figure 6.27, lower panel). Besides the impermeable nature of the crystalline bedrock in the high mountain areas and the relatively shallow soils, the steep topography results in the generation of more overland flow.
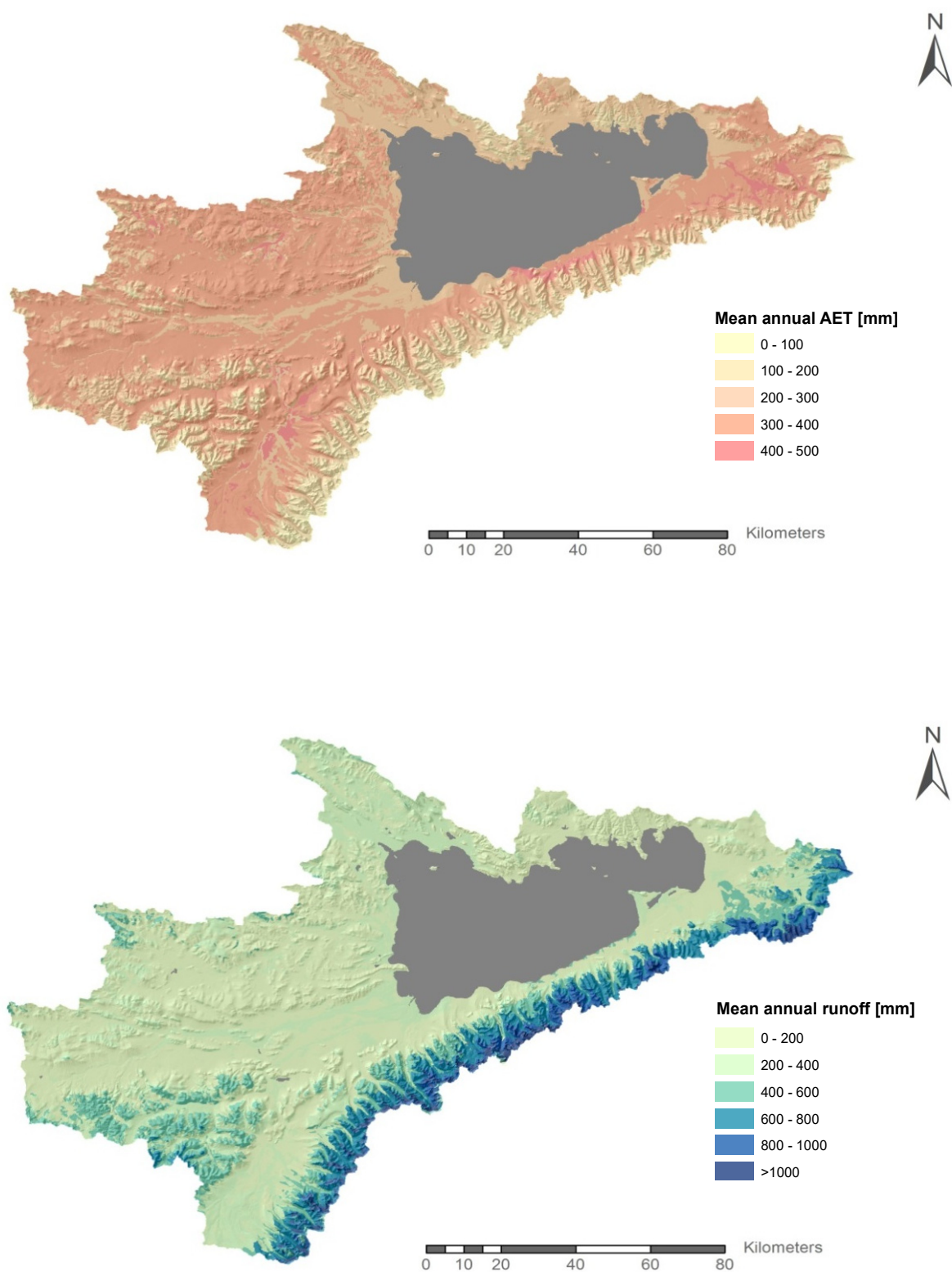
Figure 6.27: Spatial variations of simulated mean annual AET (upper panel) and runoff (lower panel) within the Nam Co basin.

Figure 6.28 illustrates the altitudinal dependence of the mean annual basin-wide precipitation totals and runoff from glaciers and non-glacierized land surface as computed by the J2000g model. The area-altitude relation (hypsometry) for glaciers and non-glacierized areas was derived based upon mean elevations of respective model entities. Larger precipitation amounts in the high mountainous and hilly headwater areas resulted in higher land runoff estimates compared to lower elevation areas (Figure 6.28). Indeed, the increase of the modeled mean annual land runoff rates with altitude was higher than the elevation-dependent increase of mean annual precipitation (Figure 6.28).

The non-glacierized high-elevation areas indicated smaller soil-water contents and lower AET rates compared to lower elevation bands, resulting in higher runoff rates. Due to high ice-melt rates in the ablation areas, the modeled runoff from low-altitude glacier areas was about four times higher than the runoff from ice-free areas in the same elevation band. Because of lower temperatures and higher snowfall rates at higher elevations, the modeled glacier runoff decreased with altitude.

In summary, the relative importance of simulated runoff contribution from glaciers and non-glacierized areas in different elevation zones to the total runoff can be determined: 19 % of the discharge within the catchment was generated in the glacier areas that account for only ~2 % of the total land surface. However, only about 12 % of the total basin runoff is glacier ice melt. The runoff from non-glacierized areas located in elevations above 5500 m a.s.l. (~5 % of the total land surface) accounted for 10 % of the total runoff. The largest runoff contribution (50 % of total runoff) came from non-glacierized areas in the elevation zone 5000-5500 m a.s.l. that account for almost half (49 %) of the total land surface. The contribution of the non-glacierized areas below 5000 m a.s.l. (44 % of the total land surface) was comparatively low (21 % of the total runoff).
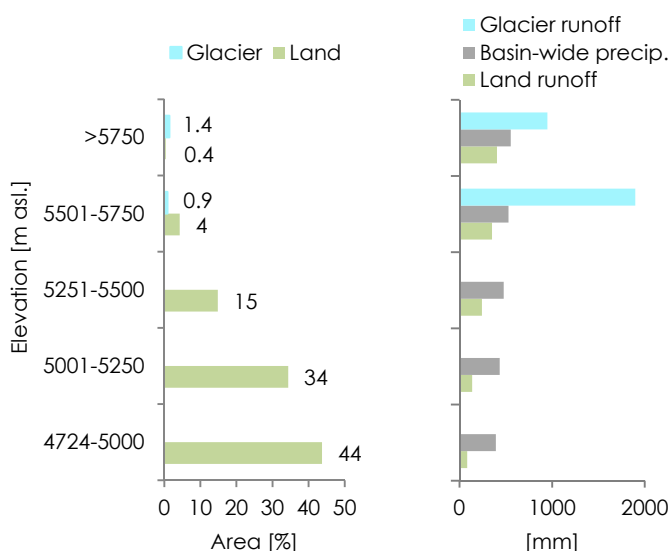
Figure 6.28: Hypsometry of glacier and non-glacierized land areas, based on mean elevations of corresponding model entities for the Nam Co basin (left panel). Altitudinal distribution of basin-wide precipitation and runoff from glacier and non-glacierized land areas for the Nam Co basin (right panel).

6.2.1.6 Lake Evaporation

The seasonal cycle of the modeled lake evaporation and the water-surface temperature is indicated in Figure 6.29 (left panel). The seasonality of the water-surface temperature, with increasing temperatures in spring and decreasing temperatures in autumn, is an indicator for the seasonal variation of the heat storage of the Nam Co (HAGINOYA *et al.*, 2009). The released heat in autumn acted as energy source for evaporation. Thus, the simulated lake evaporation was higher in autumn than in spring (Figure 6.29, left panel).

The modeled annual lake evaporation for Nam Co ranged from 710 to 860 mm yr^{-1} during the last decade, with an average of 770 mm (Figure 6.29, right panel). The years 2001 and 2002 exhibited the lowest evaporation rates; whereas, 2009 and 2010 indicated the highest evaporation amounts. Inter-annual variations in lake evaporation were related to specific combinations of air temperature, wind, radiation, lake-surface temperature, and humidity in individual years (Figure 6.30). The higher air temperatures toward the end of the study period's decade, as indicated by the HAR10 data, are primarily related to an increase in winter temperatures. This probably does not affect lake-surface water temperatures (the lake remains frozen in winter). In 2001, relatively low air temperatures, wind speeds, net radiation and water-surface temperatures, and relatively high humidity related to the other years led to less evaporation. In contrast, in 2009, net radiation, wind speeds, air temperatures, and water-surface temperatures were comparatively high and humidity relatively low, enhancing the evaporation process.
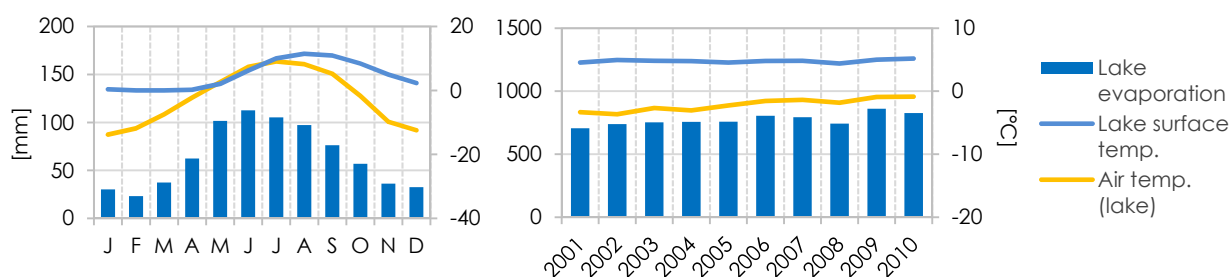
Figure 6.29: Mean monthly and inter-annual variations (2001-2010) of modeled air temperature over the lake, water-surface temperature and evaporation from the lake Nam Co.
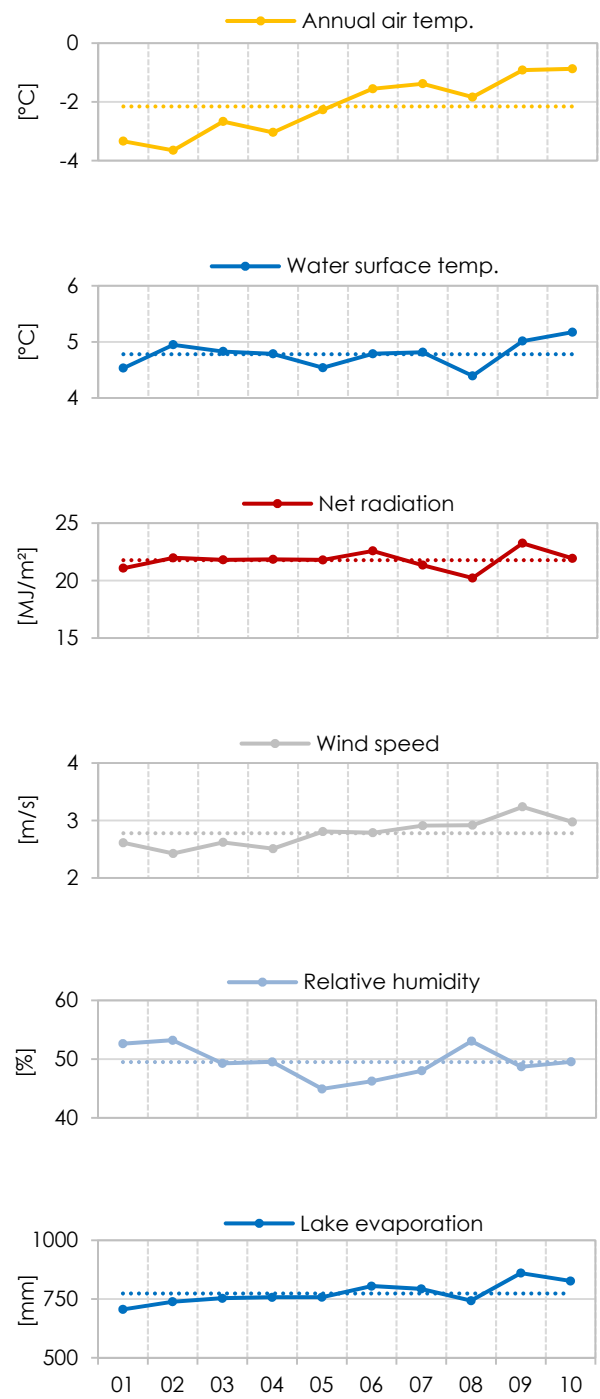
Figure 6.30: *Annual variations of modeled lake-surface water temperature, lake evaporation, and various climate factors (air temperature, net radiation, wind speed, relative humidity) over the lake Nam Co. Dashed lines represent the corresponding 10-year annual means.*

6.2.1.7 Lake-Water Storage Change

Due to higher water-volume inflow compared to outflow (i.e. lake evaporation), the simulated mean annual water balance of Nam Co was positive during the 2001-2010 period. The modeled lake volume increased about 4.7 km³ over the 10-year period. Dividing lake volume by lake area or using the water level-volume curve derived from the digital bathymetry model (Section 5.2.1), this value corresponds to a lake-level increase of 2.41 m and 2.37 m, respectively, using each calculation method.

In Table 6.12 and Figure 6.31, monthly-averaged lake-level simulations and in-situ measurements from the lake Nam Co are compared for the June-November period of the years 2006 through 2010. The overall seasonal dynamic during the June-November period was well represented by the J2000g model (r = 0.81). However, the model overestimated the lake level for the month of November. In general, the magnitude of the lake-level evolution was less well simulated than its timing. The comparison revealed a non-systematic pattern (Figure 6.31). In 2006, the model was not able to reproduce the observed increase in lake levels. The substantial lake-level rise of Nam Co in 2008 simulated by the model compared well with observed data. However, the lake-level increase in 2009 was slightly overestimated. The absolute deviation between observed and simulated relative changes of monthly-averaged lake levels during the June-November period ranged between -0.31 m (2006) and 0.30 m (2009). The simulated relative lake-level change during the June-November period averaged over the years 2006 to 2010 was 0.41 m, which is approximately 0.05 m higher than the measured one (0.36 m).

Table 6.12: Comparison of observed and simulated relative changes of monthly-average lake levels of Nam Co.

Rel. lake-level change (June-Nov.) [m]	2006	2007	2008	2009	2010	Ø
Observed	0.23	0.29	0.70	0.17	0.41	**0.36**
Simulated	-0.08	0.45	0.71	0.47	0.49	**0.41**
Δ	-0.31	0.16	0.01	0.30	0.08	**0.05**
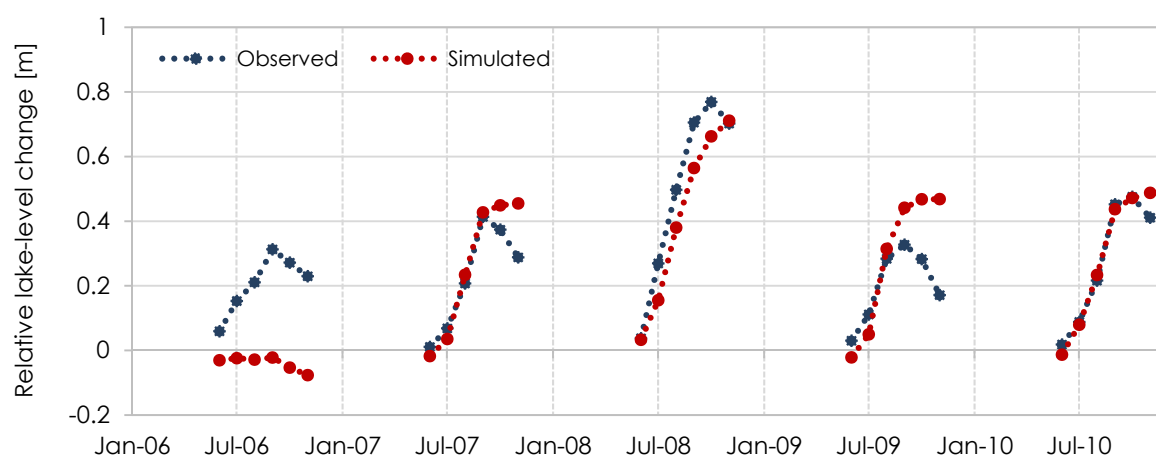
Figure 6.31: Monthly-averaged lake-level observations (blue) versus simulated lake-levels (red) for the June-November period of the years 2006 through 2010. Note that for the calculation of monthly-average lake levels, the lake-level value of the 1st of June was set to zero in each year and the subsequent values were adjusted accordingly.

Figure 6.32 (upper panel) illustrates the simulated yearly water contribution in units of km³ of each land-cover type (land, glacier, and lake) for the 2001-2010 period. Averaged over this period, the largest simulated water contribution was derived from the land runoff (~1.25 km³). The loss term (or net evaporation) accounted for ~0.95 km³ of the water budget. The simulated average annual contribution of glaciers to the total basin runoff volume was ~0.27 km³. Between the year-to-year contribution of glaciers and annual lake-volume changes, no correlation was found. The simulated annual lake-volume changes were highly correlated with annual precipitation ($r^2 = 0.95$) and land runoff ($r^2 = 0.97$).

The simulated annual percentage deviations from the 10-year average of several hydrological system components (Figure 6.32, lower panel) indicate that the anomalously high lake-level increase in 2008 was caused by higher precipitation amounts (37 % above the average), causing more land runoff (54 % above the average) than normally anticipated. The model-simulated glacier melt rate was 14 % below the average during this wet year. Although the simulated glacier runoff was 20-30 % above the average in 2005 and 2006, lower precipitation amounts (~30 % below average) led to a ~50-70 % decrease in land runoff, resulting in a decrease of the lake-water volume on an annual basis.
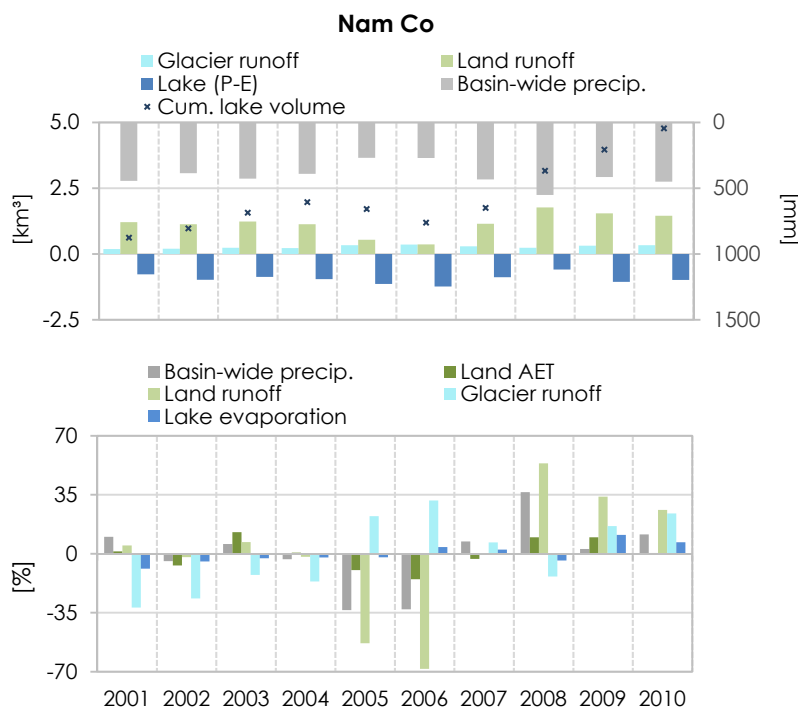
Figure 6.32: Simulated cumulative lake-volume change (km³), contribution of several water-balance components (km³) to lake-volume change and annual basin-wide precipitation amounts (mm yr⁻¹) for the Nam Co basin (upper panel). Annual percentage deviations from the 10-year average of several water-balance components (lower panel).

6.2.2 Uncertainty and Sensitivity Analysis

As described in Section 5.4.2.2, uncertainty and sensitivity analyses were conducted, in order to account for the variability of the model-calibration parameters and to assess the most critical parameters and their effects on the uncertainty of the model outputs. The uncertainty ranges of relevant model-output components were derived based upon 1479 acceptable (behavioral) models. The box-whisker plots in Figure 6.33 visualize the uncertainty ranges for 10-year annual means of several output variables and the distributions of model output values within the uncertainty ranges. The lower, median and upper values as well as the absolute and relative differences between lower and upper bounds (defined here as uncertainty ranges) are summarized in Table 6.13. The 10-year averages of the several output variables for the reference run (see Section 5.4.2.2) are also given in Table 6.13. The mean annual values of the reference run were close to the median.
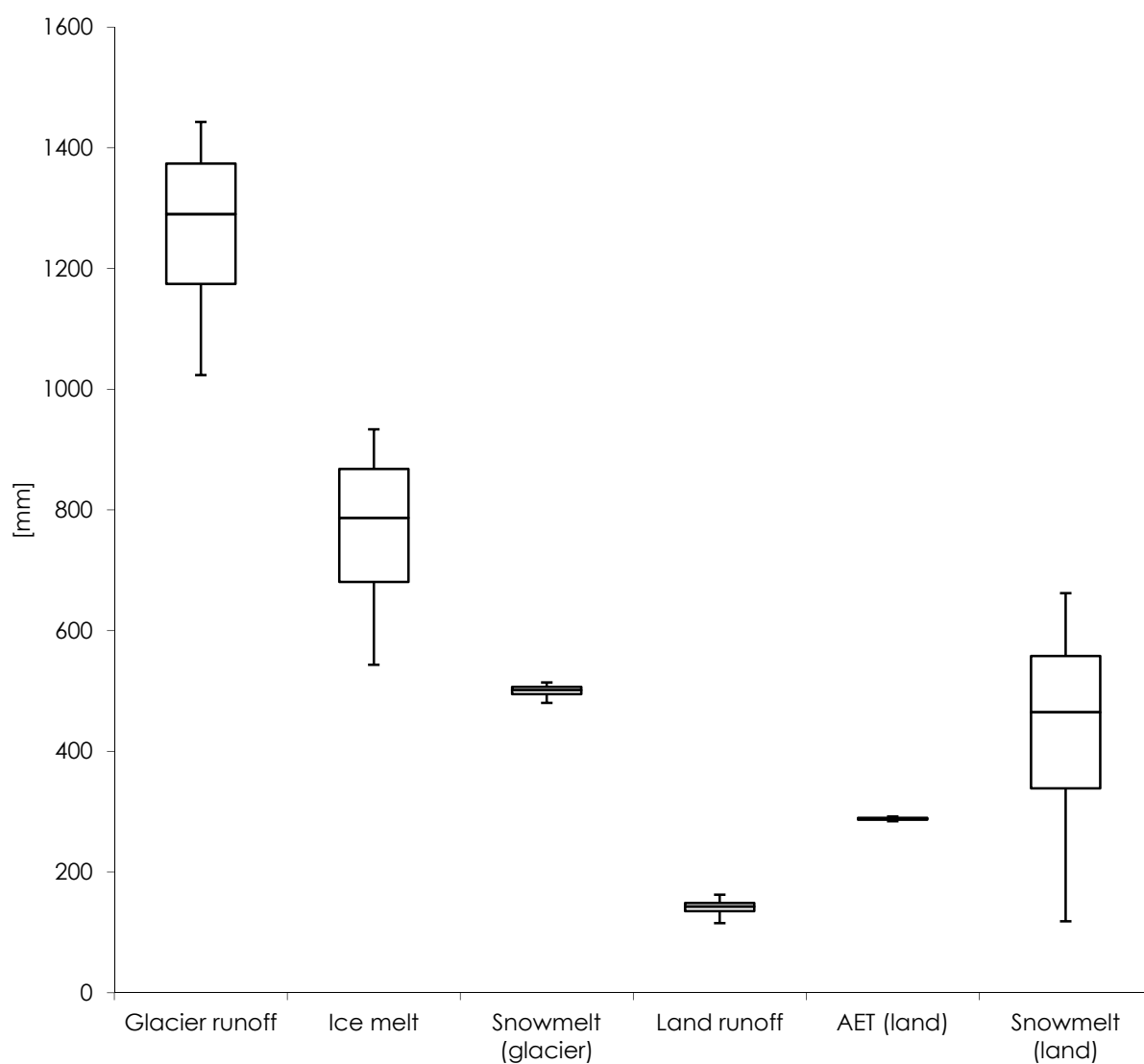
Figure 6.33: Box-whisker plots illustrating the distribution of 10-year annual means of several model-output variables. The bottom and top of the box are the first and third quartiles, and the band inside the box is the median. The ends of the whiskers represent the maximum and minimum values and correspond to the upper and lower bounds of the uncertainty range of the depicted variable.

Table 6.13: Absolute and relative percent uncertainty ranges for 10-year annual means of selected model-output variables.

Output variable	Lower limit [mm]	Median [mm]	Reference run [mm]	Upper limit [mm]	Uncertainty range [mm]	Uncertainty range [%]
Snowmelt (land)	321	347	352	367	51	13
AET	284	288	285	292	8	3
Land runoff	132	137	134	144	12	9
Snowmelt (glacier)	480	501	499	513	33	7
Ice melt	543	786	818	933	390	50
Glacier runoff	1023	1290	1318	1443	420	33

In terms of process simulations for non-glacierized land areas, the largest uncertainty range was computed for snowmelt (13 %), followed by land runoff (9 %) and AET (3 %). The uncertainty range of AET was relatively low, because the Penman-Monteith approach used for the AET calculation does not require setting of model-calibration parameters. Variations in modeled AET (including snow sublimation) resulted only from differences in the availability of water (both liquid as well as in the form of snow).

A relatively low uncertainty range was indicated in this analysis for snowmelt on glacier areas (7 %); whereas, the uncertainty range of ice melt was relatively large (50 % deviation between lower and upper bound). The uncertainty range of the total glacier runoff (combined snowmelt and ice melt) was 33 % and hence was higher than for land runoff (9 %). Because the percentage of glacier area is only 2 %, larger errors in glacier runoff simulations can be compensated for by the land runoff output component.

Figure 6.34 illustrates the monthly variations of the computed uncertainty bands (grey shaded) for several model-output components. The respective values of the median and the model reference run are presented in red and green, respectively. The uncertainty of simulated snowmelt (non-glacierized areas) was largest between May through August, particularly in July. The uncertainty plot for land runoff suggests that uncertainty was highest between May and August. This was related to uncertainties in snowmelt simulation. The lower and upper bounds of AET were close to the median throughout the year. They diverged only slightly during the beginning of the snowmelt during the spring.

The uncertainty for modeled snowmelt (glacier areas), ice melt and glacier runoff was high between June through August. Although the highest uncertainty for modeled snowmelt and glacier runoff was indicated at the beginning of the melt season, ice melt indicated the highest uncertainty during the melt peak during July. However, the uncertainty intervals for ice melt and glacier runoff in July were not symmetric around the median. The upper bound was much closer to the median (Figure 6.34), because model runs with higher ice/glacial melt rates did not meet the selection criterion for acceptability.
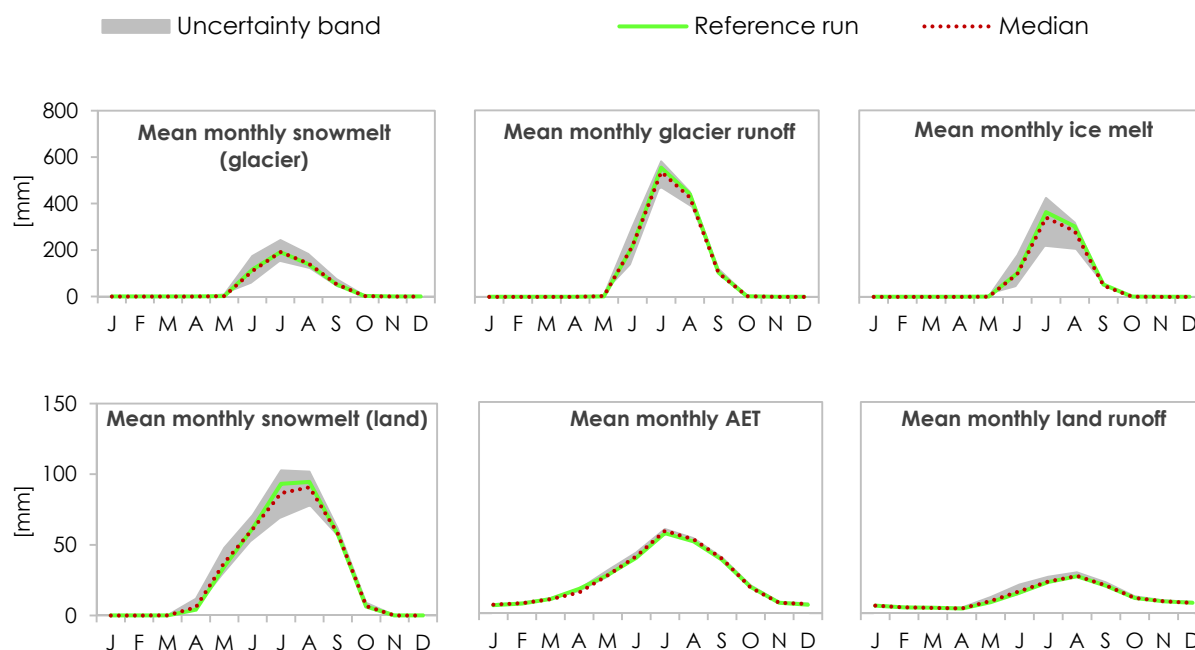
Figure 6.34: Monthly variations of uncertainty bands for several output variables from glacier areas (upper panels) and non-glacierized land areas (lower panels).

As described in Section 5.4.2.2, the RSA approach was applied to evaluate which model parameters dominate the uncertainty of several model-output components. Figure 6.35 indicates the sensitivity of the model parameters regarding the PBIAS performance criterion (see Section 5.4.2.2). The precipitation-scaling factor was the most sensitive parameter with the highest impact on the overall system response (in terms of lake-volume change). By considering all of the model runs having a PBIAS ≤ 50 % (6495 models), the precipitation-scaling factor may explain more than 70 % of the variations in modeled lake-volume change. The cumulative distributions of the precipitation-scaling factor (Figure 6.36) indicate that scaling factors between 0.8 and 0.825 indicated best performances; whereas, lower or higher values of that parameter performed worse in terms of modeled lake-volume change. Beside the precipitation-scaling factor, the parameters *baseTemp* (threshold temperature for snow and ice melt), *AWCA* (available water-capacity adaption) and *linETRed* (linear evapotranspiration-reduction factor) were more sensitive than other parameters in impacting resultant model outputs; however, their sensitivities were relatively low compared with the sensitivity analysis for the precipitation-scaling factor (Figure 6.35).

The results of the modified RSA approach for non-glacierized land areas and glacier areas are summarized in Figure 6.37 and Figure 6.38, respectively. Variations in snowmelt simulations for non-glacierized land areas were not only significantly affected by the amount of precipitation input, but also by the following: *i)* the fraction of the total precipitation that falls as snow depending upon the values of parameters *snow_trs* (threshold temperature for 50 % rain, 50 % snowfall) and *snow_trans* (half width of the transition range within which both precipitation forms occur), and *ii)* the threshold temperature for snowmelt (*baseTemp*) (Figure 6.37a). The higher the values of *snow_trs* and *snow_trans* (indicating higher fractions of snowfall), and the lower the value of *basetemp*, the higher is the simulated amount of snowmelt. Regarding the AET and land runoff, the parameters *snow_trs* and *snow_trans* were less sensitive (Figure 6.37b&c), because it doesn't make a difference whether the water available for AET and runoff process

comes from snowmelt or rainfall. Similar to the parameter sensitivities derived for the overall model response, the precipitation-scaling factor was found to be the parameter with the highest impact on the uncertainty in AET and land runoff simulations, followed by the parameters *baseTemp* and *AWCA* (Figure 6.37b&c). In terms of land runoff, the influence of the *baseTemp* parameter was greater compared with the *AWCA* parameter; whereas, the opposite was indicated for AET.

With respect to glacier areas, simulated snowmelt was highly sensitive to the precipitation-scaling factor and *basetemp* (Figure 6.38a). *Snow_trs* and *snow_trans* were less sensitive parameters, because precipitation on glaciers falls mainly as snow. In contrast to snowmelt, ice melt and glacier runoff were much more sensitive to the *basetemp* parameter than to the precipitation-scaling factor (Figure 6.38b&c), because ice-melting is only simulated in the J2000g model if the snow cover of any given glacier HRU has been melted completely. The lower the *basetemp*, then the faster the snow melts and thus the ice-melt season starts earlier in time.
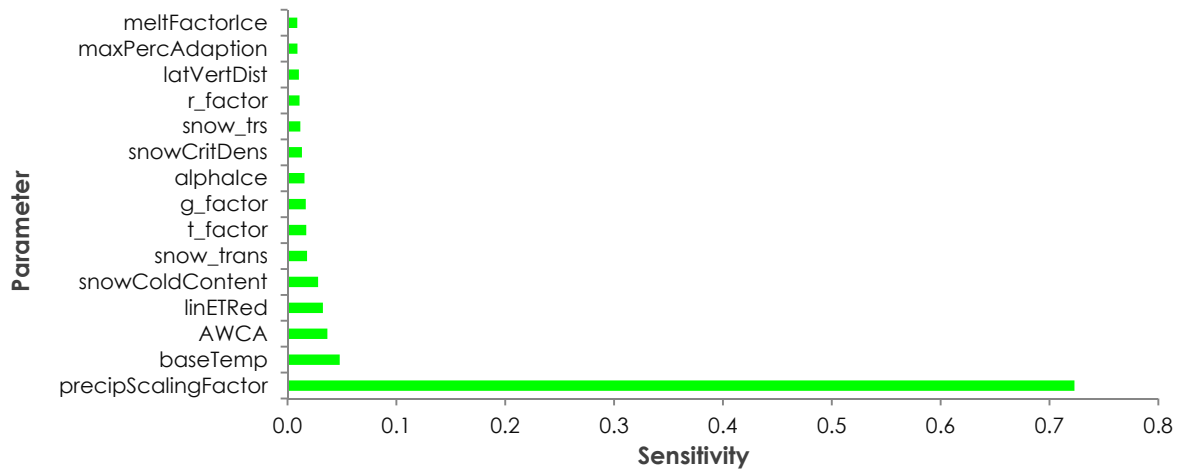
Figure 6.35: Parameter sensitivity ranking in terms of the PBIAS performance criterion, resulting from RSA.
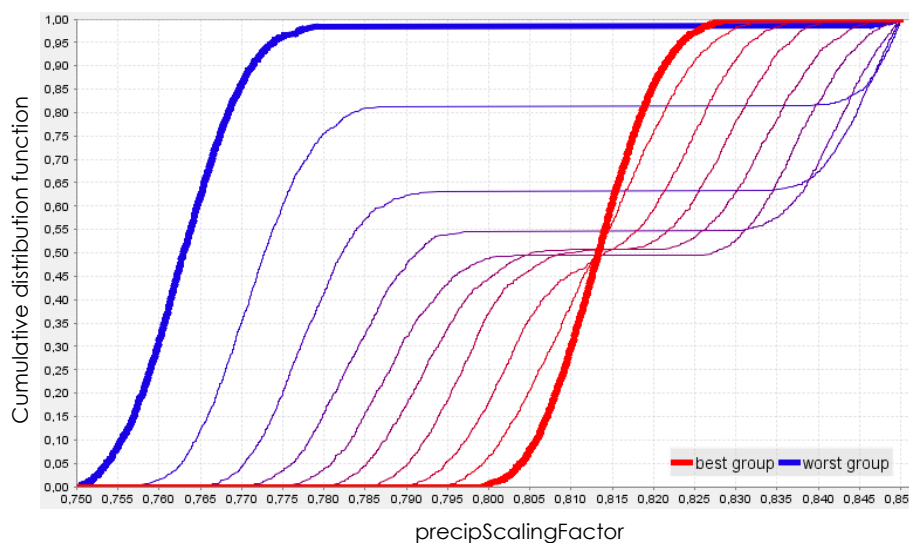
Figure 6.36: RSA plot indicating the sensitivity of the precipitation-scaling factor, based on the PBIAS performance criterion. Red/ blue colors indicate groups of better/ less performing parameter values.

(a)

Snowmelt (land)

(b)

AET (land)

(c)

Land runoff
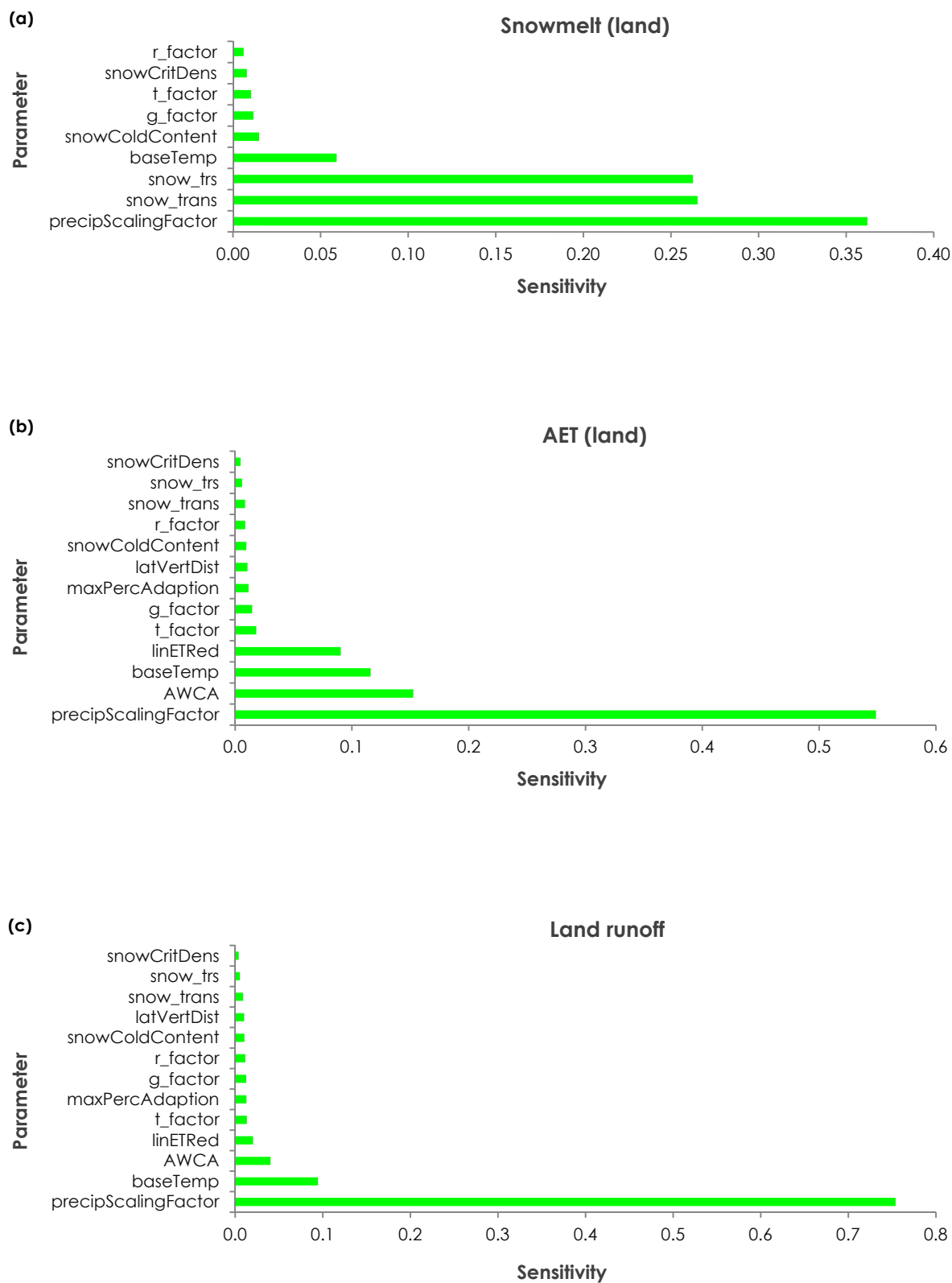
Figure 6.37: Parameter sensitivity ranking for several model outputs for non-glacierized land areas using a modified RSA.

(a)

(b)

(c)
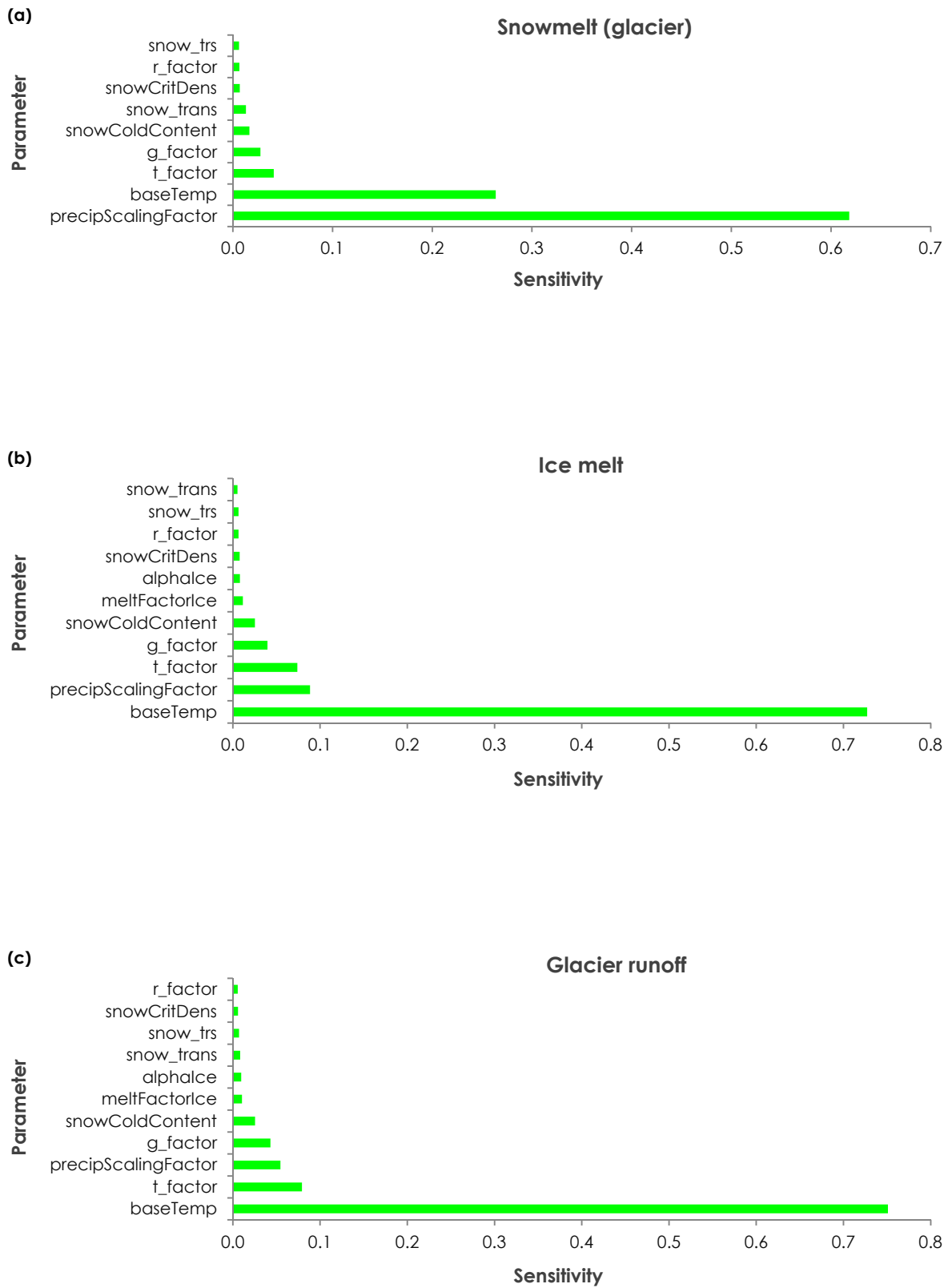
Figure 6.38: Parameter sensitivity ranking for several model outputs for glacier areas using a modified RSA.

As described in Section 5.4.2.2, the sensitivity of several hydrological model-output components to changes in input variables was analyzed. Table 6.14 summarizes the absolute (percentage) changes in mean annual hydrological components with respect to the reference run. The various sensitivity runs indicated that lake-level fluctuations are most sensitive to changes in precipitation. A 10 % increment (decrement) in precipitation resulted in an increase (decrease) in mean annual lake-level change by 163 mm (218 mm) compared to the reference run. This was primarily caused by an increase (decrease) in land runoff by approximately 20 %. Higher (lower) precipitation amounts led to increasing (decreasing) AET (±5 %), which may reduce the impact of changing precipitation on lake-level variations. An interesting feature was that simulated total glacier runoff does not change much as precipitation is changed by ±10 % (Table 6.14). This is mainly due to the fact that changes in snowmelt and ice melt may offset each other. Higher precipitation led to an increase in snowmelt by 11 %, which in turn resulted in a decrease of ice melt by 6 %. The contrary effect (decrease in snowmelt, and increase in ice melt) was found under a precipitation reduction (-10 % snowmelt versus +6 % ice melt). However, glacier runoff was more sensitive to changes in air temperature. A temperature change by +1°C or -1°C, caused a change in glacier runoff by +48 % and -37 %, respectively. Indeed, increasing (decreasing) air temperature resulted in an AET increase (decrease) of ~5 % and a land runoff decrease (increase) of ~10 %, leading to a lower (higher) lake-level rate related to the reference run.

Table 6.14: Absolute/percentage changes in mean annual hydrological components by increasing/decreasing input variables.

		Lake evaporation [mm] / [%]	Land AET [mm] / [%]	Land runoff [mm] / [%]	Glacier runoff [mm] / [%]	Lake level [mm]
Air temp.	+1°C	47 / 5	13 / 4	-12 / -9	629 / 48	-34
	-1°C	-46 / -5	-14 / -5	13 / 10	-488 / -37	55
Lake-surface temp.	+1°C	55 / 6	-	-	-	-54
	-1°C	-50 / -6	-	-	-	49
Precip.	+10 %	-	11 / 4	30 / 22	4.2 / 0.3	163
	-10 %	-	-13 / -5	-28 / -21	-9 / -0.7	-218
Rel. Humidity	+10 %	-22 / -3	-9 / -3	8 / 6	8 / 0.6	61
	-10 %	22 / 3	9 / 3	-8 / -6	-9/ 0.7	-59
Wind speed	+10 %	22 / 3	0.8 / 0.3	-0.6 / -0.5	-1.2 / -0.1	-24
	-10 %	-22 /-3	-0.9 / -0.3	0.8 / 0.6	1.3 / 0.1	25
Solar radiation	+10 %	63 / 7	9 / 3	-8 / -6	68 / 5	-93
	-10 %	-63 / -7	-10 /- 3	9 / 7	-68 / -5	96

6.3   Comparative Analysis of the Four Selected Lake Basins

The following sections deal with the assessment of similarities and differences among the four selected basins regarding spatiotemporal variability of hydrological components (Section 6.3.1) and their contributions to each basin's water balance (Section 6.3.2).

6.3.1   Spatiotemporal Patterns of Hydrological Components

The seasonal dynamics of simulated hydrological components in the Tangra Yumco, Paiku Co and Mapam Yumco basins were similar to the seasonal variations described previously in Section 6.2.2 for the Nam Co basin. The percentage of the precipitation occurring during the wet season (June through September) is more than half of the annual precipitation in all four studied basins. Specifically, June-through-September precipitation is approximately 80 % of the annual total in the Nam Co and Tangra Yumco basins and around 60 % in the Paiku Co and Mapam Yumco basins (Figure 6.39). This indicates a higher influence of the Westerlies in the Paiku Co and Mapam Yumco basins. Snowmelt, evapotranspiration and runoff processes were concentrated in the temperate-wet summer season in all basins (Figure 6.39 - Figure 6.43). However, simulated snowmelt in the Mapam Yumco started later and occurred over a shorter time period compared to the other basins (Figure 6.40). This can be explained by lower air temperatures in this basin. The land runoff peak in the Mapam Yumco basin occurred one month earlier compared to the other basins (Figure 6.41), because of a higher snowmelt contribution to the discharge.
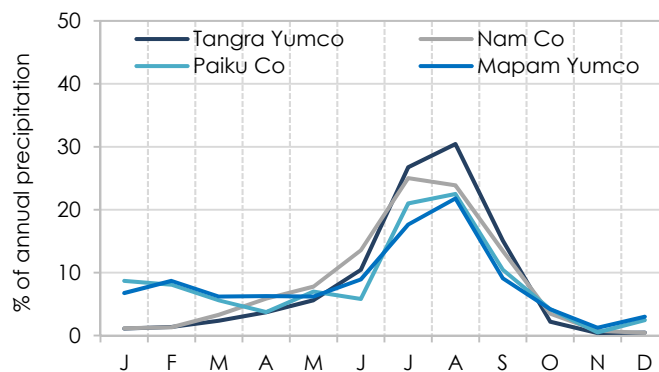
Figure 6.39: Monthly percentage of annual precipitation for the four studied basins.
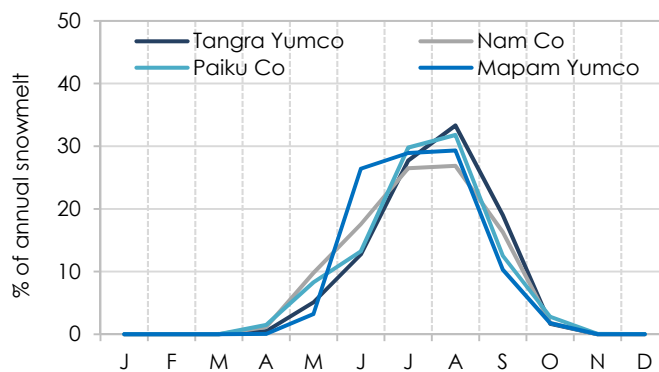
Figure 6.40: Monthly percentage of annual snowmelt for the non-glacierized land areas of the four studied basins.
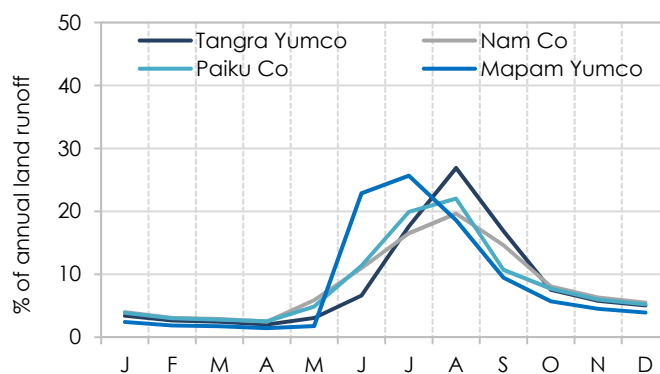
Figure 6.41: Monthly percentage of annual land runoff for the four studied basins.
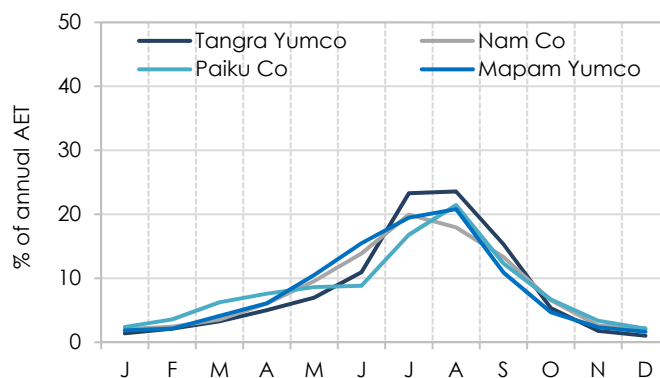
Figure 6.42: Monthly percentage of annual actual evapotranspiration (AET) for the non-glacierized land areas of the four studied basins.
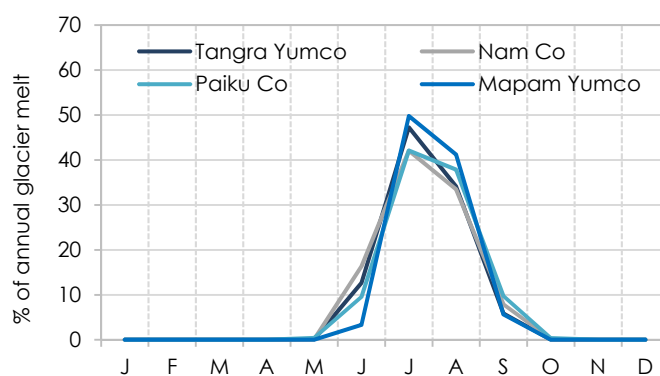
Figure 6.43: Monthly percentage of annual glacier runoff for the four studied basins.

Table 6.15 below summarizes annual means of modeled hydrological components for the 2001-2010 period for each basin.

Table 6.15: Annual means of several hydrological components for the 2001-2010 period for the four studied lake basins.

		Western basin ⟶			Eastern basin
		Mapam Yumco	**Paiku Co**	**Tangra Yumco**	**Nam Co**
Hydrological components [mm yr^{-1}]					
Lake					
	On-lake precipitation	90	140	150	290
	Lake evaporation	710	910	840	770
	Net evaporation	620	770	690	480
Land					
	Precipitation	230	250	300	420
	AET (ratio AET/precip.)	170 (0.74)	180 (0.72)	210 (0.70)	290 (0.69)
	Land runoff	60	70	90	130
Glacier					
	Precipitation	330	480	330	560
	Glacier runoff	600	320	1320	1320

As indicated in Table 6.15, the annual mean of the model-simulated lake evaporation rates varied between 700 and 900 mm yr^{-1} for the four basins averaged over the 10-year study period. Because of unlimited water availability, the model-simulated mean annual lake evaporation was substantially higher than the land AET (Table 6.15). Due to higher precipitation amounts in the eastern part of the study region, the simulated mean annual terrestrial AET was higher in the east (~290 mm in the Nam Co basin) than in the west (~170 mm in the Mapam Yumco basin) (Table 6.15).

Impacted by the decreasing precipitation gradient spatially from east to west, the model-simulated mean annual land runoff in the Nam Co basin (~130 mm) was estimated to be more than twice that in the Mapam Yumco basin (~60 mm) during the study period. The percentage of the annual precipitation which was lost by terrestrial AET increases with decreasing precipitation totals from 69 % (Nam Co basin) to 74 % (Mapam Yumco basin) (Table 6.15). For all the catchments, the AET decreased and land runoff increased with increasing altitude (Figure 6.44a-d), as described previously for the Nam Co basin.

In all studied basins, the runoff from glacier areas located in lower elevations zones (< 5750 m a.s.l.) significantly exceeded the land runoff in the same elevation zones (Figure 6.44). However, the modeled mean annual glacier runoff averaged over all glacier HRUs in the Nam Co and Tangra Yumco basins (~1300 mm) was considerably higher than in the Paiku Co (~300 mm) and Mapam Yumco (~600 mm) basins. This was judged to be caused by lower air temperatures (~2°C less) in the glacier areas of the Paiku Co and Mapam Yumco basins.
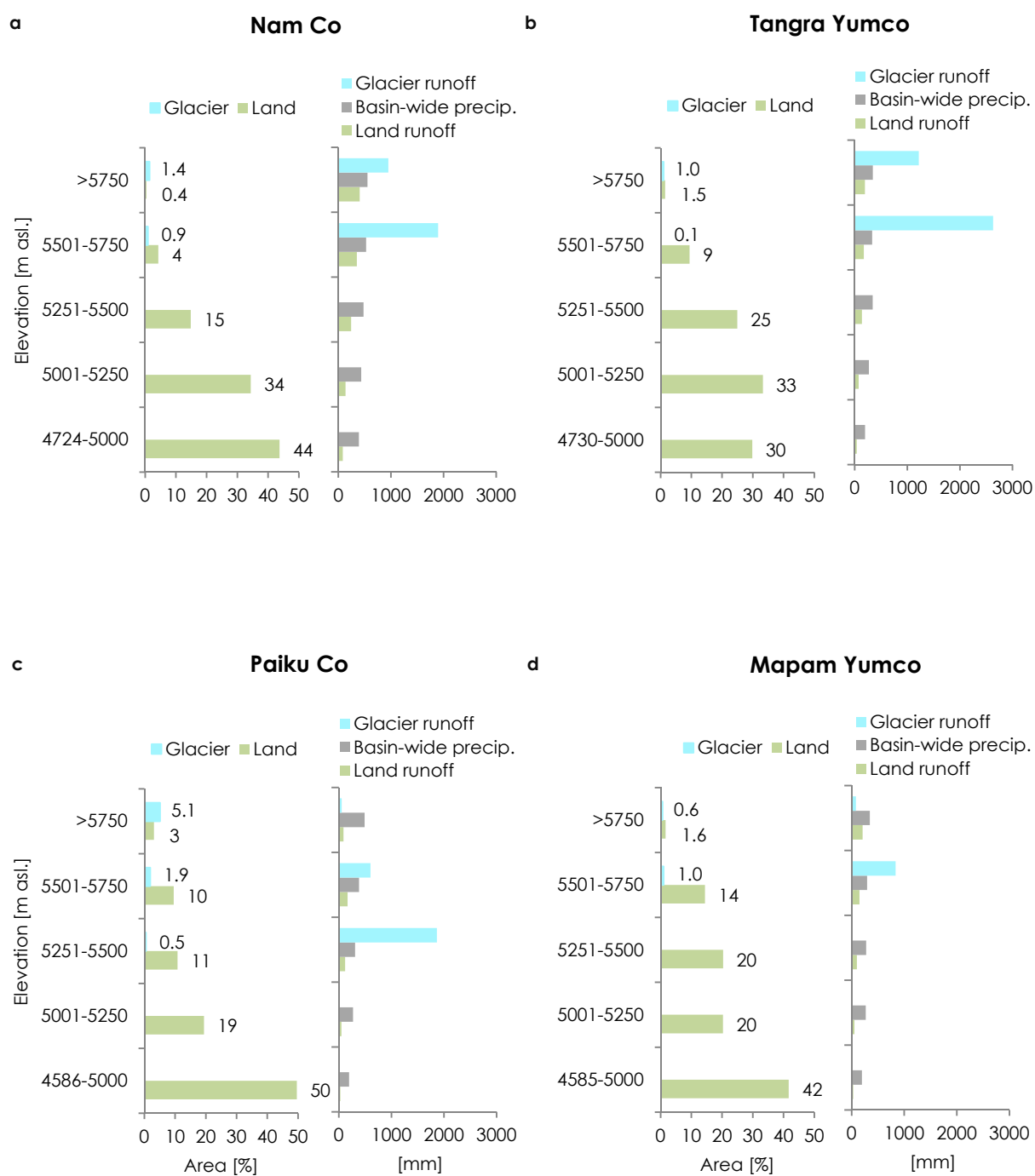
Figure 6.44: (a-d, left panel) Hypsometry of glaciers and non-glacierized land areas based on mean elevations of respective model entities for the four studied basins. (a-d, right panel) Altitudinal distribution of basin-wide precipitation and runoff from glaciers and non-glacierized land areas for the four studied basins.

6.3.2 Contributions of the Individual Hydrological Components to the Water Balance

Table 6.16 summarizes model-simulated mean annual lake-volume and water-level changes and the contribution of non-glacierized land, glacier and lake areas to the total water budget during the 2001-2010 study period for the four basins. Comparative values for the mean annual lake-level changes derived from remote-sensing data are also given in Table 6.16.

Table 6.16: Mean annual water budget and lake-level rates for the 2001-2010 period for the four studied lake basins.

	Western basin **Mapam Yumco**	**Paiku Co**	**Tangra Yumco**	Eastern basin **Nam Co**
Water budget [km³ yr⁻¹]				
<u>Water gain</u>				
Land runoff (% of total basin runoff)	0.23 (85)	0.14 (70)	0.70 (86)	1.15 (81)
Glacier runoff (% of total basin runoff)	0.04 (15)	0.06 (30)	0.11 (14)	0.27 (19)
<u>Water loss</u>				
Net evaporation	-0.26	-0.22	-0.57	-0.95
<u>Net water-budget</u>				
Lake-volume change	0.01	-0.02	0.24	0.47
Lake-level change [m yr⁻¹]				
Simulated	0.02	-0.07	0.29	0.24
ZHANG, G. *et al.* (2011) (GLAS/ICESat 2003-2009)	-0.02	-0.04	0.26	0.25
PHAN *et al.* (2012) (GLAS/ICESat 2003-2009)	-0.043	-0.118	0.291	0.230
LEGOS*	-0.05	-0.07	0.25	0.22

*Mean annual lake-level rates for the studied basins correspond to following time periods: Nam Co – 2001-2010; Tangra Yumco – 2001-2009; Paiku Co – 2004-2008; Mapam Yumco – 2003-2009.

Similar to the Nam Co basin, the contribution of glacier runoff to the total basin runoff volume in the Tangra Yumco (14 %) and Mapam Yumco (15 %) basins was relatively low compared to the runoff contribution from non-glacierized land areas. The glacierization in the Paiku Co basin (6 % of the total basin area) is about two to five times larger than in the other three basins, but the glacier-melt contribution to the total basin runoff volume was only around twice as high (30 %) due to lower glacier-melt rates. Despite the generally higher glacier contribution in the Paiku Co, the water balance was slightly negative during the study period (Table 6.16). The water loss for Paiku Co exceeded the water gain by 10 %. In contrast, the total water inflow in the Tangra Yumco and Nam Co basins exceeded the water loss by a factor of 1.4 or 1.5, respectively. In the Mapam Yumco basin the water gain and loss terms tended to balance each other out (Table 6.16), based upon the model simulation.

In order to better predict and understand the role of glaciers for the mean annual water balance, a hypothetical scenario with ice-free conditions were evaluated through model simulations for each lake basin. Therefore, the land-cover class of all glacier HRUs was changed to barren land. Table 6.17 compares the model results of the ice-free scenario with the reference run.

Table 6.17: Comparison of model results of the ice-free scenario with the reference run for the four studied basins.

	Total basin runoff [km³ yr⁻¹]	Lake-volume change [km³ yr⁻¹]	Lake-level change [m yr⁻¹]
Nam Co			
Ice-free scenario	1.24	0.29	0.15
Reference run	1.42	0.47	0.24
Δ	0.18	0.18	0.09
Tangra Yumco			
Ice-free scenario	0.71	0.14	0.17
Reference run	0.81	0.24	0.29
Δ	0.10	0.10	0.12
Paiku Co			
Ice-free scenario	0.15	-0.07	-0.25
Reference run	0.20	-0.02	-0.07
Δ	0.05	0.05	0.18
Mapam Yumco			
Ice-free scenario	0.19	-0.07	-0.18
Reference run	0.27	0.01	0.02
Δ	0.08	0.08	0.18

In the absence of glaciers, the total runoff volumes in the Nam Co and Tangra Yumco basins would be about 13 % lower than with ice-melt water contribution. Thus, the mean annual lake-level increases of Nam Co and Tangra Yumco would be reduced from 0.24 to 0.15 m and from 0.29 to 0.17 m, respectively. In the Mapam Yumco and Paiku Co basins, the total runoff volumes would decrease by approximately 30 % and the resulting mean annual lake-level changes would be decreased from 0.02 to -0.18 m and from -0.07 to -0.25 m, respectively, under an ice-free scenario.

From this latter evaluation, it can be concluded that the mean annual net water budget would noticeably change without ice-meltwater contribution; however, the water balance in the Nam Co and Tangra Yumco remains positive. Based upon the J2000g modeling results, the differences in the water balance among the four studied lakes were primarily caused by relatively higher land runoff contributions in the Nam Co and Tangra Yumco basins compared to the Paiku Co and Mapam Yumco basins. This is related to relatively higher precipitation totals in the Nam Co and Tangra Yumco basins compared to the other two basins during the 2001-2010 period.

Over the study period, annual relative lake-volume changes in the four basins indicated similar patterns (Figure 6.32, Figure 6.45 - Figure 6.47). A relatively high correlation of lake-volume changes was found between the Nam Co and Tangra Yumco basins (r = 0.82). These are the basins with a higher proportion of June-through-September precipitation compared to the Paiku Co and Mapam Yumco basins.

The annual lake-volume changes of all four lakes were highly correlated to inter-annual variations of land runoff (r ≈ 0.99). The year-to-year variability of land runoff, in turn, was strongly related to inter-annual variations of precipitation (r ≈ 0.92). Inter-annual variability of lake evaporation was low in all four studied basins and it was not correlated to lake-level changes. There was also no correlation between annual glacier-melt amounts and lake-volume changes for the four basins.

Although the modeled annual glacier runoff was greater than the 10-year average in the year 2006 in all basins, lower precipitation amounts led to less land runoff, causing a lake-volume decrease in this year in all basins (Figure 6.32, Figure 6.45 - Figure 6.47). In contrast, the year 2008 was judged as having anomalous conditions, with modeled precipitation and land runoff substantially above average and with below-average glacier melt, resulting in a lake-volume increase in all basins (Figure 6.32, Figure 6.45 - Figure 6.47). Differences in annual lake-volume changes among the basins are caused principally by regional differences in the inter-annual variations of precipitation.
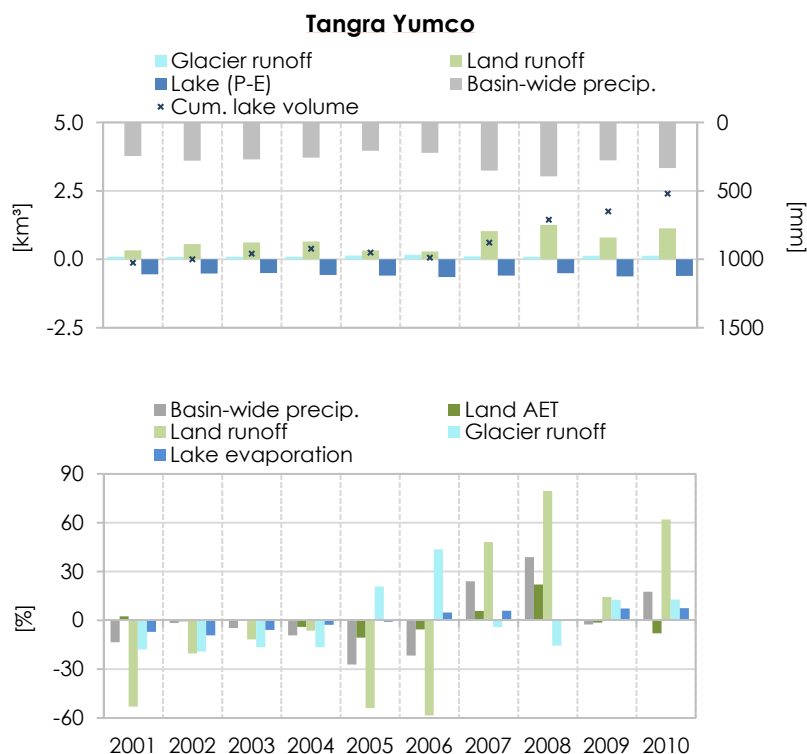
Figure 6.45: Cumulative lake-volume change (km³), contribution of several water-balance components (km³) to lake-volume change and basin-wide annual precipitation (mm yr⁻¹) for the Tangra Yumco basin (upper panel). Annual percentage deviations from the 10-year average of several water-balance components (lower panel).
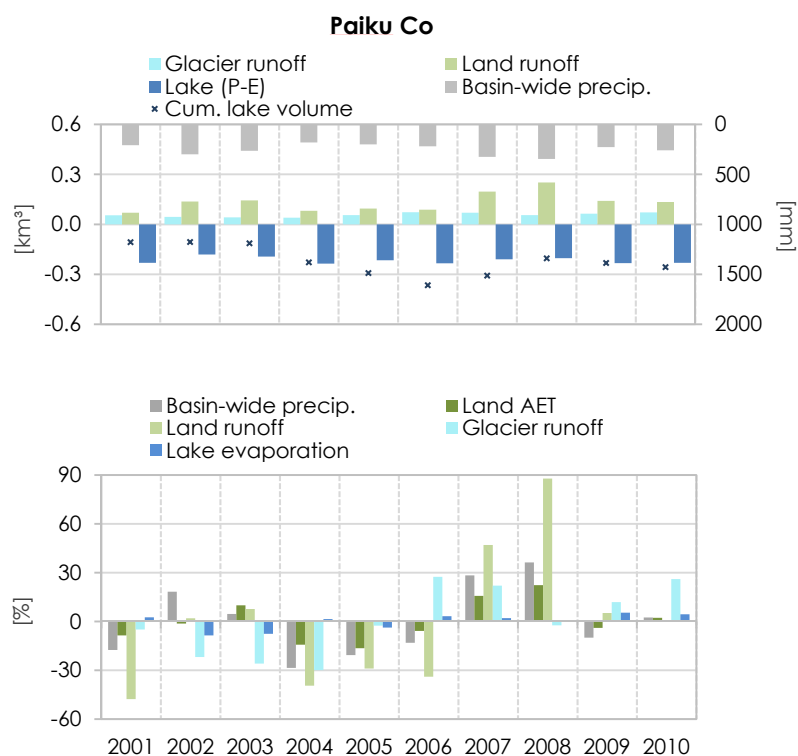
Figure 6.46: Cumulative lake-volume change (km³), contribution of several water-balance components (km³) to lake-volume change and basin-wide annual precipitation (mm yr⁻¹) for the Paiku Co basin (upper panel). Annual percentage deviations from the 10-year average of several water-balance components (lower panel).
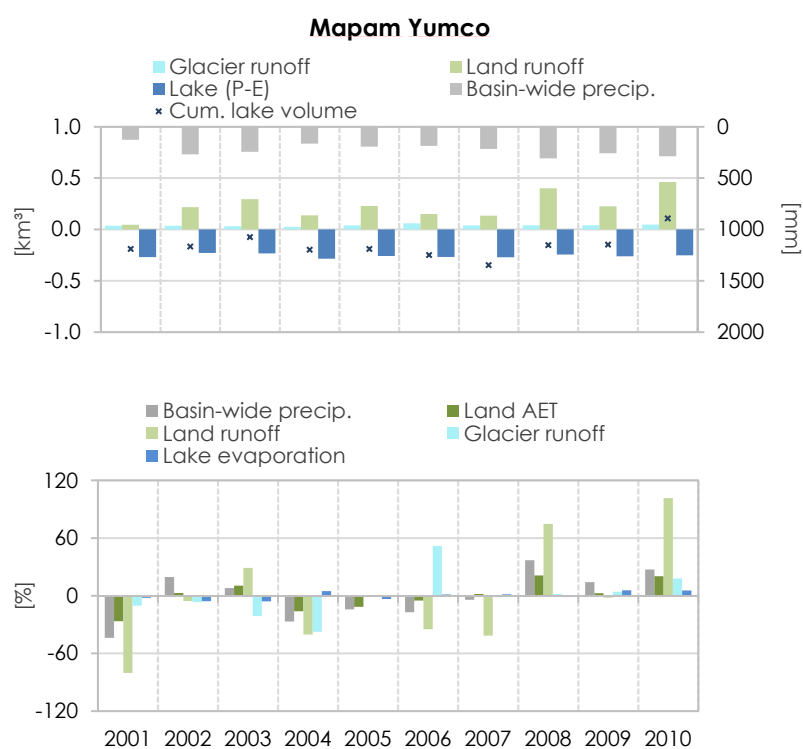
Figure 6.47: Cumulative lake-volume change (km³), contribution of several water-balance components (km³) to lake-volume change and basin-wide annual precipitation (mm yr⁻¹) for the Mapam Yumco basin (upper panel). Annual percentage deviations from the 10-year average of several water-balance components (lower panel).

7 DISCUSSION

7.1 Comparison with Other Studies

7.1.1 Estimation of the Water-Balance Components

Due to the scarcity of field measurements in the TP region, model simulations of water-balance components are limited in the TP region. Evaporation over lake surfaces has been estimated for only few lakes on the TP, based on model simulations (e.g., HAGINOYA *et al.*, 2009; MORRILL, 2004; XU *et al.*, 2009; YU *et al.*, 2011). Mean annual lake-evaporation estimates on the TP vary between 700 and 1200 mm. The lake-evaporation rates simulated with the J2000g model (between 710 and 910 mm yr^{-1}) are within this range (Table 6.15).

There are only few studies for assessing the actual evapotranspiration in the TP region, based on measurements and model simulations (e.g., GU *et al.*, 2008; YIN *et al.*, 2013; ZHU *et al.*, 2014). YIN *et al.* (2013) estimated AET over the entire TP using meteorological data available between 1981 and 2010 from 80 weather stations as model input for the Lund-Potsdam-Jena dynamic vegetation model (SITCH *et al.*, 2003). For the south-central TP, the simulated mean annual AET ranged from 100 to 300 mm, with generally higher values in the east and lower values in the drier regions in the west. The modeled AET estimates for the four studied basins varied between 170 and 290 mm yr^{-1}, decreasing from east (Nam Co basin) to west (Mapam Yumco basin) (Table 6.15). This compares favorably with the study reported by YIN *et al.* (2013).

Using a simplified procedure, YIN *et al.* (2013) developed spatial patterns of the surface-water budget over the entire TP for the 1981-2010 period by estimating the difference between precipitation and AET (P-AET). The results revealed that P-AET depends on climate regimes and gradually decreases from the east (~150 mm yr^{-1}) to the west (~50 mm yr^{-1}) in the study region. The J2000g model simulations indicate quite similar runoff patterns compared to the findings of YIN *et al.* (2013), with decreasing annual means from the east (~130 mm in the Nam Co basin) to the west (~60 mm in the Mapam Yumco basin). The calculated AET/precipitation ratio of around 0.7 in all basins is slightly higher than the ratio given by GU *et al.* (2008). They estimated that the average annual sum of AET was about 60 % of the annual precipitation for the three years 2002-2004 in an alpine meadow site in the northern TP.

The mean annual glacier runoff of 1320 mm, simulated with the J2000g model for the Nam Co basin, compares quite well with estimated glacier-melt quantities for the Zhadang glacier in the Nam Co basin using more complex SEB/MB models (HUINTJES *et al.*, 2015: 1325 mm yr^{-1}; MÖLG *et al.*, 2014: 1375 mm yr^{-1}).

7.1.2 Factors Controlling the Water Balance and Lake-Level Variability

As mentioned in Section 2.3.3, many studies emphasize the importance of glacier-meltwater contribution to the water budget of Tibetan lakes (e.g., ZHU *et al.*, 2010). However, estimates of glacier-meltwater contribution have large uncertainties due to the difficulty in quantifying glacier-volume changes in this data-scarce region (LI, B. *et al.*, 2014). Only few studies have quantitatively estimated glacier-meltwater contribution to total runoff. LI, B. *et al.* (2014) estimated a glacier-runoff contribution of 15 % of the total runoff (during 2006-2011) in a sub-basin of the Nam Co basin, the Qugaqie basin (8.4 % glacier coverage), using an energy-balance based glacier-melt model and the Gridded Subsurface Hydrologic Analysis model (DOWNER & OGDEN, 2004). Based upon the J2000g model results, the glacier contribution ranged between 14 and 30 % in the four studied basins (1-6 % glacier coverage) during the 2001-2010 period. This range of values is slightly higher than that computed by LI, B. *et al.* (2014) considering the percentage of basin area covered by glaciers.

Simulated glacier-meltwater contribution is generally lower compared to the runoff contribution from non-glacierized areas. However, glaciers make an important contribution to the water budget during the 10-year period considering the small extent of ice-covered areas in the four studied lake basins. Indeed, the water balance in the Nam Co and Tangra Yumco basins would also be positive without ice-meltwater contribution, based on the results of the ice-free scenarios. Thus, the question arises why the Nam Co and Tangra Yumco indicated a non-equilibrium state; whereas, Paiku Co and Mapam Yumco were at a state close to the hydrologic equilibrium during the study period.

As described in Section 2.3.1, endorheic lakes respond to climatic changes to maintain equilibrium between input and output, and to reach steady state. Due to the time lag of lakes in responding to climatic changes, this modeling study cannot confirm whether or not the shift towards a positive water balance in the Nam Co and Tangra Yumco basins or the negative shift in the water balance of the Paiku Co basin, respectively, was primarily caused by changes in precipitation, glacier melt, evapotranspiration, etc. However, as indicated in Section 6.3.2, inter-annual lake-level variations were highly positively correlated with precipitation and land runoff. This supports the assumption of other studies (e.g., LEI *et al.*, 2014; LI, Y. *et al.*, 2014; SONG *et al.*, 2014c) that increasing precipitation is the primary factor causing lake-level increases in the central TP (where Nam Co and Tangra Yumco are located). The results of the precipitation time-trend analysis in the Nam Co region (Section 6.1.1) also revealed a precipitation increase over the last decades (on average by ~10 % of the annual total per decade during 1981-2010).

The relative stability or slight lake-level declines in the marginal region of the TP (where Paiku Co and Mapam Yumco are located) seem to be related to relatively stable or slightly decreased precipitation (e.g., LEI *et al.*, 2014). Both changes in large-scale circulation systems and local circulation are assumed to be responsible for spatially varying changes in moisture flux over the TP (e.g., GAO *et al.*, 2014; 2015). However, these factors are still under debate and further research is needed (GAO *et al.*, 2015).

According to the J2000g model results, inter-annual variability of lake evaporation was low in all four studied basins and thus it seems to have had a minor impact on the year-to-year variability of lake levels during the last decade. Annual anomalies (Figure 6.32, Figure 6.45 - Figure 6.47)

indicated that lake evaporation has tended to increase over the last decade. This is in accordance with an overall increasing tendency of potential evaporation over the TP after 2000 (LI, Y. *et al.*, 2014, YIN, *et al.*, 2013). LI, Y. *et al.* (2014) argued that the recent rapid lake expansion in the central TP cannot be explained by changes in potential evaporation, because an increase in evaporation would negate the effect of increasing precipitation on lake levels.

However, potential evaporation decreased in most areas on the TP during 1961-2000, primarily caused by decreasing wind speeds (XIE & ZHU, 2013). Remarkably decreasing trends in wind speed were also detected in the Nam Co region (on average by ~10 % reduction per decade during 1981-2010, cf. Section 6.1.1) which agrees with trend rates given by XIE & ZHU (2013) (see Section 2.1.2). A decreasing time-trend in potential evaporation before 2000 might have resulted in rising lake levels in the central TP. However, this factor did not prevent the lake shrinkage along the south-west periphery of the TP, indicating that lake evaporation is not a primary factor for explaining the spatial differences of lake-level changes between the central and southern TP (LEI *et al.*, 2014).

No correlation was found between simulated inter-annual variations of glacier runoff and lake level. This suggests that glacier-melt runoff is not the main driving force for lake-level changes, at least for inter-annual lake variations during the last decade. Glacier-meltwater runoff played a greater role in dry years, but it could not compensate for lower precipitation totals and land runoff in the water balance (cf. Figure 6.32, Figure 6.45 - Figure 6.47). Under the assumption that glacier-melt runoff increased during the last decades due to climate warming (on average by ~0.5°C per decade during 1981-2010, cf. Section 6.1.1), it is very likely that glacier-meltwater supply augmented the precipitation-driven lake areal expansion in the Nam Co and Tangra Yumco basins. This is consistent with conclusions drawn by SONG *et al.* (2014c). This study found that few glacier-fed lakes experienced faster lake expansion than no-glacier-fed lakes. In the Mapam Yumco and Paiku Co basins, glacier-meltwater discharge might have mitigated lake-level declining and acted as a regulating factor. This is in accordance with assumptions made by YE *et al.* (2008) and NIE *et al.* (2012). A further rise in temperature would imply a probable increase in future glacier-melt runoff generation. However, this is not likely to last for a long time with continued climate warming. Glacier-meltwater runoff will eventually tend to decrease as glacier extent decreases (e.g., PRASCH *et al.*, 2013).

As previously mentioned in Section 2.3.3, some authors argued for the importance of permafrost degradation on recent lake-level changes (LI, Y. *et al.*, 2014; LIU *et al.*, 2009; 2010). LI, Y. *et al.* (2014) found a positive correlation between permafrost coverage and lake-level changes (2003-2009). Accelerated permafrost thawing might have contributed to the rapid lake expansion in the central and northern TP subregions, but the water contribution from permafrost will become limited when ground temperature increases above the melting point of the frozen soil (LI, Y. *et al.*, 2014). LI, Y. *et al.* (2014) suggest that permafrost meltwater contribution may have become already limited in the southern TP. This is difficult to corroborate given the absence of observational data for the studied lake basins. Furthermore, the Nam Co and Tangra Yumco basins in the central TP with a larger areal percentage with probable permafrost occurrence compared to the Paiku Co and Mapam Yumco basins in the south and southwest TP (according to the Global Permafrost Zonation Index Map, GRUBER, 2012; Figure A.8.1 - Figure A.8.4) indicated increasing lake levels during the last decades. The questions remain: *i)* how large is the volume of water released due to thinning and thawing of permafrost, and *ii)* to what extent can it

modulate basin runoff. These cannot be answered without adequate information about permafrost occurrence, thickness and ice content in the studied basins.

Differences in the response time or, in other words, the time required to reach an equilibrium state could also be a reason for observed differences in lake-level changes. Based upon remote sensing data, the lake areas of Nam Co and Tangra Yumco expanded by 4.6 and 1.8 %, respectively, between 1970 and 2008 (LIAO *et al.*, 2013). As illustrated in Figure 5.2, the underwater topography in the marginal areas of Nam Co reflects the topographic-relief conditions above the lake levels, with hill and mountainous terrain on the north and south sides and relatively flat floodplains west and east of Nam Co (Figure A.1). The lakeshore slopes of Tangra Yumco are steeper (Figure A.2), suggesting a steeper underwater landform distribution (bathymetry). Steep-sided lakes have a longer equilibrium response time, because of a lower rate of change of the lake area with volume (MASON, 1994). Based upon paleo-shorelines, the post-glacial lake-level high of the Nam Co and Tangra Yumco was about 29 m (SCHUETT *et al.*, 2008) and 185 m (RADES *et al.*, 2013), respectively, above the present-day lake level, supporting the assumption that the Nam Co has a shorter response time than Tangra Yumco to compensate for the increment in net inflow (i.e. faster and stronger reaction of its lake area). Moreover, the water supply coefficient (basin area/lake area ratio) for the Nam Co is smaller than for the Tangra Yumco basin (5.5 versus 11.0).

The lake extent of Paiku Co and Mapam Yumco decreased by 3.7 and 0.8 %, respectively, between 1970 and 2008 (LIAO *et al.*, 2013). The lakeshores of Mapam Yumco are generally flatter compared to the Paiku Co, which indicates gentle sandy shores to southeast and southwest, but steep-inclined shores in the northeast and northwest (Figure A.3, Figure A.4). However, due to only small lake-area variations of Mapam Yumco during the last decades (LIAO *et al.*, 2013), differences in lake morphology seem not to be the reason for the relative stability of the recent water levels of Mapam Yumco. Differences in the water-supply coefficient of the Paiku Co and Mapam Yumco basin are quite low (8.8 versus 10.6).

Based upon results of other studies in the region (e.g., LEI *et al.*, 2013), the effects of upwelling and downwelling groundwater related to fault zones and lake-groundwater exchanges on the water balance were assumed to be negligible. However, ZHOU *et al.* (2013) suggest that water leakage related to seepage might play an essential role in the hydrological cycle of the TP, due to the large numbers of lakes and the sub-surface fault system in the TP region.

Groundwater outflow from the Mapam Yumco to the Langa Co (located only a few kilometers to the west about 15 m below the Mapam Yumco) cannot be excluded and could be a reason for the relatively stable water levels of Mapam Yumco. It is assumed that Mapam Yumco and the Langa Co together once formed a much larger water body and that they have become separate water bodies, due to a warmer climate since Quaternary (GUAN *et al.*, 1984). In the more recent past, the Mapam Yumco and the Langa Co were connected by the natural river Ganga Chu having an extent about 10 km. However, currently there is no surface outflow (LIAO *et al.*, 2013).

7.2 Limitations and Uncertainties

7.2.1 Model Input Uncertainty

As stated in many studies (e.g., KNOCHE *et al.*, 2014; POHL *et al.*, 2015), precipitation input is the primary source of uncertainty in hydrological modeling studies in data-scarce regions. According to previous studies using HAR10 as input for glaciological modeling in the TP region (HUINTJES, 2014; HUINTJES *et al.*, 2015; MÖLG *et al.*, 2012, 2014), a precipitation-scaling factor < 1 was needed to be applied in the present study. Recently, HAR10 data served as input for hydrological modeling in the Pamir Mountains using the J2000g model (POHL *et al.*, 2015). However, this study also needed to apply a precipitation-scaling reduction factor. MAUSSION *et al.* (2014) could not find a systematic bias in comparison with station observations, but it is probable that overestimation of precipitation amounts occurs at high altitudes.

The precipitation-scaling factors were kept constant for the entire 10-year period, because there is no opportunity to derive varying scaling factors for individual years, due to a lack of observations in the lake basins included in this study. This may have affected the inter-annual variations of modeling results. The non-systematic deviations between simulated and measured lake levels of the Nam Co (Figure 6.31) might be related to a non-systematic error pattern in the HAR10 precipitation data. The primary issue is that HAR10 precipitation cannot be validated to a sufficient degree, because available data are for stations that are located at lower elevations, and no accuracy assessment can be done for the higher elevation zones where study basins are located. The comparison with available station data suggests that the accuracy of the precipitation data is probably regionally dependent (MAUSSION *et al.*, 2014). This makes it difficult to find a fixed precipitation-scaling factor that is applicable for different regions of the TP.

The values of the precipitation-scaling factor vary enormously among the several studies, from 0.37 in the Pamir Mountains (POHL *et al.*, 2015) to 0.79 in central TP (MÖLG *et al.*, 2014). The difficulty in obtaining meaningful precipitation-correction factors from comparison with in-situ data was demonstrated by POHL *et al.* (2015). Particularly in high mountainous regions, such a comparison may be strongly biased, depending on the location of any given meteorological station (e.g., precipitation shadows due to orographic effects) (POHL *et al.*, 2015). Thus, the only viable way to derive a precipitation-scaling factor is through evaluation of modeled hydrological quantities (POHL *et al.*, 2015). Comparing modeled hydrograph and observed discharge, POHL *et al.* (2015) concluded that a precipitation reduction by 63 % led to reliable model outputs; otherwise, the relatively high estimated precipitation amounts for higher elevations resulted in unrealistic snowmelt amounts that cannot be compensated for realistically in the model.

As described in Section 5.4.2.2, multiple model runs were conducted using precipitation-scaling factors between 0.3 and 1.0, seeking a precipitation-scaling factor that best simulates satellite-derived lake-volume changes. Figure 7.1 presents the modeled lake-volume change for each run and indicates how sensitive the model results are to the precipitation-scaling factor. There may be errors in the satellite-derived water-volume data, which in turn might have affected the estimation of the precipitation-scaling factor and thereby the accuracy of model results. However, the precipitation-scaling factors obtained for the Nam Co (0.80), Tangra Yumco (0.75) and Paiku Co (0.85) basins are relatively close to the scaling factor used for the Zhadang glacier in the Nam Co

basin in the study of MÖLG *et al.* (2014). They found very good agreement between glacier mass-balance model calculations and available in-situ measurements by applying a precipitation-scaling factor of 0.79. This gives confidence that the scaling factors used in this study seemed to be within an acceptable range.

The relatively low precipitation-scaling factor of 0.50 obtained for the Mapam Yumco basin seems to be plausible when comparing HAR10 precipitation with weather station data of Burang (30°17'N, 81°15'E, ~30 km to the south, closest station with available data) published in LIAO *et al.* (2013). The mean annual precipitation total of Burang is 150 mm yr^{-1} for the period 2001-2009; whereas, the nearest HAR10 point gives a mean annual precipitation amount of 330 mm yr^{-1}. HUINTJES (2014) also found that a reduction of the precipitation by more than 50 % leads to more reliable mass-balance results for the Naimona'nyi glacier (Gurla Mandhata, south western TP) which is located close to the Mapam Yumco basin.
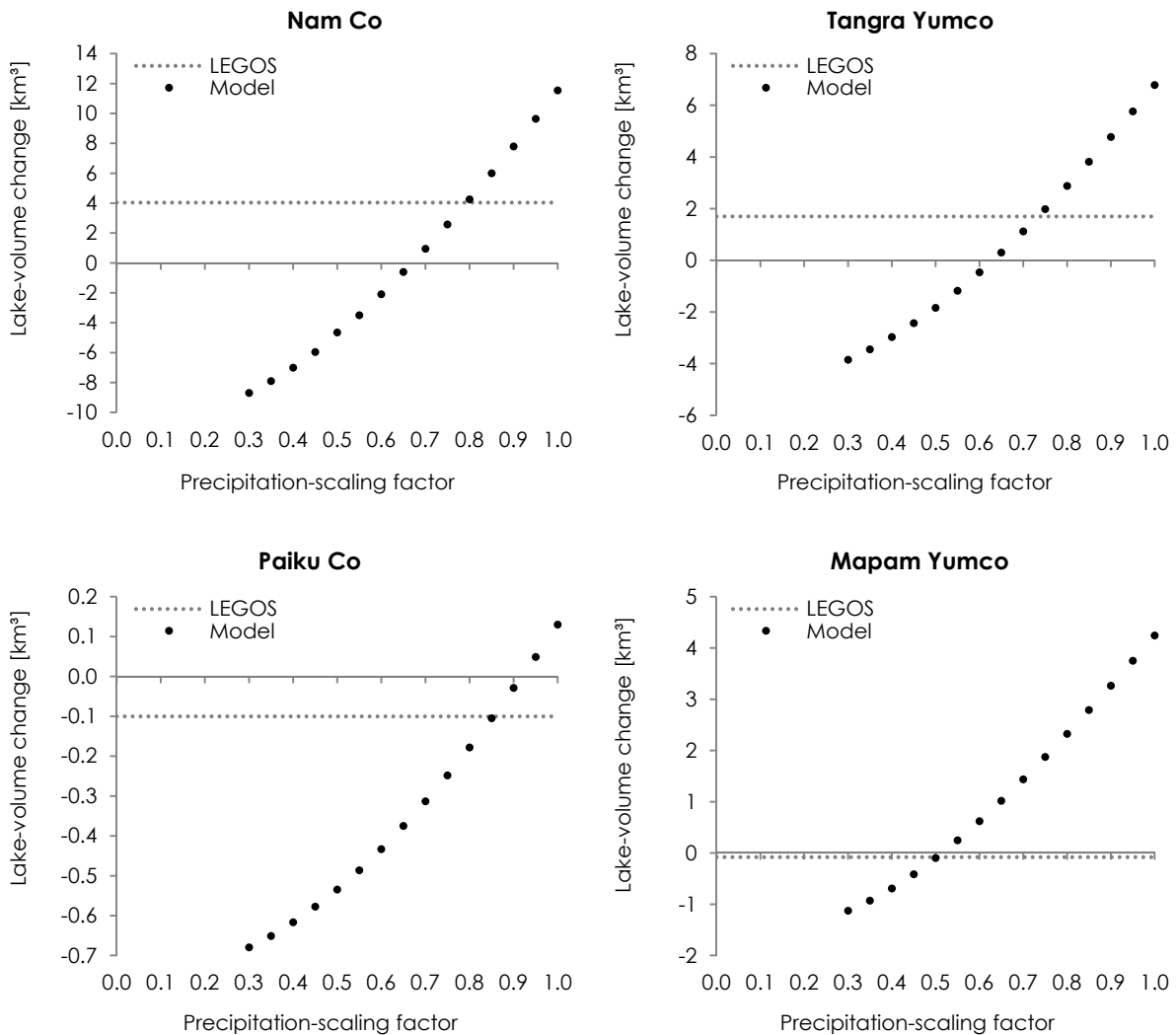
Figure 7.1: Simulated lake-volume changes for the four study lakes for the time period given in Table 3.1, using precipitation-scaling factors varying between 0.3 and 1.0. Dotted line indicates lake-volume changes derived from remote sensing data provided by LEGOS. The point where model dots are closest to the dotted line was taken as the precipitation-scaling factor.

Model-input uncertainty stems also from the fact that HAR10 grid points surrounding the lakes needed to be used as input for the modeling of lake evaporation and estimation of on-lake precipitation (cf. Section 4.2). Thus, specific climate conditions over the lake surfaces might not be represented sufficiently in the model. Furthermore, errors in air temperature calculated for single glacier HRUs might have affected glacier-melt simulations. Due to a lack of HAR10 grid points in highest elevations (glacier areas), daily temperature data of the closest HAR10 grid point combined with a constant lapse rate (0.65 K / 100 m) were used for any given glacier HRU. However, the local climate in high elevation zones, particularly in glacier areas, may vary considerably over short distances and time periods (BARRY, 2008).

7.2.2 Model Structure and Parameter Uncertainty

Besides model-input uncertainty, hydrological modeling in data-scarce regions is hindered by model parameter and structure uncertainty. In this study, model-parameter values were not estimated by calibration, except for the precipitation-scaling factor. Default settings of the J2000g model were applied or parameter values were taken from the literature, due to missing required calibration data. Because various parameter set combinations can lead to equally acceptable model outputs (BEVEN, 2001), ensemble modeling incorporating uncertainty and sensitivity assessment was conducted for the case study basin Nam Co, as suggested by other authors (e.g., MCINTYRE *et al.*, 2005; WINSEMIUS *et al.*, 2009). As discussed in Section 2.3, in the presence of data limitations statistical formal (probabilistic) methods are not applicable for uncertainty analysis and consequently an informal (non-probabilistic) method is required where subjectivity is unavoidable (MONTANARI *et al.*, 2009).

The GLUE approach, applied in this study, was used in hundreds of studies due to its simplicity and applicability (BEVEN & BINLEY, 2014). GLUE has often been criticized in the scientific literature, due to subjective determinations that influence ensemble prediction. However, as noted earlier, subjectivity cannot be prevented entirely in such informal approaches. Hence, estimated uncertainty ranges and parameter sensitivities (cf. Section 6.2.2) depend on the underlying assumptions, particularly the sampled range of the parameters and the choice of the performance criteria with associated limits of acceptability. In order to reduce the general subjectivity of the selection of thresholds for rejection criteria, the limits of acceptability should be based on best available hydrological knowledge and be estimated from an uncertainty assessment using the data with which model output would be compared (BEVEN & BINLEY, 2014; WINSEMIUS *et al.*, 2009). However, in practice it is often difficult, because the uncertainty of various data is often hard or impossible to quantify (WINSEMIUS *et al.*, 2009). Unfortunately, there was no information on errors in the satellite-derived lake-volume data that could be used to provide an acceptance range of lake-volume changes.

A general problem is that parameters may compensate for potential effects of model structure and input errors (BEVEN & BINLEY, 2014). This becomes especially clear from the analysis of estimating the precipitation-scaling factor. The precipitation-scaling factor can compensate for not only HAR10 data errors but also model-structure inadequacies. Blowing-snow sublimation was neglected in the modeling due to the complexity of this process in complex terrain (VIONNET *et al.*, 2014). However, wind-induced sublimation of suspended snow above the snow pack can be a significant water loss to the atmosphere (e.g., BOWLING *et al.*, 2004; STRASSER *et al.*, 2008; VIONNET *et al.*, 2014). VIONNET *et al.* (2014) simulated total sublimation (surface + blowing

snow) in alpine terrain (French Alps) using a fully coupled snow pack/atmosphere model. They estimated that blowing-snow sublimation is two thirds of total sublimation. This process is judged to be important in the study area, due to the relatively dry near-surface conditions and relatively higher wind speeds occurring during the winter months. Thus, the low value of the precipitation-scaling factor applied in the Mapam Yumco basin as well as in the Pamir Mountains in the study of POHL *et al.* (2015) might be an indication either that HAR10 precipitation is significantly overestimated in these specific regions or that drifting snow sublimation plays a greater role than in other regions.

The omission of processes such as snow redistribution by wind and avalanches and snow loss by blowing-snow sublimation may affect snow-cover patterns as well as the magnitude and timing of melt runoff (PELLICCIOTTI *et al.*, 2014). This could be a reason for the larger areal snow-cover extent in the model simulation during the winter season compared to MODIS (Figure 6.22). Explanations for the lower SCAF values of the model during the summer period could be related to the fact that the MODIS/Terra data are collected only in the morning (10:30 AM) rather than at several times during the day. This means that MODIS indicates snow cover at days when snow was accumulated during the previous night or early morning but which might be sublimated or melted later during the day (KROPACEK *et al.*, 2010).

Given the limited data availability, further assumptions and simplifications in the model were required. Seasonal soil freezing and thawing processes were neglected in the model, due to a lack of detailed soil data for the sub-basins. However, the impact of soil freezing and thawing on model results is assumed to be small, due to the low amount of water estimated to be stored in the soil during the winter months. It is likely that these processes have a higher effect on the timing than the magnitude of simulated runoff and the related lake-level. The currently implemented glacier-melt model component according to HOCK (1999) is a simple, robust and easy to use methodology that does not account for the transformation of snow into ice. Thus, simulated snowmelt amounts on glacier surfaces might be overestimated. Because glacier-volume changes are not considered in J2000g, unrealistic amounts of glacier-meltwater could be generated. However, the consideration of glacier-volume changes and ice redistribution would be of higher importance for long-term model simulations (e.g., SHEA *et al.*, 2015).

Effects of lake-groundwater interactions were neglected in the model, because the quantification of flow between aquifer systems and lakes is difficult (ROSENBERRY *et al.*, 2015). However, it is unclear if and to what extent intermittent (at irregular time intervals) exfiltration (flow from groundwater to a lake) and infiltration (flow from a lake to groundwater) processes might occur, thereby impacting water-level changes. The stated values of lake-groundwater exchange rates do strongly vary by more than five orders of magnitude within the literature (median exfiltration: 0.74 cm/day, median infiltration: 0.60 cm/day, ROSENBERRY *et al.*, 2015).

The lack of consideration of lake-groundwater interactions could be the reason that the observed lake-level decrease of the Nam Co was not well represented by the model. If lake levels rise higher than adjacent ground-water levels, lake water may move into the adjacent lakeshores' subsurface. This additional storage factor would basically have a dampening effect on lake-level dynamics. However, in view of multi-annual lake changes, lake-groundwater exchanges were assumed to be negligible. Another reason for the overestimation of the lake level in the months of October and November could be that lake evaporation was underestimated

in these months due to an insufficient representation of the heat-storage term. Due to the lack of lake-temperature depth profiles, the heat-storage change in the lakes was estimated using an empirical formulation (JENSEN *et al.*, 2005).

7.3   Implications for Further Research

Growing evidence indicates that mountainous areas are highly vulnerable to climate change by undergoing substantial cryospheric and hydrological changes with wide-spread implications for ecosystems and human societies (e.g., BENISTON, 2003; DIAZ *et al.*, 2003; RANGWALA *et al.*, 2013). Hydrological modeling has become an important tool for understanding how the hydrological system is functioning, i.e. the way a catchment responds to a certain input, but it is particularly challenging in mountainous regions due to data scarcity (PANDAY *et al.*, 2013). In fact, most of the basins on Earth are ungauged or poorly gauged, and it is necessary to benefit from any available hydrological information for model applications (e.g., HRACHOWITZ *et al.*, 2013). The research initiative '*Predictions in Ungauged Basins (PUB)*' (SIVAPALAN *et al.*, 2003) emphasized the need to move away from classical rainfall-runoff 'curve-fitting' approaches towards more innovative approaches integrating data sets obtained from different observation technologies and strategies.

The presented study contributes to the PUB initiative by providing a robust modeling framework that can be applied in remote regions where in-situ data are limited or even unavailable. This thesis emphasizes the value of combining hydrological modeling with atmospheric-model output and satellite-derived data to handle the data-scarcity problem in remote regions. Because model-derived atmospheric and remote sensing data cannot achieve the precision of in-situ measurements, the modeling has inherent uncertainties which should be perceived as useful information for further research rather than a lack of basic knowledge or understanding (BLÖSCHL & MONTANARI, 2010).

Research effort must be directed towards emerging observation techniques which are able to capture space and time variability of hydrological processes as well as of their controlling factors such climatic and landscape properties (surface and subsurface) (e.g., WAGENER *et al.*, 2010). As ground observations are often limited by financial, logistical and time constraints, increasingly available remote sensing data (e.g., soil-moisture content, evapotranspiration, etc.) with high spatial and temporal resolution can be highly valuable for improving distributed hydrological models and thereby reducing model uncertainties in data-scarce regions. A key question today is how, and to what extent remote sensing and satellite information can be integrated into hydrological modeling to provide more robust water balance estimates at ungauged or poorly gauged catchments and to help better represent the variability of water-cycle components in space and time (e.g., HRACHOWITZ *et al.*, 2013). Innovative remote-sensing methods, e.g. the terrestrial water storage-change observations from GRACE (TAPLEY *et al.*, 2004), offer advances in monitoring hydrological patterns to account for scale heterogeneity and to infer changes at larger scales.

Because most of the catchments are increasingly affected by anthropogenic impacts such as urban/agricultural development under changing climatic boundary conditions, a new initiative for the Scientific Decade 2013-2022, entitled '*Panta Rhei - Everything Flows*', has been proposed (MONTANARI *et al.*, 2013). The overall goal of the Panta Rhei initiative is to improve the understanding of changing process dynamics governing the water cycle and the capability to

make hydrological predictions by advancing monitoring, data analysis and modeling techniques (MONTANARI *et al.*, 2013). The modeling framework presented in this study has the potential to make an important contribution to the Panta Rhei initiative. Due to the modular model structure, the model has high flexibility and adaptability to integrate new components within the model framework, opening new directions of research. Linking paleo lake-level high stands and hydrological modeling will allow for a better understanding of past hydrological and related paleo-climate conditions. Understanding hydrological system behavior under past and present climate conditions is essential to forecast its evolution in the near future, which is critically important for ecosystem and water-resources management (BLÖSCHL & MONTANARI, 2010). The developed modeling tool was specially designed for investigations of the hydrological system behavior of endorheic lake basins across the TP. However, it may form the basis for hydrological predictions in other semi-arid cold regions in Asia, North America, etc. and thereby support societal development in terms of water-related demands in a changing environment.

8 CONCLUSION AND FUTURE NEEDS

8.1 Overall Conclusions

The contrasting patterns of lake-level fluctuations across the TP are sensitive indicators for regional differences in water-balance estimates. However, quantitative water-balance estimates of endorheic lakes in the TP are limited in this data-scarce region. Hydrological modeling is required to allow for a quantitative assessment of differences in the water balance and thus a better understanding of the factors affecting water balance in the TP region.

Addressing this research need, the overall objective of this study was the development and application of a hydrological modeling approach, in order to contribute to a more quantitative understanding of the factors controlling the water balance and lake-level variability in the TP. In this study, four endorheic lakes across the southern-central part of the TP were selected to investigate differences in the water balance on catchment scale: Nam Co and Tangra Yumco with increasing water levels, and Mapam Yumco and Paiku Co with stable or slightly decreasing water levels, respectively.

Hydrological modeling in data-scarce regions faces many challenges, mainly due to a lack of reliable data for model input, calibration and validation. This study demonstrates the feasibility of a methodological approach combining distributed hydrological modeling with atmospheric-model output and various satellite-based data to overcome the data-scarcity problem in the TP. To meet the challenge of applying a model that is simple enough to account for data limitations and complex enough to represent relevant hydrological processes, a distributed, conceptual model structure of the J2000g model was judged to be appropriate.

The J2000g model was adapted and extended according to the local conditions in endorheic lake basins on the TP, focusing on the implementation of robust model routines facing data scarcity and process complexity. The model-derived atmospheric data HAR10 and satellite-derived lake-water surface temperature served as input for the modeling period 2001-2010. Due to missing continuous lake-level in-situ data, satellite-derived lake-volume changes were used as a model-performance criterion.

The adapted J2000g model version reasonably captured seasonal dynamics of relevant hydrological processes. The overall agreement between lake-level simulations and in-situ observations from the Nam Co confirms the capability of the model to provide reliable simulated estimates of monthly-averaged lake-level fluctuations. However, water-balance estimates of individual years should be considered carefully, due to possible unsystematic error patterns in HAR10 precipitation. Nevertheless, uncertainties which appear to be related to the precipitation-scaling factor, should not affect the overall conclusions drawn from the model-application results.

The major outcomes can be summarized as follows:

- The seasonal hydrological dynamics and spatial variations of runoff generation within the basins were similar for all the studied lake basins; however, the several water-balance components varied quantitatively among the four basins.

- Differences in the mean annual water balances among the four basins were primarily related to higher precipitation totals and attributed runoff generation in the basins with a higher monsoon influence (Nam Co and Tangra Yumco). The incoming water into to the Nam Co and Tangra Yumco exceeded the water loss term by a factor of approximately 1.5; whereas, the water input in the Mapam Yumco and Paiku Co basins was not large enough to compensate for the water output.

- The glacier-meltwater contribution to the total basin runoff volume (between 14 and 30 % averaged over the 10-year period) played a less important role compared to runoff generation from rainfall and snowmelt on non-glacierized land areas. Indeed, glaciers made an important contribution to the water budget during the 10-year period considering the small part of glacier areas (1 to 6 % of the total basin area).

- Based upon hypothetical ice-free scenarios in the hydrological model, ice-melt water constitutes an important water-supply component for basins with lower precipitation (Mapam Yumco and Paiku Co), in order to maintain a state close to equilibrium; whereas, the water balance in the basins with higher precipitation (Nam Co and Tangra Yumco) would be still positive under ice-free conditions.

- Precipitation and related runoff were the main driving forces for inter-annual lake-level variations during the 2001-2010 period. Both were highly positively correlated with annual lake-level changes during the 10-year period; whereas, no correlation was found between inter-annual variability of lake levels and glacier runoff or lake evaporation.

For the 10-year modeling period used in this study, it is not possible to draw definitive conclusions regarding the hydrological changes that might have led to imbalances in the water budgets of the four studied lakes. However, the model results support the assumptions of other studies that contrasting patterns in lake-level fluctuations across the TP are closely linked to spatial differences in precipitation. Relatively stable or slightly decreased precipitation might have kept the level of Paiku Co and Mapam Yumco with little or no change; whereas, increased precipitation in the central TP could have caused the lake-level increases of Nam Co and Tangra Yumco during the last decades.

This study highlights the possible benefits of combining hydrological modeling with atmospheric-model output and satellite-derived data to investigate quantitatively differences in the water-balance components of endorheic lake basins in the TP. The integration of readily available model-derived atmospheric and remote-sensing data with hydrological modeling has the potential to improve our understanding of spatiotemporal hydrological patterns and to quantify water-balance components, even in ungauged or poorly gauged basins. The results of this study provide a useful basis for future regionally focused investigations on the space-time transition of lake changes in the TP. This thesis provides a robust modeling framework that serves as a valuable tool for improving our understanding of atmosphere, cryosphere and hydrosphere linkages not only in the TP, but also in other remote regions of the world where observational data are scarce.

8.2 Future Research Needs

Given the constraints of this study, following main research needs were identified, in order to provide a better representation of local conditions and further understanding of the hydrological response of high-altitude endorheic lakes in the TP to climate variability and change:

- A higher spatial resolution of the atmospheric-model output to better represent the vertical distribution of meteorological variables.

- Meteorological observations (particularly precipitation in high mountain regions) to confirm the plausibility of model-derived atmospheric data.

- Emerging earth and ground observations which are able to incorporate both space and time variability of landscape properties (surface and subsurface) and thereby to reduce the model uncertainties arising from land-surface parameterization.

- Continuous lake-level in-situ measurements or water-level and volume estimations with a higher temporal resolution from new satellite-altimetry data, such as from Cryosat (continuously data available since 2012, planed until 2017), Sentinel-3 (2015) and Jason-CS (2017) (KLEINHERENBRINK *et al.*, 2015) for a better calibration or validation in further model applications in the future.

- Model-independent data describing spatiotemporal patterns of hydrological system components which can be used for multi-response validation, providing more reliable assumptions on the suitability of the different model components apart from indicating where further improvements would be useful.

- Information on bathymetry and lake-temperature depth profiles to implement an energy budget based thermal model for the simulation of freezing and melting of water on the lake surface and a more reliable estimation of the heat-storage term.

- Investigations to assess and monitor ground water aquifers to clarify the role of lake-groundwater interactions in deriving the water balance.

- Detailed soil data to include the simulation of seasonal soil freezing and thawing processes in the model.

- Detailed information on permafrost occurrence, thickness and ice content to enable permafrost-melt simulations, aiming to quantify potentially permafrost meltwater contribution to lake-level changes.

- In-situ measurements of snow depth and density as well as wind and radiative fluxes from the upper sections of the glaciers and the surroundings to take into account processes such as snow redistribution by wind and avalanches and snow loss by blowing-snow sublimation.

- The estimation of glacier ice storage changes to allow for long-term model simulations (e.g., SHEA *et al.*, 2015).

REFERENCES

AD-HOC Arbeitsgruppe Boden (2005). *Bodenkundliche Kartieranleitung* (5th ed.). Hannover: Schweizerbart'sche Verlagsbuchhandlung.

Allen, R. G., Pereira, L. S., Raes, D., & Smith, M. (1998). *Crop evapotranspiration: Guidelines for computing crop water requirements. FAO Irrigation and drainage paper 56*. Rome, Italy.

Andréassian, V., Le Moine, N., Perrin, C., Ramos, M.-H., Oudin, L., Mathevet, T., … Berthet, L. (2012). All that glitters is not gold: the case of calibrating hydrological models. *Hydrological Processes*, *26*(14), 2206–2210.

Anslow, F. S., Hostetler, S., Bidlake, W. R., & Clark, P. U. (2008). Distributed energy balance modeling of South Cascade Glacier, Washington and assessment of model uncertainty. *Journal of Geophysical Research*, *113*, F02019, doi:10.1029/2007JF000850.

Atkinson, S. E., Woods, R. A., & Sivapalan, M. (2002). Climate and landscape controls on water balance model complexity over changing timescales. *Water Resources Research*, *38*(12), doi:10.1029/2002WR001487.

Barnes, W. L., Pagano, T. S., & Salomonson, V. V. (1998). Prelaunch characteristics of the Moderate Resolution Imaging Spectroradiometer (MODIS) on EOS-AM1. *Geoscience and Remote Sensing, IEEE Transactions on*, *36*(4), 1088–1100.

Barry, R. G. (2008). *Mountain Weather and Climate* (3rd ed.). Cambridge University Press.

Barry, R. G., & Chorley, R. J. (2003). *Atmosphere, weather and climate* (8th ed.). London: Routledge.

Beniston, M. (2003). Climatic change in mountain regions: A review of possible impacts. *Climatic Change*, *59*(1-2), 5–31.

Benn, D. I., & Owen, L. A. (1998). The role of the Indian summer monsoon and the mid-latitude westerlies in Himalayan glaciation: review and speculative discussion, *155*(1992), 353–363.

Bertle, F. A. (1966). *Effects of Snow Compaction on Runoff from Rain on Snow*. Bureau of Reclamation, Engineering Monograph No. 35, Washington.

Beven, K. (2001). How far can we go in distributed hydrological modelling? *Hydrology and Earth System Sciences*, *5*(1), 1–12.

Beven, K. (2006). A manifesto for the equifinality thesis. *Journal of Hydrology*, *320*(1-2), 18–36.

Beven, K., & Binley, A. (1992). The future of distributed models: Model calibration and uncertainty prediction. *Hydrological Processes*, *6*, 279–298.

Beven, K., & Binley, A. (2014). GLUE: 20 years on. *Hydrological Processes*, *28*(24), 5897–5918.

Beven, K., & Freer, J. (2001). Equifinality, data assimilation, and uncertainty estimation in mechanistic modelling of complex environmental systems using the GLUE methodology. *Journal of Hydrology*, *249*, 11–29.

Biermann, T., Babel, W., Ma, W., Chen, X., Thiem, E., Ma, Y., & Foken, T. (2013). Turbulent flux observations and modelling over a shallow lake and a wet grassland in the Nam Co basin, Tibetan Plateau. *Theoretical and Applied Climatology*, *116*(1-2), 301–316.

Blöschl, G. (2001). Scaling in hydrology. *Hydrological Processes*, *15*(4), 709–711.

Blöschl, G. (2006). Hydrologic synthesis: Across processes, places, and scales. *Water Resources Research*, *42*, W03S02, doi:10.1029/2005WR004319.

Blöschl, G., & Montanari, A. (2010). Climate change impacts-throwing the dice? *Hydrological Processes*, *24*, 374–381.

Blöschl, G., & Sivapalan, M. (1995). Scale issues in hydrological modelling: a review. *Hydrological Processes*, *9*, 251–290.

Blöschl, G., Sivapalan, M., Wagener, T., Viglione, A., & Savenije, H. (2013). *Runoff Prediction in Ungauged Basins: Synthesis Across Processes, Places and Scales*. Cambridge University Press.

Bolch, T. (2011). *Assessment of Cryospheric Variations in Different Climatic Regimes and Their Impacts Using Geomatics*. Habilitation, TU Dresden.

Bolch, T., Kulkarni, A., Kääb, A., Huggel, C., Paul, F., Cogley, J. G., … Stoffel, M. (2012). The state and fate of Himalayan glaciers. *Science*, *336*(6079), 310–314.

Bolch, T., Yao, T., Kang, S., Buchroithner, M. F., Scherer, D., Maussion, F., … Schneider, C. (2010). A glacier inventory for the western Nyainqentanglha Range and the Nam Co Basin, Tibet, and glacier changes 1976–2009. *The Cryosphere*, *4*(3), 419–433.

Boltzmann, L. (1884). Ableitung des Stefan'schen Gesetzes, betreffend die Abhängigkeit der Wärmestrahlung von der Temperatur aus der electromagnetischen Lichttheorie. *Ann. Phys.*, 258, 291–294. doi: 10.1002/andp.18842580616.

Bonan, G. (2008). *Ecological Climatology. Concepts and Applications*. Cambridge University Press.

Boos, W. R., & Kuang, Z. (2010). Dominant control of the South Asian monsoon by orographic insulation versus plateau heating. *Nature*, *463*, 218–22.

Bothe, O., Fraedrich, K., & Zhu, X. (2011). Large-scale circulations and Tibetan Plateau summer drought and wetness in a high-resolution climate. *International Journal of Climatology*, *31*, 832–846.

Bothe, O., Fraedrich, K., & Zhu, X. (2012). Tibetan Plateau summer precipitation: covariability with circulation indices. *Theoretical and Applied Climatology*, *108*, 293–300.

Bowling, L. C., Pomeroy, J. W., & Lettenmaier, D. P. (2004). Parameterization of Blowing-Snow Sublimation in a Macroscale Hydrology Model. *Journal of Hydrometeorology*, *5*, 745–762.

Branstator, G. (2002). Circumglobal Teleconnections, the Jet Stream Waveguide, and the North Atlantic Oscillation. *Journal of Climate*, *15*(14), 1893–1910.

Brutsaert, W. (1975). On a Derivable Formula for Long-Wave Radiation From Clear Skies. *Water Resources Research*, *11*(5), 742–744.

Burn, D., & Hag Elnur, M. (2002). Detection of hydrologic trends and variability. *Journal of Hydrology*, *255*(1-4), 107–122.

Cao, J., Qin, D., Kang, E., & Li, Y. (2006). River discharge changes in the Qinghai-Tibet Plateau. *Chinese Science Bulletin*, *51*(5), 594–600.

Chang, D. H. S. (1981). The Vegetation Zonation of the Tibetan Plateau. *Mountain Research and Development*, *1*(1), 29–48.

Che, T., Xin, L., Jin, R., Armstrong, R., & Zhang, T. (2008). Snow depth derived from passive microwave remote-sensing data in China. *Annals of Glaciology*, *49*, 145–154.

Chen, B., Chao, W., & Liu, X. (2003). Enhanced climatic warming in the Tibetan Plateau due to doubling CO2: a model study. *Climate Dynamics*, *20*, 401–413.

Chen, B., Xu, X.-D., Yang, S., & Zhang, W. (2012). On the origin and destination of atmospheric moisture and air mass over the Tibetan Plateau. *Theoretical and Applied Climatology*, *110*(3), 423–435.

Cheng, G., & Jin, H. (2013). Permafrost and groundwater on the Qinghai-Tibet Plateau and in northeast China. *Hydrogeology Journal*, *21*(1), 5–23.

Clark, M. P., Hendrikx, J., Slater, A. G., Kavetski, D., Anderson, B., Cullen, N. J., … Woods, R. A. (2011). Representing spatial variability of snow water equivalent in hydrologic and land-surface models: A review. *Water Resources Research*, *47*, W07539, doi:10.1029/2011WR010745.

Crawford, T. M., & Duchon, C. E. (1999). An Improved Parameterization for Estimating Effective Atmospheric Emissivity for Use in Calculating Daytime Downwelling Longwave Radiation. *Journal of Applied Meteorology*, *38*, 474–480.

Crétaux, J.-F., Jelinski, W., Calmant, S., Kouraev, A., Vuglinski, V., Bergé-Nguyen, M., … Maisongrande, P. (2011). SOLS: A lake database to monitor in the Near Real Time water level and storage variations from remote sensing data. *Advances in Space Research*, *47*(9), 1497–1507.

Cuo, L., Zhang, Y., Zhu, F., & Liang, L. (2014). Characteristics and changes of streamflow on the Tibetan Plateau: A review. *Journal of Hydrology: Regional Studies*, *2*, 49–68.

Curio, J., Maussion, F., & Scherer, D. (2014). A twelve-year high-resolution climatology of atmospheric water transport on the Tibetan Plateau. *Earth Syst. Dynam.*, *6*, 109–124.

Daniel, E. B., Camp, J. V, Leboeuf, E. J., Penrod, J. R., Dobbins, J. P., & Abkowitz, M. D. (2011). Watershed Modeling and its Applications: A State-of-the-Art Review. *The Open Hydrology Journal*, *5*, 26–50.

Deardorff, J. W. (1978). Efficient prediction of ground surface temperature and moisture, with inclusion of a layer of vegetation. *Journal of Geophysical Research*, *83*(C4), 1889–1903.

Dehotin, J., & Braud, I. (2008). Which spatial discretization for distributed hydrological models? Proposition of a methodology and illustration for medium to large-scale catchments. *Hydrology and Earth System Sciences*, *12*(3), 769–796.

Deus, D., Gloaguen, R., & Krause, P. (2013). Water Balance Modeling in a Semi-Arid Environment with Limited in situ Data Using Remote Sensing in Lake Manyara, East African Rift, Tanzania. *Remote Sensing*, *5*, 1651–1680.

Diaz, H., Grosjean, M., & Graumlich, L. (2003). Climate Variability and Change in High Elevation Regions: Past, Present and Future. *Climatic Change*, *59*(1), 1–4.

Ding, Q., & Wang, B. (2005). Circumglobal Teleconnection in the Northern Hemisphere Summer. *Journal of Climate*, *18*(17), 3483–3505.

Doorenboos, J., & Pruitt, W. O. (1977). *Guidelines for predicting crop water requirements. FAO irrigation and drainage paper 24*. Rome, Italy.

Downer, C., & Ogden, F. (2004). GSSHA: Model To Simulate Diverse Stream Flow Producing Processes. *Journal of Hydrologic Engineering*, *9*(3), 161–174.

Du, M., Kawashima, S., Yonemura, S., Yamada, T., Zhang, X., Liu, J., … Tang, Y. (2007). Temperature distribution in the high mountain regions on the Tibetan Plateau-Measurement and simulation. In L. Oxley & D. Kulasiri (Eds.), *MODSIM2007 International Congress on Modelling and Simulation, 10-13 December 2007* (pp. 2146–2152). Christchurch, New Zealand: Modelling and Simulation Society of Australia and New Zealand.

DVWK (1996). *Ermittlung der Verdunstung von Land- und Wasserflächen*. In Merkblätter zur Wasserwirtschaft, Nr. 238.

Efstratiadis, A., & Koutsoyiannis, D. (2010). One decade of multi-objective calibration approaches in hydrological modelling: a review. *Hydrological Sciences Journal*, *55*(1), 58–78.

Ehret, U., Gupta, H. V, Sivapalan, M., Weijs, S. V, Schymanski, S. J., Blöschl, G., … Harman, C. (2014). Advancing catchment hydrology to deal with predictions under change. *Hydrology and Earth System Sciences*, *18*, 649–671.

Farr, T. G., Rosen, P. A., Caro, E., Crippen, R., Duren, R., Hensley, S., … Alsdorf, D. E. (2007). The shuttle radar topography mission. *Reviews of Geophysics*, *45*, RG2004, doi:10.1029/2005RG000183.

Feng, L., & Zhou, T. (2012). Water vapor transport for summer precipitation over the Tibetan Plateau: Multidata set analysis. *Journal of Geophysical Research: Atmospheres*, *117*, D20114, doi:10.1029/2011JD017012.

Fischer, C. (2013). *Automatische Kalibrierung hydrologischer Modelle*. Dissertation, FSU Jena.

Fischer, C., Kralisch, S., Krause, P., Fink, M., & Flügel, W. (2009). Calibration of hydrological model parameters with the JAMS framework. In R. S. Anderssen, R. D. Braddock, & L. T. H. Newham (Eds.), *18th World IMACS Congress and MODSIM09 International Congress on Modelling and Simulation, 13-17 July 2009.* (pp. 866–872). Cairns, Australia: Modelling and Simulation Society of Australia and New Zealand and International Association for Mathematics and Computers in Simulation.

Flügel, W.-A. (1995). Delineating Hydrological Response Units by Geographical Information System analyses for regional hydrological modelling using PRMS/MMS in the drainage basin of the river Bröl, Germany. *Hydrological Processes*, *9*, 423–436.

Frauenfeld, O. W., Zhang, T., & Serreze, M. C. (2005). Climate change and variability using European Centre for Medium-Range Weather Forecasts reanalysis (ERA-40) temperatures on the Tibetan Plateau. *Journal of Geophysical Research*, *110*, D2101, doi:10.1029/2004JD005230.

Freer, J., Beven, K., & Ambroise, B. (1996). Bayesian Estimation of Uncertainty in Runoff Prediction and the Value of Data: An Application of the GLUE Approach. *Water Resources Research*, *32*(7), 2161–2173.

Fuhrer, O., & Schär, C. (2005). Embedded cellular convection in moist flow past topography. *Journal of the Atmospheric Sciences*, *62*(8), 2810–2828.

Fujita, K., & Ageta, Y. (2000). Effect of summer accumulation on glacier mass balance on the Tibetan Plateau revealed by mass-balance model. *Journal of Glaciology*, *46*(153), 244–252.

Gao, T., Kang, S., Krause, P., Cuo, L., & Nepal, S. (2011). A test of J2000 model in a glacierized catchment in the central Tibetan Plateau. *Environmental Earth Sciences*, *65*(6), 1651–1659.

Gao, Y., Cuo, L., & Zhang, Y. (2014). Changes in moisture flux over the tibetan plateau during 1979-2011 and possible mechanisms. *Journal of Climate*, *27*(5), 1876–1893.

Gao, Y., Leung, L. R., Zhang, Y., & Cuo, L. (2015). Changes in Moisture Flux over the Tibetan Plateau during 1979–2011: Insights from a High-Resolution Simulation. *Journal of Climate*, *28*(10), 4185–4197.

Gao, Y., Xie, H., Yao, T., & Xue, C. (2010). Integrated assessment on multi-temporal and multi-sensor combinations for reducing cloud obscuration of MODIS snow cover products of the Pacific Northwest USA. *Remote Sensing of Environment*, *114*(8), 1662–1675.

Gruber, S. (2012). Derivation and analysis of a high-resolution estimate of global permafrost zonation. *The Cryosphere*, *6*(1), 221–233.

Gu, S., Tang, Y., Cui, X., Du, M., Zhao, L., Li, Y., … Zhao, X. (2008). Characterizing evapotranspiration over a meadow ecosystem on the Qinghai-Tibetan Plateau. *Journal of Geophysical Research*, *113*, D08118, doi:10.1029/2007JD009173.

Guan, Z. H., Chen, C. Y., Ou, Y. X. (1984). *Rivers and Lakes of Xizang, the Series of the Scientific Expedition to the Qinghai-Xizang Plateau.* Beijing: Science Press (in Chinese).

Guo, D., Wang, H., & Li, D. (2012). A projection of permafrost degradation on the Tibetan Plateau during the 21st century. *Journal of Geophysical Research*, *117*, D05106, doi:10.1029/2011JD016545.

Guo, Z. G., Zhou, X. R., & Hou, Y. (2012). Effect of available burrow densities of plateau pika (Ochotona curzoniae) on soil physicochemical property of the bare land and vegetation land in the Qinghai-Tibetan Plateau. *Acta Ecologica Sinica*, *32*(2), 104–110.

Gupta, H., Sorooshian, S., & Yapo, P. (1999). Status of Automatic Calibration for Hydrologic Models: Comparison with Multilevel Expert Calibration. *Journal of Hydrologic Engineering*, *4*(2), 135–143.

Gupta, H. V., Sorooshian, S., & Yapo, P. O. (1998). Toward improved calibration of hydrologic models: Multiple and noncommensurable measures of information. *Water Resources Research*, *34*(4), 751–763.

Gupta, H. V, Beven, K. J., & Wagener, T. (2006). Model Calibration and Uncertainty Estimation. In M. G. Anderson (Ed.), *Encyclopedia of Hydrological Sciences. 11:131*. John Wiley & Sons, Ltd. doi:10.1002/0470848944.hsa138.

Gupta, H. V, Perrin, C., Blöschl, G., Montanari, A., Kumar, R., Clark, M., & Andréassian, V. (2014). Large-sample hydrology: a need to balance depth with breadth. *Hydrological Earth System Sciences*, *18*, 463–477.

Haginoya, S., Fujii, H., Kuwagata, T., Xu, J., Ishigooka, Y., Kang, S., & Zhang, Y. (2009). Air Lake Interaction Features Found in Heat and Water Exchanges over Nam Co on the Tibetan Plateau. *Scientific Online Letters on the Atmosphere*, *5*, 172–175.

Hahn, D. G., & Manabe, S. (1975). The role of Mountains in the South Asian Monsoon Circulation. *Journal of Atmospheric Sciences*, *32*, 1515–1541.

Hall, D. K., Riggs, G. A., Salomonson, V. V, DiGirolamo, N. E., & Bayr, K. J. (2002). MODIS snow-cover products. *Remote Sensing of Environment*, *83*(1-2), 181–194.

Hazewinkel, M. (2001). *Trigonometric functions. Encyclopedia of Mathematics*, Springer.

He, Y., Zhang, Z., Theakstone, W. H., Chen, T., Yao, T., & Pang, H. (2003). Changing features of the climate and glaciers in China's monsoonal temperate glacier region. *Journal of Geophysical Research*, *108*(D17), 4530, doi:10.1029/2002JD003365.

Henderson-Sellers, B. (1986). Calculating the Surface Energy Balance for Lake and Reservoir Modeling: A Review. *Reviews of Geophysics*, *24*(3), 625–649.

Heynen, M., Pellicciotti, F., & Carenzo, M. (2013). Parameter sensitivity of a distributed enhanced temperature-index melt model. *Annals of Glaciology*, *54*(63), 311–321.

Hock, R. (1999). A distributed temperature-index ice- and snowmelt model including potential direct solar radiation. *Journal of Glaciology*, *45*(149), 101–111.

Hock, R. (2003). Temperature index melt modelling in mountain areas. *Journal of Hydrology*, *282*(1-4), 104–115.

Hornberger M., G., & Spear C., R. (1981). An approach to the preliminary analysis of environmental systems. *Journal of Environmental Management*, *12*(1), 7–18.

Hrachowitz, M., Savenije, H. H. G., Blöschl, G., McDonnell, J. J., Sivapalan, M., Pomeroy, J. W., … Cudennec, C. (2013). A decade of Predictions in Ungauged Basins (PUB)-a review. *Hydrological Sciences Journal*, *58*(6), 1198–1255.

Huintjes, E. (2014). *Energy and mass balance modelling for glaciers on the Tibetan Plateau - Extension, validation and application of a coupled snow and energy balance model*. Dissertation, RWTH Aachen.

Huintjes, E., Sauter, T., Schröter, B., Maussion, F., Yang, W., Kropácek, J., … Schneider, C. (2015). Evaluation of a Coupled Snow and Energy Balance Model for Zhadang Glacier, Tibetan Plateau, Using Glaciological Measurements and Time-Lapse Photography. *Arctic, Antarctic, and Alpine Research*, *47*(3), 573–590.

Huss, M., Farinotti, D., Bauder, A., & Funk, M. (2008). Modelling runoff from highly glacierized alpine drainage basins in a changing climate. *Hydrological Processes*, *22*, 3888–3902.

Hutchinson, M. F. (1989). A new procedure for gridding elevation and stream line data with automatic removal of spurious pits. *Journal of Hydrology*, *106*(3–4), 211–232.

Ihaka, R., & Gentleman, R. (1996). R: A Language for Data Analysis and Graphics. *Journal of Computational and Graphical Statistics*, *5*(3), 299–314.

Iman, R. L., & Helton, J. C. (1988). An Investigation of Uncertainty and Sensitivity Analysis Techniques for Computer Models. *Risk Analysis*, *8*(1), 71–90.

Immerzeel, W. W., Droogers, P., de Jong, S. M., & Bierkens, M. F. P. (2009). Large-scale monitoring of snow cover and runoff simulation in Himalayan river basins using remote sensing. *Remote Sensing of Environment*, *113*(1), 40–49.

Immerzeel, W. W., Pellicciotti, F., & Bierkens, M. F. P. (2013). Rising river flows throughout the twenty-first century in two Himalayan glacierized watersheds. *Nature Geoscience*, *6*, 742–745.

Immerzeel, W. W., van Beek, L. P. H., & Bierkens, M. F. P. (2010). Climate Change Will Affect the Asian Water Towers. *Science*, *328*, 1382–1385.

Jakeman, A. J., Letcher, R. A., & Norton, J. P. (2006). Ten iterative steps in development and evaluation of environmental models. *Environmental Modelling & Software*, *21*(5), 602–614.

Jayatilaka, C. J., Storm, B., & Mudgway, L. B. (1998). Simulation of water flow on irrigation bay scale with MIKE-SHE. *Journal of Hydrology*, *208*(1–2), 108–130.

Jensen, M., Dotan, A., & Sanford, R. (2005). Penman-Monteith Estimates of Reservoir Evaporation. In P. E. Raymond Walton (Ed.), *World Water and Environmental Resources Congress 2005: Impacts of Global Climate Change, 15-19 May 2005* (pp. 1–24). Anchoraga, Alaska, USA: American Society of Civil Engineers. doi:10.1061/40792(173)548.

Jensen, M. E. (2010). Estimating evaporation from water surfaces. *Presented at the CSU/ARS Evapotranspiration Workshop, 12 March 2010*. Retrieved from http://deepcreekanswers.com/info/evaporation/ET_water_surf.pdf

Jenson, S. K., & Domingue, J. O. (1988). Extracting Topographic Structure from Digital Elevation Data for Geographic Information System Analysis. *Photogrammetric Engineering and Remote Sensing*, *54*(11), 1593–1600.

Kääb, A., Berthier, E., Nuth, C., Gardelle, J., & Arnaud, Y. (2012). Contrasting patterns of early twenty-first-century glacier mass change in the Himalayas. *Nature*, *488*(7412), 495–8.

Kaiser, K. (2007). *Soils and terrestrial sediments as indicators of Holocene environmental changes on the Tibetan Plateau*. Habilitation Thesis, University of Marburg.

Kaiser, K., Miehe, G., Barthelmes, A., Ehrmann, O., Scharf, A., Schult, M., … Frenzel, B. (2008). Turf-bearing topsoils on the central Tibetan Plateau, China: Pedology, botany, geochronology. *Catena*, *73*(3), 300–311.

Kampf, S. K., & Burges, S. J. (2007). A framework for classifying and comparing distributed hillslope and catchment hydrologic models. *Water Resources Research*, *43*, W05423, doi:10.1029/2006WR005370.

Kang, S., Chen, F., Gao, T., Zhang, Y., Yang, W., Yu, W., & Yao, T. (2009). Early onset of rainy season suppresses glacier melt: a case study on Zhadang glacier, Tibetan Plateau. *Journal of Glaciology*, *55*(192), 755–758.

Kang, S., Xu, Y., You, Q., Flügel, W.-A., Pepin, N., & Yao, T. (2010). Review of climate and cryospheric change in the Tibetan Plateau. *Environmental Research Letters*, *5*(1), 1–8.

Kattel, D. B., Yao, T., Yang, K., Tian, L., Yang, G., & Joswiak, D. (2012). Temperature lapse rate in complex mountain terrain on the southern slope of the central Himalayas. *Theoretical and Applied Climatology*, *113*(3-4), 671–682.

Kendall, M. G. (1975). *Rank Correlation Methods*. London: Charles Griffin.

Kirchner, J. W. (2006). Getting the right answers for the right reasons: Linking measurements, analyses, and models to advance the science of hydrology. *Water Resources Research*, *42*, W03S04, doi:10.1029/2005WR004362.

Kirshbaum, D. J., & Durran, D. R. (2004). Factors Governing Cellular Convection in Orographic Precipitation. *Journal of the Atmospheric Sciences*, *61*(6), 682–698.

Kleinhans, M. G., Bierkens, M. F. P., & van der Perk, M. (2010). On the use of laboratory experimentation: "Hydrologists, bring out shovels and garden hoses and hit the dirt." *Hydrology and Earth System Sciences*, *14*(2), 369–382.

Kleinherenbrink, M., Lindenbergh, R. C., & Ditmar, P. G. (2015). Monitoring of lake level changes on the Tibetan Plateau and Tian Shan by retracking Cryosat SARIn waveforms. *Journal of Hydrology*, *521*, 119–131.

Knauf, D. (1980). Die Berechnung des Abflusses aus einer Schneedecke. *Schriftenreihe des Deutschen Verbandes für Wasserwirtschaft und Kulturbau*, *46*, 97–135.

Knoche, M., Fischer, C., Pohl, E., Krause, P., & Merz, R. (2014). Combined uncertainty of hydrological model complexity and satellite-based forcing data evaluated in two data-scarce semi-arid catchments in Ethiopia. *Journal of Hydrology*, *519*, 2049–2066.

Kocis, L., & Whiten, W. J. (1997). Computational investigations of low-discrepancy sequences. *ACM Transactions on Mathematical Software*, *23*(2), 266–294.

Kralisch, S., & Fischer, C. (2012). Model representation, parameter calibration and parallel computing – the JAMS approach. In R. Seppelt, A. A. Voinov, S. Lange, & D. Bankamp (Eds.), *International Congress on Environmental Modelling and Software: Managing Resources of a Limited Planet: Pathways and Visions under Uncertainty, Sixth Biennial Meeting, 1-5 July* (pp. 1177–1184). Leipzig, Germany: International Environmental Modelling and Software Society (iEMSs).

Kralisch, S., & Krause, P. (2006). JAMS – A Framework for Natural Resource Model Development and Application. In A. Voinov, A. Jakeman, & A. E. Rizzoli (Eds.), *International Congress on Environmental Modelling and Software: Summit on Environmental Modelling and Software, Third Biannual Meeting, 9-13 July*. Burlington, Vermont, USA: International Environmental Modelling and Software Society.

Kralisch, S., Krause, P., Fink, M., Fischer, C., & Flügel, W.-A. (2007). Component based environmental modelling using the JAMS framework. In L. Oxley & D. Kulasiri (Eds.), *MODSIM 2007 International Congress on Modelling and Simulation, 10-13 December 2007* (pp. 812–818). Christchurch, New Zealand: Modelling and Simulation Society of Australia and New Zealand.

Krause, P. (2002). Quantifying the impact of land use changes on the water balance of large catchments using the J2000 model. *Physics and Chemistry of the Earth*, *27*, 663–673.

Krause, P., Bäse, F., Bende-Michl, U., Fink, M., Flügel, W.-A., & Pfennig, B. (2006). Multiscale investigations in a mesoscale catchment – hydrological modelling in the Gera catchment project. *Advances in Geosciences*, *9*, 53–61.

Krause, P., Biskop, S., Helmschrot, J., Flügel, W.-A., Kang, S., & Gao, T. (2010). Hydrological system analysis and modelling of the Nam Co basin in Tibet. *Advances in Geosciences*, *27*, 29–36.

Krause, P., & Hanisch, S. (2009). Simulation and analysis of the impact of projected climate change on the spatially distributed waterbalance in Thuringia, Germany. *Advances in Geosciences*, *21*, 33–48.

Krause, P., & Kralisch, S. (2005). The hydrological modelling system J2000 - knowledge core for JAMS. In A. Zerger & R. M. Argent (Eds.), *MODSIM 2005 International Congress on Modelling and Simulation.* (pp. 676–682). Melbourne, Australia: Modelling and Simulation Society of Australia and New Zealand.

Kropacek, J., Braun, A., Kang, S., Feng, C., Ye, Q., & Hochschild, V. (2012). International Journal of Applied Earth Observation and Geoinformation Analysis of lake level changes in Nam Co in central Tibet utilizing synergistic satellite altimetry and optical imagery. *International Journal of Applied Earth Observation and Geoinformation*, *17*, 3–11.

Kropacek, J., Feng, C., Alle, M., Kang, S., & Hochschild, V. (2010). Temporal and Spatial Aspects of Snow Distribution in the Nam Co Basin on the Tibetan Plateau from MODIS Data. *Remote Sensing*, *2*(12), 2700–2712.

Kuchment, L. S., Demidov, V. N. & Motovolov, Y. G. (1983). Formirovanie rechnogo stok (fiziko- matematichestde modeli) (River runoff formation/physically based models) (in Russian). Nauka, Moscow.

Kuczera, G., Kavetski, D., Franks, S., & Thyer, M. (2006). Towards a Bayesian total error analysis of conceptual rainfall-runoff models: Characterising model error using storm-dependent parameters. *Journal of Hydrology*, *331*(1-2), 161–177.

Kuczera, G., & Mroczkowski, M. (1998). Assessment of hydrologic parameter uncertainty and the worth of multiresponse data. *Water Resources Research*, *34*(6), 1481–1489.

Leavesley, G. H., Lichty, R. W., Troutman, B. M., & Saindon, L. G. (1983). Precipitation-Runoff Modeling System: User´s Manual. *U.S. Geological Survey, Water-Resources Investigations Report 83-4238*.

Leber, D., Holawe, F., & Häusler, H. (1995). Climatic Classification of the Tibet Autonomous Region Using Multivariate Statistical Methods. *GeoJournal*, *37*(4), 451–472.

Lei, Y., Yang, K., Wang, B., Sheng, Y., Bird, B. W., Zhang, G., & Tian, L. (2014). Response of inland lake dynamics over the Tibetan Plateau to climate change. *Climatic Change*, *125*, 281–290.

Lei, Y., Yao, T., Bird, B. W., Yang, K., Zhai, J., & Sheng, Y. (2013). Coherent lake growth on the central Tibetan Plateau since the 1970s: Characterization and attribution. *Journal of Hydrology*, *483*, 61–67.

Li, B., Yu, Z., Liang, Z., & Acharya, K. (2014). Hydrologic response of a high altitude glacierized basin in the central Tibetan Plateau. *Global and Planetary Change*, *118*, 69–84.

Li, F., Zhang, Y., Xu, Z., Liu, C., Zhou, Y., & Liu, W. (2014). Runoff predictions in ungauged catchments in southeast Tibetan Plateau. *Journal of Hydrology*, *511*, 28–38.

Li, F., Zhang, Y., Xu, Z., Teng, J., Liu, C., Liu, W., & Mpelasoka, F. (2013). The impact of climate change on runoff in the southeastern Tibetan Plateau. *Journal of Hydrology*, *505*, 188–201.

Li, L., Li, J., Yao, X., Luo, J., Huang, Y., & Feng, Y. (2014). Changes of the three holy lakes in recent years and quantitative analysis of the influencing factors. *Quaternary International*, *349*, 339–345.

Li, R., Zhao, L., Ding, Y., Wu, T., Xiao, Y., Du, E., … Qiao, Y. (2012). Temporal and spatial variations of the active layer along the Qinghai-Tibet Highway in a permafrost region. *Chinese Science Bulletin*, *57*(35), 4609–4616.

Li, X., Jin, R., Pan, X., Zhang, T., & Guo, J. (2012). Changes in the near-surface soil freeze–thaw cycle on the Qinghai-Tibetan Plateau. *International Journal of Applied Earth Observation and Geoinformation*, *17*, 33–42.

Li, Y., Liao, J., Guo, H., Liu, Z., & Shen, G. (2014). Patterns and Potential Drivers of Dramatic Changes in Tibetan Lakes, 1972–2010. *PLoS ONE*, *9*(11), e111890, doi:10.1371/journal.pone.0111890.

Liao, J., Shen, G., & Li, Y. (2013). Lake variations in response to climate change in the Tibetan Plateau in the past 40 years. *International Journal of Digital Earth*, *6*(6), 534–549.

Lin, C., Yang, K., Qin, J., & Fu, R. (2012). Observed Coherent Trends of Surface and Upper-Air Wind Speed over China since 1960. *Journal of Climate*, *26*(9), 2891–2903.

Lin, X., Zhang, Y., Yao, Z., Gong, T., Wang, H., Chu, D., … Zhang, F. (2008). The trend on runoff variations in the Lhasa River Basin. *Journal of Geographical Sciences*, *18*(1), 95–106.

Linacre, E. T. (1993). Data-sparse estimation of lake evaporation, using a simplified Penman equation. *Agriculture and Forest Meteorology*, *64*, 237–256.

Liu, J., Kang, S., Gong, T., & Lu, A. (2010). Growth of a high-elevation large inland lake, associated with climate change and permafrost degradation in Tibet. *Hydrological Earth System Sciences*, *14*, 481–489.

Liu, J., Wang, S., Yu, S., Yang, D., & Zhang, L. (2009). Climate warming and growth of high-elevation inland lakes on the Tibetan Plateau. *Global and Planetary Change*, *67*(3-4), 209–217.

Liu, X., & Chen, B. (2000). Climate Warming in the Tibetan Plateau during recent decades. *International Journal of Climatology*, *20*, 1729–1742.

Liu, X., Yin, Z.-Y., Shao, X., & Qin, N. (2006). Temporal trends and variability of daily maximum and minimum, extreme temperature events, and growing season length over the eastern and central Tibetan Plateau during 1961–2003. *Journal of Geophysical Research*, *111*, D19109, doi:10.1029/2005JD006915.

Liu, X., Zheng, H., Zhang, M., & Liu, C. (2011). Identification of dominant climate factor for pan evaporation trend in the Tibetan Plateau. *Journal of Geographical Sciences*, *21*(4), 594–608.

Ly, S., Charles, C., & Degré, A. (2013). Different methods for spatial interpolation of rainfall data for operational hydrology and hydrological modeling at watershed scale. A review. *Biotechnol. Agron. Soc. Environ.*, *17*(2), 392–406.

MacCallum, S. N., & Merchant, C. J. (2012). Surface water temperature observations of large lakes by optimal estimation. *Canadian Journal of Remote Sensing*, *38*(01), 25–45.

Maidment, D. R. (1993). *Handbook of Hydrology*. New York: McGraw-Hill.

Mann, H. (1945). Nonparametric tests against trend. *Econometrica*, *12*, 245–249.

Mason, I. M. (1994). The response of lake levels and areas to climatic change. *Climatic Change*, *27*(2), 161–197.

Maussion, F. (2014). *A new atmospheric dataset for High Asia: Development, validation and applications in climatology and in glaciology.* Dissertation, TU Berlin.

Maussion, F., Scherer, D., Mölg, T., Collier, E., Curio, J., & Finkelnburg, R. (2014). Precipitation Seasonality and Variability over the Tibetan Plateau as Resolved by the High Asia Reanalysis. *Journal of Climate*, *27*(5), 1910–1927.

McDonnell, J. J., Sivapalan, M., Vaché, K., Dunn, S., Grant, G., Haggerty, R., … Weiler, M. (2007). Moving beyond heterogeneity and process complexity: A new vision for watershed hydrology. *Water Resources Research*, *43*, W07301, doi:10.1029/2006WR005467.

McIntyre, N., Lee, H., Wheater, H., Young, A., & Wagener, T. (2005). Ensemble predictions of runoff in ungauged catchments. *Water Resources Research*, *41*, W12434, doi:10.1029/2005WR004289.

Meng, K., Shi, X., Wang, E., & Liu, F. (2012). High-altitude salt lake elevation changes and glacial ablation in Central Tibet, 2000–2010. *Chinese Science Bulletin*, *57*(5), 525–534.

Miehe, G., Miehe, S., & Bach, K. (2011). Plant communities of central Tibetan pastures in the Alpine Steppe/ Kobresia pygmaea ecotone. *Journal of Arid Environments*, *75*(8), 711–723.

Miehe, G., Miehe, S., Kaiser, K., Liu, J., & Zhao, X. (2008). Status and dynamics of the Kobresia pygmaea ecosystem on the Tibetan plateau. *Ambio*, *37*(4), 272–279.

Miehe, S., Miehe, G., Leeuwen, J. F. N., Wrozyna, C., Knaap, W. O., Duo, L., & Haberzettl, T. (2014). Persistence of Artemisia steppe in the Tangra Yumco Basin, west-central Tibet, China: despite or in consequence of Holocene lake-level changes? *Journal of Paleolimnology*, *51*(2), 267–285.

Mölg, T., Maussion, F., & Scherer, D. (2014). Mid-latitude westerlies as a driver of glacier variability in monsoonal High Asia. *Nature Climate Change*, *4*(1), 68–73.

Mölg, T., Maussion, F., Yang, W., & Scherer, D. (2012). The footprint of Asian monsoon dynamics in the mass and energy balance of a Tibetan glacier. *The Cryosphere*, *6*(6), 1445–1461.

Montanari, A. (2007). What do we mean by "uncertainty"? The need for a consistent wording about uncertainty assessment in hydrology. *Hydrological Processes*, *21*, 841–845.

Montanari, A., & Koutsoyiannis, D. (2012). A blueprint for process-based modeling of uncertain hydrological systems. *Water Resources Research*, *48*, W09555, doi:10.1029/2011WR011412.

Montanari, A., Shoemaker, C. A., & van de Giesen, N. (2009). Introduction to special section on Uncertainty Assessment in Surface and Subsurface Hydrology: An overview of issues and challenges. *Water Resources Research*, *45*(12), W00B00, doi:10.1029/2009WR008471.

Montanari, A., & Toth, E. (2007). Calibration of hydrological models in the spectral domain: An opportunity for scarcely gauged basins? *Water Resources Research*, *43*, W05434, doi:10.1029/2006WR005184.

Montanari, A., Young, G., Savenije, H. H. G., Hughes, D., Wagener, T., Ren, L. L., … Belyaev, V. (2013). "Panta Rhei-Everything Flows": Change in hydrology and society-The IAHS Scientific Decade 2013–2022. *Hydrological Sciences Journal*, *58*(6), 1256–1275.

Monteith, J. L. (1965). Evaporation and environment. *Symp. Soc. Exp. Biol.*, *19*, 205–234.

Moore, I. D., Grayson, R. B., & Ladson, A. R. (1991). Digital Terrain Modelling: a review of hydrological, geomorphological, and biological applications. *Hydrological Processes*, *5*, 3–30.

Morrill, C. (2004). The influence of Asian summer monsoon variability on the water balance of a Tibetan lake. *Journal of Paleolimnology*, *32*(3), 273–286.

Neckel, N., Kropáček, J., Bolch, T., & Hochschild, V. (2014). Glacier mass changes on the Tibetan Plateau 2003–2009 derived from ICESat laser altimetry measurements. *Environmental Research Letters*, *9*, doi:10.1088/1748–9326/9/1/014009.

Nepal, S. (2012). *Evaluating Upstream-Downstream Linkages of Hydrological Dynamics in the Himalayan Region*.

Nepal, S., Krause, P., Flügel, W.-A., Fink, M., & Fischer, C. (2014). Understanding the hydrological system dynamics of a glaciated alpine catchment in the Himalayan region using the J2000 hydrological model. *Hydrological Processes*, *28*(3), 1329–1344.

Nie, Y., Zhang, Y., Ding, M., Liu, L., & Wang, Z. (2012). Lake change and its implication in the vicinity of Mt. Qomolangma (Everest), central high Himalayas, 1970–2009. *Environmental Earth Sciences*, *68*(1), 251–265.

Panday, P. K., Williams, C. a., Frey, K. E., & Brown, M. E. (2013). Application and evaluation of a snowmelt runoff model in the Tamor River basin, Eastern Himalaya using a Markov Chain Monte Carlo (MCMC) data assimilation approach. *Hydrological Processes*, doi: 10.1002/hyp.10005.

Parajka, J., & Blöschl, G. (2008). Spatio-temporal combination of MODIS images – potential for snow cover mapping. *Water Resources Research*, *44*, W03406, doi:10.1029/2007WR006204.

Pellicciotti, F., Buergi, C., Immerzeel, W. W., Konz, M., & Shrestha, A. B. (2012). Challenges and Uncertainties in Hydrological Modeling of Remote Hindu Kush–Karakoram–Himalayan (HKH) Basins: Suggestions for Calibration Strategies. *Mountain Research and Development*, *32*(1), 39–50.

Pellicciotti, F., Ragettli, S., Carenzo, M., & McPhee, J. (2014). Changes of glaciers in the Andes of Chile and priorities for future work. *The Science of the Total Environment*, *493*, 1197–1210.

Penman, H. L. (1948). Natural evaporation from open water, bare and grass. *Proceedings of the Royal Society of London. Series A, Mathematical and Physical*, *193*(1032), 120–145.

Phan, V. H., Lindenbergh, R. C., & Menenti, M. (2013). Geometric dependency of Tibetan lakes on glacial runoff. *Hydrology and Earth System Sciences*, *17*, 4061–4077.

Phan, V. H., Lindenbergh, R., & Menenti, M. (2012). ICESat derived elevation changes of Tibetan lakes between 2003 and 2009. *International Journal of Applied Earth Observation and Geoinformation*, *17*, 12–22.

Phan, V. H., Lindenbergh, R., & Menenti, M. (2012). Seasonal trends in Tibetan lake level changes as observed by ICESAT Laser Altimetry. *ISPRS Annals of the Photogrammetry, Remote Sensing and Spatial Information Sciences*, *I*(7), 237–242.

Plüss, C. G. (1996). The energy balance over an alpine snowcover point measurements and areal distribution. *Züricher Geographische Schriften*, *65*, 128.

Pohl, E., Knoche, M., Gloaguen, R., Andermann, C., & Krause, P. (2015). Sensitivity analysis and implications for surface processes from a hydrological modelling approach in the Gunt catchment, high Pamir Mountains. *Earth Surface Dynamics*, *3*(3), 333–362.

Pokhrel, P., Yilmaz, K. K., & Gupta, H. V. (2012). Multiple-criteria calibration of a distributed watershed model using spatial regularization and response signatures. *Journal of Hydrology*, *418-419*, 49–60.

Prasch, M., Mauser, W., & Weber, M. (2013). Quantifying present and future glacier melt-water contribution to runoff in a central Himalayan river basin. *The Cryosphere*, *7*(3), 889–904.

Pu, Z., & Xu, L. (2008). MODIS/Terra observed snow cover over the Tibet Plateau: distribution, variation and possible connection with the East Asian Summer Monsoon (EASM). *Theoretical and Applied Climatology*, *97*(3-4), 265–278.

Qin, J., Yang, K., Liang, S., & Guo, X. (2009). The altitudinal dependence of recent rapid warming over the Tibetan Plateau. *Climatic Change*, *97*(1-2), 321–327.

Qiu, J. (2008). The third pole. *Nature*, *454*, 393–396.

Qiu, Y., Guo, H., Shi, J., & Lemmetyinen, J. (2012). Satellite-Based Snow Cover Analysis and the Snow Water Equivalent Retrieval Perspective over China. In Y. Chemin (Ed.), *Remote Sensing of Planet Earth* (pp. 47–74). InTech.

Quin, D., Liu, S., & Li, P. (2006). Snow Cover Distribution , Variability, and Response to Climate Change in Western China. *Journal of Climate*, *19*, 1820–1833.

Rades, E. F., Hetzel, R., Xu, Q., & Ding, L. (2013). Constraining Holocene lake-level highstands on the Tibetan Plateau by 10Be exposure dating: a case study at Tangra Yumco, southern Tibet. *Quaternary Science Reviews*, *82*, 68–77.

Ragettli, S., & Pellicciotti, F. (2012). Calibration of a physically based, spatially distributed hydrological model in a glacierized basin: On the use of knowledge from glaciometeorological processes to constrain model parameters. *Water Resources Research*, *48*, W03509, doi:10.1029/2011WR010559.

Ragettli, S., Pellicciotti, F., Bordoy, R., & Immerzeel, W. W. (2013). Sources of uncertainty in modeling the glaciohydrological response of a Karakoram watershed to climate change. *Water Resources Research*, *49*, 6048–6066.

Raghavan, B. K. (1973). Tibetan Anticyclone and Tropical Easterly Jet. *Pageoph*, *110*, 2130–2142.

Rajagopalan, B., & Molnar, P. (2013). Signatures of Tibetan Plateau heating on Indian summer monsoon rainfall variability. *Journal of Geophysical Research: Atmospheres*, *118*(3), 1170–1178.

Rangwala, I., Sinsky, E., & Miller, J. R. (2013). Amplified warming projections for high altitude regions of the northern hemisphere mid-latitudes from CMIP5 models. *Environmental Research Letters*, *8*, 024040, doi:10.1088/1748–9326/8/2/024040.

Refsgaard, J. C. (1997). Parameterisation, calibration and validation of distributed hydrological models. *Journal of Hydrology*, *198*(1-4), 69–97.

Refsgaard, J. C., & Henriksen, H. J. (2004). Modelling guidelines – terminology and guiding principles. *Advances in Water Resources*, *27*, 71–82.

Riggs, G. A., Hall, D. K., & Salomonson, V. V. (2006). *MODIS Snow Products User Guide to Collection 5*.

Rödiger, T., Geyer, S., Mallast, U., Merz, R., Krause, P., Fischer, C., & Siebert, C. (2014). Multi-response calibration of a conceptual hydrological model in the semiarid catchment of Wadi al Arab, Jordan. *Journal of Hydrology*, *509*, 193–206.

Rodríguez, E., Morris, C. S., & Belz, J. E. (2006). A Global Assessment of the SRTM Performance. *Photogramm. Eng. & Remote Sens.*, *72*(3), 249–260.

Rogers, R. R., & Yau, M. K. (1989). *A Short Course in Cloud Physics*. Oxford: Pergamon Press.

Rohrer, M. B. (1992). Die Schneedecke im Schweizer Alpenraum und ihre Modellierung. Analyse langjähriger Schneemessungen und Modellierung des Wasseräquivalentes aufgrund zeitlich hoch aufgelöster operationell gemessener meteorologischer Daten. *Züricher Geographische Schriften*, *49*, 178.

Rosenberry, D. O., Lewandowski, J., Meinikmann, K., & Nützmann, G. (2015). Groundwater - the disregarded component in lake water and nutrient budgets. Part 1: effects of groundwater on hydrology. *Hydrological Processes*, *29*(13), 2895–2921.

Saltelli, A., Tarantola, S., Campolongo, F., & Ratto, M. (2004). *Sensitivity analysis in practice. A guide to assessing scientific models*. John Wiley & Sons, Ltd.

Schaefli, B., Harman, C. J., Sivapalan, M., & Schymanski, S. J. (2011). HESS Opinions: Hydrologic predictions in a changing environment: behavioral modeling. *Hydrology and Earth System Sciences*, *15*(2), 635–646.

Schaefli, B., & Zehe, E. (2009). Hydrological model performance and parameter estimation in the wavelet-domain. *Hydrology and Earth System Sciences*, *13*, 1921–1936.

Scherler, D., Bookhagen, B., & Strecker, M. R. (2011). Spatially variable response of Himalayan glaciers to climate change affected by debris cover. *Nature Geoscience*, *4*(3), 156–159.

Schiemann, R., Lüthi, D., & Schär, C. (2009). Seasonality and Interannual Variability of the Westerly Jet in the Tibetan Plateau Region. *Journal of Climate*, *22*(11), 2940–2957.

Schuett, B., Berking, J., Frechen, M., & Yi, C. (2008). Late Pleistocene Lake Level Fluctuations of the Nam Co, Tibetan Plateau, China. *Z. Geomorph. N.F.*, *52*(2), 57–74.

Schulla, J. (2013). *Model Description WaSiM. Technical report.* Zürich.

Schulz, K., Seppelt, R., Zehe, E., Vogel, H. J., & Attinger, S. (2006). Importance of spatial structures in advancing hydrological sciences. *Water Resources Research*, *42*, W03S03, doi:10.1029/2005WR004301.

Seibert, J. (2000). Multi-criteria calibration of a conceptual runoff model using a genetic algorithm. *Hydrology and Earth System Sciences*, *4*(2), 215–224.

Seibert, J., & Beven, K. (2009). Gauging the ungauged basin: how many discharge measurements are needed? *Hydrology and Earth System Sciences*, *13*, 883–892.

Seibert, J., & McDonnell, J. J. (2002). On the dialog between experimentalist and modeler in catchment hydrology: Use of soft data for multicriteria model calibration. *Water Resources Research*, *38*(11), 1241, doi:10.1029/2001WR000978.

Sen, P. K. (1968). Estimates of the Regression Coefficient Based on Kendall's Tau. *Journal of the American Statistical Association*, *63*(324), 1379–1389.

Shea, J. M., Immerzeel, W. W., Wagnon, P., Vincent, C., & Bajracharya, S. (2015). Modelling glacier change in the Everest region, Nepal Himalaya. *The Cryosphere*, *9*, 1105–1128. doi:10.5194/tc-9-1105-2015

Shuttleworth, W. J. (1993). *Evaporation.* In Maidment, D. R. (ed.), New York: McGraw-Hill.

Sieber, A., & Uhlenbrook, S. (2005). Sensitivity analyses of a distributed catchment model to verify the model structure. *Journal of Hydrology*, *310*(1-4), 216–235.

Singh, V. P., & Xu, C.-Y. (1997). Evaluation and generalization of 13 mass-transfer equations for determining free water evaporation. *Hydrological Processes*, *11*, 311–323.

Sitch, S., Smith, B., Prentice, I. C., Arneth, A., Bondeau, A., Cramer, W., … Venevsky, S. (2003). Evaluation of ecosystem dynamics, plant geography and terrestrial carbon cycling in the LPJ dynamic global vegetation model. *Global Change Biology*, *9*, 161–185.

Sivakumar, B. (2000). Chaos theory in hydrology: important issues and interpretations. *Journal of Hydrology*, *227*(1-4), 1–20.

Sivakumar, B., & Singh, V. P. (2012). Hydrologic system complexity and nonlinear dynamic concepts for a catchment classification framework. *Hydrology and Earth System Sciences*, *16*(11), 4119–4131.

Sivapalan, M. (2003). Prediction in ungauged basins: a grand challenge for theoretical hydrology. *Hydrological Processes*, *17*(15), 3163–3170.

Sivapalan, M. (2006). *Pattern, Process and Function: Elements of a Unified Theory of Hydrology at the Catchment Scale. Encyclopedia of Hydrological Sciences. 1:13*. doi:10.1002/0470848944.hsa012

Sivapalan, M., & Kalma, J. D. (1995). Scale problems in hydrology: contributions of the Robertson Workshop. *Hydrological Processes*, *9*, 243–250.

Sivapalan, M., Takeuchi, K., Franks, S. W., Gupta, V. K., Karambiri, H., Lakshmi, V., … Zehe, E. (2003). IAHS Decade on Predictions in Ungauged Basins (PUB), 2003–2012: Shaping an exciting future for the hydrological sciences. *Hydrological Sciences Journal*, *48*(6), 857–880.

Skamarock, W. C., & Klemp, J. B. (2008). A time-split nonhydrostatic atmospheric model for weather research and forecasting applications. *Journal of Computational Physics*, *227*(7), 3465–3485.

Sobol, I. M. (1967). On the distribution of points in a cube and the approximate evaluation of integrals. *USSR Computational Mathematics and Mathematical Physics*, *7*(4), 86–112.

Song, C., Huang, B., & Ke, L. (2013). Modeling and analysis of lake water storage changes on the Tibetan Plateau using multi-mission satellite data. *Remote Sensing of Environment*, *135*, 25–35.

Song, C., Huang, B., & Ke, L. (2014). Inter-annual changes of alpine inland lake water storage on the Tibetan Plateau: Detection and analysis by integrating satellite altimetry and optical imagery. *Hydrological Processes*, *28*(4), 2411–2418.

Song, C., Huang, B., Ke, L., & Richards, K. S. (2014). Seasonal and abrupt changes in the water level of closed lakes on the Tibetan Plateau and implications for climate impacts. *Journal of Hydrology*, *514*, 131–144.

Song, C., Huang, B., Richards, K., Ke, L., & Hien, V. P. (2014). Accelerated lake expansion on the Tibetan Plateau in the 2000s: Induced by glacial melting or other processes? *Water Resources Research*, *50*(4), 3170–3186.

Song, C., Ye, Q., & Cheng, X. (2015). Shifts in water-level variation of Namco in the central Tibetan Plateau from ICESat and CryoSat-2 altimetry and station observations. *Science Bulletin*, *60*(14), 1287–1297.

Stedinger, J. R., Vogel, R. M., Lee, S. U., & Batchelder, R. (2008). Appraisal of the generalized likelihood uncertainty estimation (GLUE) method. *Water Resources Research*, *44*, W00B06, doi:10.1029/2008WR006822.

Stefan, J. (1879). *Über die Beziehung zwischen der Wärmestrahlung und der Temperatur*. In Sitzungsberichte der mathematisch-naturwissenschaftlichen Classe der kaiserlichen Akademie der Wissenschaften, Bd. 79, Wien.

Strasser, U., Bernhardt, M., Weber, M., Liston, G. E., & Mauser, W. (2008). Is snow sublimation important in the alpine water balance? *The Cryosphere*, *2*, 53–66.

Sturm, K. (2013). *Spatial-temporal snow cover dynamics in the Central Taurus Mountains, Turkey*. Master Thesis, FSU Jena.

Sun, W., Ishidaira, H., Bastola, S., & Yu, J. (2015). Estimating daily time series of streamflow using hydrological model calibrated based on satellite observations of river water surface width: Toward real world applications. *Environmental Research*, *139*, 36–45.

Tahir, A. A., Chevallier, P., Arnaud, Y., Neppel, L., & Ahmad, B. (2011). Modeling snowmelt-runoff under climate scenarios in the Hunza River basin, Karakoram Range, Northern Pakistan. *Journal of Hydrology*, *409*(1-2), 104–117.

Tang, B.-H., Shrestha, B., Li, Z.-L., Liu, G., Ouyang, H., Gurung, D. R., … Aung, K. S. (2013). Determination of snow cover from MODIS data for the Tibetan Plateau region. *International Journal of Applied Earth Observation and Geoinformation*, *21*, 356–365.

Tang, Y., Reed, P., Wagener, T., & van Werkhoven, K. (2007). Comparing sensitivity analysis methods to advance lumped watershed model identification and evaluation. *Hydrology and Earth System Sciences*, *11*(2), 793–817.

Tapley, B. D., Bettadpur, S., Ries, J. C., Thompson, P. F., & Watkins, M. M. (2004). GRACE measurements of mass variability in the Earth system. *Science*, *305*, 503–505.

Tian, K., Liu, J., Kang, S., Campbell, I. B., Zhang, F., Zhang, Q., & Lu, W. (2008). Hydrothermal pattern of frozen soil in Nam Co lake basin, the Tibetan Plateau. *Environmental Geology*, *57*(8), 1775–1784.

Troch, P. A., Carrillo, G. A., Heidbüchel, I., Rajagopal, S., Switanek, M., Volkmann, T. H. M., & Yaeger, M. (2009). Dealing with Landscape Heterogeneity in Watershed Hydrology: A Review of Recent Progress toward New Hydrological Theory. *Geography Compass*, *3*(1), 375–392.

Uhlenbrook, S., Seibert, J., Leibundgut, C., & Rodhe, A. (1999). Prediction uncertainty of conceptual rainfall-runoff models caused by problems in identifying model parameters and structure. *Hydrological Sciences Journal*, *44*(5), 779–797.

Vaché, K. B., & McDonnell, J. J. (2006). A process-based rejectionist framework for evaluating catchment runoff model structure. *Water Resources Research*, *42*, W02409, doi:10.1029/2005WR004247.

Valiantzas, J. D. (2006). Simplified versions for the Penman evaporation equation using routine weather data. *Journal of Hydrology*, *331*(3-4), 690–702.

Van Engelen, V. W. P., & Dijkshoorn, J. A. (2013). *Global and National Soils and Terrain Digital Databases (SOTER). Procedures Manual, Version 2.0*. Wageningen: ISRIC - World Soil Information.

Vehvilaeinen, B. (1992). *Snow cover models in operational watershed forecasting. Yhteenveto: Lumimallit vesistöjen ennustemalleissa.* Publications of the Water and Environment Research Institute 11. National Board of Waters and the Environment. Finland, Helsinki.

Venkatesh, T. N., Kulkarni, A. V., & Srinivasan, J. (2012). Relative effect of slope and equilibrium line altitude on the retreat of Himalayan glaciers. *The Cryosphere*, *6*(2), 301–311.

Vettermann, F. (2014). *Hydrologische Systemanalyse und Modellierung des Einzugsgebietes Tangra Yumco, Tibet*. Master Thesis, FSU Jena.

Vionnet, V., Martin, E., Masson, V., Guyomarc'h, G., Naaim-Bouvet, F., Prokop, A., … Lac, C. (2014). Simulation of wind-induced snow transport and sublimation in alpine terrain using a fully coupled snowpack/atmosphere model. *The Cryosphere*, *8*(2), 395–415.

Vrugt, J. A., Gupta, H. V., Bastidas, L. A., Bouten, W., & Sorooshian, S. (2003). Effective and efficient algorithm for multiobjective optimization of hydrologic models. *Water Resources Research*, *39*(8), 1214, doi:10.1029/2002WR001746.

Wagener, T. (2007). Can we model the hydrological impacts of environmental change? *Hydrological Processes*, *21*, 3233–3236.

Wagener, T., Boyle, D. P., Lees, M. J., Wheater, H. S., Gupta, H. V, & Sorooshian, S. (2001). A framework for development and application of hydrological models. *Hydrological Earth System Sciences*, *5*(1), 13–26.

Wagener, T., & Kollat, J. (2007). Numerical and visual evaluation of hydrological and environmental models using the Monte Carlo analysis toolbox. *Environmental Modelling & Software*, *22*(7), 1021–1033.

Wagener, T., McIntyre, N., Lees, M. J., Wheater, H. S., & Gupta, H. V. (2003). Towards reduced uncertainty in conceptual rainfall-runoff modelling: dynamic identifiability analysis. *Hydrological Processes*, *17*(2), 455–476.

Wagener, T., Sivapalan, M., McDonnell, J., Hooper, R., Lakshmi, V., Liang, X., & Kumar, P. (2004). Predictions in Ungauged Basins As a Catalyst for Multidisciplinary Hydrology. *Eos, Trans. AGU*, *85*(44), 451–457.

Wagener, T., Sivapalan, M., Troch, P. A., McGlynn, B. L., Harman, C. J., Gupta, H. V., … Wilson, J. S. (2010). The future of hydrology: An evolving science for a changing world. *Water Resources Research*, *46*(5), W05301, doi:10.1029/2009WR008906.

Wahba, G. (1990). *Spline models for Observational data*. Philadelphia: Soc. Ind. Appl. Maths.

Wan, Z. (2009). *MODIS Land Surface Temperature Products Users ' Guide*.

Wang, B., Bao, Q., Hoskins, B., Wu, G., & Liu, Y. (2008). Tibetan Plateau warming and precipitation changes in East Asia. *Geophysical Research Letters*, *35*(14), L14702, doi:10.1029/2008GL034330.

Wang, J., Zhu, L., Daut, G., Ju, J., Lin, X., Wang, Y., & Zhen, X. (2009). Investigation of bathymetry and water quality of Lake Nam Co, the largest lake on the central Tibetan Plateau, China. *Limnology*, *10*(2), 149–158.

Wang, X., Siegert, F., Zhou, A., & Franke, J. (2013). Glacier and glacial lake changes and their relationship in the context of climate change, Central Tibetan Plateau 1972–2010. *Global and Planetary Change*, *111*, 246–257.

Winsemius, H. C., Savenije, H. H. G., & Bastiaanssen, W. G. M. (2008). Constraining model parameters on remotely sensed evaporation: justification for distribution in ungauged basins? *Hydrology and Earth System Sciences*, *12*(6), 1403–1413.

Winsemius, H. C., Schaefli, B., Montanari, A., & Savenije, H. H. G. (2009). On the calibration of hydrological models in ungauged basins: A framework for integrating hard and soft hydrological information. *Water Resources Research*, *45*(12), W12422, doi:10.1029/2009WR007706.

Wu, G., Liu, Y., He, B., Bao, Q., Duan, A., & Jin, F.-F. (2012). Thermal controls on the Asian summer monsoon. *Scientific Reports*, *2*(404), 1–7.

Wu, Q., & Zhang, T. (2008). Recent permafrost warming on the Qinghai-Tibetan Plateau. *Journal of Geophysical Research*, *113*, D13108, doi:10.1029/2007JD009539.

Wu, Q., & Zhang, T. (2010). Changes in active layer thickness over the Qinghai Tibetan Plateau from 1995 to 2007. *Journal of Geophysical Research*, *115*, D09107, doi:10.1029/2009JD012974.

Wu, Y., & Zhu, L. (2008). The response of lake-glacier variations to climate change in Nam Co Catchment, central Tibetan Plateau, during 1970–2000. *Journal of Geographical Sciences*, *18*(2), 177–189.

Xie, H., Wang, X., & Liang, T. (2009). Development and assessment of combined Terra and Aqua snow cover products in Colorado Plateau, USA and northern Xinjiang, China. *Journal of Applied Remote Sensing*, *3*(1), 033559, doi:10.1117/1.3265996.

Xie, H., Ye, J., Liu, X., & E, C. (2009). Warming and drying trends on the Tibetan Plateau (1971–2005). *Theoretical and Applied Climatology*, *101*(3-4), 241–253.

Xie, H., & Zhu, X. (2013). Reference evapotranspiration trends and their sensitivity to climatic change on the Tibetan Plateau (1970-2009). *Hydrological Processes*, *27*(25), 3685–3693.

Xu, J., Yu, S., Liu, J., Haginoya, S., Ishigooka, Y., Kuwagata, T., … Yasunari, T. (2009). The Implication of Heat and Water Balance Changes in a Lake Basin on the Tibetan Plateau. *Hydrological Research Letters*, *5*, 1–5.

Xu, L. (2010). MODIS Snow Monitoring Over the Tibetan Plateau. In E. Chuvieco, J. Li, & X. Yang (Eds.), *Advances in Earth Observation of Global Change* (pp. 111–124). Springer Netherlands. doi:10.1007/978-90-481-9085-0_9.

Xu, Y., Shen, Y., & Wu, Z. (2013). Spatial and Temporal Variations of Land Surface Temperature Over the Tibetan Spatial and Temporal Variations of Land Surface Temperature Over the Tibetan Plateau Based on Harmonic Analysis. *Mountain Research and Development*, *33*(1), 85–94.

Xu, Z., Gong, T., & Li, J. (2008). Decadal trend of climate in the Tibetan Plateau—regional temperature and precipitation. *Hydrological Processes*, *22*, 3056–3065.

Yang, D., Zhou, C., Ouyang, H., & Chen, C. (2012). Characteristics of Variation in Runoff Across the Nyangqu River Basin in the Qinghai-Tibet Plateau. *Journal of Resources and Ecology*, *3*(1), 80–86.

Yang, K., Chen, Y.-Y., & Qin, J. (2009). Some practical notes on the land surface modeling in the Tibetan Plateau. *Hydrology and Earth System Sciences*, *13*, 687–701.

Yang, K., Wu, H., Qin, J., Lin, C., Tang, W., & Chen, Y. (2014). Recent climate changes over the Tibetan Plateau and their impacts on energy and water cycle: A review. *Global and Planetary Change*, *112*, 79–91.

Yang, K., Ye, B., Zhou, D., Wu, B., Foken, T., Qin, J., & Zhou, Z. (2011). Response of hydrological cycle to recent climate changes in the Tibetan Plateau. *Climatic Change*, *109*(3-4), 517–534.

Yang, M., Nelson, F. E., Shiklomanov, N. I., Guo, D., & Wan, G. (2010). Permafrost degradation and its environmental effects on the Tibetan Plateau: A review of recent research. *Earth-Science Reviews*, *103*(1-2), 31–44.

Yao, H. (2009). Long-Term Study of Lake Evaporation and Evaluation of Seven Estimation Methods: Results from Dickie Lake, South-Central Ontario, Canada. *Journal of Water Resource and Protection*, *2*, 59–77.

Yao, T. (2010). Glacial fluctuations and its impacts on lakes in the southern Tibetan Plateau. *Chinese Science Bulletin*, *55*(20), 2071–2071.

Yao, T., Pu, J., Lu, A., Wang, Y., & Yu, W. (2007). Recent Glacial Retreat and Its Impact on Hydrological Processes on the Tibetan Plateau, China, and Surrounding Regions. *Arctic, Antarctic, and Alpine Research*, *39*(4), 642–650.

Yao, T., Thompson, L. G., Mosbrugger, V., Zhang, F., Ma, Y., Luo, T., … Fayziev, R. (2012). Third Pole Environment (TPE). *Environmental Development*, *3*, 52–64.

Yao, T., Thompson, L., Yang, W., Yu, W., Gao, Y., Guo, X., … Joswiak, D. (2012). Different glacier status with atmospheric circulations in Tibetan Plateau and surroundings. *Nature Climate Change*, 1–5.

Ye, Q., Yao, T., Chen, F., Kang, S., Zhang, X., & Wang, Y. (2008). Response of Glacier and Lake Covariations to Climate Change in Mapam Yumco Basin on Tibetan Plateau during 1974 – 2003. *Journal of China University of Geosciences*, *19*(2), 135–145.

Yin, A., & Harrison, T. M. (2000). Geologic evolution of the Himalayan - Tibetan orogen. *Annu. Rev. Earth Planet. Sci.*, *28*, 211–280.

Yin, Y., Wu, S., Zhao, D., Zheng, D., & Pan, T. (2013). Modeled effects of climate change on actual evapotranspiration in different eco-geographical regions in the Tibetan Plateau. *Journal of Geographical Sciences*, *23*(2), 195–207.

Yin, Y., Wu, S., Zheng, D., & Yang, Q. (2008). Radiation calibration of FAO56 Penman-Monteith model to estimate reference crop evapotranspiration in China. *Agricultural Water Management*, *95*, 77–84.

You, Q., Fraedrich, K., Ren, G., Pepin, N., & Kang, S. (2013). Variability of temperature in the Tibetan Plateau based on homogenized surface stations and reanalysis data. *International Journal of Climatology*, *33*(6), 1337–1347.

You, Q., Fraedrich, K., Ren, G., Ye, B., Meng, X., & Kang, S. (2012). Inconsistencies of precipitation in the eastern and central Tibetan Plateau between surface adjusted data and reanalysis. *Theoretical and Applied Climatology*, *109*(3-4), 485–496.

You, Q., Kang, S., Aguilar, E., & Yan, Y. (2008). Changes in daily climate extremes in the eastern and central Tibetan Plateau during 1961–2005. *Journal of Geophysical Research*, *113*, D07101, doi:10.1029/2007JD009389.

You, Q., Kang, S., Pepin, N., Flügel, W.-A., Sanchez-Lorenzo, A., Yan, Y., & Zhang, Y. (2010). Climate warming and associated changes in atmospheric circulation in the eastern and central Tibetan Plateau from a homogenized dataset. *Global and Planetary Change*, *72*(1-2), 11–24.

You, Q., Kang, S., Pepin, N., Flügel, W.-A., Yan, Y., Behrawan, H., & Huang, J. (2010). Relationship between temperature trend magnitude, elevation and mean temperature in the Tibetan Plateau from homogenized surface stations and reanalysis data. *Global and Planetary Change*, *71*(1-2), 124–133.

Yu, H., Luedeling, E., & Xu, J. (2010). Winter and spring warming result in delayed spring phenology on the Tibetan Plateau. *Proceedings of the National Academy of Sciences of the United States of America*, *107*(51), 22151–22156.

Yu, S., Liu, J., Xu, J., & Wang, H. (2011). Evaporation and energy balance estimates over a large inland lake in the Tibet-Himalaya. *Environmental Earth Sciences*, *64*, 1169–1176.

Zehe, E., & Blöschl, G. (2004). Predictability of hydrologic response at the plot and catchment scales: Role of initial conditions. *Water Resources Research*, *40*, W10202, doi:10.1029/2003WR002869.

Zhang, B., Wu, Y., Lei, L., Li, J., Liu, L., Chen, D., & Wang, J. (2013). Monitoring changes of snow cover, lake and vegetation phenology in Nam Co Lake Basin (Tibetan Plateau) using remote sensing (2000–2009). *Journal of Great Lakes Research*, *39*(2), 224–233.

Zhang, B., Wu, Y., Zhu, L., Wang, J., Li, J., & Chen, D. (2011). Estimation and trend detection of water storage at Nam Co Lake, central Tibetan Plateau. *Journal of Hydrology*, *405*(1-2), 161–170.

Zhang, G., Kang, S., Fujita, K., Huintjes, E., Xu, J., Yamazaki, T., … Yao, T. (2013). Energy and mass balance of Zhadang glacier surface, central Tibetan Plateau. *Journal of Glaciology*, *59*(213), 137–148.

Zhang, G., Xie, H., Kang, S., Yi, D., & Ackley, S. F. (2011). Monitoring lake level changes on the Tibetan Plateau using ICESat altimetry data (2003–2009). *Remote Sensing of Environment*, *115*(7), 1733–1742.

Zhang, G., Xie, H., Yao, T., Liang, T., & Kang, S. (2012). Snow cover dynamics of four lake basins over Tibetan Plateau using time series MODIS data (2001-2010). *Water Resources Research*, *48*, W10529, doi:10.1029/2012WR011971.

Zhang, G., Yao, T., Xie, H., Kang, S., & Lei, Y. (2013). Increased mass over the Tibetan Plateau: From lakes or glaciers? *Geophysical Research Letters*, *40*, 2125–2130.

Zhang, L., Su, F., Yang, D., Hao, Z., & Tong, K. (2013). Discharge regime and simulation for the upstream of major rivers over Tibetan Plateau. *Journal of Geophysical Research: Atmospheres*, *118*(15), 8500–8518.

Zhang, Q., Liu, C., Xu, C., Xu, Y., & Jiang, T. (2006). Observed trends of annual maximum water level and streamflow during past 130 years in the Yangtze River basin, China. *Journal of Hydrology*, *324*(1-4), 255–265.

Zhang, T. (2007). Perspectives on Environmental Study of Response to Climatic and Land Cover/Land Use Change over the Qinghai-Tibetan Plateau: an Introduction Environmental Study of Response to Climatic and Land Cover / Land Use Change over the Qinghai-T. *Arctic, Antarctic, and Alpine Research*, *39*(4), 631–634.

Zhang, X., Ren, Y., Yin, Z.-Y., Lin, Z., & Zheng, D. (2009). Spatial and temporal variation patterns of reference evapotranspiration across the Qinghai-Tibetan Plateau during 1971–2004. *Journal of Geophysical Research*, *114*, D15105, doi:10.1029/2009JD011753.

Zhang, Y., Liu, S., Xu, J., & Shangguan, D. (2007). Glacier change and glacier runoff variation in the Tuotuo River basin, the source region of Yangtze River in western China. *Environmental Geology*, *56*(1), 59–68.

Zhang, Y., Yao, T., & Ma, Y. (2011). Climatic changes have led to significant expansion of endorheic lakes in Xizang (Tibet) since 1995. *Sciences in Cold and Arid Regions*, *3*(6), 463–467.

Zhang, Y., Zhang, S., Zhai, X., & Xia, J. (2012). Runoff variation and its response to climate change in the Three Rivers Source Region. *Journal of Geographical Sciences*, *22*(5), 781–794.

Zhao, L., Ping, C.-L., Yang, D., Cheng, G., Ding, Y., & Liu, S. (2004). Changes of climate and seasonally frozen ground over the past 30 years in Qinghai–Xizang (Tibetan) Plateau, China. *Global and Planetary Change*, *43*(1-2), 19–31.

Zhao, L., Yang, K., Qin, J., Chen, Y., Tang, W., Montzka, C., … Vereecken, H. (2013). Spatiotemporal analysis of soil moisture observations within a Tibetan mesoscale area and its implication to regional soil moisture measurements. *Journal of Hydrology*, *482*, 92–104.

Zhou, S., Kang, S., Chen, F., & Joswiak, D. R. (2013). Water balance observations reveal significant subsurface water seepage from Lake Nam Co, south-central Tibetan Plateau. *Journal of Hydrology*, *491*, 89–99.

Zhu, G., Su, Y., Li, X., & Zhang, K. (2014). Modelling evapotranspiration in an alpine grassland ecosystem on Qinghai-Tibetan plateau. *Hydrological Processes*, *28*(3), 610–619.

Zhu, L., Xie, M., & Wu, Y. (2010). Quantitative analysis of lake area variations and the influence factors from 1971 to 2004 in the Nam Co basin of the Tibetan Plateau. *Chinese Science Bulletin*, *55*(13), 1294–1303.
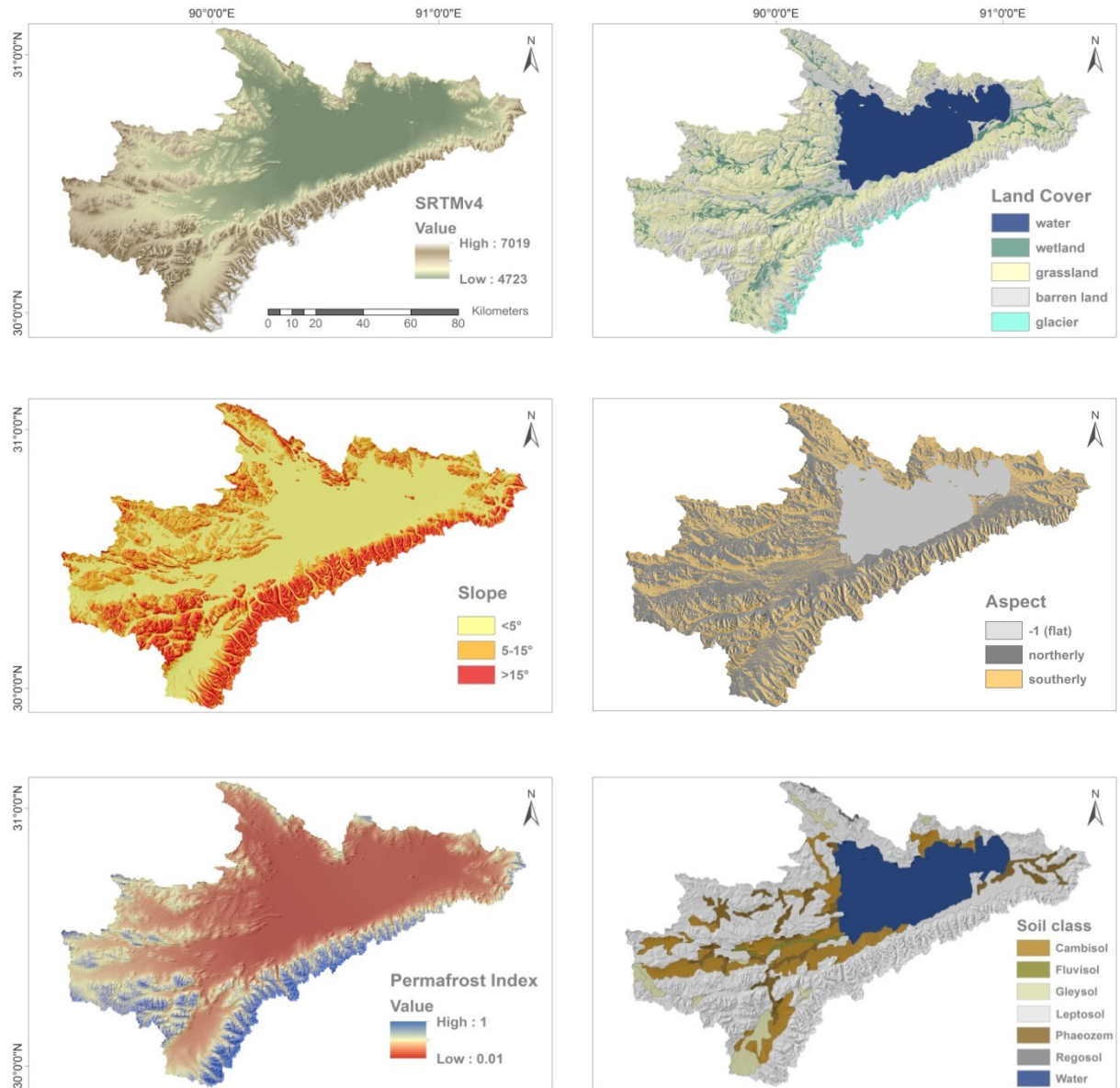
Figure A.1:   SRTM-DEM, land cover, slope, aspect, permafrost index and soil map for the Nam Co basin.
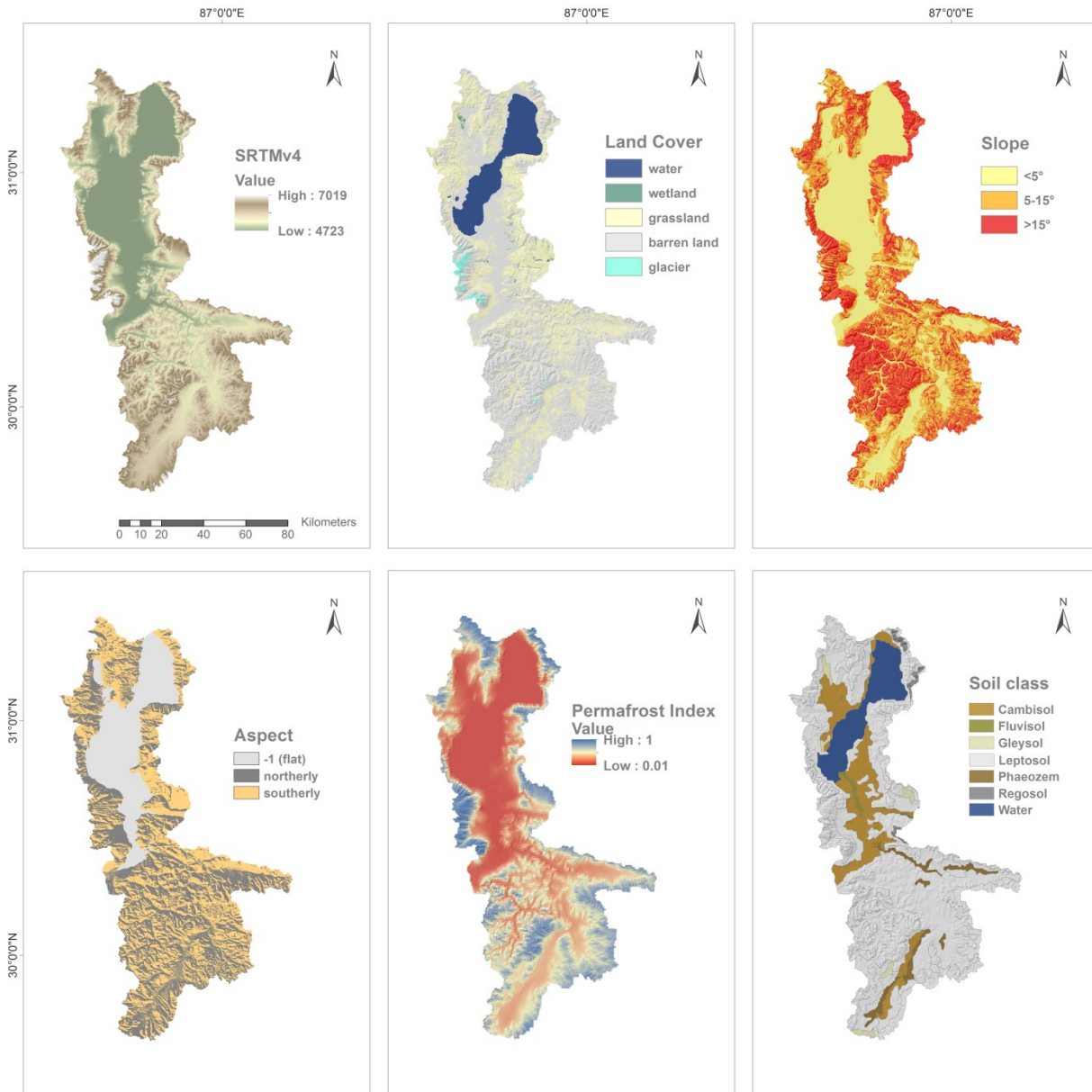
Figure A.2:   SRTM-DEM, land cover, slope, aspect, permafrost index and soil map for the Tangra Yumco basin.
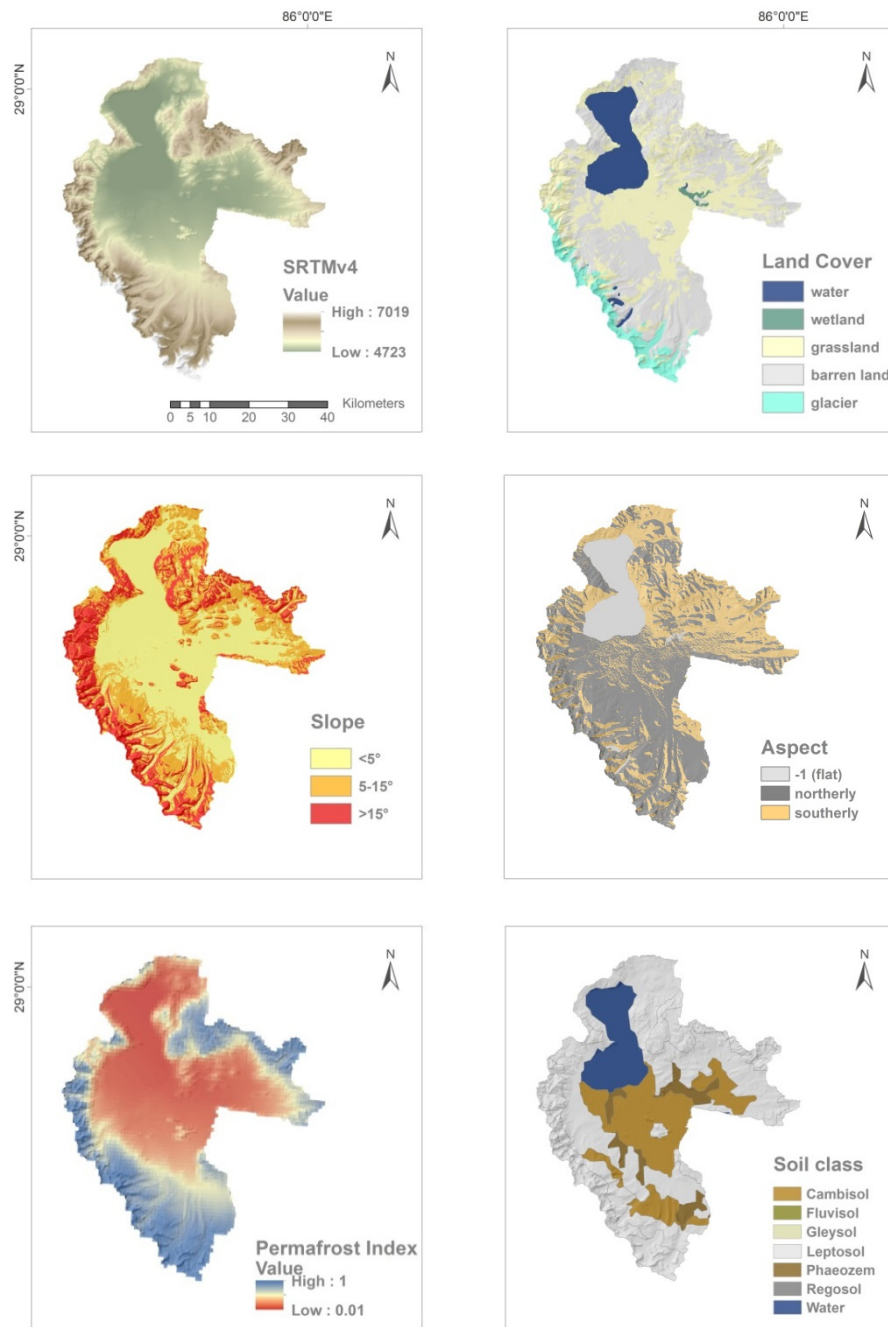
Figure A.3: SRTM-DEM, land cover, slope, aspect, permafrost index and soil map for the Paiku Co basin.
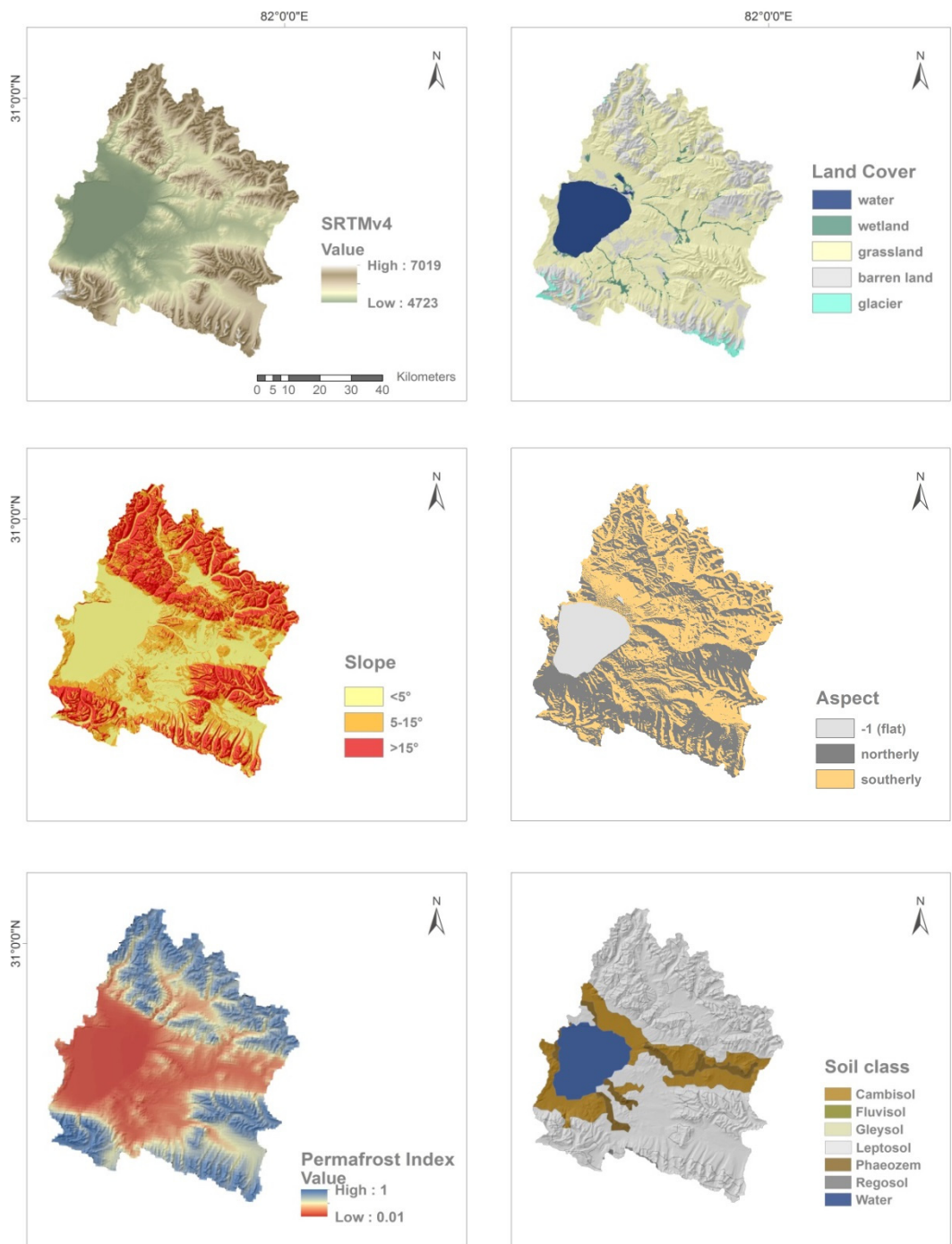
Figure A.4:   SRTM DEM, land cover, slope, aspect, permafrost index and soil map for the Mapam Yumco basin.

Table A.1: Area percentages of topographic features in the four study basins.

Lake name	Elevation (area proportion in %)		
	<5000	5000-5500	>5500
Nam Co	54	39	7
Tangra Yumco	38	48	13
Paiku Co	55	28	17
Mapam Yumco	47	34	18
	Slope (area proportion in %)		
	<5°	5-15°	>15°
Nam Co	55	28	17
Tangra Yumco	38	32	29
Paiku Co	46	31	23
Mapam Yumco	38	32	30
	Aspect (area proportion in %)		
	flat	southerly (SE-SW/112.5-292.5)	northerly (NW-NE/292.5-112.5)
Nam Co	19	36	45
Tangra Yumco	20	40	20
Paiku Co	11	37	52
Mapam Yumco	9	46	45

Selbständigkeitserklärung

Ich erkläre, dass ich die vorliegende Arbeit selbständig und unter Verwendung der angegebenen Hilfsmittel, persönlichen Mitteilungen und Quellen angefertigt habe.

Jena, Oktober 2015 (Sophie Biskop)

Tabellarischer Lebenslauf

Persönliche Daten

Name	Sophie Biskop
Nationalität	Deutsch
Familientsand	Ledig
Geburtsdatum	03.05.1984
Geburtsort	Weimar

Kurzbiographie

Juni 2002	Abitur, Goethegymnasium Weimar
10/2002 - 01/2009	Studium der Geographie (Diplom) mit dem Nebenfach Geologie und Ökologie Friedrich-Schiller-Universität Jena
01/2009	Abschluss als Diplom-Geograph (Gesamtnote: sehr gut) Friedrich-Schiller-Universität Jena
	Diplomarbeit: "Anwendung des J2000 Modells in vergletscherten Einzugsgebieten im Venedigergebiet"
04/2009 – 02/2010	Doktorandenstipendium Friedrich-Schiller-Universität Jena
seit 03/2010	Wissenschaftlicher Mitarbeiter am Lehrstuhl für Geoinformatik, Institut für Geographie, Friedrich-Schiller-Universität Jena

Jena, Oktober 2015   (Sophie Biskop)